

**ASPECTS OF QUANTUM RESOURCES IN THERMAL
ENVIRONMENT**

By
CHIRANJIB MUKHOPADHYAY
PHYS08201305006

Harish-Chandra Research Institute, Allahabad

*A thesis submitted to the
Board of Studies in Physical Sciences
In partial fulfillment of requirements
for the Degree of*
DOCTOR OF PHILOSOPHY
of
HOMI BHABHA NATIONAL INSTITUTE



November 2019

Homi Bhabha National Institute¹

Recommendations of the Viva Voce Committee

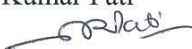
As members of the Viva Voce Committee, we certify that we have read the dissertation prepared by Chiranjib Mukhopadhyay entitled "Aspects of quantum resources in thermal environment" and recommend that it may be accepted as fulfilling the thesis requirement for the award of Degree of Doctor of Philosophy.

Chairman - Prof. Pinaki Majumdar



Date: 18/2/20

Guide / Convener – Arun Kumar Pati



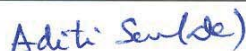
Date: 18-2-20

Examiner - Prof. Anil Shaji



Date: 18 February 2020

Member 1- Prof. Aditi Sen (De)



Date: 18.02.2020

Member 2- Prof. Ujjwal Sen



Date: 18/02/2020

Member 3- Prof. Sumathi Rao



Date: 18/2/2020

Final approval and acceptance of this thesis is contingent upon the candidate's submission of the final copies of the thesis to HBNI.

I/We hereby certify that I/we have read this thesis prepared under my/our direction and recommend that it may be accepted as fulfilling the thesis requirement.

Date: 18-02-2020

Place: Prayagraj



Prof. Arun Kumar Pati

Guide

¹ This page is to be included only for final submission after successful completion of viva voce.

STATEMENT BY AUTHOR

This dissertation has been submitted in partial fulfillment of requirements for an advanced degree at Homi Bhabha National Institute (HBNI) and is deposited in the Library to be made available to borrowers under rules of the HBNI.

Brief quotations from this dissertation are allowable without special permission, provided that accurate acknowledgement of source is made. Requests for permission for extended quotation from or reproduction of this manuscript in whole or in part may be granted by the Competent Authority of HBNI when in his or her judgement the proposed use of the material is in the interests of scholarship. In all other instances, however, permission must be obtained from the author.



Chiranjib Mukhopadhyay

DECLARATION

I hereby declare that the investigation presented in the thesis has been carried out by me.
The work is original and has not been submitted earlier as a whole or in part for a degree
/ diploma at this or any other Institution / University.



Chiranjib Mukhopadhyay

List of Publications arising from the thesis

Journal

1. "Exact master equation for a spin interacting with a spin bath: Non-Markovianity and negative entropy production rate", Samyadeb Bhattacharya, Avijit Misra, Chiranjib Mukhopadhyay, Arun Kumar Pati, *Physical Review A*, **2017**, 95, 012122.
2. "Dynamics and thermodynamics of a central spin immersed in a spin bath", Chiranjib Mukhopadhyay, Samyadeb Bhattacharya, Avijit Misra, Arun Kumar Pati, *Physical Review A*, **2017** 96, 052125.
3. "Quantum speed limit constraints on a nanoscale autonomous refrigerator", Chiranjib Mukhopadhyay, Avijit Misra, Samyadeb Bhattacharya, Arun Kumar Pati, *Physical Review E*, **2018**, 97, 062116.
4. "Coherence makes quantum systems magical", Chiranjib Mukhopadhyay, Sk Sazim, Arun Kumar Pati, *Journal of Physics A : Mathematical and Theoretical*, **2018**, 51, 414006.
5. "Generating steady quantum coherence and magic through an autonomous thermodynamic machine by utilizing a spin bath", Chiranjib Mukhopadhyay, *Physical Review A*, **2018**, 98, 012102.

Preprint

1. "Superposition of causal order as a metrological resource in quantum thermometry", Chiranjib Mukhopadhyay, Manish Kumar Gupta, Arun Kumar Pati, arXiv 1812.07508 [quant-ph]
2. "Quantum precision thermometry with weak measurement", Arun Kumar Pati, Chiranjib Mukhopadhyay, Sagnik Chakrabarty, Sibasish Ghosh, arXiv 1901.07415 [quant-ph].

List of Publications of the candidate not substantially used in the thesis

Journal

1. "Stronger error disturbance relations for incompatible quantum observables", Chiranjib Mukhopadhyay, Namrata Shukla, Arun Kumar Pati, *Europhysics Letters*, **2016**, 113, 50002.
2. "Quantum uncertainty relation based on the mean deviation", Gautam Sharma, Chiranjib Mukhopadhyay, Sk Sazim, Arun Kumar Pati, *Physical Review A*, **2018**, 98, 032106.

3. "A note on robustness of coherence or multipartite quantum states", Chiranjib Mukhopadhyay, Udit Kamal Sharma, Indranil Chakrabarty, *Pramana*, **2018**, 93, 69.

Preprint

1. "Steerability of quantum coherence in accelerated frame", Debasis Mondal, Chiranjib Mukhopadhyay, arXiv 1510.07556 [quant-ph].
2. "Wave particle duality employing quantum coherence in superposition with indistinguishable pointers", Sreetama Das, Chiranjib Mukhopadhyay, Sudipto Singha Roy, Samyadeb Bhattacharya, Aditi Sen (De), Ujjwal Sen, arXiv 1705.04343 [quant-ph].
3. "Quantifying coherence with quantum addition", Chiranjib Mukhopadhyay, Arun Kumar Pati, Sk Sazim, arXiv 1803.06982 [quant-ph].
4. "Stronger classes of sum uncertainty and reverse uncertainty relations", Chiranjib Mukhopadhyay, Arun Kumar Pati, arxiv 1806.11347 [quant-ph].
5. "Superposition of causal order enables perfect quantum teleportation with very noisy singlets", Chiranjib Mukhopadhyay, Arun Kumar Pati, arXiv 1901.07626 [quant-ph].
6. "Coherence of purification", Arun Kumar Pati, Long-Mei Yang, Chiranjib Mukhopadhyay, Shao-Ming Fei, Zhi-Xi Wang, arXiv 1907.13067 [quant-ph].
7. "Many-body systems as resources for universal fault tolerant quantum computation", Saubhik Sarkar, Chiranjib Mukhopadhyay, Abolfazl Bayat, arXiv 1908.08058 [quant-ph].

Conference presentations

Oral presentations

1. *Young Quantum 2017*, Harish-Chandra Research Institute, Allahabad, India (2017).
2. *Recent Trends in Quantum Theory*, University of Calcutta, Kolkata, India (2017).
3. *Physics and Applied Mathematics Researchers' Meet*, Indian Statistical Institute, Kolkata, India (2017).
4. *Nanyang Quantum 2017*, Nanyang Technological University, Singapore (2017).
5. *Quantum Frontiers and Fundamentals*, Raman Research Institute, Bengaluru, India (2018).
6. *Quantum Metrology and Open Quantum Systems*, Kodaikanal, Institute of Mathematical Sciences, India (2018).

7. *Quantum Information Processing and Applications*, Harish-Chandra Research Institute, Allahabad, India (2018).
8. *Asia Pacific Conference and Workshop on Quantum Information Sciences*, Indian Institute of Science Education and Research, Kolkata, India (2018).

Poster presentations

1. *International Conference on Quantum Foundations*, National Institute of Technology, Patna (2015).
2. *International Conference on Quantum Foundations*, National Institute of Technology, Patna (2017).
3. *Quantum Roundabout 2018*, University of Nottingham, United Kingdom (2018).

Other activities

1. Tutored a graduate course on *Mathematical Methods - I* in fall 2016 semester, taught by Prof. T.P. Pareek.
2. Tutored a graduate course on *Quantum Information and Computation* in fall 2018 semester, taught by Prof. Aditi Sen De.

DEDICATIONS

Dedicated to the memories of my grandfather, and Kalyanbabu.

ACKNOWLEDGEMENTS

First of all, it is a pleasure to thank Arun Pati, my doctoral supervisor. Arun is one of the nicest as well the most creative persons I have ever met. I can only wish everyone get the same amount of creative and collaborative freedom from their doctoral advisors. It is a privilege and pleasure to be thanking other members of the quantum information group at HRI. Apart from academic discussions, I will miss Ujjwal-da's baritone laughter at our jokes at the pantry, or the invites to Aditi-di's office for sweets. I am grateful to Samya-da and Avijit-da who had given me courage and company in a particularly challenging time, and privileged to have worked with them. During the later part of time at HRI, it was wonderful to have all those chats with Sazim-da, Shiladitya-da, Saubhik-da, Brij, Stav, Sankha, Susobhan, Ratul, and Manish about physics as well as politics, sports, and arm-chair philosophy - with or without stimulants. I remember looking forward half in dread and half in excitement of Sohail's latest jokes. The fond memories of playing football in HRI will stay forever with me. Manab-da, Samrat, Joshi-bhaiya, Ritobroto, Mallesham, Mani, Pandey-ji, Manna-da, Pallab-da, Bibek-da, Sudhir-bhai, Ramdin, Sarif, Himadri-da, Niloy-da, Nirnoy, Kushal, Niyogi-da, Joydeep-da, Anirban-da - if any of you chance upon this, thank you for the great memories we shared. Cricket was another of my pastimes, and thanks to people like Stav, Brij, Chanchal, Srijon, Rohit, Chirag, Sohail, Abhishek - I enjoyed most thoroughly. I'd like to thank many non-academic members of HRI for making my life as smooth as possible at HRI. The library people, the computing centre stuff, Archana Tandon-ji, Seema-ji, Rachna-ji, Swapna ma'm, Sushant-bhaiya, Yashpal-ji - a big thank you to everyone. As far as HRI friends go, Dipyaman, Shouvik, and I have come to share a camaraderie which I will cherish for a long time to come, and if our antics are put to print, I'm sure it will be at least ten times the size of this thesis. Tanaya, my wonder woman, has put up with me for past few years. Long may that continue. I have always

enjoyed visiting IMSc in Chennai, and would like to acknowledge Sibasish-da, Chandru, Prof. Simon, Sagnik-da, Atanu-da, Arpan, Amlan, Aravinda, Tanmoy, Sahil, and others for letting me have a wonderful time whenever at Chennai. It is also a pleasure to acknowledge Debasis Mondal, Namrata Shukla, Gautam Sharma, Abolfazl Bayat, Sougato Bose, Gerardo Adesso, Sai Vinjanampathy, Kunal Sharma, Varun Narasimhachar, Manik Banik, Shao Ming Fei, Suman Chand, Bartosz Regula, Manish Gupta, Ben Morris, and Mike Vasmer for discussions at various points of my PhD, and especially Mario Ziman for enabling the journey thereafter. Looking back on it, I consider myself immensely fortunate to have attended masters level courses from Dileep Jatkar, Ashoke Sen, Jayanta Bhattacharjee, Pinaki Majumdar, Biswarup Majumdar, and especially late G. Venkat Pai, whose wonderful course on condensed matter physics almost succeeded in tempting me towards cond-matt. I warmly remember my (to date) only experimental research project at IGCAR, especially Deepak Gupta and B.V.R. Tata. Apart from HRI or academia, it was a joy to make friends with people like Tania, Siddartha-jethu, or continue my friendship with Shounak, Bhaskar, Abhirup, Avik, Ranita and others. I am thankful to the teacher who inspired me to take up physics, Dr. Gopal Sett, and Mr. Kalyan Kumar Bhattacharjee. Last, but definitely not the least, I can't express in words my gratitude to have grown up in a household that was stable, fun, and lively in equal measure.

Contents

SUMMARY	1
LIST OF FIGURES	3
LIST OF TABLES	11
1 Introduction	13
1.1 Resource theoretic framework : an overview	15
1.1.1 Resources available in the quantum world	15
1.1.2 Generic structure of convex quantum resource theories	23
1.1.3 Effect of environment on quantum resources	26
1.2 Outline of Thesis	27
1.3 Summary	27
2 A primer on open quantum systems	29
2.1 Kraus operator formalism	29
2.1.1 Examples of quantum channels	31
2.2 Dynamics of noisy quantum systems : quantum master equations	33
2.2.1 Lindblad master equation	34
2.3 Memory effects and Markovianity	35
2.3.1 Measures of non-Markovianity	35
2.4 Connection with thermodynamics	37

2.5	Summary	39
3	Linking coherence with magic	41
3.1	Coherence Quantifiers through magic monotones	42
3.1.1	Coherence monotone inspired from another magic monotone . . .	44
3.1.2	Hierarchy of stabilizer operations	46
3.2	Concrete results in small quantum systems	49
3.2.1	Explicit expression for magic in the qutrit case	49
3.2.2	Effect of coherent and incoherent noise on magic states	50
3.2.3	Relation between quantum coherence, quantum entanglement, and magic content	53
3.3	Summary	55
4	Non Markovian dynamics of central spin systems I : Infinite temperature case	57
4.1	Central spin model and its reduced dynamics	60
4.1.1	The model	60
4.1.2	Canonical master equation	62
4.1.3	Operator sum representation	66
4.1.4	Non-Markovianity	67
4.2	Negative entropy production rate	72
4.2.1	Rate of change of purity: Detection of non-Markovianity	76
4.3	Summary	77
5	Non Markovian dynamics of central spin systems II : Finite temperature case	79
5.1	Central spin model and its reduced dynamics	80
5.1.1	The model	80
5.1.2	Dynamical map of the central spin	81
5.1.3	Operator sum representation	83
5.1.4	Coherence and Entanglement dynamics of the central spin	85
5.2	Analysis of time averaged dynamical map	87

5.2.1	Resonance Condition for long lived quantum coherence	90
5.2.2	Information trapping in the Central Spin System	91
5.3	Canonical master equation and the process of equilibration	93
5.3.1	The principle of detailed balance	95
5.3.2	Irreversible Entropy production	99
5.4	Summary	102
6	Quantum speed limit constraints on absorption refrigerators	105
6.1	Absorption refrigerator at steady state	107
6.2	Quantum speed limit	109
6.3	Effects on the performance of quantum refrigerator from quantum speed limit	110
6.3.1	Dependence of the figure of merit on model parameters : role of initial coherence	114
6.3.2	Efficiency at maximal figure of merit	117
6.4	Summary	120
7	Autonomous creation of quantum resources	121
7.1	Autonomous thermal machine	122
7.1.1	Scheme and master equation	123
7.2	Quantum coherence generation in the reduced qubit	126
7.3	Generation of magic in the reduced qubit	127
7.4	Summary	135
8	Indefinite causal order as a resource for thermometry	137
8.1	A brief prologue on quantum thermometry	138
8.2	Quantum switch enhanced thermometry	140
8.2.1	Protocol	140
8.2.2	Thermodynamic uncertainty relations	144
8.2.3	Performance advantage	146
8.3	Summary	148

9	Thermometry using weak quantum measurements	149
9.1	Weak measurement	150
9.2	Assessing temperature through weak values	152
9.3	Precision in measurement of temperature	157
9.3.1	Precision analysis for imperfect thermalization	157
9.3.2	Precision analysis for unsharp post-selection	162
9.4	Quantum Fisher Information based analysis of precision of weak thermometry protocol	164
9.5	Summary	167
10	Future directions of work	169
	REFERENCES	170

SUMMARY

Quantum technologies have come a long way since the early days, and commercial exploitation of quantum resources is well underway. On the other hand, environments, especially in the form of thermal baths, often exert a rather destructive effect on these quantum resources. In this thesis, we seek to understand some aspects of links between these two sides - the first one is to consider how quantum resources get affected in presence of thermal environments, and the second one is to envisage the possible role of quantum features towards obtaining better performing machines in the thermal setting.

After a brief introduction to the dynamics of open quantum systems, we show that the amount of magic created by converting the quantum coherence content present in a state is itself a coherence monotone, and given a distance based magic monotone, it is possible to construct a coherence monotone. We next turn towards exploring the nature of non-Markovian dynamics for the central spin model, whose importance, especially in the context of NV-centre based quantum computation schemes, may hardly be overstated. We provide the exact time local master equations in the Lindblad form, and utilize them to investigate the nature of thermalization, or lack thereof, in these models, for infinite temperature spin baths, as well as generalizing in the subsequent chapter to arbitrary finite temperatures. The analysis turns up a few surprising facts, among them, a resonance condition for survival of quantum coherence in the long-time averaged state. We next

turn towards autonomous thermal machines, and assuming a recently proposed model of quantum absorption refrigerators, show that there is a trade off involved in the optimizing steady state cooling performance, and the waiting time involved in reaching the steady state, the latter being quantified through the quantum speed limit. The existence of this trade off prompts us to propose a new figure of merit for the performance of the refrigerator, and to demonstrate that injection of coherence in the initial configuration is highly beneficial as far as the increment in the proposed figure of merit is concerned. We further propose an autonomous thermodynamic machine for the purpose of creation of steady quantum coherence, and magic. We show the existence of a critical temperature below which it is possible to create magic in a single qubit at its steady configuration through this machine. Subsequently we propose two new avenues of quantum thermometry. The first of them is based on the use of a quantum switch, which shows marked improvement over the analogous case without using quantum switches. The second one shows that it is possible to use a weak measurement based scheme for thermometric purposes, thus enabling potentially fragile thermometric probes to measure temperature of a given bath. Both of these schemes can be easily generalized to more general quantum parameter estimation tasks. We hope the present thesis is helpful towards further clarifying the bidirectional link between quantum resources on the one hand, and thermodynamics on the other.

List of Figures

1.1	Pictorial representation of free states in resource theories of magic and coherence in the qubit case. The stabilizer polytope is an octahedron within the Bloch sphere. Any qubit state represented by a point outside the octahedron is a magic state. All incoherent states in the computational basis lie on the yellow line.	19
3.1	Hierarchy of various free operations in the resource theory of magic. . . .	46
3.2	Response of two different maximally magical pure states, viz a strange state (red), and a Norrell state (blue), for admixture with maximally incoherent noise (left) and coherent noise (right). The sum negativity of the resulting states has been plotted with respect to the admixture parameter $p \in [0, 1]$	51
3.3	Interplay between quantum coherence, magic and entanglement in a qutrit (left) and a qutrit-qubit system (right).	53
4.1	Schematic diagram of the central spin model. The central spin (red circle) interacts with the bath (green) constituting of spins (blue circles).	58

4.2	Variation of $q(t)$ with time t for various interaction strength α . Number of bath spins is kept fixed at $N = 20$. Positive $q(t)$ implies the non-Markovian nature of the dynamics according to the RHP measure.	69
4.3	Variation of $q_{dis}(t)$ with time t for various interaction strength α . Number of bath spins is kept fixed at $N = 20$. To distinguish the effect on the thermal part of the quantum channel, we separately plot $q_{dis}(t)$. It can be seen from the plot that the non-Markovian revival for the thermal part of the channel increases with the increase of the interaction strength α for fixed N	70
4.4	Variation of $q(t)$ with time t for different number of bath spins N . Interaction strength $\alpha = 0.03$ is taken.	71
4.5	Variation of $q_{dis}(t)$ with time t for different number of bath spins N . Interaction strength $\alpha = 0.03$ is taken. Magnified view of the rectangular region is shown in the inset. The plot depicts that the revival of $q_{dis}(t)$ increases with the increase of bath spins N	72
4.6	Variation of $p(t)$ with time t for the two states $ \pm\rangle = \frac{1}{\sqrt{2}} 0 \pm 1\rangle$, for different interaction strength α (where $N = 20$). Positive $p(t)$ implies non-Markovianity according to the BLP measure.	73
4.7	Variation of $p(t)$ with time t for two density matrices $ \pm\rangle = \frac{1}{\sqrt{2}} 0 \pm 1\rangle$, for different number of bath spins N , and interaction strength $\alpha = 0.03$. Magnified view of the rectangular region is shown in the inset.	74

4.8	Variation of rate of change of the irreversible entropy production $\sigma(t)$, rate of change of the purity $\frac{dP}{dt}$, and Γ_{dis} with time t for the initial state $ 1\rangle$ with the interaction strength $\alpha = 0.03$ and number of bath spins $N = 20$. It is evident that $\sigma(t)$ and $\frac{dP}{dt}$ are negative and positive respectively, whenever Γ_{dis} is negative. This implies that the non-Markovian information back-flow revives purity of the state and causes negative irreversible entropy production rate.	77
5.1	Dynamics of quantum coherence and entanglement for the central qubit immersed in the spin bath.	88
5.2	Variation of the ratio of long time averaged populations at excited and ground state $\bar{\rho}_{11}/\bar{\rho}_{22}$ with (a) initial population of the excited state $\rho_{11}(0)$ and (b) interaction strength ϵ , keeping the number of bath spins N as a parameter.	92
5.3	Variation of information trapping \mathcal{T} with temperature T , keeping the number of bath spins N as a parameter.	93
5.4	Variation of information trapping \mathcal{T} with interaction strength ϵ at (a) low temperature and (b) high temperature, keeping the number of bath spins N as a parameter.	94
5.5	Variation of $D(t)$ with time, keeping temperature T as a parameter. $\rho_{11}(0) = 0.5, \rho_{12}(0) = 0$	98
5.6	Variation of $D(t)$ with time, keeping temperature T as a parameter. $\rho_{11}(0) = 0.5, \rho_{12}(0) = 0.2$	99
5.7	Variation of $D(t)$ with time, keeping interaction strength ϵ as a parameter. $\rho_{11}(0) = 0.5, \rho_{12}(0) = 0$	100

5.8	Variation of $D(t)$ with time, keeping N as a parameter. $\rho_{11}(0) = 0.5, \rho_{12}(0) = 0$	101
5.9	Variation of IEP rate $\Sigma(t)$ and Lindblad coefficients for absorption $\Gamma_{abs}(t)$ and dissipation $\Gamma_{dis}(t)$ with time t . Initial state $\rho(0)$ is chosen as $\frac{4}{5} 1\rangle\langle 1 + \frac{1}{5} 1\rangle\langle 0 + \frac{1}{5} 0\rangle\langle 1 + \frac{1}{5} 0\rangle\langle 0 $	102
5.10	Variation of IEP rate $\Sigma(t)$ with time t for different bath temperatures. Initial state $\rho(0) = \frac{4}{5} 1\rangle\langle 1 + \frac{1}{5} 1\rangle\langle 0 + \frac{1}{5} 0\rangle\langle 1 + \frac{1}{5} 0\rangle\langle 0 $	103
5.11	Variation of IEP rate $\Sigma(t)$ with time t for different number of bath spins. Initial state $\rho(0) = \frac{4}{5} 1\rangle\langle 1 + \frac{1}{5} 1\rangle\langle 0 + \frac{1}{5} 0\rangle\langle 1 + \frac{1}{5} 0\rangle\langle 0 $	104
6.1	Schematic diagram of the absorption refrigerator model used in this work.	107
6.2	Demonstration that high equilibrium cooling power Q_c can come at the cost of slow evolution to equilibrium state. When all parameters other than g are fixed, steady cooling rate Q_c and the inverse of evolution time $1/\tau$, both functions of g , are parametrically plotted by varying the interaction strength g from 10^{-4} to 10^{-1} . The parameters are chosen as $E_c = 1, p_c = p_r = p_h = 0.1, \eta = 1, T_c = 1, T_r = 5, T_h = 10$	112
6.3	Variation of BSOCR with interaction strength g . <i>Left</i> : for different strengths of initial coherence κ applied to the $ 000\rangle\langle 111 $ subspace as well as <i>Right</i> : for same amount of coherence in different subspaces viz., the $ 101\rangle\langle 010 $, and the $ 000\rangle\langle 111 $ subspaces. The reset probabilities have been taken as $p_c = p_r = p_h = p$ throughout. The other parameters are taken as $T_c = 1, T_r = 2, T_h = 10, \eta = 0.5, p = 0.05, E_c = 1$	114

6.4	Variation of BSOCR with reset probability $p_c = p_r = p_h = p$. <i>Left</i> : for different strengths of initial coherence κ in the $ 000\rangle\langle 111 $ subspace as well as <i>Right</i> : for same amount of coherence in different subspaces viz. the $ 101\rangle\langle 010 $, and the $ 000\rangle\langle 111 $ subspaces. The other parameters are taken as $T_c = 1, T_r = 2, T_h = 10, \eta = 0.5, g = 0.05, E_c = 1$	116
6.5	Variation of BSOCR with steady state efficiency η for fixed parameter values $p_c = 0.01, p_r = 0.02, p_h = 0.05, T_c = 1, T_r = 2, T_h = 10, E_c = 1, g = 0.01$	117
7.1	Schematic diagram of model used in the work.	122
7.2	Dependence of the steady state coherence of the first qubit on the heat bath temperature T_1 (left) and the reset probability for the spin bath p_2 (right).	126
7.3	If a qubit state equilibrates on the z -axis of the Bloch sphere (blue blob) or on the x -axis of the Bloch sphere (golden blob) - the state lies within the stabilizer polytope. The first scenario is associated with the thermal state of the heat bath, the second with the equilibrium state of the angular momentum bath depicted in our model.	128
7.4	Values of linear functions of Bloch vector (cf. 7.8 of the reduced qubit attached to the heat bath vs. the reset probability $p_1 = p_2 = p$ (left) and the heat bath temperature T_1 (right). Any one of the curves falling in the pale yellow region indicates the presence of magic. If all three lines lie in the light grey region, that indicates the state is within the stabilizer polytope.	129

7.5 Magic creation in the limit of low spin bath temperature T_2 . Left : dependence of critical temperature T_{crit} on the reset probability $p_1 = p_2 = p$. Creation of magic is possible in the pale yellow region and impossible in the light gray region. Right : allowed interval for interaction strength g with respect to heat bath temperature T_1 for creation of magic. Creation of magic is possible in the pale yellow region and impossible in the dark brown region. 132

7.6 Condition for creation of magic for high spin bath temperature T_2 . Left : dependence of critical temperature T_{crit} on the reset probability $p_1 = p_2 = p$. Creation of magic is possible in the pale yellow region and impossible in the light gray region. Right : Allowed interval for interaction strength g with respect to heat bath temperature T_1 for creation of magic. Creation of magic is possible in the pale yellow region and impossible in the dark brown region. 132

7.7 Effect of asymmetry μ between the reset probabilities p_1 and $p_2 = \mu p_1$ on the critical temperature T_{crit} for creation of magic in the low spin bath temperature T_2 limit (left) and high spin bath temperature T_2 limit (right). Creation of magic is possible in the pale yellow region and impossible in the light gray region. 134

8.1 Schematic of the protocol. The input probe is being sent in two possible pathways (red solid line, which implements $N \circ M$ and blue dashed line, which implements $M \circ N$) based upon the configuration of the control. N and M are identical thermalizing channels. 140

8.2 Density plot of QFI for the inverse temperature β on the gap ϵ as well as the superposition parameter α . Temperature is fixed at $T = 1$ 144

8.3	<p><i>Left</i>: QFI for temperature T vs. temperature T. <i>Right</i>: Relative advantage in terms of QFI gained through the use of quantum switch. The red solid line indicates the qubit probe used without any switch, the blue dash-dotted line indicates the qubit probe used with a maximally coherent switch. Green shaded regions are only accessible when using a quantum switch in the qubit protocol.</p>	145
8.4	<p>Comparison of the QFI for temperature with temperature T for the qubit probe without quantum switch (red solid line), qubit probe with a maximally coherent quantum switch (blue dash dotted line), and a harmonic oscillator probe (orange dotted line). The energy level spacing in every case is $\epsilon = 1$.</p>	147
9.1	<p>Schematic of the weak measurement based thermometric scheme. The bath is a collection of thermalized qubits. We couple the measuring apparatus to one of these qubits for a very small time-interval.</p>	152
9.2	<p>Precision of the scheme plotted against the temperature for the specific choice of post-selected states $\psi_f\rangle = \sqrt{1-\epsilon} \psi_1\rangle + \sqrt{\epsilon} \psi_2\rangle$ (green dotted curve), $\psi_f\rangle = \frac{1}{\sqrt{2}}(\psi_1\rangle + \psi_2\rangle)$ (red dashed curve). Energy gap between ground and excited states is unity in each case. $\epsilon = 0.01$ is assumed.</p>	160
9.3	<p>The temperature at which the optimal precision is achieved is plotted against the parameters ξ and ν of the post selected state $\psi_f\rangle$.</p>	160
9.4	<p>The magnitude of precision at optimal temperature is plotted against the parameters ξ and ν of the post selected state $\psi_f\rangle$.</p>	161
9.5	<p>The magnitude of precision is plotted against the parameters ξ and ν of the post selected state $\psi_f\rangle$ for (<i>left</i>) low temperature $T = 0.05$, and (<i>right</i>) high temperature $T = 100$.</p>	161

- 9.6 The magnitude of precision at optimal temperature is plotted against the temperature T and the polar angle ξ of the post selected state $|\psi_f\rangle$ 163
- 9.7 *Left-* optimal temperature, and *Right-* precision at optimal temperature, as a function of the polar angle ξ of the post measurement state $|\psi_f\rangle$ 164
- 9.8 Scaled precision \tilde{F} plotted against temperature for various choices of post-selected state parameter θ . The energy gap Δ is taken to be unity, and the azimuthal angle ϕ of the post-selected state is assumed to be zero. 166

List of Tables

1.1	Structure of three popular quantum resource theories.	25
2.1	Some well-known qubit channels	32
2.2	Different Witness based measures for non-Markovianity.	36

Introduction

In the first half of the twentieth century, it became obvious that classical Newtonian physics, based on which the scientific and industrial revolutions were largely built, was grossly inadequate to describe phenomenon on very large as well as very small length scales. While Einsteinian concepts of relativity took steps towards understanding the former, the latter necessitated an even more profound way of thinking. This new theory, known as quantum mechanics, has so far stood the test of every experiment until now. Yet, as its first practitioners realised [1], the premises of quantum mechanics turned out run counter to everyday common sense intuition. Faced with this dichotomy, most physicists established an uncomfortable truce by adopting the mantra “shut up and calculate”. Decades later, inspired by Feynman [2] and Benioff [3], physicists began to wonder whether the troublesome bugs of quantum theory may turn out to be useful features for practical tasks. On the more foundational side, Bell’s work [4] showed that according to quantum mechanical laws, nature turns out to be impossible to be described in a local and realistic framework. Kochen and Specker showed that quantum mechanics is a fundamentally contextual theory [5]. In conjunction with the new spirit of exploiting the peculiarities of quantum mechanics for practical ends, the operational importance of such foundational aspects of quantum theory began to be realized in the last decades of the twentieth century. The development of quantum technologies was now afoot, and it was

to be profoundly affected by, among others, the burgeoning fields of information theory and computer science.

Scientists, like all human beings, explore nature, that is, they attempt to obtain information about natural laws. Thus, one has to begin with the simple sounding question “what is information ?” - vague and philosophical responses notwithstanding, the first comprehensive quantitative framework to address this question had to wait until the end of World War II and the middle of the twentieth century, when Claude Shannon pioneered the mathematical theory of information and communication [6]. Since then, in the last several decades, information theory has blossomed into a topic with wide ranging facets, from a quantitative understanding of capacity of noisy communication channels [7], to the study of computational linguistics [8], to financial analysis [9], among others. The deep connection of information with physics was indicated even earlier than Shannon’s entropic quantification of information, with the Szilard engine [10] version of Maxwell’s demon thought experiment, which seeks to convert information about gas molecules to extractible work. 1960’s saw another profound discovery by Landauer [11] - that the erasure of every bit of information costs $k_B T$ amount of energy. Since the Boltzmann constant is $10^{-24} JK^{-1}$, this cost was almost imperceptible on a practical level at that time. Hence no bottleneck was encountered when computing power began to double roughly every eighteen months, this phenomenon was informally described as the Moore’s law. However, as computing elements have come down in size, Landauer’s limit is finally almost upon us. For example, the laptop on which the present thesis is being written, is powered by 14 nm chips, which are only about two hundred times the size of the Bohr radius. Hence, the quest for reversible computation has grown in recent years. Unitary quantum mechanics is inherently reversible - and as has been discovered, contains several useful features to augment information processing as well as computation. Thus, it was perhaps inevitable that we seek to build nanoscale devices which exploit these useful features. In this chapter, we shall briefly review some of these features pertinent to the present thesis before providing a brief outline of the chapters contained in the thesis.

1.1 Resource theoretic framework : an overview

Resources are intrinsically defined in terms of their usefulness in accomplishing certain tasks. From this operational viewpoint, any feature which allows a certain task to be performed which would be more difficult or impossible otherwise, is to be viewed as a resource. If this feature is quantum mechanical in nature, the resource is called a quantum resource. In the following subsections, we briefly describe the resources relevant to our purpose.

1.1.1 Resources available in the quantum world

Entanglement

Perhaps the most well studied quantum resource is *entanglement*. This arises from the combination of two postulates of quantum mechanics - the linearity postulate and the tensor product postulate. Suppose there are two parties A , and B , with the corresponding Hilbert spaces \mathcal{H}_A , and \mathcal{H}_B respectively. Hence, the combined state is an element of the combined Hilbert space $\mathcal{H}_A \otimes \mathcal{H}_B$. If the combined pure state $|\psi\rangle_{AB} \in \mathcal{H}_{AB}$ can be written in the product form $|\psi_1\rangle_A \otimes |\psi_2\rangle_B$, where $|\psi_1\rangle_A \in \mathcal{H}_A$, and $|\psi_2\rangle_B \in \mathcal{H}_B$ - then the combined pure state is said to be *separable*. Else, the combined pure state is said to be *entangled*. For arbitrary mixed states, a separable state is defined as a state ρ_{AB} which can be written as a probabilistic mixture of product states, i.e., when

$$\rho_{\text{sep}} = \sum_i p_i \rho_A^i \otimes \rho_B^i \quad (1.1)$$

That entanglement is a peculiar quantum phenomenon was realized early on in the history of quantum mechanics, with the famous EPR paper by Einstein, Podolsky, and Rosen [1] in 1935. However, operational use of entangled resources towards practical communication tasks had to wait for another half a century. Bennett and Wiesner showed entangled

states can be a resource for dense coding [12]. That is, if two parties share an EPR pair, then one of the parties can send two bits of classical information by sending only a single physical qubit to the other party. In what is perhaps the most famous example of a task with genuinely quantum mechanical communicational advantage, Bennett and co-workers showed [13] that it is possible to send all the information about a qubit to a blank qubit at a distant location without sending the qubit physically, provided the sender and the receiver share an EPR pair.

That there was a link between entanglement and quantum non-locality, as described by CHSH-Bell type inequalities, was realized immediately. Gisin *et al* proved that every pure bipartite entangled state violated some judiciously constructed Bell inequality. For bipartite pure states, it was realized that there was an unique quantifier of quantum entanglement, known as *entanglement entropy*, and defined as the local entropy of any of the subsystem's states, that suffices to completely describe the entanglement content of a pure quantum state, which is given by

$$E(|\psi_{AB}\rangle) = S(\rho_A) = S(\rho_B). \quad (1.2)$$

However, the study of mixed state entanglement turns out to be lot more subtle than its pure state counterpart. A particularly important realization was that there existed mixed quantum states whose entanglement can not be distilled into a pure EPR pair. These states, dubbed *bound* entangled states, have long evaded easy and general characterization. For example, it was long believed that bound entangled states do not violate Bell-type inequalities, as per the Peres conjecture [14], but this has been disproved recently [15]. Mixed states also do not admit a single entanglement measure that completely quantifies the entanglement. Hence there have been several entanglement measures proposed in the recent years. Some of the measures are directly motivated from operational tasks, for example, entanglement of formation [16], entanglement cost [17], or distillable entanglement [18]; while other measures like negativity [19], or squashed entanglement [20] etc. are either

easier to compute or satisfy certain nice mathematical properties.

From an operational standpoint, beyond the canonical examples like dense coding, teleportation, or remote state preparation [21] in the field of quantum communication, entanglement turns out to be useful in several other areas as well. For example, entangled probes can beat the shot noise $\frac{1}{\sqrt{N}}$ scaling for metrological tasks, and offer much better precision as the error scales as $\frac{1}{N}$, which is the so called *Heisenberg scaling*. In addition, entanglement has also asserted as a resource for tasks like state discrimination [22], or speeding up quantum evolution [23]. Apart from the operational efficacy of entanglement in the above schemes, there is a vast and growing literature on entanglement in realistic many body quantum systems, for example, the entanglement, or more precisely its first derivative is an important tool to witness quantum phase transition in transverse Ising type spin models.

Another facet of entanglement theory is the study of multipartite entanglement, which unfortunately turns out to be a subtler and more complicated than bipartite entanglement. For example, there exists inequivalent classes of genuinely multipartite entangled states, which are impossible to transform into each other by local operations and classical communications (LOCC), even in a probabilistic way (stochastic LOCC or SLOCC). For three parties, there are two such inequivalence classes [24] - namely the GHZ class and the W class. Even worse, for as little as four parties, there are an infinite number of such SLOCC inequivalent classes[25]. It is easy to see that separable states are of vanishing volume in the state space. Thus, it is natural to wonder why entanglement is so difficult to observe in practice. The reason for this goes back to another fundamental property of entanglement - viz, the monogamy property. The monogamy property, roughly stated, asserts that the more a party is entangled with another party, the less the entanglement between any of these parties with yet another. This explains why long range quantum entanglement among multi-component bodies is so hard to observe.

As far as genuinely quantum correlations go, entanglement is not the end of the story as

newer quantum correlation measures like quantum discord [26, 27, 28], quantum work deficit [29], local quantum uncertainty [30] and yet many others have been proposed. Among them, quantum discord is probably the most studied correlation measure and claims of quantum discord being an useful resource in computational tasks [31] have been put forward. However, the chief difficulty with constructing formal resource theories for these quantities is the lack of convexity in the free state structure. That is, classical mixture of free quantum states in the relevant context may have non-zero resource value. From a practical point of view, these correlation measures generally do not satisfy monogamy relations [32], so they are not useful resources for several tasks where monogamy is a key ingredient, for example in cryptographic tasks. In the present thesis, we shall not be concerned with these measures of quantum correlation.

Coherence

The one postulate of quantum mechanics that sets it apart from its classical counterpart is the superposition principle. A state can simultaneously be in a superposition of two or more basis states. However, a formal quantification of the superposition content of a state had to wait until relatively recently. The concept of quantum coherence [33] is inherently basis dependent. A state of the form $\frac{1}{\sqrt{2}}(|0\rangle + |1\rangle)$ may be considered coherent from the perspective of a computational basis, but not the perspective of the complementary $\{|\pm\rangle\}$ basis. Hence, in contrast to the quantum correlation measures, we need to fix a basis $\{i\}$ when treating quantum coherence.

The states which have no quantum coherence in such a basis are denoted as *incoherent states*, and defined as

$$\rho_{\text{incoherent}} = \sum_i \alpha_i |i\rangle\langle i| \quad (1.3)$$

The states which are not incoherent states, turn out to be useful in their own right. For example, these states are useful resources for phase discrimination tasks [34, 35, 36], or

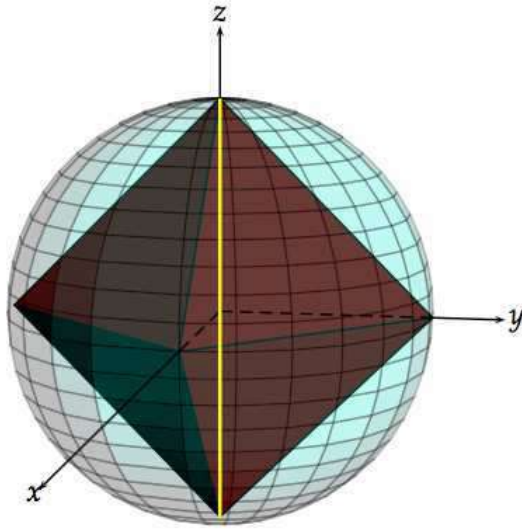


Figure 1.1: Pictorial representation of free states in resource theories of magic and coherence in the qubit case. The stabilizer polytope is an octahedron within the Bloch sphere. Any qubit state represented by a point outside the octahedron is a magic state. All incoherent states in the computational basis lie on the yellow line.

creation of other quantum resources [37, 28, 38, 39]. In a slightly altered formalism of quantification of asymmetry, thermodynamic work extraction is also improved with the presence of off-diagonal states [40, 41].

Magic

One of the principle scientific developments in last few decades has been the emergence of the theory of quantum computation. Quantum computers are touted to be vastly more powerful than their classical counterparts. For example, they are supposed to be able to run algorithms to factorize non-prime numbers [42], or perform search in a database [43], with a smaller time complexity than classical algorithms. Resources like quantum entanglement and quantum coherence have at various points been shown to lead to quantum advantage vis-a-vis classical computers. For example, to implement Shor's algorithm, one needs a large amount of entanglement [44], whereas, to implement Grover's algorithm, one needs a small amount of entanglement [45, 46]. Similarly, it has recently been demonstrated that in order to implement the Deutsch-Jozsa algorithm [47], one requires

coherence as a resource [48]. Quantum coherence has also been related to the success probability of the Grover search algorithm [49, 50]. Thus, the important question arises - what kind of genuine quantum resources do quantum computers exploit ? To answer this question - it is first useful to note that fault tolerance through error correction schemes have to be built in to any potential quantum computer, since they are delicate to both incoherent as well as coherent noise. These fault tolerance schemes often use stabilizer gates, which is a subset of all possible unitary transformations, as their building blocks [51]. However, by the Gottesman-Knill theorem [52] this stabilizer circuit architecture turns out to be efficiently, that is, with at most a polynomial overhead, simulable, using probabilistic classical computers. Thus, in addition to stabilizer gates, one needs other gates to obtain genuine quantum computing advantages. In the magic state injection paradigm of quantum computing [53], this is done by using some auxiliary states in addition to the input, and global stabilizer operations. If these auxiliary states thus enable beyond-classical computational advantage, then they are called *magic* states. Utilising these quantum states, which lie outside of the stabilizer polytope enable the implementation of gates which are not classically simulable, e.g., the T-gate. A resource theory for such magic states was recently proposed [54] and is a topic of active interest [55, 56]. The pure free states in this resource theory are the ones reachable via Clifford unitaries acting on any member of the computational basis states. The total family of free states, denoted as *stabilizer states* \mathcal{S} , consists of the convex hull formed by the pure free states. The free operations consist of Clifford unitaries, measurement in the computational basis, composition with other stabilizer states and partial trace, as well as these operations conditioned on measurement results. Magic monotones are relatively less studied until now, although some monotones have been found ranging from distance based monotones [54] to robustness type monotones [57] to monotones inspired from the Wigner function representation of states in discrete phase space [54]. The magic states also turn out to have an intimate connection to another foundational aspect of quantum mechanics - namely, the contextuality of the theory[58], and inter-alia, linked to the continuous variable resource

of non-Gaussianity.

Memory effects and non-Markovianity

The above resources were all properties of a state, now we shall discuss about a resource that manifests itself in dynamical processes. For vast majority of stochastic processes, at any particular time of the dynamics, the resultant outcome generically depends on the previous history of the dynamics, that is, the dynamics is predicated on its previous memory. For quantum processes, this type of generic dynamics is harder to theoretically investigate than memoryless, i.e., Markovian processes, because of the generic build up of quantum correlations between the system and the environment during the run time of the dynamical process. Nonetheless, non-Markovian processes are now shown to be important from an operational point of view in quantum thermodynamics [59], metrology [60], or entanglement preservation [61].

Unlike classical stochastic processes, there is a lively debate on what constitutes Markovianity in quantum processes. At one end of the spectrum, one concentrates on the CP-divisibility of the dynamical maps into arbitrary small blocks. One may look for witnesses of violation of completely positive evolution, for example via trace distance between arbitrary pairs of input states [62, 63], or via the increase of coherence [64]. This spirit is captured in the so called Rivas-Huelga-Plenio measure of non-Markovianity which captures the deviation of the Choi matrix from positivity during the entire duration of the dynamics [65, 66]. However, other attempts of defining non-Markovianity in terms of the so called *process tensor* formalism are also in the literature [67, 68] - according to which, even CP divisible dynamical maps can turn out to be non-Markovian.

Superposition of quantum processes

In one of the previous sections, we discussed quantum coherence, which arises due to the superposition between distinct quantum states that form a basis. In the context of quantum dynamics, this leaves us with the idea of superposing quantum evolutions as well [69] via a control. The basic idea is simple - if the control state is in one of the basis states, the dynamics proceeds via one pathway. Now, if the control state is in superposition of these basis states, the dynamics is coherently controlled.

This basic idea turned out to be extremely fruitful for quantum walks, where the walker's dynamics is predicated on the behavior of the quantum coin. Quantum walks have been observed to enable greater, i.e., ballistic, dissipation, over and above classical random walks. In the recent years, a related scheme, known as the quantum switch, has seen several interesting developments [70, 71, 72], as well as experimental verifications [73, 74]. For the simplest case of a quantum switch, there are two pathways, each which have two quantum processes in common, but the order of these processes are reversed in one of the pathways. The pathway taken by a quantum particle depends on a control qubit.

The quantum switch turns out to be useful in several operational aspects. The presence of a quantum switch enables one to send classical information through an otherwise zero capacity channel [75, 72, 76], confers advantage over other quantum as well as classical algorithms in a black box unitary guessing game [77], gives advantage in quantum teleportation with noisy singlets [78], and as we shall show in one of the latter chapters - provides metrological advantage.

One must mention at this point that there is an ongoing debate about the nature of the quantum switch - whether the indefinite causal order of quantum operations [79, 73] is really the resource for the operational advantage gained through the use of a quantum switch, or whether it is a manifestation of coherently controlled quantum processes with no recourse to indefinite causal order being necessary [80, 81] to obtain the same effects.

However, this is beyond the scope of the present thesis.

1.1.2 Generic structure of convex quantum resource theories

It may give one the impression that the study of quantum resources described so far, along with other possible quantum resources, are disparate disciplines, with little in common. However, in the recent years, a resource theoretic formulation has been developed, which seeks to underline the common traits to quantum resources in a mathematically consistent fashion [82]. The advantage of a general resource theoretic formalism over studying individual resources separately is twofold - first, it allows one to organize and efficiently observe the nature of individual quantum resources, and secondly, any result that holds true in this generic formalism is also true for any other resource hitherto not discovered, provided it follows the constraints incorporated in the original resource theoretic framework.

Following Brandao and Gour's seminal paper [83], we outline the following features of a generic convex resource theory. The convexity stems from the notion that a genuinely quantum resource can not be created through classical mixing alone.

1. There is a set of states \mathcal{F} , whose elements are called free states, that is, states which do not have a given resource.
2. There is a set of free operations Λ_F , which preserves the set of free states \mathcal{F} , for a given resource. Other operations, which may create quantum resources from a free states, are assumed to be expensive. The important point to notice is that not all such operations may turn out to actually be operationally easy to implement. Hence, a realistic resource theory will have to consider subsets of the above set, which are easily implementable in practice.

The typical questions one tries to address, given the structure of resource theories are the

following..

1. How to quantify the amount of resource possessed by a state ?
2. Whether a state ρ_1 is convertible to another state ρ_2 under the free operations ?
3. How to interconvert quantum resources ?

To this end, Brandao and Gour [83] has laid down five basic postulates that a reasonable quantum resource theory might be expected to follow.

1. Free states are closed under tensor product. That is, if σ_1 , and σ_2 both belong to free states with respective dimensions d_1 , and d_2 , then $\sigma_1 \otimes \sigma_2$ is again a free state with the dimension $d_1 d_2$.
2. Free states are closed under partial trace. That is, if ρ_{AB} for a bipartite AB system is a free state, then ρ_A , and ρ_B are also free states, albeit in requisite reduced dimension.
3. The set of free states \mathcal{F} is closed under permutation of subsystems.
4. The set of free states \mathcal{F} is a closed one.
5. The set of free states \mathcal{F} is a convex set. That is, if σ_1 , and σ_2 are free states, then any convex mixture $\mu\sigma_1 + (1 - \mu)\sigma_2 \in \mathcal{F}$, where $\mu \in [0, 1]$. This ensures that the resource in question is a genuinely quantum mechanical one in the sense that it is not possible to create resources through classical mixing alone.

The final property is not satisfied by so called non-convex quantum resources like discord, or non-Gaussianity. In the table 1.1.2, we summarize the structure of the resource theories of coherence, entanglement, and magic.

A point should be noted here. Brandao and Gour assumes that the free operations are any operations that preserve the set of free states \mathcal{F} . Under this assumption, they go on to

Resource theory	Free states	Free operation
Entanglement	Separable states $\sigma = \sum_i p_i \rho_i^A \otimes \rho_i^B$	Local operations and Classical Communication (LOCC)
Coherence	diagonal incoherent states $\sigma = \sum_i c_i i\rangle\langle i $ in the basis $\{ i\rangle\}$	Incoherent operation <ul style="list-style-type: none"> • If $\sigma \in \mathcal{I}$, $\Lambda_{IC}[\sigma] \in \mathcal{I}$ • If $\sigma \in \mathcal{I}$ then for each Kraus channel $\{K_i\}$ corresponding to incoherent operation, $K_i \sigma K_i^\dagger \in \mathcal{I}$
Magic	States inside polytope accessible via Clifford unitary rotation of computational basis	Stabilizer operation <ul style="list-style-type: none"> • Clifford unitary • Measurement in computational basis • Partial trace • Composition with other stabilizer states

Table 1.1: Structure of three popular quantum resource theories.

prove that the resource theories satisfying the postulates above are reversible. However, from an operational standpoint, this result does not hold in general if one restricts the set of free operations to operations which are actually easy to implement. For example, in entanglement theory, such operationally important free operations are the LOCC protocols. However, under LOCC, it is possible to show the existence of irreversibility in the form of bound entangled states, which require non-zero number of singlets to be assembled, yet can not be distilled with LOCC protocols.

1.1.3 Effect of environment on quantum resources

Quantum systems rarely exist in isolation. Even if a certain state contains some degree of a quantum resource, it is continuously subject to interaction with an environment, which most often is a thermal bath at a certain temperature. Therefore, from an experimental point of view, it is important to investigate the effect that the presence of the environment has on the resource content of the original system. As it often turns out, ubiquitous thermal environments often lead to decoherence, and consequently may partially or fully destroy quantum features of a state, and are detrimental to the resource content of the original quantum state. For everyday macroscopic objects, the decoherence time scale is extremely small [84], therefore quantum effects are not apparent in our daily lives. Thus, in order to make the most of quantum resources, one has to design a workaround. One of the possible ways is the decoherence-free subspace approach [85], which relies on finding a (often small) subspace of the system, which is effectively decoupled from the environment. Thus, any quantum features present in that subspace may be preserved. Another strategy, known as dynamic decoupling [86, 87], relies on periodically running large control pulses through a system to ensure that the effective coupling between the system and the environment vanishes. However, in this thesis, we shall not be concerned with these methods of suppressing decoherence.

1.2 Outline of Thesis

In this section, we briefly outline the plan of the thesis. In this chapter, we have provided a brief introduction to various resources pertaining to quantum states and dynamics. In Chapter 2, we review some of the basic aspects of the theory of the dynamics of quantum open systems. Chapter 3 concerns itself with the demonstration of the connection between resource theories of quantum coherence and magic. Chapter 4 contains an exact treatment of the non-Markovian central spin model for infinite bath temperatures, corresponding master equations, and the quantitative formulation of non-Markovianity. Chapter 5 extends the treatment to arbitrary finite temperature central spin baths. In chapter 6, we investigate the steady state performance of a popular model of quantum autonomous refrigerators vis-a-vis the minimal time taken to reach the state through the lens of the quantum speed limit. Chapter 7 is dedicated to the proposal and detailed investigation of a protocol for the generation of steady quantum coherence and magic. We discuss how superposition of temporal order may bolster the precision of single qubit thermometry in chapter 8. Chapter 9 contains another proposal for quantum thermometry utilizing a weak measurement scheme. We conclude by sketching some possible directions for future work in Chapter 10.

1.3 Summary

- Different operational tasks call for different features of quantum mechanics.
- Operationally useful features of quantum mechanics can be considered as resources.
- It is possible to construct generic resource theoretic formulations which bring different resources under a common umbrella.
- Quantum entanglement is the most well known resource. Especially quantum enhanced communication schemes generally owe their advantage to the presence of

entanglement.

- Quantum coherence is a basis-dependent resource, which seeks to quantify the superposition content in quantum states.
- Magic states are resources for stabilizer circuit based quantum computation.
- Superposition of quantum processes may facilitate new tasks impossible with the constituent processes considered in isolation.
- Memory effects in the dynamics of open quantum systems, formalized under the notion of non-Markovianity, are operational resources.
- Thermal environments are generally detrimental to the resource content of pure quantum states.

A primer on open quantum systems

In the previous chapter, we have briefly discussed about various quantum resources at our disposal. In this chapter, we review some of the basic theory pertaining to the dynamics of open quantum systems, that is, quantum systems in contact with an environment, about whose detailed dynamics we are not interested in, and which is assumed to be unaffected by the presence of the system by virtue of being significantly larger than the system.

The familiar Schroedinger equation, or the analogous Heisenberg equation of motion, describes the dynamical evolution of a closed quantum system. However, it is practically impossible to obtain fully isolated quantum systems, and in cases where the exact dynamics of the environment is either unknown or of very little interest, we must obtain the dynamical equations corresponding to the system state, represented by the density matrix ρ_S alone. As we shall see in this chapter, there are several ways of tackling the problem.

2.1 Kraus operator formalism

The simplest possible description of any dynamics is the following - what is the state of the system at the end of a certain specified time interval ? Note that this question excludes the additional demand of formulating a dynamical differential equation. For example, for

closed quantum systems, we know that the evolution is a norm-preserving one, which is endowed with its physical meaning via the Born rule, that is, in a closed system, ipso facto, one must find any particle somewhere in the initially defined parameter space. Thus the evolution is unitary in that case, and any initial quantum state $\rho(0)$, and final quantum state $\rho(t)$ is connected through an unitary $U(t, 0)$, that is,

$$\rho(t) = U(t, 0)\rho(0)U(t, 0)^\dagger \quad (2.1)$$

For open systems, non-conservation of particles in the form of dissipation or absorption leads to a departure from unitarity, and the dynamics is no longer in the simple form above. However, the Kraus operator formalism, originally developed by Sudarshan [88], takes advantage of the following dictum, known as the Stinespring dilation theorem.

Every open quantum evolution on the state space of a system S , which forms a Hilbert space \mathcal{H}_S , may be extended to an unitary evolution on the joint Hilbert space $\mathcal{H} \otimes \mathcal{H}_A$, where A is some auxiliary system.

Following the Stinespring dilation theorem, it is clear that corresponding to every dynamical map Λ from the initial state $\rho_S(0)$ to the final state $\rho_S(t)$ for a system S , there exists a joint unitary U_{SA} , whose action, followed by forgetting, that is, tracing out, of the auxiliary system A , leads to the final state $\rho(t)$, i.e., the dynamical map for the system alone follows

$$\rho_S(t) \longrightarrow \Lambda(\rho_S(0)) = \rho_S(t) = \text{tr}_A U_{SA} (\rho_S(0) \otimes |0\rangle_A \langle 0|) U_{SA}^\dagger. \quad (2.2)$$

Note that a highly non-trivial assumption has been made here, that the initial system-auxiliary joint state is a product state. Clearly, this is a limiting assumption, yet, this assumption ensures that the dynamics turns out to be completely positive, that is adding

any number of further trivial auxiliaries to this dynamics does not change the fact that the density matrix is always positive semi-definite. On the contrary, initially entangled joint states may engender dynamics that is not, in fact, guaranteed to be complete positivity preserving, as observed by Pechukas [89]. While there is a debate in the literature whether non-CP maps, when restricted to a certain sector of the parameter space, may turn out to be physically relevant, it is beyond the scope of the present elementary discussion. We refer the interested reader to Shaji and Sudarshan's relevant work [90] in this context. We shall further assume that all the Hilbert spaces in question are finite dimensional.

Now, let us assume a basis $\{|a_i\rangle\}$ pertaining to the auxiliary A . This allows the equation above to be written as

$$\rho_S(t) = \sum_l \langle a_l | U_{SA} (\rho_S(0) \otimes |0\rangle_A \langle 0|) U_{SA}^\dagger |a_l\rangle = \sum_i K_i \rho_S(0) K_i^\dagger. \quad (2.3)$$

The above is known as the Kraus operator representation of the dynamical map, and $K_i = \langle a_i | U_{SA} |0\rangle$, are called the corresponding Kraus operators. Note that the choice of different bases for the environment yields different Kraus operators. Hence the Kraus operator representation is not unique. It is easy to check the following property of the Kraus operators, by starting from the fact that $\text{tr}(\rho_S(0)) = \text{tr}(\rho_S(t)) = 1$.

$$\sum_i K_i^\dagger K_i = \mathbb{I} \quad (2.4)$$

2.1.1 Examples of quantum channels

In this subsection, we list some of the most popular quantum channels acting on qubits, and their possible Kraus operator representations in tabular form. It is to be noted that all the Kraus operators below have been expressed in the computational basis.

Let us now ask the following question - what is the most general form of a quantum

Channel	Kraus Operator Representation	Physical Interpretation
Bit-flip	$K_0 = \sqrt{1-p} \begin{pmatrix} 1 & 0 \\ 0 & 1 \end{pmatrix}, K_1 = \sqrt{p} \begin{pmatrix} 0 & 1 \\ 1 & 0 \end{pmatrix}$	Flips quantum states $ 0\rangle \leftrightarrow 1\rangle$ with probability p .
Phase-flip	$K_0 = \sqrt{1-p} \begin{pmatrix} 1 & 0 \\ 0 & 1 \end{pmatrix}, K_1 = \sqrt{p} \begin{pmatrix} 1 & 0 \\ 0 & -1 \end{pmatrix}$	Flips the polar phase of the quantum states $\theta \leftrightarrow -\theta$ with probability p .
Bit-Phase flip	$K_0 = \sqrt{1-p} \begin{pmatrix} 1 & 0 \\ 0 & 1 \end{pmatrix}, K_1 = \sqrt{p} \begin{pmatrix} 0 & -i \\ i & 0 \end{pmatrix}$	A combination of the bit flip and the phase flip channel acting in sequence.
Amplitude damping	$K_0 = \begin{pmatrix} 1 & 0 \\ 0 & \sqrt{1-\gamma} \end{pmatrix}, K_1 = \begin{pmatrix} 0 & \sqrt{\gamma} \\ 0 & 0 \end{pmatrix}$	A model of thermalization for zero temperature environments where the probability of transition from the excited state to the ground state is γ .
Generalized amplitude damping	$K_0 = \sqrt{p} \begin{pmatrix} 1 & 0 \\ 0 & \sqrt{1-\gamma} \end{pmatrix}, K_1 = \sqrt{p} \begin{pmatrix} 0 & \sqrt{\gamma} \\ 0 & 0 \end{pmatrix}, K_2 = \sqrt{1-p} \begin{pmatrix} \sqrt{1-\gamma} & 0 \\ 0 & 1 \end{pmatrix}, K_3 = \sqrt{1-p} \begin{pmatrix} 0 & 0 \\ \sqrt{\gamma} & 0 \end{pmatrix}$	A model of thermalization for finite temperature environments where the probability of transition from the excited state to the ground state is γ , and the eventual corresponding temperature $k_B T = \ln(p/1-p)$.
Depolarizing	$K_0 = \sqrt{1-\frac{3p}{4}} \begin{pmatrix} 1 & 0 \\ 0 & 1 \end{pmatrix}, K_1 = \sqrt{\frac{p}{4}} \begin{pmatrix} 0 & 1 \\ 1 & 0 \end{pmatrix}, K_2 = \sqrt{\frac{p}{4}} \begin{pmatrix} 0 & -i \\ i & 0 \end{pmatrix}, K_3 = \sqrt{\frac{p}{4}} \begin{pmatrix} 1 & 0 \\ 0 & -1 \end{pmatrix}$	A model of mixing with a maximally mixed state with probability p .

Table 2.1: Some well-known qubit channels

channel ? To answer this question, let us first remember the following two properties of a density matrix - firstly, any quantum density matrix should be positive semi-definite, and secondly, it should have a trace equal to unity. Hence, it is easy to deduce the following two properties of a legitimate quantum channel Λ , namely

1. $\Lambda(\rho) \geq 0 \forall \rho$ (*Positivity*)
2. $\text{tr}(\Lambda(\rho)) = \text{tr} \rho = 1$ (*Trace-Preserving*).

However, the above list does not exhaust the possible limitations on a dynamical map. There may exist dynamical maps which are positive, yet when the system is coupled to some ancilla, and prepared without loss of generality in a state $|\psi\rangle$, is considered, even when acted upon by a trivial identity channel, the resulting map $\Lambda \otimes \mathbb{I}$ may turn out to be non-positive for some ancilla. For example, let us consider the transposition map, that is, $\Lambda(\rho) = \rho^T$. Since the spectrum of any Hermitian operator remains invariant under transposition, it is clear that the map is a positive one. However, if one applies the map $\Lambda \otimes \mathbb{I}$ to a two qubit entangled state, say, $\frac{1}{\sqrt{2}}(|00\rangle + |11\rangle)$, the resulting matrix is not positive semi-definite, and consequently not a legitimate density matrix.

2.2 Dynamics of noisy quantum systems : quantum master equations

Sometimes, it is not sufficient to know about the output state corresponding to a specific quantum channel, given the input. In particular, if one is interested in the continuous time evolution of the system, the relevant differential equation (or integro-differential equation) for the evolution must be found. Such an equation is often called a *master equation*. Note that in principle, the set of Kraus operators at all times contains all possible information about the system. However, in practice, it is often easier to work with master

equations. Unlike Kraus operators, an arbitrary master equation, for example one in the Bloch-Redfield form [91], is not guaranteed to preserve positivity, let alone complete positivity, throughout the dynamical evolution. However, for a certain restricted class of master equations, in the so called Lindblad form [92, 93], complete positivity is always guaranteed, and thus this form has become the workhorse of studying open quantum dynamics.

2.2.1 Lindblad master equation

The first restriction required, in addition to the lack of initial quantum correlations between the system and environment, for the general derivation of a Lindblad master equation is the so called *Born* approximation, which assumes that the strength of coupling between the system and the environment is weak throughout the duration of the dynamics. The second restriction is the *Markov* approximation, which dictates that the correlation times corresponding to the dynamics is so small that the dynamics is effectively memoryless. The third restriction is the so called *Secular* approximation, which mandates that one should neglect fast oscillating terms. With these restrictions, one can write down a master equation in the Lindblad form in the following way.

$$\boxed{\frac{d\rho_S}{dt} = \partial_t \rho_S - \frac{i}{\hbar} [H_S, \rho] + \sum_j L_j \left(a_j \rho_S a_j^\dagger - \frac{1}{2} \{a_j^\dagger a_j, \rho_S\} \right)} \quad (2.5)$$

Where H_S is the Hamiltonian acting on the system, $\{\cdot\}$ is the anti-commutator, and a_j , and a_j^\dagger are the relevant lowering and raising operators respectively, and $\{L_j\}$ are corresponding Lindblad coefficients which characterize the strength of various processes characterizing energy absorption or leaking from the system.

2.3 Memory effects and Markovianity

The Markovian approximation is a drastic assumption. Even in the case of classical stochastic processes, memoryless processes are vastly outnumbered by processes with some form of memory, and non-Markovian processes are the rule, not the exception. In the quantum case, as discussed in the previous chapter, there are lots of approaches towards defining non-Markovianity. For the sake of brevity, we shall only discuss one of the most popular approaches, based on CP-divisibility of the dynamics. For another approach based on the process tensor formalism, the interested reader may consult Pollock *et al*'s work [94].

A dynamical map Λ running from $t = t_i$ to $t = t_f$ is said to be Markovian when it can be chopped up in infinitesimal CP maps, i.e., $\Lambda_{t_i, t_f} \equiv \Lambda_{t_f - \delta t, t_f} \circ \dots \Lambda_{t, t + \delta t} \circ \Lambda_{t - \delta t, t} \dots \circ \Lambda_{t_i, t_i + \delta t}$.

Any process which does not satisfy the above mentioned property is said to be non-Markovian. Physically, such Markovian processes mandate that the flow of information is always from the system towards environment, and consequently, any non-monotonic behavior unseen for CP dynamics indicates the backflow of information, thus indicating the prevalence of a non-Markovian dynamics. Quantifying non-Markovianity of any arbitrary given dynamics is discussed in the next subsection.

2.3.1 Measures of non-Markovianity

Like other quantum resources, it is possible to quantify non-Markovianity using witness operators. Below we list a few of those witnesses in a tabular form. For a more detailed list, we refer to Ref. [95].

However, one of the most popular measures of non-Markovianity in the CP divisibility

Witness	Physical Origin
Breuer-Laine-Piilo measure[63]	For a quantum system undergoing CPTP evolution, the trace distance between any two initial density matrices monotonically decreases with time. Hence, if the trace distance between two chosen initial points grows with time for certain temporal regions of the dynamics, the dynamics is non-Markovian.
Coherence based witness [64]	A quantum system undergoing incoherent CPTP evolution should always lose coherence. Any intermediate gain in coherence is thus a signifier of non-Markovian dynamics.
Irreversible Entropy Production Rate	Spohn's theorem asserts that a system in a thermal environment must always have a positive rate of production of irreversible entropy. Any signature of temporary decrease in irreversible dynamics is thus a signature of non-Markovianity
Data-processing violation [96]	The quantum data processing inequality asserts that the mutual information between two systems undergoing a CP evolution decreases monotonically. Hence the violation of the data processing inequality in intermediate times indicates the breakdown of CP, and consequent onset of non-Markovianity.
Purity	For a qubit system going through a Lindbladian CP evolution, the purity of the state always goes down monotonically. Hence, any temporary increase in purity heralds a non-Markovian dynamics.

Table 2.2: Different Witness based measures for non-Markovianity.

sense is the so called *Rivas-Huelga-Plenio* (RHP) measure, which seeks to quantify the amount of CP violation in the following way. A complete positive and trace preserving (CPTP) dynamical map $\Lambda(t, 0)$ is divisible, or not based upon whether [65]

$$q(t) = \lim_{\epsilon \rightarrow 0^+} \frac{\|(\mathbb{I}_d \otimes \Lambda(t + \epsilon, t)) \Phi_+\| - 1}{\epsilon}, \quad (2.6)$$

is zero or greater than zero, respectively. Here, d is the dimension of the Hilbert space and $\|\cdot\|$ denotes for trace norm and $\Phi_+ = |\Phi_+\rangle\langle\Phi_+|$ is the $d \times d$ dimensional maximally entangled state. By computing $q(t)$ from above, the RHP measure of non-Markovianity can be defined [97, 65] based on the positive definiteness of $q(t)$ as

$$G = \frac{\eta}{\eta + 1}, \quad (2.7)$$

where $\eta = \int_0^\infty q(t) dt$.

2.4 Connection with thermodynamics

One of the most ubiquitous kind of environments one encounters is the thermal environment. For such thermal environments, there are a few different ways of proceeding. The first approach, due to classical thermodynamics, is to concern ourselves with only macroscopic emergent parameters like pressure, volume, etc. This approach, within its limitations, has been supremely successful in terms of practical utility. However, this approach largely does not distinguish between microscopic models of underlying physics, notwithstanding the indistinguishability-motivated corrections. From the perspective of quantum open systems, it is remarkable that with a suitably chosen measure of ergotropy, it is possible to prove that only the thermal state is completely passive, that is, we are unable to extract work out of it even when infinite number of copies are available. The critical caveat one has to keep in mind is that many of results for thermodynamics in the

quantum regime depend on how one chooses to quantify work in terms of microscopic parameters. One of the rather popular choices is to ascribe the change of average energy owing to the change in Hamiltonian levels as the rate of work \dot{W} , and that owing to the change in level occupancies as the rate of heat absorption or dissipation \dot{Q} , that is, for a Hamiltonian H ,

$$\dot{W} = \text{tr} \rho \dot{H}, \dot{Q} = \text{tr} \dot{\rho} H. \quad (2.8)$$

However, we shall not dwell on the appropriate definition of work and heat in the quantum context, and move on to discussing quantum thermal machines. These machines are, by design, supposed to consist of small quantum systems, yet function in much the same way as macroscopic thermal machines. The motivations come from numerous areas of research, from algorithmic cooling protocols to the possibility of creating molecular motors to biological considerations. Theoretical as well as experimental study of quantum thermodynamic machines have attracted a great deal of interest in recent times. One key ingredient for analysis of performance of these machines is the master equation of the dynamics pertaining to the setup where a single or few quantum systems are coupled with their heat baths in general. For example, in recently proposed quantum absorption refrigerators [98], three qubits interact among themselves while they are coupled to their respective baths. The Lindblad operators corresponding to the qubits interacting with heat baths become crucial to the study the performance of the thermal machines in both steady and transient regimes [99, 100, 101, 102, 103, 104]. Quantum thermal transistors [105] whose performance is analogous to the usual transistors have also been explored. Thus, we conclude that the master equation based approach outlined in this chapter provides a whole host of tools in hitherto less explored regimes which might have far-reaching impacts to enhance the performance of quantum thermodynamic machines.

2.5 Summary

- Evolution of open quantum systems is non-unitary and expressible in the Kraus operator-sum form

$$\rho \longrightarrow \sum_i K_i \rho K_i^\dagger \quad (2.9)$$

- Although severely limited by approximations, the Lindblad form of quantum master equations is guaranteed to preserve complete positivity of the dynamics.
- Non-Markovianity in quantum dynamical systems may be defined from the CP-divisibility perspective, and quantified using various witnesses.
- Master equation based approaches are crucial to quantitatively analyse the performance of nascent quantum thermodynamic machines.

Linking coherence with magic

1

We have introduced various quantum resources in the previous chapter, including the notions of quantum coherence and magic. The resource theories of coherence and magic states, as reviewed, seem quite disjoint. But are they really so? This is the question we seek to address. In this chapter, we provide a link between these two resource theories. Firstly we show, using contractive distance based monotones, that the magic generated in a quantum state through incoherent operations [33] is upper bounded by the amount of coherence initially in the state. Subsequently, we prove that the maximum amount of magic generated through such incoherent operations can, by itself, be shown to be a coherence monotone. Next, we turn towards obtaining a full coherence monotone based on the discrete Wigner function representation [106, 107, 108] of quantum states, the latter being useful for providing a calculable measure of magic. Next, we propose the counterparts to various types of incoherent operations in the resource theory of magic states. We subsequently move on to revealing the link between magic and other quantum resources like quantum coherence and entanglement, in small quantum systems.

¹This chapter is based on the paper "*Coherence makes quantum systems magical*", published in Journal of Physics A : Mathematical and Theoretical, **51**, 414006 (2018).

3.1 Coherence Quantifiers through magic monotones

In this section, we demonstrate how the presence or lack of quantum coherence in systems constrains the amount of magic in the system. In doing so, we reveal that quantum coherence can be quantified by the maximum amount of magic generated through incoherent operation on arbitrary quantum states. In subsequent work, unless otherwise stated, the basis with respect to which quantum coherence is defined, is the computational basis and the pure stabilizer states are the ones obtainable through Clifford unitary rotation of one of the basis elements, say $|0\rangle$, of the computational basis. We now state our first result.

For any distance based coherence quantifier C_D and corresponding magic quantifier M_D , the amount of magic generated through incoherent operations Λ_{IC} on a quantum state is upper bounded by the amount of coherence originally present in that state, that is,

$$M_D[\Lambda_{IC}(\rho)] \leq C_D[\rho]. \quad (3.1)$$

The proof of this lemma is simple. The left hand side equals, by definition, $\min_{\mu \in \mathcal{S}} D[\Lambda_{IC}(\rho), \mu] \leq \min_{\sigma \in \mathcal{I}} D[\Lambda_{IC}(\rho), \sigma] = C_D[\Lambda_{IC}(\rho)] \leq C_D[\rho]$, where we used the fact that any incoherent state in the computational basis is a stabilizer state.

Thus, the amount of magic created through incoherent operations in a quantum system is upper bounded by the amount of quantum coherence originally present. However, we can prove an even stronger result - namely, the amount of magic thus created, quantifies, in itself, the amount of quantum coherence originally present in the system. To this end, we propose the following set of coherence monotones corresponding to every distance based magic monotone

$$C_M[\rho] = \sup_{\Lambda_{IC}} M[\Lambda_{IC}(\rho)] \quad (3.2)$$

Now, we shall prove that the proposed quantity above is indeed a coherence monotone.

It is trivial to see that any incoherent state with respect to the adequately chosen basis is a stabilizer state. Monotonicity under CPTP maps is guaranteed for any contractive distance based measure. Therefore, we only present the proof for strong monotonicity under selective measurements. The proof is identical in spirit to the one presented in Ref. [37] for entanglement.

If $\sigma_i = \frac{K_i \rho K_i^\dagger}{\text{tr}[K_i \rho K_i^\dagger]}$ and $p_i = \text{tr}[K_i \rho K_i^\dagger]$ where $\{K_i\}$ are the Kraus operators corresponding to some incoherent operation, then

$$\sum_i p_i C_M[\sigma_i] \leq C_M[\rho]. \quad (3.3)$$

Proof- Let us assume that the condition above is false. Then there will exist at least one set of incoherent operations $\{\Lambda_i\}$ for which

$$\sum_i p_i M[\Lambda_i \sigma_i] > C_M[\rho]. \quad (3.4)$$

Note that each Λ_i here is individually an incoherent operation and should not be confused as being merely one Kraus element of a quantum operation. Now, since magic monotones are non-increasing on average under measurements in the computational basis ,

$$M \left[\sum_i p_i \rho_i \otimes |i\rangle\langle i| \right] \geq \sum_i p_i M[\rho_i] \quad (3.5)$$

$$\Rightarrow M \left[\sum_i p_i \Lambda_i \sigma_i \otimes |i\rangle\langle i| \right] > C_M[\rho] \quad (3.6)$$

$$\Rightarrow M \left[\sum_i \Lambda_i (K_i \rho K_i^\dagger) \otimes |i\rangle\langle i| \right] > C_M[\rho]. \quad (3.7)$$

Where the last step follows from the definition of $\sigma_i = K_i \rho K_i^\dagger / p_i$. Now, one can write a bipartite incoherent operation $\tilde{\Lambda}$ such that the Kraus operators for $\tilde{\Lambda}$ are written as $M_{ij} =$

$L_{ij}(K_i) \otimes U_i$, where L_{ij} are the Kraus operators corresponding to the incoherent operation Λ_i and U_i is the incoherent unitary $\sum_j |\text{mod}(i+j, \dim(\text{ancilla}))\rangle\langle j|$. For this operation, the LHS =

$$M[\tilde{\Lambda}(\rho \otimes |0\rangle\langle 0|)] > C_M[\rho] = C_M[\rho \otimes |0\rangle\langle 0|]. \quad (3.8)$$

This is in contradiction with the result (3.1) proved earlier, thus completing the proof.

3.1.1 Coherence monotone inspired from another magic monotone

Historically, phase space methods in quantum optics and continuous variable quantum information theory, have been very successful. In particular, the phase space (quasi)-probability distributions like the Wigner distribution, the Sudarshan-Glauber p -distribution or the Husimi q -distribution are extremely helpful in characterizing optical states [109]. Of these, the Wigner distribution is particularly notable for the fact that it additionally reproduces the correct marginal probability distributions. Since the introduction of phase space distributions are so successful for CV systems, it was inevitable that attempts to create analogues of such distributions for qudit states were to be made. There exist many such proposed constructions in the literature, [110, 111, 112], of which we shall make use of the construction of discrete Wigner function by Wootters [110]. Above, we showed how to construct coherence monotones from distance based magic monotones. In most cases, these monotones are extremely hard to exactly calculate. There is however, a computable monotone, called sum negativity, already in the literature [54] in terms of the negativity of the discrete Wigner function representation of a state. We show that the discrete Wigner function representation can also give rise to a coherence monotone.

For finite Hilbert space dimension d , the expression for characteristic function associated with each point (p, q) on the $d \times d$ phase grid is given by

$$A_{(p,q)} = D_{p,q} A_0 D_{p,q}^\dagger, \quad (3.9)$$

where $D_{p,q} = \omega^{-2^{-1}pq} Z^p X^q$ and $A_0 = \frac{1}{d} \sum_{p,q=0}^{d-1} D_{p,q}$. X and Z are the well known Shift and Boost operators respectively, and $\omega = e^{2\pi i/d}$ is the d -th root of unity and 2^{-1} is shorthand for $\frac{d+1}{2} \bmod (d)$. The Wigner function of a quantum state represented by the density matrix ρ , at a phase space point (p, q) , is given by $W_{(p,q)} = \text{tr}(\rho A_{(p,q)})$. Sum of Wigner functions along a line $W_q = \sum_p W_{(p,q)}$ is always positive semidefinite. Now let us propose the following candidate for a coherence monotone

$$C_w[\rho] = \min_{\sigma \in \mathcal{I}, \lambda \geq 0} \|\vec{K}_\rho - \lambda \vec{K}_\sigma\| \quad (3.10)$$

Here \vec{K}_ρ is a probability vector whose elements are the sums of Wigner functions ($W_1(\rho), W_2(\rho), \dots$) along parallel lines in the phase grid and $\|P - Q\|$ is the statistical distance between probability distributions P and Q .

Clearly, $C_w[\rho]$ vanishes for incoherent states. Moreover, from the monotonicity of trace distance under CPTP maps, C_w is monotonically decreasing under any CPTP map. The remaining, i.e., strong monotonicity and convexity conditions have been shown in literature [113] to be equivalent to the equality condition

$$C[p\rho_1 \oplus (1-p)\rho_2] = pC[\rho_1] + (1-p)C[\rho_2]. \quad (3.11)$$

The LHS of the above condition now reads as $C_w[p\rho_1 \oplus (1-p)\rho_2] = \min_{\sigma_1, \sigma_2 \in \mathcal{I}, \lambda_1, \lambda_2 \geq 0} \|\vec{K}_{p\rho_1 \oplus (1-p)\rho_2} - \vec{K}_{\lambda_1 \sigma_1 \oplus \lambda_2 \sigma_2}\| = \min_{\sigma_1, \sigma_2 \in \mathcal{I}, \lambda_1, \lambda_2 \geq 0} \|p\vec{K}_{\rho_1} + (1-p)\vec{K}_{\rho_2} - \lambda_1\vec{K}_{\sigma_1} - \lambda_2\vec{K}_{\sigma_2}\| = \min_{\sigma_1, \sigma_2 \in \mathcal{I}, \lambda_1, \lambda_2 \geq 0} \|p\vec{K}_{\rho_1} - \lambda_1\vec{K}_{\sigma_1} + (1-p)\vec{K}_{\rho_2} - \lambda_2\vec{K}_{\sigma_2}\| = p \min_{\sigma_1 \in \mathcal{I}, \lambda'_1 \geq 0} \|\vec{K}_\rho - \lambda'_1\vec{K}_{\sigma_1}\| + (1-p) \min_{\sigma_2 \in \mathcal{I}, \lambda'_2 \geq 0} \|\vec{K}_{\rho_2} - \lambda'_2\vec{K}_{\sigma_2}\| = pC_w[\rho_1] + (1-p)C_w[\rho_2]$ where $\lambda'_1 = \lambda_1/p$ and $\lambda'_2 = \lambda_2/(1-p)$. This completes the proof of the assertion that C_w is a full coherence monotone.



Figure 3.1: Hierarchy of various free operations in the resource theory of magic.

3.1.2 Hierarchy of stabilizer operations

In analogy with the resource theories of quantum coherence or entanglement, we may formulate various generalizations and specializations of stabilizer operations. A tentative hierarchy of such operations, roughly following the corresponding formulation for incoherent operations in Ref. [114, 115] is depicted in Fig. 3.1.

Genuinely Stabilizer Operations : The most stringent of all the stabilizer operations must be the genuinely stabilizer operations (GSO) similar to genuinely incoherent operations introduced in [116] for which every stabilizer state is supposed to be a fixed point for the dynamics. In the following proposition- we prove that such an operation is impossible unless it is the trivial identity transformation.

There is no non-trivial Genuinely Stabilizer Operation.

Let us illustrate the proof for $d = 2$. Suppose there is such a CPTP operation Λ which is a Genuinely Stabilizer Operation. This implies Λ is a genuinely incoherent operation with

respect to both the eigenbasis of σ_z and σ_x . Thus the Kraus operators corresponding to this operation are diagonal in both z basis as well as x basis, which holds true only for the trivial identity operation.

Incoherent Stabilizer Operations - Stabilizer operations can still generate quantumness in the form of quantum coherence. Thus, if we are to construct a resource theory encompassing both the stabilizer formalism and quantum superposition, it is relevant to consider incoherent stabilizer operations. In the stabilizer protocol, two operations stand out as potentially generators of quantum coherence. One being the Clifford unitary operation, the other being composition with different stabilizer states. The other operations, viz. measurement in computational basis or partial trace, can easily be shown to be incoherent operations as well. Thus, we write down the following subset of these two operations -

1. *Incoherent Clifford Unitary* - Defined as those clifford unitaries which do not generate quantum coherence, these now represent permutations of computation basis vectors. For example, in the qubit case, the bit-flip gate σ_x or the phase-gate $\begin{pmatrix} 1 & 0 \\ 0 & i \end{pmatrix}$ are incoherent Clifford unitaries, but the Hadamard gate $H = \frac{1}{\sqrt{2}} \begin{pmatrix} 1 & 1 \\ 1 & -1 \end{pmatrix}$ is not.
2. *Composition with other incoherent states* Incoherent states are by definition, within the stabilizer polytope, and composition with other incoherent states keeps quantum coherence fixed [117]. Thus this represents a suitable incoherent stabilizer operation.

Clearly every coherence monotone is a monotone under this formalism.

The l_p -norm is a monotone under incoherent stabilizer operations for every $p \geq 1$

For the proof of the above assertion, let us note that every stabilizer protocol Λ on a state ρ_S can be expressed as $\Lambda[\rho_S] = \text{Tr}_{A'} [U_{SA} (\rho_S \otimes \sigma_A) U_{SA}^\dagger]$ where U is a Clifford unitary

and σ is an ancilla stabilizer state. According to the conditions above, we must restrict σ to the set of incoherent stabilizer states and U to the set of incoherent Clifford unitaries. The effect of incoherent unitaries is either to permute the basis labellings for coherence, or to lend a phase term to the off-diagonal elements of the density matrix, the latter, for example, is illustrated by an incoherent unitary $\begin{pmatrix} 1 & 0 \\ 0 & i \end{pmatrix}$. Both of these effects can be easily verified to leave the l_p -norm invariant. The l_p -norm of a state ρ is given by

$$C_{l_p}[\rho] = \left(\sum_i \sum_{j, i \neq j} |\rho_{ij}|^p \right)^{1/p}. \quad (3.12)$$

Now, for an incoherent ancilla state $\sigma = \sum_k q_k |k\rangle\langle k|$, the l_p norm $C_{l_p}[\rho \otimes \sigma] = (\sum_k q_k^p)^{1/p} C_{l_p}[\rho] \leq C_{l_p}[\rho]$, where we have used Hölder's inequality. Similarly one can also check using the triangle inequality for the p -norm, that partial tracing doesn't increase C_{l_p} . Thus, l_p -norm is indeed a monotone for every $p \geq 1$ under incoherent stabilizer protocols.

Operationally, it is natural to wonder about the strength of stabilizer operations vis-a-vis the strength of incoherent stabilizer operations. A simple example is to consider the Hadamard operation, which is a stabilizer unitary, but can generate coherence in the computational basis.

Incoherent Stabilizer Preserving Operations- Continuing in the spirit of connecting the two resource theories, one can impose on the set of incoherent operations only the constraint that it does not generate any magic from stabilizer states. For example, the phase rotation is an incoherent operation, which may easily be seen to create magic starting from a stabilizer state. The mathematical characterization of incoherent stabilizer preserving operations is beyond the scope of the present work and we invite the reader to embark upon the same. An especially pressing concern would be to identify whether there exists any incoherent stabilizer preserving operation which is not an incoherent stabilizer operation, or even a stabilizer operation. Tentatively, Fig. 3.1 reflects that such operations are not ruled out, however, we have not succeeded in finding explicit counterexamples or

proofs either refuting or supporting this statement.

Stabilizer Preserving Operations - This is the most general type of free operation in the resource theory of magic that one can envisage. One only imposes the constraint that no stabilizer state is mapped to a magic state. In fact, such operations were studied in detail in Ref. [56] and a family of monotones derived.

3.2 Concrete results in small quantum systems

In this section, we shift our focus towards linking magic with other quantum resources in low dimensional systems. The smallest dimension for which we have a concrete computable expression for magic is $d = 3$, which is expressed via the sum negativity of discrete Wigner functions. Let us now look at the interplay between quantum coherence and magic in this scenario. Since signature of the connection between magic and contextuality has already been revealed [118, 58], our method of relating magic to other resource theories connects contextuality *inter alia* with these resources. The nascent resource theoretic formulation of contextuality [119, 120] can shed further light on the results we obtain here.

3.2.1 Explicit expression for magic in the qutrit case

We know from the discrete version of Hudson's theorem, that at least in the odd-dimensional case, a pure state with a positive discrete Wigner distribution, must be a stabilizer state. Accordingly, a measure of magic named *sum negativity*, embodying the negativity of the discrete Wigner function for a given state, was proposed and proved as a magic monotone for odd prime power dimensions under stabilizer operations [54]. It is defined as the following -

For any quantum state with discrete Wigner distribution W_u , the sum negativity is the

sum of absolute values of the negative elements of the discrete Wigner (quasiprobability) distribution.

For the qutrit case, after some algebra, we have the following discrete Wigner distribution corresponding to a qutrit density matrix ρ .

$$\begin{aligned}
W_{(1,1)} &= \frac{1}{3}(2\lambda_3 + \rho_{11}), W_{(1,2)} = \frac{1}{3}(2\lambda_2 + \rho_{22}), W_{(1,3)} = \frac{1}{3}(2\lambda_1 + \rho_{33}), \\
W_{(2,1)} &= \frac{1}{3}(-\lambda_3 - \sqrt{3}\mu_3 + \rho_{11}), W_{(2,2)} = \frac{1}{3}(-\lambda_2 + \sqrt{3}\mu_2 + \rho_{22}), \\
W_{(2,3)} &= \frac{1}{3}(-\lambda_1 - \sqrt{3}\mu_1 + \rho_{33}), W_{(3,1)} = \frac{1}{3}(-\lambda_3 + \sqrt{3}\mu_3 + \rho_{11}), \\
W_{(3,2)} &= \frac{1}{3}(-\lambda_2 - \sqrt{3}\mu_2 + \rho_{22}), W_{(3,3)} = \frac{1}{3}(-\lambda_1 + \sqrt{3}\mu_1 + \rho_{33}). \tag{3.13}
\end{aligned}$$

Where density matrix elements $\rho_{12} = \lambda_1 + i\mu_1, \rho_{13} = \lambda_2 + i\mu_2, \rho_{23} = \lambda_3 + i\mu_3, \lambda_i, \mu_i \in \mathbb{R}$.

Now the sum negativity $M_{SN}[\rho]$ is simply given by

$$M_{SN}[\rho] = \sum_{\mathbf{u}} |W_{\mathbf{u}}| - 1. \tag{3.14}$$

Similar to the case of logarithmic negativity in the resource theory of entanglement, it is possible to come up with another monotone, which is the logarithm of the sum negativity.

This measure was dubbed the *Mana* [54].

3.2.2 Effect of coherent and incoherent noise on magic states

As with many other quantum resource theories, the maximally mixed state is a free state in the resource theory of magic states while the maximally resourceful state turns out to be a pure state. In the qutrit scenario, the maximally magical pure states come in two different varieties, viz. the Strange states [54] and the Norrell states [54]. The strange states are pure states which are invariant under the symplectic component of the Clifford

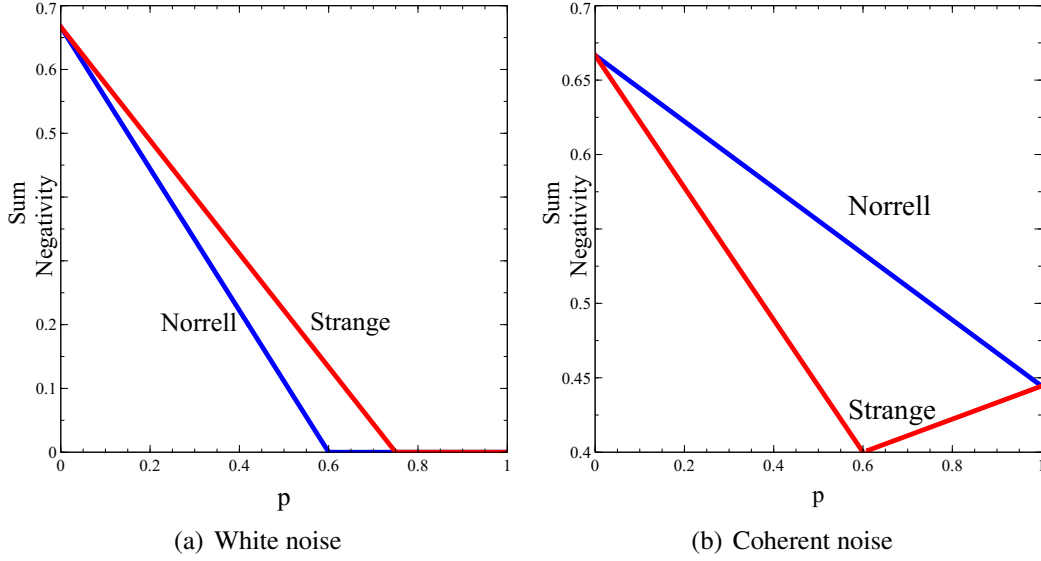


Figure 3.2: Response of two different maximally magical pure states, viz a strange state (red), and a Norrell state (blue), for admixture with maximally incoherent noise (left) and coherent noise (right). The sum negativity of the resulting states has been plotted with respect to the admixture parameter $p \in [0, 1]$.

group and of the form $\frac{1}{\sqrt{2}}(0, 1, \pm 1)^T$ and the corresponding permutations. Geometrically speaking, the Strange states are the pure states maximally distant from the *faces* of the stabilizer polytope. The Norrell states, in contrast, are pure states maximally distant from the *edges* of the stabilizer polytope. They are thus natural qutrit generalizations to the T and H states for qubits respectively.

It may therefore be interesting to have an answer to the question that which class of states remain more magical under admixture of noise. However, noise can be either coherent or incoherent. As we demonstrate below, depending on the character of the noise, the relative robustness of two types of magical states may be of different nature.

Strange states are more robust under mixture with maximally incoherent, i.e. white noise than Norrell states.

Proof- Due to symmetry, it suffices to check for one strange state and one Norrell state, respectively. Let this strange state be $|\psi_S\rangle = \frac{1}{\sqrt{2}}(0, 1, -1)^T$ and this Norrell state be $|\psi_N\rangle = \frac{1}{\sqrt{6}}(-1, 2, -1)^T$. Let us consider the strange state (Norrell state) $|\psi_S\rangle(|\psi_N\rangle)$ mixed with the

maximally mixed state to have the family of states $\rho_S(\rho_N) = (1 - p)|\psi_S\rangle\langle\psi_S| + \frac{p}{3}\mathbb{I}$ $((1 - p)|\psi_N\rangle\langle\psi_N| + \frac{p}{3}\mathbb{I})$. With the explicit expression for sum negativity given previously, it is easy to check that the sum negativity for the noisy strange state is given by

$$M_{SN}[\rho_S] = \begin{cases} \frac{2}{9}(3 - 4p), & \text{if } 0 \leq p \leq \frac{3}{4} \\ 0, & \text{if } \frac{3}{4} \leq p \leq 1 \end{cases} \quad (3.15)$$

while the corresponding sum negativity for the noisy Norrell state is given by

$$M_{SN}[\rho_N] = \begin{cases} \frac{2}{9}(3 - 5p), & \text{if } 0 \leq p \leq \frac{3}{5} \\ 0, & \text{if } \frac{3}{5} \leq p \leq 1 \end{cases} \quad (3.16)$$

Therefore, we see that the strange state remains more robust against admixture with white noise than the Norrell state.

Now, let us consider an example of a purely coherent noise, i.e. admixture of a maximally magical pure state with a maximally coherent state $|c\rangle = \frac{1}{\sqrt{3}}(|0\rangle - |1\rangle + |2\rangle)$.

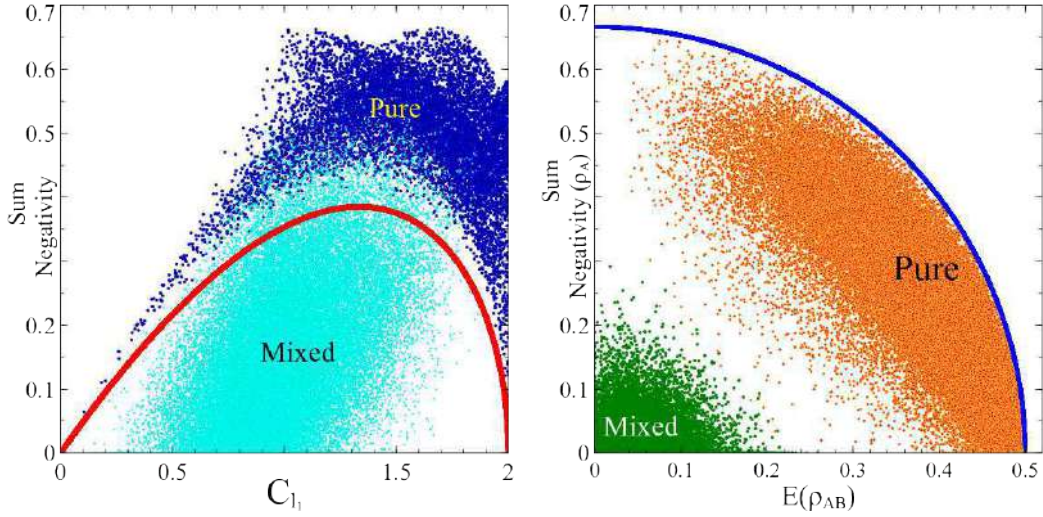
The Norrell state above is more robust under the admixture of aforementioned coherent noise than the strange state above.

Proof- Proceeding similarly as before, the expression for sum negativity of the noisy strange state is now given by

$$M_{SN}[\rho_S] = \begin{cases} \frac{2}{9}(3 - 2p), & \text{if } 0 \leq p \leq \frac{3}{5} \\ \frac{1}{9}(3 + p), & \text{if } \frac{3}{5} \leq p \leq 1 \end{cases}, \quad (3.17)$$

while the corresponding expression for sum negativity of the noisy Norrell state is given by

$$M_{SN}[\rho_N] = \frac{2}{9}(3 - p). \quad (3.18)$$



(a) Magic (quantified by sum negativity) vs l_1 - (b) Magic (quantified by sum negativity) of the norm coherence for randomly chosen qutrit pure reduced qutrit system vs negativity measure of entanglement (deep blue) and mixed (light blue) states. The tanglement for randomly chosen qutrit-qubit pure red line corresponds to the bound conjectured in (3.19) and mixed (green) states. The blue line corresponds to the bound conjectured in (3.20).

Figure 3.3: Interplay between quantum coherence, magic and entanglement in a qutrit (left) and a qutrit-qubit system (right).

Thus, throughout the range of the noise parameter p , the noisy Norrell state contains more magic than the corresponding noisy strange state, which is demonstrated in Fig. 3.2(b).

3.2.3 Relation between quantum coherence, quantum entanglement, and magic content

Continuing with our theme of attempting to unearth the relation of coherence and magic in quantum systems, it is a natural question to ask whether we can find a bound for the quantity of magic in terms of coherence in the qutrit scenario. One bound is quite obvious. Every incoherent state lies within the stabilizer polytope, therefore it is easy to see that any quantum state, pure or mixed, is at least as close to a stabilizer state as to an incoherent state. Thus, the magic of a quantum state is upper bounded by the amount of coherence in the system. However, for qutrit pure states, numerical simulation in Fig. 3.3(a) leads us to conjecture the following inequality, which gives a reverse, i.e., lower bound to the magic in terms of quantum coherence.

The following condition on quantum coherence, quantified via the l_1 -norm, and magic, quantified by the sum negativity, holds for qutrit pure states

$$M_{SN}[|\psi\rangle] \geq \frac{C_{l_1}[|\psi\rangle]}{2} \sqrt{1 - \frac{C_{l_1}[|\psi\rangle]}{2}} \quad (3.19)$$

It has already been shown that the presence of entanglement in a bipartite state adversely affects the coherence [121, 122] as well as contextuality [123] in the reduced state. Since magic as a resource in quantum computation has ultimately been ascribed to the contextual nature of quantum mechanics [58], it is important to quantify the corresponding trade off for entanglement in the joint system and magic in the reduced system. The simplest case is that of a qutrit qubit joint system. In this situation, we conjecture the following trade off relation between bipartite entanglement, quantified by the negativity, of a qutrit qubit joint system AB , and that of magic, quantified by sum negativity, in the reduced qutrit system A .

The negativity of entanglement E_{AB} and the sum negativity SN_A satisfies the following trade off relation

$$16E_{AB}^2 + 9M_{SN_A}^2 < 4 \quad (3.20)$$

Although an analytical proof is lacking, the numerical result furnished in Fig. 3.3(b) strongly suggests that the proposition above is true and indeed, almost tight for pure 3×2 states.

3.3 Summary

- The maximal amount of magic, quantified by a contractive distance based measure, liberated through incoherent operations on a quantum system is upper bounded by the amount of quantum coherence originally present in the system.
- The maximal amount of magic obtainable through incoherent operations on a quantum system, in itself, is a coherence monotone.
- It is possible to obtain a measure of coherence from the discrete Wigner function representation of finite dimensional quantum systems.
- There are no genuinely incoherent stabilizer operations.
- Distance based measures which are not coherent monotones under incoherent operations, may become monotones under incoherent stabilizer operations.
- Two families of qutrit magic states, namely, the Strange states and the Norrell states, are differentially affected by the nature of noise.
- For qubit-qutrit systems, there is a complementarity relation between the bipartite entanglement content, and the magic content of the reduced qutrit system.

Non Markovian dynamics of central spin systems I : Infinite temperature case

1

In the previous chapter, we have discussed about a link between two static resources, that is, resources pertaining to quantum states. In this chapter and the next one, we shall study the effect of a dynamical resource, namely, non-Markovianity, on the behaviour of a spin system.

In many body problems, when we deal with microscopic (e.g. spin systems) or mesoscopic (e.g. SQUIDs) physical systems, the analysis of dynamics often becomes complicated by virtue of the system's interaction with a background environment, as outlined in the second chapter. For the purpose of such an analysis, the environment is often modelled as a collection of oscillators or spin half particles [124]. They constitute two different universal classes of quantum environment [125]. In the oscillator bath model,

¹This chapter is based on the paper "*Exact master equation for a spin interacting with a spin bath: Non-Markovianity and negative entropy production rate*", published in Physical Review A, **95**, 012122 (2017).

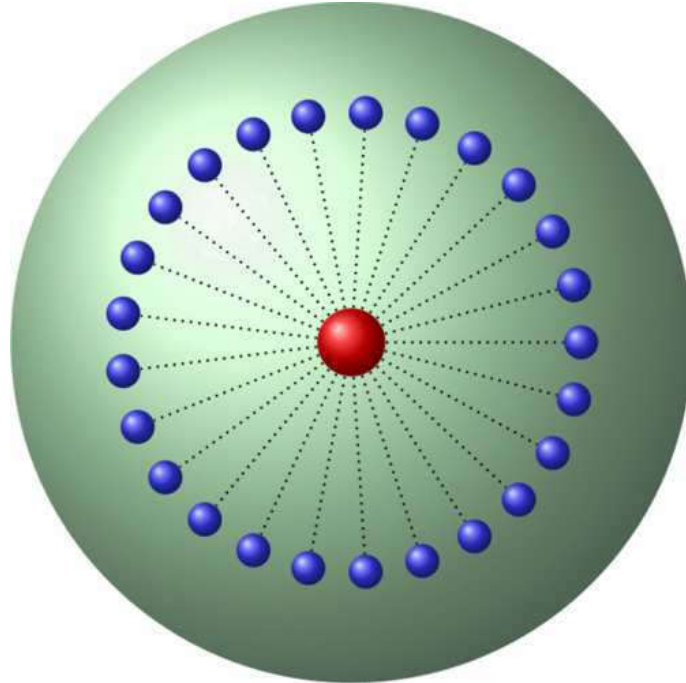


Figure 4.1: Schematic diagram of the central spin model. The central spin (red circle) interacts with the bath (green) constituting of spins (blue circles).

the environment is described as a set of uncoupled Harmonic oscillators, for example, the spin-boson [126, 127] and the Caldeira-Leggett models [127, 128] fall under its ambit. These oscillator models have been widely studied in the context of various physical phenomena under Markovian approximation [92, 93, 124]. On the other hand, the spin bath models remain relatively less explored. However, the spin bath models play a pivotal role in the quantum theory of magnetism [129], quantum spin glasses [130], theory of conductors and superconductors [131]. Solving for the exact dynamics of quantum systems under the spin bath models is thus of significant operational importance yet a technically challenging task. Indeed, in most of the cases the dynamics cannot be described exactly and several approximation techniques, both local and nonlocal in time, have been employed [124, 132, 133, 107, 134, 135, 136].

In this chapter, we will focus on the dynamical behavior of a central spin interacting uniformly with a spin bath and derive an exact time-local master equation of the Lindblad type. By virtue of the master equation being in this form, the dynamics is guaranteed to

be completely positive even in the strong coupling regime. Moreover, the Kraus representation of the dynamical map is also derived. Reduced dynamics of this particular spin bath model has been considered before [135, 136] where correlated projection operator techniques have been used to approximate the master equation of the central spin. However, the master equation furnished previously is time nonlocal and not of the standard Lindblad form. We take a different approach and start from the exact reduced state of the central spin at an arbitrary given time [135] to derive the canonical master equation without considering any approximations. We emphasise that the master equation is not only exact but allows one to systematically unravel the less explored but far reaching consequences of the strong coupling regimes which can be instrumental in performing information theoretic, quantum thermodynamic and several other quantum technological tasks. Moreover, the relaxation rates in the canonical master equation are insightful to understand several physical processes such as the dissipation, absorption and dephasing and thus the nature of decoherence.

One of the characteristics of the central spin models is to exhibit the non-Markovian features [137, 66]. As we discussed in the first chapter, non-Markovianity has been identified as a key resource in information theoretic [138, 61, 139], thermodynamic [59, 140, 141] and precision measurement protocols [142, 60, 143]. We study the non-Markovian features of the reduced dynamics and demonstrate that the non-Markovianity increases with the interaction strength. We next focus on the thermodynamic implications of non-Markovianity in this system. Irreversible increase of entropy due to dissipation of energy and work into the environment is inevitable for systems out of equilibrium [144, 145, 146, 147, 148, 149]. According to the Spohn's theorem [150], the irreversible entropy production rate is always non-negative under the Markovian dynamics. We show in this chapter that the non-Markovianity of the dynamics allows for negative irreversible entropy production rate. The resulting partial reversibility of the work and entropy influences the performance of quantum heat engines, refrigerators and memory devices. More specifically, we investigate the entropy production rate and show that the non-Markovianity of

the dynamics is always associated with a negative entropy production rate of the central spin for a certain initial state. We also investigate the non-Markovianity in terms of the rate of change of the purity of the central qubit and demonstrate that the rate of change of the purity of the qubit is positive for the same aforesaid initial state, whenever the dynamics is non-Markovian. Experimental detection of the non-Markovianity and the entropy production rates for quantum systems are of paramount interest in current research. As purity can be measured in the laboratory, this section hints at the possibility to experimentally demonstrate non-Markovian features and negative entropy production rate in spin bath models.

4.1 Central spin model and its reduced dynamics

In this section we first describe the central spin bath model. Then we derive the exact canonical master equation of the Lindblad type. From the master equation of the Lindblad form we show that the reduced dynamics of the central spin exhibits non-Markovian features throughout. We also derive the Kraus operators for the dynamical map.

4.1.1 The model

Let us first describe the central spin bath model, as depicted in the schematic Fig. 4.1. We consider a spin- $\frac{1}{2}$ particle that interacts uniformly with N other spin- $\frac{1}{2}$ particles constituting the bath. We further take the simplifying assumption that the spins of the bath do not interact with each other. The Hamiltonian for this spin bath model is thus given by

$$H = H_S + H_{SB} = \frac{\hbar}{2}\omega_0\sigma_z^0 + \frac{\hbar}{2}\sum_{i=1}^N\alpha(\sigma_x^0\sigma_x^i + \sigma_y^0\sigma_y^i + \sigma_z^0\sigma_z^i), \quad (4.1)$$

where σ_k^i ($k = x, y, z$) are the Pauli matrices of the i -th spin of the bath and σ_k^0 ($k = x, y, z$)

are the Pauli matrices for the central spin, α is the interaction strength. Here H_S and H_{SB} are the system and interaction Hamiltonian respectively. We shall make the usual assumption that initially the central spin and the spin bath is uncorrelated and the reservoir is in a thermal state at infinite temperature i.e., completely unpolarized state [135]. The composite state of the system and bath evolves unitarily under the total Hamiltonian $H + H_B$, starting from the factorized initial state, $\rho_{SB}(0) = \rho_S(0) \otimes \frac{1}{2^N} \mathbb{I}_B$, where \mathbb{I}_B is an N qubit maximally mixed state and H_B is the bath Hamiltonian. Since we are only concerned with the reduced dynamics of the central spin and the bath is completely unpolarized when initialized, there is no loss of generality by dropping any reference to the bath Hamiltonian. Therefore, the reduced quantum state $\rho_S(t)$ of the central spin at time t , can be obtained by tracing out the bath degrees of freedom as

$$\rho_S(t) = \text{Tr}_B[e^{-i(H+H_B)t/\hbar} \{\rho_S(0) \otimes \frac{1}{2^N} \mathbb{I}_B\} e^{i(H+H_B)t/\hbar}]. \quad (4.2)$$

Hereafter in this chapter, we drop the subscript S for the central spin unless otherwise mentioned. The total angular momentum of the bath is given by $\mathbf{J} = \frac{1}{2} \sum_i \boldsymbol{\sigma}^i$. The basis $|j, m\rangle$ is defined as the simultaneous eigenbases of both \mathbf{J}^2 and J_z . For even N , j takes the values $j = 0, 1, 2, \dots, N/2$ and for odd N , we have $j = 1/2, 3/2, \dots, N/2$ and m goes from $-j$ to j . It can be shown that [135] the z -component of the total angular momentum $\frac{1}{2}\sigma_z^0 + \frac{1}{2} \sum_i \sigma_z^i$ as well as \mathbf{J}^2 are conserved quantities. There are now two dimensional subspaces spanned by $|+\rangle \otimes |j, m\rangle$ and $|-\rangle \otimes |j, m + 1\rangle$ which are invariant under time evolution. Now the task of finding the analytical solution to the reduced dynamics of the central spin is broken down into solving the equations of motion in each subspace. Solving the equation of motion exactly vide Ref. [135], the initial reduced state of the

central spin, $\rho = \begin{pmatrix} \rho_{11} & \rho_{12} \\ \rho_{21} & \rho_{22} \end{pmatrix}$ can be shown to evolve as

$$\begin{aligned} \rho_{11}(t) &= A(t)\rho_{11}(0) + B(t)\rho_{22}(0), \\ \rho_{12}(t) &= C(t)\rho_{12}(0). \end{aligned} \quad (4.3)$$

Where,

$$\begin{aligned}
A(t) &= \sum_{j,m} \frac{N_j}{2^N} \left[\cos^2(\mu_+(j,m)t) + \frac{\Omega_+^2(m)}{4\mu_+^2(j,m)} \sin^2(\mu_+(j,m)t) \right], \\
B(t) &= \sum_{j,m} \frac{N_j}{2^N} \frac{\alpha^2 b^2(j,m)}{4\mu_+^2(j,m)} \sin^2(\mu_+(j,m)t), \\
C(t) &= e^{i\omega_0 t} \sum_{j,m} \frac{N_j}{2^N} \left[\cos(\mu_+(j,m)t) - \frac{i\Omega_+(m)}{2\mu_+(j,m)} \sin(\mu_+(j,m)t) \right] \\
&\quad \times \left[\cos(\mu_-(j,m)t) + \frac{i\Omega_-(m)}{2\mu_-(j,m)} \sin(\mu_-(j,m)t) \right],
\end{aligned}$$

$$N_j = \binom{N}{\frac{N}{2} + j} - \binom{N}{\frac{N}{2} + j + 1},$$

and

$$\begin{aligned}
\Omega_{\pm} &= \pm\omega_0 + \alpha(\pm m + 1/2), \\
\mu_{\pm} &= \frac{1}{2} \sqrt{\Omega_{\pm}^2 + \alpha^2 b_{\pm}^2}, \\
b_{\pm} &= \sqrt{j(j+1) - m(m \pm 1)}.
\end{aligned}$$

It follows from the above expressions that $A(t) + B(t) = 1$, which implies the dynamical map is unital. The unitality of the dynamics has to be satisfied as the environment and the systems starts from a product state while the environment being in the maximally mixed state. We are now in position to derive the canonical master equation.

4.1.2 Canonical master equation

In what follows, we derive the exact canonical master equation of the Lindblad type for the central spin starting from dynamical map given in Eq. 4.3. The dynamical map described in Eq. 4.3 can be notationally represented as

$$\rho(t) = \Phi[\rho(0)]. \quad (4.4)$$

The equation of motion of the reduced density matrix of the form

$$\dot{\rho}(t) = \Lambda[\rho(t)] \quad (4.5)$$

can be obtained from Eq. 4.3, which is characterized by the time dependent generator $\Lambda[.]$. By following the method [151] given below, we find the master equation and thus the generator of the specific reduced dynamics. Consider a convenient orthonormal basis set $\{G_a\}$ with the properties $G_a^\dagger = G_a$ and $\text{Tr}[G_a G_b] = \delta_{ab}$. The map given in Eq. 5.12 can now be represented as

$$\Phi[\rho(0)] = \sum_{k,l} \text{Tr}[G_k \Phi[G_l]] \text{Tr}[G_l \rho(0)] G_k = [F(t)r(0)]G^T, \quad (4.6)$$

where $F_{kl} = \text{Tr}[G_k \Phi[G_l]]$, $r_l = \text{Tr}[G_l \rho(0)]$. Differentiating Eq. 4.6, we get

$$\dot{\rho}(t) = [\dot{F}(t)r(0)]G^T. \quad (4.7)$$

Let us consider a matrix L , with elements $L_{kl} = \text{Tr}[G_k \Lambda[G_l]]$. We can now represent Eq. 5.13 as

$$\dot{\rho}(t) = \sum_{k,l} \text{Tr}[G_k \Lambda[G_l]] \text{Tr}[G_l \rho(t)] G_k = [L(t)r(t)]G^T. \quad (4.8)$$

By comparing Eq. 4.7 and 4.8, we find

$$\dot{F}(t) = L(t)F(t) \Rightarrow L(t) = \dot{F}(t)F(t)^{-1}. \quad (4.9)$$

We can arrive at Eq. 4.9 given the inverse of $F(t)$ does exist and $F(0) = \mathbb{I}$. Considering the specific map of the central spin in Eq. 4.3, and taking the Orthonormal basis set $\{G_a\}$ as $\{\frac{\mathbb{I}_2}{\sqrt{2}}, \frac{\sigma_x}{\sqrt{2}}, \frac{\sigma_y}{\sqrt{2}}, \frac{\sigma_z}{\sqrt{2}}\}$, we find the $L(t)$ matrix to be

$$L(t) = \begin{pmatrix} 0 & 0 & 0 & 0 & 0 \\ 0 & \frac{C_R(t)\dot{C}_R(t)+C_I(t)\dot{C}_I(t)}{C_R(t)^2+C_I(t)^2} & -\frac{C_I(t)\dot{C}_R(t)-C_R(t)\dot{C}_I(t)}{C_R(t)^2+C_I(t)^2} & 0 & 0 \\ 0 & \frac{C_I(t)\dot{C}_R(t)-C_R(t)\dot{C}_I(t)}{C_R(t)^2+C_I(t)^2} & \frac{C_R(t)\dot{C}_R(t)+C_I(t)\dot{C}_I(t)}{C_R(t)^2+C_I(t)^2} & 0 & 0 \\ (\dot{A}(t) + \dot{B}(t)) + \left(\frac{\dot{A}(t)-\dot{B}(t)}{A(t)-B(t)}\right)(1 - (A(t) + B(t))) & 0 & 0 & 0 & \left(\frac{\dot{A}(t)-\dot{B}(t)}{A(t)-B(t)}\right) \end{pmatrix}, \quad (4.10)$$

where $C_R(t)$ and $C_I(t)$ are the real and imaginary part of $C(t)$ respectively. Now from the Eq. 4.8, we get the equation of motion as given by

$$\begin{aligned}\dot{\rho}_{11}(t) &= \frac{L_{z0}+L_{zz}}{2}\rho_{11}(t) + \frac{L_{z0}-L_{zz}}{2}\rho_{22}(t), \\ \dot{\rho}_{12}(t) &= (L_{xx} + iL_{xy})\rho_{12}(t).\end{aligned}\tag{4.11}$$

Eq. 4.11 gives the time rate of change of the density matrix. However, one needs to have the Lindblad type master equation to understand various processes like dissipation, absorption, dephasing in a more convincing way. Moreover, it is of prime importance to have the master equation to study the non-Markovian behavior of the reduced dynamics as we will see later. Therefore, our immediate aim is to derive the Lindblad type master equation starting from Eq. 4.11. Eq. 5.13 can be written in the form [122]

$$\dot{\rho}(t) = \Lambda[\rho(t)] = \sum_k X_k(t)\rho(t)Y_k(t)^\dagger,\tag{4.12}$$

where $X_k(t) = \sum_i G_i x_{ik}(t)$, $Y_k(t) = \sum_i G_i y_{ik}(t)$ and $\{G_a\}$ are the basis operators as defined before. Using this decomposition of $X(t)$ and $Y(t)$, Eq. 4.12 can be rewritten as

$$\dot{\rho}(t) = \sum_{i,j=\{0,x,y,z\}} z_{ij}(t)G_i\rho(t)G_j,\tag{4.13}$$

where $z_{ij}(t) = \sum_k x_{ik}(t)y_{jk}(t)^*$ are the elements of a Hermitian matrix. Using a new set of operators [122] $\mathcal{F}(t) = (z_{00}(t)/8)\mathbb{I}_2 + \sum_i (z_{i0}/2)G_i$ and $H(t) = \frac{i}{2}\hbar(\mathcal{F}(t) - \mathcal{F}^\dagger(t))$, after some algebra, the Eq. 4.13 can be written as

$$\begin{aligned}\dot{\rho}(t) &= \frac{i}{\hbar}[\rho(t), H(t)] \\ &+ \sum_{i,j=\{x,y,z\}} z_{ij}(t) \left(G_i\rho G_j - \frac{1}{2}\{G_j G_i, \rho(t)\} \right),\end{aligned}\tag{4.14}$$

where the curly braces stand for anti-commutator. Hence, the canonical master equation of the Lindblad form read as

$$\begin{aligned}\dot{\rho}(t) &= \frac{i}{\hbar}U(t)[\rho(t), \sigma_z] + \Gamma_{deph}(t) [\sigma_z\rho(t)\sigma_z - \rho(t)] \\ &+ \Gamma_{dis}(t) \left[\sigma_- \rho(t) \sigma_+ - \frac{1}{2} \{ \sigma_+ \sigma_-, \rho(t) \} \right] \\ &+ \Gamma_{abs}(t) \left[\sigma_+ \rho(t) \sigma_- - \frac{1}{2} \{ \sigma_- \sigma_+, \rho(t) \} \right],\end{aligned}\tag{4.15}$$

where $\sigma_{\pm} = \frac{\sigma_x \pm i\sigma_y}{2}$, and $\Gamma_{dis}(t), \Gamma_{abs}(t), \Gamma_{deph}(t)$ are the rates of dissipation, absorption and dephasing processes respectively, and $U(t)$ corresponds to the unitary evolution. $A(t) + B(t) = 1$, for this specific system, is used to derive the master equation. The rates of dissipation, absorption, dephasing and the unitary evolution are, respectively, given as

$$\begin{aligned}\Gamma_{dis}(t) &= -\frac{L_{z0} + L_{zz}}{2} = \frac{d}{dt} \left[\ln \left(\frac{1}{\sqrt{A(t)-B(t)}} \right) \right], \\ \Gamma_{abs}(t) &= -\frac{L_{zz} - L_{z0}}{2} = \frac{d}{dt} \left[\ln \left(\frac{1}{\sqrt{A(t)-B(t)}} \right) \right], \\ \Gamma_{deph}(t) &= -\frac{2L_{xx} - L_{zz}}{4} = \frac{1}{4} \frac{d}{dt} \left[\ln \left(\frac{A(t)-B(t)}{|C(t)|^2} \right) \right], \\ U(t) &= -\frac{L_{xy}}{2} = -\frac{1}{2} \frac{d}{dt} \left[\ln \left(1 + \left(\frac{C_R(t)}{C_I(t)} \right)^2 \right) \right].\end{aligned}\tag{4.16}$$

Note that the system environment interaction generates a time dependent driving Hamiltonian evolution in the form of $U(t)$. Since the coefficients of dissipation and absorption are equal, the master equation (5.29) can also be rewritten as

$$\begin{aligned}\dot{\rho}(t) &= \frac{i}{\hbar}U(t)[\rho(t), \sigma_z] + \frac{\Gamma_{dis}(t)}{2} [\sigma_x \rho(t) \sigma_x - \rho(t)] \\ &+ \frac{\Gamma_{dis}(t)}{2} [\sigma_y \rho(t) \sigma_y - \rho(t)] + \Gamma_{deph}(t) [\sigma_z \rho(t) \sigma_z - \rho(t)].\end{aligned}\tag{4.17}$$

The above equation implies that $\frac{\mathbb{1}}{2}$ is a fixed point of the reduced dynamics and hence, it confirms the unitality of the dynamical map. As the bath is in a thermal state at infinite temperature, the probabilities of losing energy to the bath modes and absorbing from it

become equal which makes the dissipation and absorption rates to be the same. This is quite similar to the bosonic thermal baths, as it follows from the KMS condition [124] that given the baths having canonical equilibrium distribution the rates of the absorption and dissipation process are balanced by the equation $\Gamma(-\omega) = \Gamma(\omega) \exp(-\beta\omega)$. Here β is the inverse temperature of the bath and it implies that $\Gamma(-\omega) = \Gamma(\omega)$, iff $\beta = 0$.

One of the important properties of a quantum dynamical map is complete positivity [137, 66, 152, 153, 154, 62, 63, 65, 155, 156]. The notion “complete” comes with the argument that for any valid quantum dynamical map, the positivity must be preserved if the map is acting on a system which is correlated to an ancilla of any possible dimension. For a Lindblad type canonical master equation with time dependent coefficients, as in Eq. 5.29, the complete positivity is guaranteed by the following condition $\int_0^t \Gamma_i(s) ds \geq 0$ [157], which can be easily verified for the specific decay rates given in (5.30). It is worth mentioning that since the dynamical map for this specific spin bath model is derived starting from an initial product system plus environment state, it is always guaranteed to be completely positive [158, 89]. However, the complete positivity of the dynamical map for the reduced system can break down in the presence of system-environment initial correlation [89].

4.1.3 Operator sum representation

Other important aspect of general quantum evolution is the Kraus operator sum representation, given as $\rho(t) = \sum_i K_i(t) \rho(0) K_i^\dagger(t)$. The Kraus operators can be constructed [159] from the eigenvalues and eigenvectors of the corresponding Choi-Jamiolkowski state [160]. The Choi-Jamiolkowski state for a dynamical map $\Phi[\rho]$ acting on a d dimensional system is given by $(\mathbb{I}_d \otimes \Phi)[\Phi_+]$, with $\Phi_+ = |\Phi_+\rangle\langle\Phi_+|$ being the maximally entangled state in $d \times d$ dimension. For the particular evolution considered here, we find the Choi

state to be

$$\begin{pmatrix} A(t)/2 & 0 & 0 & C(t)/2 \\ 0 & B(t)/2 & 0 & 0 \\ 0 & 0 & B(t)/2 & 0 \\ C^*(t)/2 & 0 & 0 & A(t)/2 \end{pmatrix}. \quad (4.18)$$

The positive semi-definiteness of the above density matrix demands $B(t) \geq 0$; $A(t) \geq |C(t)|$. From the eigensystem of the Choi state given in (5.15), we derive the Kraus operators as

$$\begin{aligned} K_1(t) &= \sqrt{B(t)} \begin{pmatrix} 0 & 1 \\ 0 & 0 \end{pmatrix}, \\ K_2(t) &= \sqrt{B(t)} \begin{pmatrix} 0 & 0 \\ 1 & 0 \end{pmatrix}, \end{aligned} \quad (4.19)$$

$$K_3(t) = \sqrt{\frac{A(t)-|C(t)|}{2}} \begin{pmatrix} -e^{i\theta(t)} & 0 \\ 0 & 1 \end{pmatrix},$$

$$K_4(t) = \sqrt{\frac{A(t)+|C(t)|}{2}} \begin{pmatrix} e^{i\theta(t)} & 0 \\ 0 & 1 \end{pmatrix},$$

where $\theta(t) = \arctan[C_I(t)/C_R(t)]$. It is straight forward to verify that the Kraus operators satisfies the unitality property $\sum_i K_i(t)K_i^\dagger(t) = \mathbb{I}$.

4.1.4 Non-Markovianity

The charecterization and quantification of the non-Markovianity is a fundamental aspect of open quantum dynamics. There are several proposed measures based on CP divisibility [65, 97] and non-Markovianity witness [63, 62, 161, 162, 163, 164, 64, 165]. One of the well accepted characterization and quantification of non-Markovianity based on

the composition law of the dynamical map has been introduced by Rivas-Huelga-Plenio [65], commonly known as RHP measure of non-Markovianity. In this approach, the non-Markovian behaviour is attributed to the deviation from divisibility and the quantification of non-Markovianity is done based on the amount of the deviation, as outlined in the second chapter of the thesis. Note that for the Markovian evolution G is zero and the maximum non-Markovianity corresponds to $G = 1$, i.e., when $\eta \rightarrow \infty$. The positivity of the function $q(t)$ or indivisibility of the map appears when the relaxation rates ($\{\Gamma_i(t)\}$ s) take negative values. We will show in the following that for the specific dynamical evolution considered in the present chapter, the decay rates periodically get negative and hence break the divisibility of the map, although they always maintain the complete positivity condition by construction. For this particular evolution, we get

$$\begin{aligned} q(t) &= [|\Gamma_{dis}(t)| - \Gamma_{dis}(t)] + [|\Gamma_{deph}(t)| - \Gamma_{deph}(t)] \\ &= q_{dis}(t) + q_{deph}(t), \end{aligned} \tag{4.20}$$

where $q_{deph}(t) = |\Gamma_{deph}(t)| - \Gamma_{deph}(t)$, is the non-Markovianity for the dephasing channel and $q_{dis}(t) = |\Gamma_{dis}(t)| - \Gamma_{dis}(t)$, is that for the thermal part of the channel including the dissipation and absorption process.

In Fig. 4.2 and 4.3, we plot the total non-Markovianity $q(t)$ and the contribution due to the thermal channel $q_{dis}(t)$ with different values of α to show the non-Markovian behavior of the dynamics. We see that the revival of $q_{dis}(t)$ increases with the increasing interaction strength α . In Fig. 4.4 and 4.5, we plot $q(t)$ and total non-Markovianity $q_{dis}(t)$ respectively, but for different number of bath spins N with a fixed interaction strength.

Let us now investigate the aspect of non-Markovianity from another well known perspective, namely the distinguishability of two quantum states [63, 62]. Consider any distance measure $D(\cdot)$ between two quantum states, following contraction property

$$D(\Phi[\rho^1], \Phi[\rho^2]) \leq D(\rho^1, \rho^2), \tag{4.21}$$

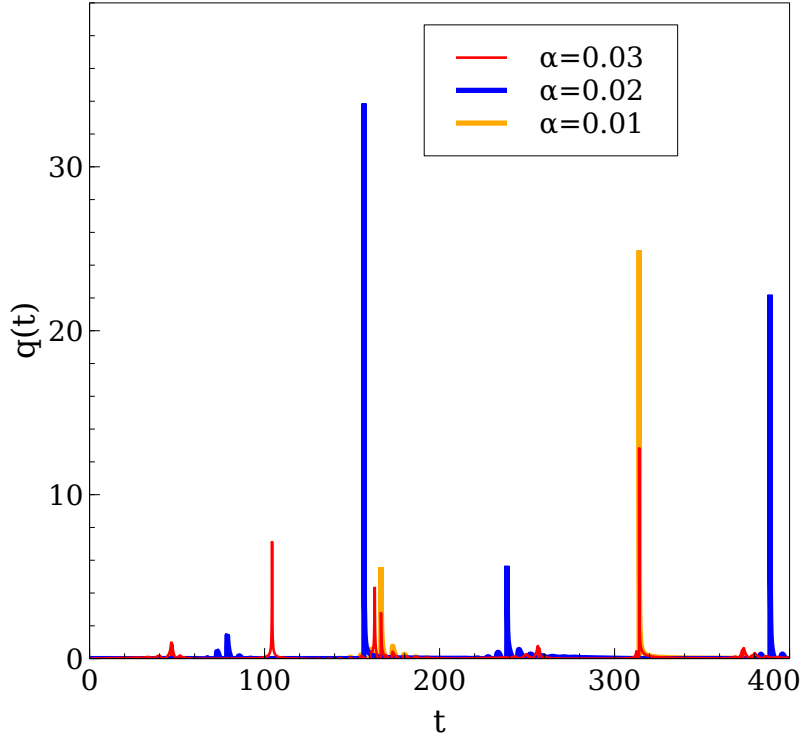


Figure 4.2: Variation of $q(t)$ with time t for various interaction strength α . Number of bath spins is kept fixed at $N = 20$. Positive $q(t)$ implies the non-Markovian nature of the dynamics according to the RHP measure.

where $\Phi[.]$ represents any CPTP map. Under any Markovian evolution, the time derivative of $D(.)$ will always be negative, owing to this contraction property. Therefore, non-monotonicity of these distances can be understood as a witness of the non-Markovian information feedback into the system. One such distance measure is the trace distance between quantum states [166]. Taking the trace distance between two states $D_T(\rho_1, \rho_2) = \frac{1}{2}\|\rho_1 - \rho_2\|$ a quantity can be defined as

$$p(t) = \frac{d}{dt} D_T(\Phi[\rho^1], \Phi[\rho^2]). \quad (4.22)$$

Breuer-Laine-Piilo (BLP) proposed a measure of non-Markovianity [63, 62] by summing over all the positive contributions of $p(t)$ and maximizing over the input states, which is given by

$$\zeta = \max_{\rho^{1,2}} \int_{p(t)>0} p(t) dt. \quad (4.23)$$

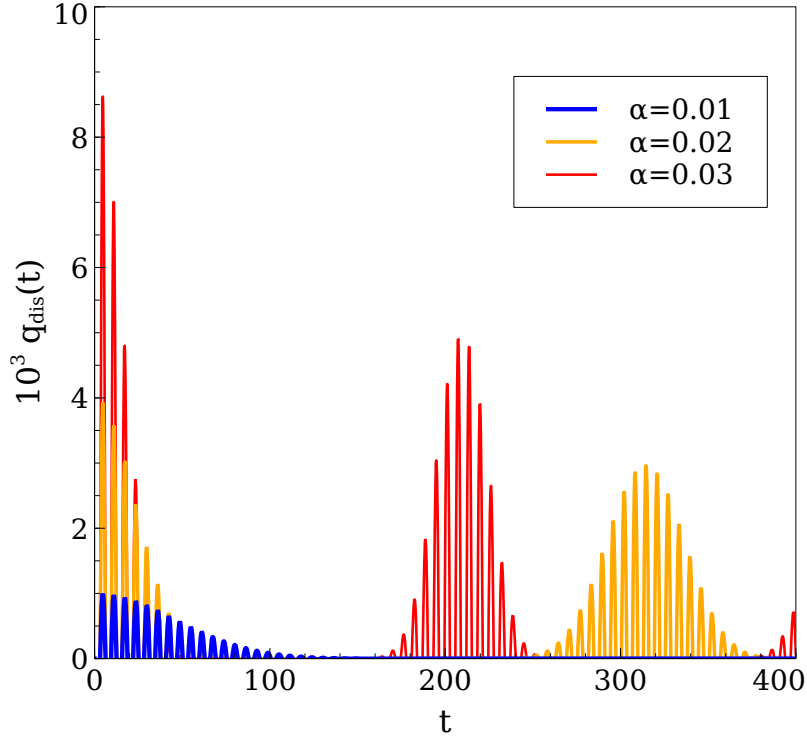


Figure 4.3: Variation of $q_{dis}(t)$ with time t for various interaction strength α . Number of bath spins is kept fixed at $N = 20$. To distinguish the effect on the thermal part of the quantum channel, we separately plot $q_{dis}(t)$. It can be seen from the plot that the non-Markovian revival for the thermal part of the channel increases with the increase of the interaction strength α for fixed N .

It can readily be taken as a witness of non-Markovian information feedback into the system under any local decoherence channel. We find that for our specific quantum channel, the trace distance fidelity between two quantum states $\rho_1(t)$ and $\rho_2(t)$, at any arbitrary time after the action of the mentioned channel can be expressed as

$$D(\Phi[\rho^1], \Phi[\rho^2]) = \sqrt{a^2(A(t) - B(t))^2 + |b|^2|C(t)|^2}, \quad (4.24)$$

with $a = \rho_{11}^1(0) - \rho_{11}^2(0)$ and $b = \rho_{12}^1(0) - \rho_{12}^2(0)$. In Fig. 4.6, we plot the function $p(t)$ for the two states $|\pm\rangle = \frac{1}{\sqrt{2}}(|0\rangle \pm |1\rangle)$. The time evolution of the same is plotted in Fig. 4.7, but for the case of increasing number of bath particles N . Note that calculating the maximized measure defined in Eq. (4.23), requires optimization over a and b , which is difficult in general. However, consideration of two specific states can demonstrate the

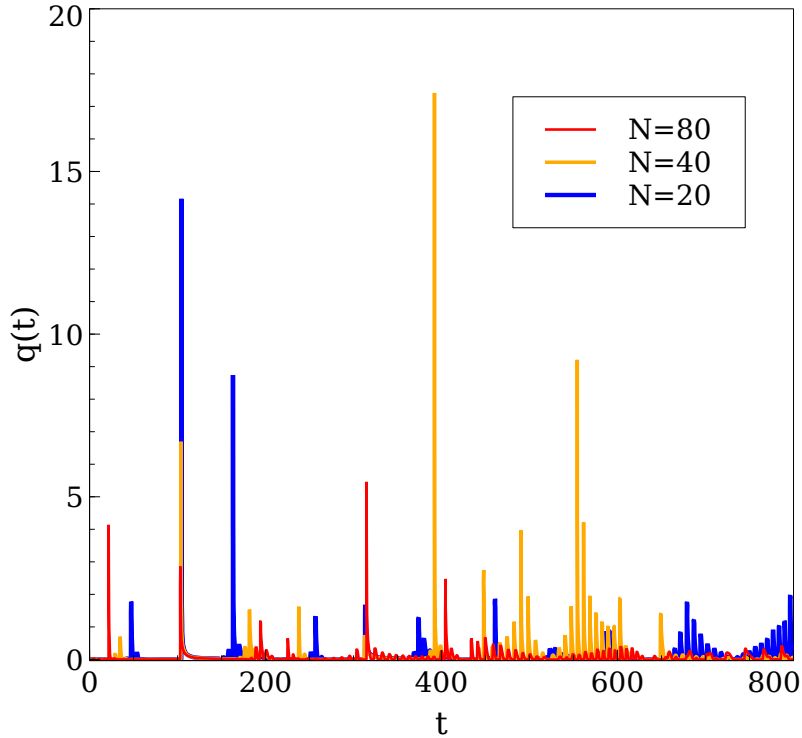


Figure 4.4: Variation of $q(t)$ with time t for different number of bath spins N . Interaction strength $\alpha = 0.03$ is taken.

non-Markovianity providing a lower bound of the measure. The two measures of non-Markovianity based on divisibility of the map (RHP measure, η) and distinguishability of two states under the action of the map (BLP measure, ζ) respectively, that we discuss here, may not agree in general [97, 167]. If a map is divisible, the evolution is Markovian and so the RHP measure of non-Markovianity η is zero. Consequently the BLP measure ζ is also zero. But the converse is generally not true, i.e., there exist some non-Markovian domain that are “bound” in terms of BLP measure and hence not captured by it. The reason behind this is that the notion of complete positivity does not enter in BLP measure and hence the divisibility breaking cannot be fully captured by it [97]. In this chapter we also consider the BLP measure of non-Markovianity to study whether the non-Markovian feature of our proposed master equation can be captured by BLP measure also.

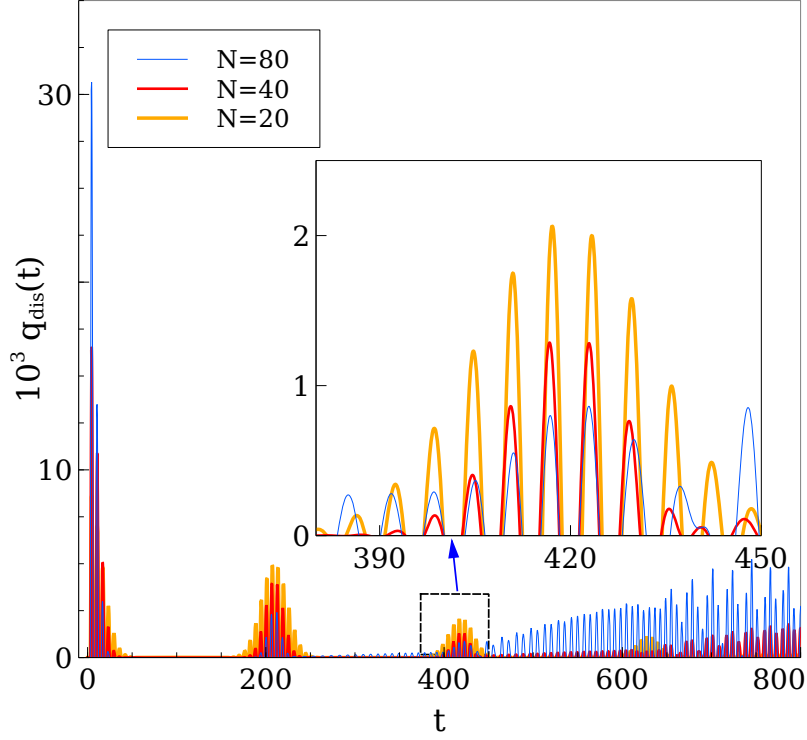


Figure 4.5: Variation of $q_{dis}(t)$ with time t for different number of bath spins N . Interaction strength $\alpha = 0.03$ is taken. Magnified view of the rectangular region is shown in the inset. The plot depicts that the revival of $q_{dis}(t)$ increases with the increase of bath spins N .

4.2 Negative entropy production rate

The irreversible or nonequilibrium entropy production and its rate are two fundamental concepts in the analysis of the nonequilibrium processes and the performance of thermodynamic devices [144, 145, 146, 147, 148, 149]. The reduction of the nonequilibrium entropy production can significantly alter the performance of thermodynamic devices and thereby it is of utmost interest in various technological domains. The nonequilibrium entropy production rate is defined as

$$\sigma(t) = \frac{dS}{dt} + \mathcal{J}, \quad (4.25)$$

where S is the von-Neumann entropy of the system and $\mathcal{J} = \frac{1}{kT} \frac{dQ}{dt} = \frac{1}{kT} \text{Tr}[H(t)\Lambda[\rho(t)]]$ is the entropy flux of the system. It can also be expressed as the time derivative of the

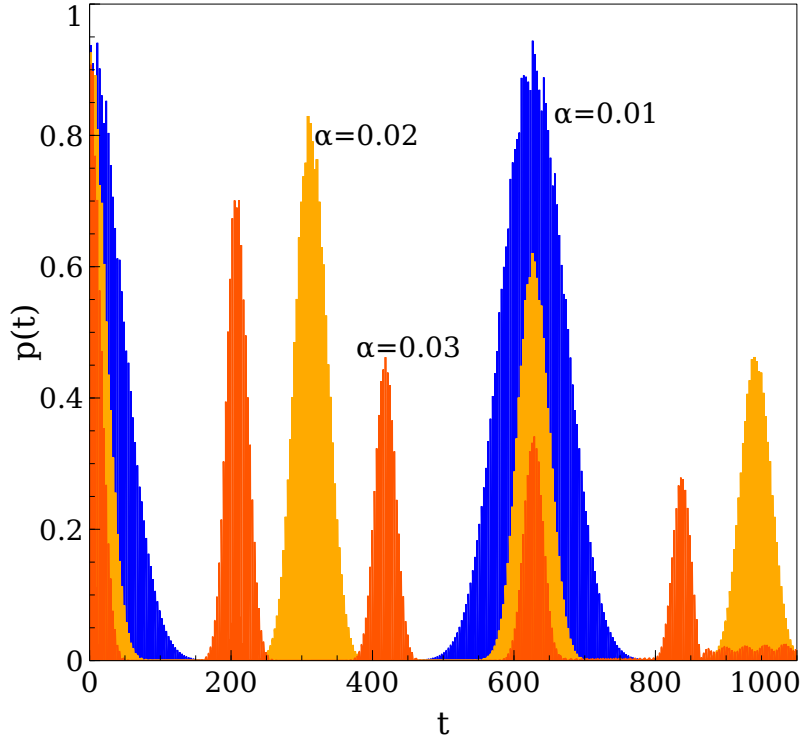


Figure 4.6: Variation of $p(t)$ with time t for the two states $|\pm\rangle = \frac{1}{\sqrt{2}}|0 \pm 1\rangle$, for different interaction strength α (where $N = 20$). Positive $p(t)$ implies non-Markovianity according to the BLP measure.

relative entropy of the state ρ with respect to the thermal equilibrium state ρ_{eq} [150, 158]

$$\sigma(t) = -\frac{d}{dt}S(\rho||\rho_{eq}), \quad (4.26)$$

where, $S(\rho||\tau) = -S(\rho) - \text{Tr}(\rho \ln \tau)$. According to the Spohn's theorem [150], the nonequilibrium entropy production rate σ is always non-negative. The Spohn's theorem is another statement of the second law of thermodynamics dictating the arrow of time. However, its validity essentially depends on the Markov approximation [62]. Under the non-Markovian dynamics σ can be negative [168, 169]. Therefore, the non-Markovianity of the dynamics is a thermodynamic resource providing partial reversibility of work and entropy. In addition, as negative $\sigma(t)$ is a prominent signature of the non-markovianity and hence it can be used to detect and quantify the non-Markovianity. Since, for the specific system considered here, the absorption and the dissipation rates are equal due to the infinite temperature of the bath, the net heat flow $\frac{dQ}{dt}$ is always zero. Therefore, for this specific model, we

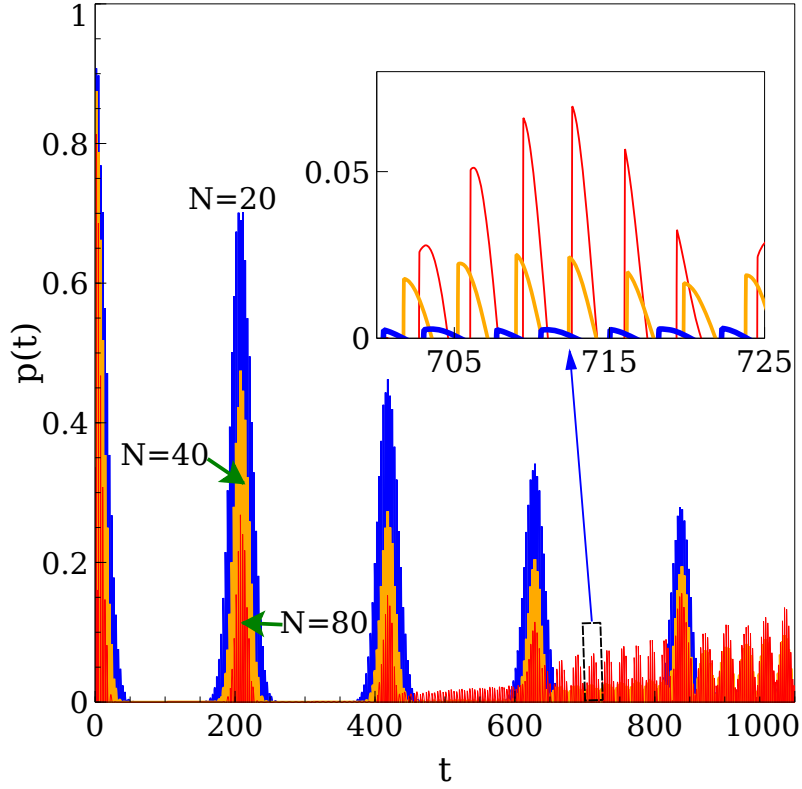


Figure 4.7: Variation of $p(t)$ with time t for two density matrices $|\pm\rangle = \frac{1}{\sqrt{2}}|0 \pm 1\rangle$, for different number of bath spins N , and interaction strength $\alpha = 0.03$. Magnified view of the rectangular region is shown in the inset.

have

$$\sigma(t) = \frac{dS}{dt}. \quad (4.27)$$

It is worth mentioning that under the action of the unital channel von-Neumann entropy of a system always increases in Markovian dynamics, as it is also a doubly stochastic map. Since the given channel is unital, the negative $\frac{dS}{dt}$ also ensures the deviation from Markovianity. Note that the rate of change of entropy is given as

$$\frac{dS}{dt} = -\frac{d}{dt} (\text{Tr}[\rho(t) \ln \rho(t)]) = -\text{Tr}[\ln \rho(t) \Lambda[\rho(t)]]. \quad (4.28)$$

Here $\Lambda[.]$ represents a general quantum evolution of the form

$$\Lambda[\rho(t)] = -\frac{i}{\hbar}[\rho(t), H_S(t)] + \sum_j \Gamma_j(t) \left[V_j \rho(t) V_j^\dagger - \frac{1}{2} \{V_j^\dagger V_j, \rho(t)\} \right]. \quad (4.29)$$

If the Lindblad operators $\{V_j\}$ are Hermitian, then Eq. 4.28 reads as

$$\frac{dS}{dt} = \frac{1}{2} \sum_{jkl} \Gamma_j(t) (\lambda_k(t) - \lambda_l(t)) \times [\ln \lambda_k(t) - \ln \lambda_l(t)] |\langle \lambda_k(t) | V_j | \lambda_l(t) \rangle|^2. \quad (4.30)$$

where we take the spectral decomposition of the density matrix $\rho(t) = \sum_i \lambda_i(t) |\lambda_i(t)\rangle \langle \lambda_i(t)|$. The above equation also implies that $\frac{dS}{dt}$ is non-negative if the relaxation rates $\{\Gamma_j(t)\}$ are non-negative. However, $\frac{dS}{dt}$ can be negative if one or more of the relaxation rates $\{\Gamma_j(t)\}$ are negative, i.e, in the non-Markovian domain. For the dynamics considered here, $\sigma(t)$ can be expressed as

$$\sigma(t) = \frac{1}{2} \ln \left(\frac{1-x}{1+x} \right) \frac{dx}{dt}, \quad (4.31)$$

where $x = \sqrt{(\rho_{11}(t) - \rho_{22}(t))^2 + 4|\rho_{12}(t)|^2}$. We plot the nonequilibrium entropy production rate $\sigma(t)$ starting from the pure initial state $|1\rangle$ in Fig. 4.8, which clearly shows that $\sigma(t)$ becomes negative whenever $\Gamma_{dis}(t)$ becomes negative. It has been shown in Ref. [168] that for a diagonal qubit state, σ can be negative only when the non-Markovian dynamics drives the system away from its thermal equilibrium. The example considered here completely agrees with this fact.

From Eq. (4.30) it is quite evident that the time rate of change of the entropy can be negative, only when the divisibility of the dynamical map breaks down. Therefore, a witness of non-Markovianity can be constructed from the negative entropy production rate for unital channels as follows

$$\varphi = \max_{\rho_{in}} \int_{\kappa(t)>0} \kappa(t) dt, \quad (4.32)$$

where $\kappa(t) = -\frac{dS}{dt}$. Measure of the non-Markovianity based on the entropy production rate has been considered before for unital dynamical maps [165].

4.2.1 Rate of change of purity: Detection of non-Markovianity

Let us investigate the non-Markovian behavior by the rate of change of the purity of the central qubit. If the Lindblad operators $\{V_j\}$ in Eq. 4.29 are Hermitian then the rate of change of the purity $P(= \text{Tr}\rho^2)$, of the central qubit can be given as

$$\frac{dP}{dt} = 2\text{Tr}[\rho(t)\Lambda[\rho(t)]] = - \sum_i \Gamma_i(t)Q_i(t), \quad (4.33)$$

where $Q_i(t) = \|[V_i, \rho(t)]\|_{HS}^2$. The abbreviation in the subscript stands for Hilbert-Schmidt norm ($\|X\|_{HS} = \sqrt{\text{Tr}(X^\dagger X)}$). As $\{Q_i(t)\}$ are always positive, the positive rate of change of purity can only occur for the negativity of one or more of $\{\Gamma_i(t)\}$ which corresponds to the divisibility breaking of the dynamical map. Note that the dynamics considered here can be expressed as a master equation with the Pauli matrices being the Lindblad operators (see Eq. 4.17) and the relaxation rates given as $\Gamma_x(t) = \Gamma_y(t) = \Gamma_{dis}(t)/2$, $\Gamma_z(t) = \Gamma_{deph}(t)$. Since the Pauli matrices are Hermitian operators and thereby positive rate of change of purity of the central spin clearly signifies the non-Markovianity of the dynamical map. It is also worth mentioning that when the Lindblad operators $\{V_j\}$ are Hermitian or in other words when they represent observables, then $Q_i(t) = \|[V_i, \rho(t)]\|_{HS}^2$, measures the quantumness [170, 171] of the state $\rho(t)$. Therefore, Eq. 4.33 implies that the more is the quantumness of the state the more it is sensitive to the environment. After a little algebra, we find that the rate of change of purity for the initial central qubit state $|1\rangle$, is given as

$$\frac{dP}{dt} = [A(t) - B(t)] \frac{d}{dt}[A(t) - B(t)]. \quad (4.34)$$

We plot the rate change of the purity with time in Fig. 4.8. From Fig. 4.8 it can be seen that the positive rate of change of purity occurs periodically, whenever the relaxation rate $\Gamma_{dis}(t)$ is negative. Since we are taking a initial diagonal state in the computational basis, there is no effect of the dephasing channel on the central qubit. For a qubit system, its eigenvalues have the form $\lambda = \frac{(1\pm z)}{2}$, where $0 \leq z \leq 1$, and hence, the entropy of a qubit

system is a monotonically decreasing function of the purity of the qubit. Therefore, signs of the rates of change of purity and entropy (See Fig. 4.8) are opposite.

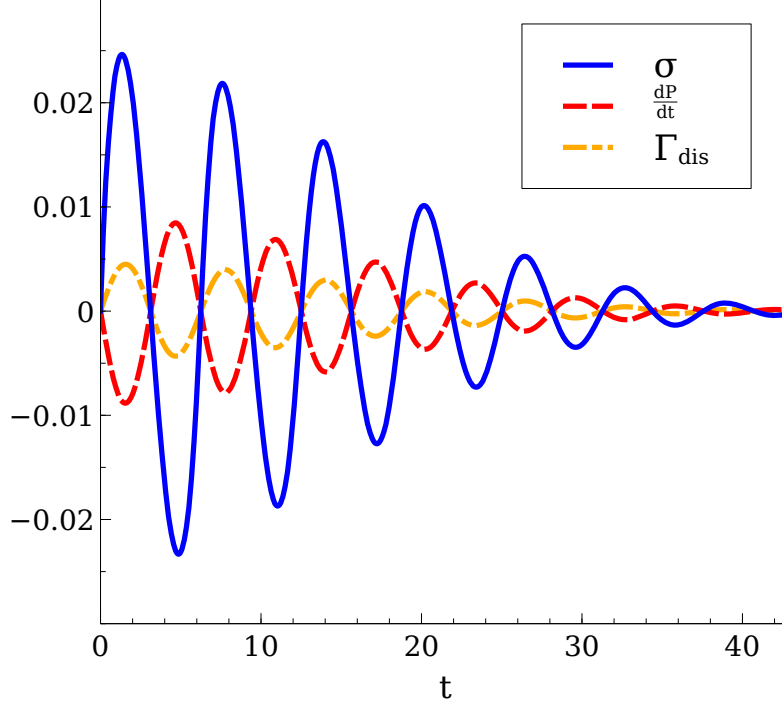


Figure 4.8: Variation of rate of change of the irreversible entropy production $\sigma(t)$, rate of change of the purity $\frac{dP}{dt}$, and Γ_{dis} with time t for the initial state $|1\rangle$ with the interaction strength $\alpha = 0.03$ and number of bath spins $N = 20$. It is evident that $\sigma(t)$ and $\frac{dP}{dt}$ are negative and positive respectively, whenever Γ_{dis} is negative. This implies that the non-Markovian information backflow revives purity of the state and causes negative irreversible entropy production rate.

Nowadays with advanced experimental techniques, the purity of a quantum system can be directly measured [172, 173, 174]. Hence, the non-Markovian revival of purity can be experimentally verified to demonstrate the non-Markovianity and the negative nonequilibrium entropy production rate in the laboratory.

4.3 Summary

- Dynamics of a central spin immersed in a completely unpolarized, non-interacting spin bath is studied.

- The Lindblad type master equation corresponding to the exact dynamics is derived.
- The dynamics is proved to be non-Markovian using witness based measures like the BLP measure, as well as the RHP measure, which is a CP divisibility-checking measure.
- Negative entropy production rate, and positive rate of change of purity has been put forward as non-Markovianity witnesses, and verified in the case of central spins.

Non Markovian dynamics of central spin systems II : Finite temperature case

1

In the previous chapter, we have analyzed the central spin model for the case of completely unpolarized, that is, infinite temperature spin baths. In this chapter, we analyze the more realistic case of finite temperature spin bath and the dynamic and thermodynamic properties of the central spin model in such a scenario. This is of considerable relevance for quantum computing schemes with NV centre [175] defects within a diamond lattice. We show that it is possible to sustain quantumness in this system for relatively longer by choosing bath parameter values appropriately. Perhaps fascinatingly, we shall show that quantum coherence persists in the system even for the time averaged state provided certain resonance conditions are met. The existence of such resonance conditions highlight the importance of bath engineering techniques. We shall also analyse the trapped information [176] content in the central spin system, and investigate the ergodicity or lack thereof in

¹This chapter is based on the paper "*Dynamics and thermodynamics of a central spin immersed in a spin bath*", published in Physical Review A, **96**, 052125 (2017).

the process of equilibration.

5.1 Central spin model and its reduced dynamics

In this section we reiterate the central spin model before deriving the exact dynamical map for the central spin, and furnish the corresponding Kraus operators. .

5.1.1 The model

We consider a spin- $\frac{1}{2}$ particle interacting uniformly with N other mutually non-interacting spin- $\frac{1}{2}$ particles constituting the bath.

The total Hamiltonian for this spin bath model is given by

$$\begin{aligned} H &= H_S + H_B + H_{SB} \\ &= \frac{\hbar\omega}{2}\omega_0\sigma_z^0 + \frac{\hbar\omega}{2N}\sum_{i=1}^N\sigma_z^i + \frac{\hbar\epsilon}{2\sqrt{N}}\sum_{i=1}^N(\sigma_x^0\sigma_x^i + \sigma_y^0\sigma_y^i), \end{aligned} \quad (5.1)$$

with σ_k^i ($k = x, y, z$) as the Pauli matrices of the i -th spin of the bath and σ_k^0 ($k = x, y, z$) as the same for the central spin and ϵ is the system bath interaction strength. H_S , H_B and H_{SB} are the system, bath and interaction Hamiltonians respectively. N is the number of bath atoms directly interacting with the central spin. The bath frequency and the system bath interaction strengths have been rescaled as ω/N and ϵ/\sqrt{N} respectively. Utilising collective angular momentum operators for bath spins $J_l = \sum_{i=1}^N\sigma_l^i$ (where $l = x, y, z, +, -$), we may write the corresponding Hamiltonians as

$$\begin{aligned} H_B &= \frac{\hbar\omega}{2N}J_z, \\ H_{SB} &= \frac{\hbar\epsilon}{2\sqrt{N}}(\sigma_x^0J_x + \sigma_y^0J_y). \end{aligned} \quad (5.2)$$

Now, it is possible to shift the problem to a Bosonic setting using the well known Holstein-

Primakoff transformation [127].

$$J_+ = \sqrt{N}b^\dagger \left(1 - \frac{b^\dagger b}{2N}\right)^{1/2}, \quad J_- = \sqrt{N} \left(1 - \frac{b^\dagger b}{2N}\right)^{1/2} b, \quad (5.3)$$

where b and b^\dagger are the respective annihilation and creation operators with the commutation rule $[b, b^\dagger] = 1$. The Hamiltonians can now be expressed as

$$\begin{aligned} H_B &= -\frac{\hbar\omega}{2} \left(1 - \frac{b^\dagger b}{N}\right), \\ H_{SB} &= \hbar\epsilon \left[\sigma_0^+ \left(1 - \frac{b^\dagger b}{2N}\right)^{1/2} b + \sigma_0^- b^\dagger \left(1 - \frac{b^\dagger b}{2N}\right)^{1/2} \right]. \end{aligned} \quad (5.4)$$

5.1.2 Dynamical map of the central spin

We assume that the initial system bath joint state is a product state $\rho_{SB}(0) = \rho_S(0) \otimes \rho_B(0)$, which ensures the complete positivity of the reduced dynamics [93, 92]. The initial bath state is considered as a thermal state $\rho_B(0) = e^{-H_B/k_B T} / Z$, where k_B , T and Z are the Boltzmann constant, bath temperature, and the partition function respectively. Now let us the evolution of the state $|\psi(0)\rangle = |1\rangle|x\rangle$, where $|1\rangle$ is the system excited state and $|x\rangle$ is an arbitrary bath state. Let the unitary orbit $U(t) = \exp\left(-\frac{iHt}{\hbar}\right)$, transform the state to $|\psi(t)\rangle = \gamma_1(t)|1\rangle|x'\rangle + \gamma_2(t)|0\rangle|x''\rangle$. We shall now introduce two operators $\hat{A}(t)$ and $\hat{B}(t)$ corresponding to the bath Hilbert space, which follow the relations $\hat{A}(t)|x\rangle = \gamma_1(t)|x'\rangle$ and $\hat{B}(t)|x\rangle = \gamma_2(t)|x''\rangle$. Then, we have $|\psi(t)\rangle = \hat{A}(t)|1\rangle|x'\rangle + \hat{B}(t)|0\rangle|x''\rangle$. Now from the equation of motion $\frac{d}{dt}|\psi(t)\rangle = -\frac{i}{\hbar}H|\psi(t)\rangle$, we have

$$\begin{aligned} \frac{d\hat{A}(t)}{dt} &= -i\left(\frac{\omega_0}{2} - \omega\left(1 - \frac{b^\dagger b}{2N}\right)\right)\hat{A}(t) - i\epsilon\left(1 - \frac{b^\dagger b}{2N}\right)^{1/2} b\hat{B}(t), \\ \frac{d\hat{B}(t)}{dt} &= i\left(\frac{\omega_0}{2} + \omega\left(1 - \frac{b^\dagger b}{2N}\right)\right)\hat{B}(t) - i\epsilon b^\dagger\left(1 - \frac{b^\dagger b}{2N}\right)^{1/2} \hat{A}(t). \end{aligned} \quad (5.5)$$

Writing $\hat{A}(t) = \hat{A}_1(t)$ and $\hat{B}(t) = b^\dagger \hat{B}_1(t)$, we have

$$\begin{aligned} \frac{d\hat{A}_1(t)}{dt} &= -i\left(\frac{\omega_0}{2} - \omega\left(1 - \frac{\hat{n}}{2N}\right)\right)\hat{A}_1(t) - i\epsilon\left(1 - \frac{\hat{n}}{2N}\right)^{1/2} (\hat{n} + 1)\hat{B}_1(t), \\ \frac{d\hat{B}_1(t)}{dt} &= i\left(\frac{\omega_0}{2} + \omega\left(1 - \frac{\hat{n}+1}{2N}\right)\right)\hat{B}_1(t) - i\epsilon\left(1 - \frac{\hat{n}}{2N}\right)^{1/2} \hat{A}_1(t), \end{aligned} \quad (5.6)$$

where $\hat{n} = b^\dagger b$ is the number operator. The operator equations 5.6 can be straightforwardly solved and the solutions are functions of \hat{n} and t . We note that $\hat{A}_1(t)|n\rangle = A_1(n, t)|n\rangle$, where $\hat{n}|n\rangle = n|n\rangle$. The time-evolved reduced state of the qubit ($|1\rangle\langle 1|$) is now obtained by tracing out the bath

$$\begin{aligned} \phi(|1\rangle\langle 1|) &= Tr_B [|\psi(t)\rangle\langle\psi(t)|] = \\ &= \frac{1}{2} \sum_{n=0}^N \left(|A_1(n, t)|^2 |1\rangle\langle 1| + (n+1)|B_1(n, t)|^2 |0\rangle\langle 0| \right) e^{-\frac{\hbar\omega}{k_B T}(n/2N-1/2)}, \end{aligned} \quad (5.7)$$

where, from the solution of 5.6, we have $|B_1(n, t)|^2 = 4\epsilon^2(1-n/2N)\frac{\sin^2(\eta t/2)}{\eta}$ and $|A_1(n, t)|^2 = 1 - (n+1)|B_1(n, t)|^2$.

We similarly define $\chi(0) = |0\rangle\langle x|$ and $\chi(t) = \hat{C}(t)|0\rangle\langle x| + \hat{D}(t)|1\rangle\langle x|$. Proceeding as above and substituting $\hat{C}(t) = \hat{C}_1(t)$, $\hat{D}(t) = b\hat{D}_1(t)$, we find

$$\begin{aligned} \frac{d\hat{C}_1(t)}{dt} &= i\left(\frac{\omega_0}{2} + \omega\left(1 - \frac{\hat{n}}{2N}\right)\right)\hat{C}_1(t) - i\epsilon\hat{n}\left(1 - \frac{\hat{n}-1}{2N}\right)^{1/2}\hat{D}_1(t), \\ \frac{d\hat{D}_1(t)}{dt} &= -i\left(\frac{\omega_0}{2} - \omega\left(1 - \frac{\hat{n}-1}{2N}\right)\right)\hat{D}_1(t) - i\epsilon\left(1 - \frac{\hat{n}-1}{2N}\right)^{1/2}\hat{C}_1(t), \end{aligned} \quad (5.8)$$

By solving the equation above, we find

$$\begin{aligned} \phi(|0\rangle\langle 0|) &= Tr_B [|\chi(t)\rangle\langle\chi(t)|] \\ &= \frac{1}{2} \sum_{n=0}^N \left(n|D_1(n, t)|^2 |1\rangle\langle 1| + |C_1(n, t)|^2 |0\rangle\langle 0| \right) e^{-\frac{\hbar\omega}{k_B T}(n/2N-1/2)}, \end{aligned} \quad (5.9)$$

with $|D_1(n, t)|^2 = 4\epsilon^2(1 - (n-1)/2N)\frac{\sin^2(\eta' t/2)}{\eta'}$ and $|C_1(n, t)|^2 = 1 - n|D_1(n, t)|^2$. For the coherences of the reduced density matrix, we can derive the following expression,

$$\begin{aligned} \phi(|1\rangle\langle 0|) &= Tr_B [|\psi(t)\rangle\langle\chi(t)|] \\ &= \frac{1}{2} \sum_{n=0}^N \left(A_1(n, t)C_1^*(n, t)|1\rangle\langle 0| \right) e^{-\frac{\hbar\omega}{k_B T}(n/2N-1/2)}, \end{aligned} \quad (5.10)$$

with $A_1(n, t)C_1^*(n, t) = \Delta(t)$.

Armed with these results, we can finally write down the time-evolved state of the central

spin qubit as

$$\begin{aligned}\rho_S(t) &= \text{Tr}_B \left[e^{-iHt/\hbar} \rho_S(0) \otimes \rho_B(0) e^{iHt/\hbar} \right], \\ &= \begin{pmatrix} \rho_{11}(t) & \rho_{12}(t) \\ \rho_{21}(t) & \rho_{22}(t) \end{pmatrix},\end{aligned}\tag{5.11}$$

where the elements of the central spin qubit density matrix are given as

$$\begin{aligned}\rho_{11}(t) &= \rho_{11}(0)(1 - \alpha(t)) + \rho_{22}(0)\beta(t), \\ \rho_{12}(t) &= \rho_{12}(0)\Delta(t),\end{aligned}\tag{5.12}$$

with

$$\begin{aligned}\alpha(t) &= \frac{1}{Z} \sum_{n=0}^N 4(n+1)\epsilon^2 \left(1 - \frac{n}{2N}\right) \frac{\sin^2(\eta t/2)}{\eta^2} e^{-\frac{\hbar\omega}{k_B T}(n/2N-1/2)}, \\ \beta(t) &= \frac{1}{Z} \sum_{n=0}^N 4n\epsilon^2 \left(1 - \frac{n-1}{2N}\right) \frac{\sin^2(\eta' t/2)}{\eta'^2} e^{-\frac{\hbar\omega}{k_B T}(n/2N-1/2)},\end{aligned}\tag{5.13}$$

$$\begin{aligned}\Delta(t) &= \frac{1}{Z} \sum_{n=0}^N e^{-i\omega t/2N} (\cos(\eta t/2) - i(\omega_0 - \omega/2N) \sin(\eta t/2)) \times \\ &\quad (\cos(\eta' t/2) + i(\omega_0 - \omega/2N) \sin(\eta' t/2)) e^{-\frac{\hbar\omega}{k_B T}(n/2N-1/2)},\end{aligned}$$

and,

$$\begin{aligned}\eta &= \sqrt{\left(\omega_0 - \frac{\omega}{2N}\right)^2 + 4\epsilon^2(n+1)\left(1 - \frac{n}{2N}\right)}, \\ \eta' &= \sqrt{\left(\omega_0 - \frac{\omega}{2N}\right)^2 + 4\epsilon^2 n\left(1 - \frac{n-1}{2N}\right)},\end{aligned}\tag{5.14}$$

where the partition function is $Z = \sum_{n=0}^N e^{-\frac{\hbar\omega}{k_B T}(n/2N-1/2)}$.

5.1.3 Operator sum representation

As a stepping stone towards deriving the master equation, first we derive the Kraus operator representation of the dynamics, which is expressible in the form $\rho(t) = \sum_i K_i(t)\rho(0)K_i^\dagger(t)$. The Kraus operators can be constructed [159] from the eigenvalues and eigenvectors of the corresponding Choi-Jamiolkowski (CJ) state [160, 159]. The CJ state for a dynamical map $\Phi[\rho]$ acting on a d dimensional system is given by $(\mathbb{I}_d \otimes \Phi)[\Phi_+]$, with $\Phi_+ = |\Phi_+\rangle\langle\Phi_+|$

being the maximally entangled state in $d \times d$ dimension. For the particular evolution considered here, we find the CJ state to be

$$\begin{pmatrix} \frac{1-\alpha(t)}{2} & 0 & 0 & \frac{\Delta(t)}{2} \\ 0 & \frac{\alpha(t)}{2} & 0 & 0 \\ 0 & 0 & \frac{\beta(t)}{2} & 0 \\ \frac{\Delta^*(t)}{2} & 0 & 0 & \frac{1-\beta(t)}{2} \end{pmatrix}. \quad (5.15)$$

From the eigensystem of the CJ state given in (5.15), we derive the Kraus operators as

$$\begin{aligned} K_1(t) &= \sqrt{\beta(t)} \begin{pmatrix} 0 & 1 \\ 0 & 0 \end{pmatrix}, \\ K_2(t) &= \sqrt{\alpha(t)} \begin{pmatrix} 0 & 0 \\ 1 & 0 \end{pmatrix}, \end{aligned} \quad (5.16)$$

$$K_3(t) = \sqrt{\frac{X_1}{1+Y_1^2}} \begin{pmatrix} Y_1 e^{i\theta(t)} & 0 \\ 0 & 1 \end{pmatrix},$$

$$K_4(t) = \sqrt{\frac{X_2}{1+Y_2^2}} \begin{pmatrix} Y_2 e^{i\theta(t)} & 0 \\ 0 & 1 \end{pmatrix},$$

where $\theta(t) = \arctan[\Delta_I(t)/\Delta_R(t)]$ and

$$X_{1,2} = \left(1 - \frac{\alpha(t) + \beta(t)}{2}\right) \pm \frac{1}{2} \sqrt{(\alpha(t) - \beta(t))^2 + 4|\Delta(t)|^2},$$

$$Y_{1,2} = \frac{\sqrt{(\alpha(t) - \beta(t))^2 + 4|\Delta(t)|^2} \mp (\alpha(t) - \beta(t))}{2|\Delta(t)|}.$$

5.1.4 Coherence and Entanglement dynamics of the central spin

It is well-known that for usual Markovian systems, quantum features like entanglement or coherence decay monotonically over time and eventually disappear [33, 64, 177]. Hence, the obvious question arises, whether it is possible to preserve quantum features for long periods of time for the non-Markovian central spin system.

Quantum Coherence: We choose the l_1 -norm of coherence as a quantifier of quantum coherence. For a qubit, the l_1 -norm of coherence [33] C_{l_1} is simply given by twice the absolute value of any off-diagonal element, i.e., $2|\rho_{12}(t)|$. The temporal dependence of coherence now goes as

$$C_{l_1}(t) = C_{l_1}(0)|\Delta(t)|. \quad (5.17)$$

One immediate corollary of the above is that we cannot create coherence over and above the coherence present in the system initially, even though this is a strongly non-Markovian system. In subsequent analysis, we can thus take the initial state to be maximally coherent without loss of generality.

Quantum Entanglement: Quantum entanglement is a fragile resource[178], and fades quickly in the Markovian scenario [177]. We envisage a situation where the central spin is initially entangled to an ancilla qubit A in addition to being acted on by the spin bath. There is no subsequent interaction between the ancilla qubit and the central spin. We shall analyze entanglement dynamics of the two-qubit state ρ_{SA} . The factorization theorem for quantum entanglement [179] yields,

$$E(\rho_{SA}(t)) = E(\rho_{SA}(0))E(\chi_{SA}(t)), \quad (5.18)$$

where $\chi_{SA}(t)$ is the CJ State in 5.15 and the entanglement quantifier E is chosen as concurrence [106], which, for a two qubit system is expressed as $E(\rho_{AB}) = \max\{0, \lambda_1 - \lambda_2 - \lambda_3 - \lambda_4\}$, where $\lambda_1, \dots, \lambda_4$ are the square roots of the eigenvalues of $\rho_{AB}\tilde{\rho}_{AB}$ in decreasing order, $\tilde{\rho}_{AB} = (\sigma_y \otimes \sigma_y)\rho_{AB}^*(\sigma_y \otimes \sigma_y)$. The entanglement of the Choi state can now be ex-

pressed as $E(\chi_{SA}(t)) = \max(0, |\Delta(t)| - \sqrt{\alpha(t)\beta(t)})$. Again, since the initial entanglement $E(\rho_{SA}(0))$ is simply a constant scaling term, we may assume a maximally entangled initial state $\rho_{SA}(0)$ without loss of generality.

Now we discuss the temporal behaviour of quantum coherence and entanglement with the bath temperature T , the interaction parameter ϵ and bath size (N). If the spin bath is in a very high temperature, thermal noise may be expected to triumph over quantum features, this intuition is backed up by Fig. 5.1(a) and 5.1(d). However, small fluctuations in quantum coherence persist for a long time due to the non-Markovianity of the dynamics. On the contrary, for low bath temperature, as demonstrated in Fig. 5.1(a), quantum coherence remains almost frozen. The dynamics of entanglement as shown in Fig. 5.1(d), is quite similar to that of coherence, albeit with greater fragility. This is in line with the usual observation of persistence of coherence, but not of entanglement, in similar situations[180, 181, 182]. In the opposite regime, for low enough temperatures, entanglement dynamics is very much similar to that of coherence. Another tuneable parameter is the system-bath interaction strength ϵ , which depends on the physical realization of the spins. For small enough interaction, the system expectedly evolves almost independently from the bath and therefore the coherence and entanglement of the system persists quite long, as shown in Fig. 5.1(b) and 5.1(e). On the other hand, if ϵ is of the same order as the energy difference of the spin levels of the central spin, we observe a rapid decay in quantum coherence with the presence of usual non-Markovian fluctuations. In this case, entanglement decays to zero almost immediately with no revival detected in the time span considered in Fig. 5.1(e). Eq. 5.13 enables us to investigate the effect of the bath size on the dynamics of coherence and entanglement. If the bath is large, as depicted in Fig. 5.1(c), quantum features like entanglement or coherence drop off rapidly. In case the number of spins in the bath is not very large, the evolution of coherence undergoes periodic revivals.

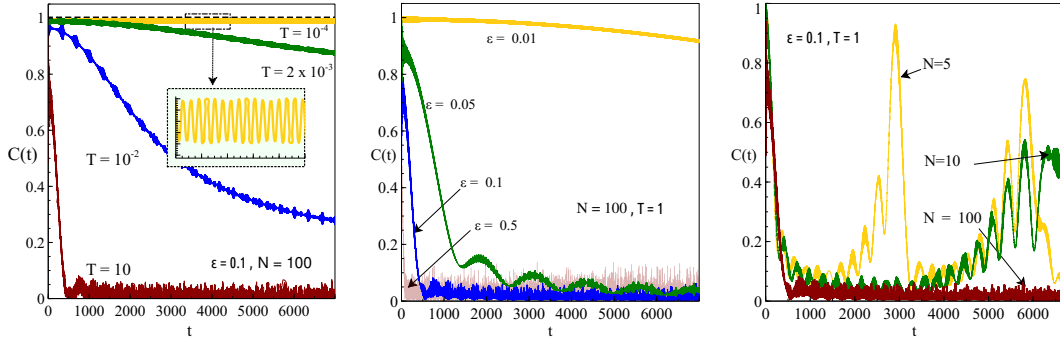
For the sake of concreteness, assuming typical order of magnitude values of various param-

eters governing the dynamics of quantum coherence, we are able to estimate the timescale for which coherence is sustained. Supposing the coupling strength $\epsilon \sim 1$ MHz, and assuming the spins having intrinsic energies ~ 100 MHz, we can conclude that at room temperature ($T = 300$ K) and for $N = 100$, the value of coherence is guaranteed to be at least 80 percent of the initial coherence for at least $\sim 100 \mu s$. Interestingly, this timescale for guaranteeing at least 80 percent of the initial coherence is not too sensitive on the bath temperature in practice. For example, if we assume the bath to be in a very low temp, say 10^{-4} K, then this time increases to only around $\sim 300 \mu s$. It implies that for the open system considered in this paper, the environment can be designed in such particular ways that quantum signatures like coherence or entanglement can be preserved for a long period of time. For diminishing number of bath spins, steady oscillations of both coherence and entanglement increases both in magnitude and frequency, which can be attributed to the finite size effect. We can contrast the situation with the the extreme case where only one auxillary spin is coupled to the central spin. In that extremal case, the coherence merely oscillates steadily, which is to be expected. But as the number of bath spin increases, the coherence suppression also increases.

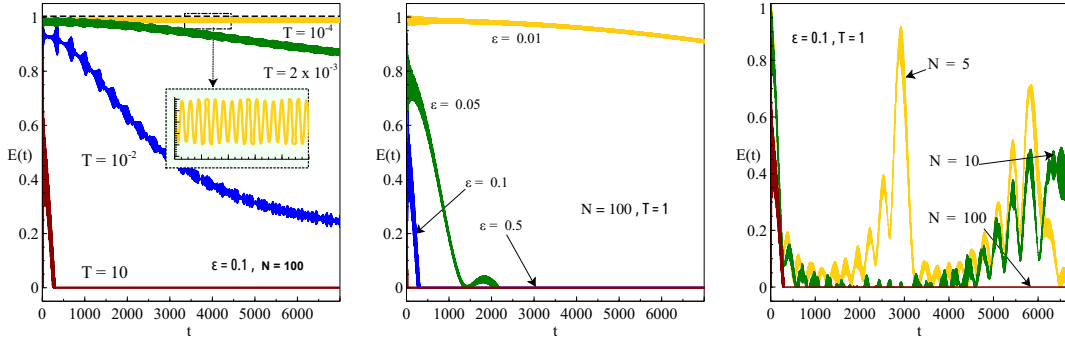
5.2 Analysis of time averaged dynamical map

We now focus our attention on the long time averaged state of the central spin, and its coherence. Another question we address is whether the long time averaged state is a true fixed point of the dynamical map, i.e. independent of initial condition. The time-averaged state of the central qubit is expressible as

$$\bar{\rho} = \lim_{\tau \rightarrow \infty} \frac{\int_0^\tau \rho(t) dt}{\tau}. \quad (5.19)$$



(a) Variation of coherence $C(t)$ with time t for different bath temperature. (b) Variation of coherence $C(t)$ with time t for different system-bath interaction strength. (c) Variation of coherence $C(t)$ with time t for different number of bath spins.



(d) Variation of entanglement $E(t)$ with time t for different bath temperature. (e) Variation of entanglement $E(t)$ with time t for different system-bath interaction strength. (f) Variation of entanglement $E(t)$ with time t for different number of bath spins.

Figure 5.1: Dynamics of quantum coherence and entanglement for the central qubit immersed in the spin bath.

Explicitly,

$$\begin{aligned}\overline{\rho_{11}} &= \lim_{\tau \rightarrow \infty} \frac{\int_0^\tau \rho_{11}(t) dt}{\tau} = \rho_{11}(0) (1 - \overline{\alpha}) + \rho_{22}(0) \overline{\beta}, \\ \overline{\rho_{12}} &= \rho_{12}(0) \overline{\Delta},\end{aligned}$$

where $\overline{\alpha}$, $\overline{\beta}$ and $\overline{\Delta}$ are long time averages of $\alpha(t)$, $\beta(t)$ and $\Delta(t)$ respectively. They can be simplified in the following way,

$$\overline{\alpha} = \sum_{n=0}^N 2(n+1)\epsilon^2 \left(1 - \frac{n}{2N}\right) \frac{1}{\eta^2} \frac{e^{-\frac{\hbar\omega_s}{k_B T}(n/2N-1/2)}}{Z}, \quad (5.20)$$

The above result is obtained by noting that the average of $\sin^2(\theta(t))$ over any integer number of time periods $= \frac{1}{2}$. Similarly we obtain,

$$\bar{\beta} = \sum_{n=0}^N 2n\epsilon^2 \left(1 - \frac{n-1}{2N}\right) \frac{1}{\eta'^2} \frac{e^{-\frac{\hbar\omega}{k_B T}(n/2N-1/2)}}{Z} \quad (5.21)$$

The equation for population dynamics shows that even the very long time averaged state retains the memory of the initial state, which is a signature of the system being strongly non-Markovian. This initial state dependence is depicted in Fig. 5.2(a). It is observed that the parameter $\overline{\left(\frac{\rho_{11}}{\rho_{22}}\right)}$ which captures the population distribution for long time averaged state is heavily dependent on the initial ground state population. If the initial population of the ground state increases, so does the population of the ground state for long time averaged state. However, in case the bath is very large, the population statistics for the long time averaged state is markedly less sensitive to the initial population. This leads us to posit that the only true fixed point independent of the initial conditions for this system exists only in the limit $N \rightarrow \infty$. We also observe that in the limit $\rho_{11}(0) = \rho_{22}(0) = \frac{1}{2}$, $\overline{\left(\frac{\rho_{11}}{\rho_{22}}\right)}$ tends towards 1 regardless of bath size N indicating the dynamics is almost unital. Also we should mention that in the thermodynamic limit ($N \rightarrow \infty$), when the temperature of the bath is infinite, the state $\bar{\rho}_{11} = \bar{\rho}_{22} = 1/2$ is not only the fixed point of the dynamics but the canonical equilibrium state also. Thus we can conclude that in the limit $N \rightarrow \infty$ and $T \rightarrow \infty$, the present open system dynamics is ergodic. Moreover, we see that the system-bath coupling strength not only affects the timescale of evolution but also plays significant role in the population statistics of the time averaged state. This we can see from Eq.s 5.20 and 5.21, which is also depicted in Fig. 5.2(b). Also for most of the cases, we have $\bar{\Delta} = 0$. It is interesting to note that the long-time averaged state $\bar{\rho}$ is incoherent in general. This implies, even though quantum coherence or entanglement persists for quite a long time if the bath temperature is very low, as depicted in Fig. 5.1(a) or Fig. 5.1(d) respectively, they must eventually decay. It is important to mention that there are specific resonance conditions under which $\bar{\Delta}$ can have finite value, which will be analysed in the

following section.

5.2.1 Resonance Condition for long lived quantum coherence

We have mentioned previously that the long time averaged state is in general diagonal, but for very specific choices of parameter values, this is not true and there indeed is long lived quantum coherence even in the long time averaged state. This can be of significant interest for theoretical and experimental purposes. For the off-diagonal component, the real and imaginary parts of $\Delta(t)$, defined as $\Delta_R(t)$ and $\Delta_I(t)$ respectively equals to

$$\begin{aligned}
\Delta_R(t) &= \\
&\sum_n \cos \frac{\omega t}{2N} \left[\cos \frac{\eta t}{2} \cos \frac{\eta' t}{2} + \frac{(\omega_0 - \frac{\omega}{2N})^2}{\eta \eta'} \sin \frac{\eta t}{2} \sin \frac{\eta' t}{2} \right] \frac{e^{-\frac{\hbar \omega}{k_B T} (n/2N - 1/2)}}{Z} \\
&+ \sum_n \left(\omega_0 - \frac{\omega}{2N} \right) \left[\frac{\sin \frac{\omega t}{2N} \cos \frac{\eta t}{2} \sin \frac{\eta' t}{2}}{\eta'} - \frac{\sin \frac{\omega t}{2N} \sin \frac{\eta t}{2} \cos \frac{\eta' t}{2}}{\eta} \right] \frac{e^{-\frac{\hbar \omega}{k_B T} (n/2N - 1/2)}}{Z}, \\
\Delta_I(t) &= \\
&- \sum_n \sin \frac{\omega t}{2N} \left[\cos \frac{\eta t}{2} \cos \frac{\eta' t}{2} + \frac{(\omega_0 - \frac{\omega}{2N})^2}{\eta \eta'} \sin \frac{\eta t}{2} \sin \frac{\eta' t}{2} \right] \frac{e^{-\frac{\hbar \omega}{k_B T} (n/2N - 1/2)}}{Z} \\
&+ \sum_n \left(\omega_0 - \frac{\omega}{2N} \right) \left[\frac{\cos \frac{\omega t}{2N} \cos \frac{\eta t}{2} \sin \frac{\eta' t}{2}}{\eta'} - \frac{\cos \frac{\omega t}{2N} \sin \frac{\eta t}{2} \cos \frac{\eta' t}{2}}{\eta} \right] \frac{e^{-\frac{\hbar \omega}{k_B T} (n/2N - 1/2)}}{Z}.
\end{aligned} \tag{5.22}$$

We always have

$$\overline{\sin \theta_1(t) \sin \theta_2(t) \sin \theta_3(t)} = \overline{\sin \theta_1(t) \cos \theta_2(t) \cos \theta_3(t)} = 0.$$

For each of the rest of the terms, it can be shown that the criteria for non-zero time averaged coherence reads

$$\frac{\omega}{2N} = \left| \frac{\eta \pm \eta'}{2} \right|.$$

For the condition $\frac{\omega}{2N} = \left| \frac{\eta + \eta'}{2} \right|$ to hold, it is easily shown that

$$N \leq \frac{\omega}{\omega_0}. \tag{5.23}$$

This, given that ω and ω_0 are usually of the same order of magnitude, is an unrealistic demand. We thus concentrate on the other condition $\frac{\omega}{2N} = \left(\frac{\eta-\eta'}{2}\right)$. The equation $\frac{\omega}{2N} = \left(\frac{\eta-\eta'}{2}\right)$ can be explicitly expanded out and the following quadratic equation in n is obtained

$$\begin{aligned} & \left(\frac{\epsilon^4}{N^2} + \frac{\epsilon^2\omega^2}{2N^3}\right)n^2 - \left(\frac{2\epsilon^4}{N} + \frac{\epsilon^2\omega^2}{N^2}\right)n + \\ & \left(\frac{\omega_0\omega^3}{4N^3} - \frac{\omega^2\omega_0^2}{4N^2} - \frac{\epsilon^2\omega^2}{2N^2} + \epsilon^4\right) = 0. \end{aligned} \quad (5.24)$$

By solving this quadratic and putting in the constraint that n is an integer, we derive the following resonance condition.

$$N \pm \frac{\epsilon\omega}{2} \frac{\sqrt{\frac{q_1}{8N^3} + \frac{q_2}{16N^4} + \frac{q_3}{32N^5} - \frac{q_4}{64N^6}}}{\frac{\epsilon^4}{4N^2} + \frac{\epsilon^2\omega^2}{8N^3}} \in \mathbb{Z}^+ \quad (5.25)$$

with

$$\begin{aligned} q_1 &= \epsilon^4, \quad q_2 = (\epsilon^2\omega^2 + \epsilon^2\omega_0^2 + 2\epsilon^4), \\ q_3 &= (\omega^2\omega_0^2 + 2\epsilon^2\omega^2 - 2\epsilon^2\omega\omega_0), \quad q_4 = 2\omega_0\omega^3, \end{aligned}$$

where \mathbb{Z}^+ is the set of integers in the range $\in [0, N]$. Assuming $\omega = \omega_0 = 1$, we obtain the resonance condition as the following in the limit $N \gg 1$,

$$N \pm \frac{\sqrt{N}}{\epsilon\sqrt{2}} \in \mathbb{Z}^+, \quad (5.26)$$

Thus, in order to ensure that a non zero amount of quantum coherence survives in the long time averaged state, we have to tune the interaction parameter exactly in such a way that $N \pm \frac{\sqrt{N}}{\epsilon\sqrt{2}}$ is a positive integer. This simple illustration demonstrates the importance of precise bath engineering in sustaining coherence.

5.2.2 Information trapping in the Central Spin System

Let us now investigate whether or under what condition the dynamical map considered here does have a true fixed point. The time averaging map $\bar{\Lambda}$ takes any initial state ρ to the

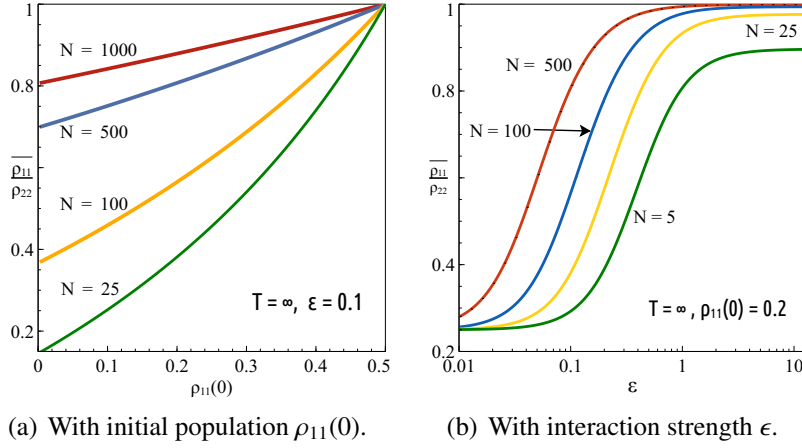


Figure 5.2: Variation of the ratio of long time averaged populations at excited and ground state $\bar{\rho}_{11}/\bar{\rho}_{22}$ with (a) initial population of the excited state $\rho_{11}(0)$ and (b) interaction strength ϵ , keeping the number of bath spins N as a parameter.

corresponding time averaged state $\bar{\rho}$ as given above. Let us now assume that the system is in an initial state ρ . Now let us consider whether the corresponding time averaged state $\bar{\rho}$ invariant under the map $\bar{\Lambda}$?" This can only happen when the map $\bar{\Lambda}$ is an idempotent one, i.e. $\bar{\Lambda}^2 = \bar{\Lambda}$. Clearly, if the time averaged state did not retain the memory of the initial state, this would be the case. Therefore the deviation from idempotence of the map $\bar{\Lambda}$ can serve as a useful measure of the initial state dependence of the system in the long run, which is termed as **Information Trapping** [176] and defined by

$$\mathcal{T}(\bar{\Lambda}) = \max_{\rho \in \mathcal{H}_S} D\left[\bar{\Lambda}^2 \rho, \bar{\Lambda} \rho\right], \quad (5.27)$$

where $D[.,.]$ is a suitable distance measure on the Hilbert space of the system. Choosing the trace norm as our distance measure, the expression for \mathcal{T} in the central spin model is computed as

$$\mathcal{T}(\bar{\Lambda}) = |\bar{\beta} - \bar{\alpha}|. \quad (5.28)$$

We immediately note that this quantity vanishes iff $\bar{\beta} = \bar{\alpha}$, which is the case only in the limit $N \rightarrow \infty, T \rightarrow \infty$, i.e. the thermodynamic and high temperature limit. The above statement is confirmed in Fig. 5.3. As we increase the temperature of the bath, the trapped information \mathcal{T} asymptotically vanishes. It is also observed that at any given temperature,

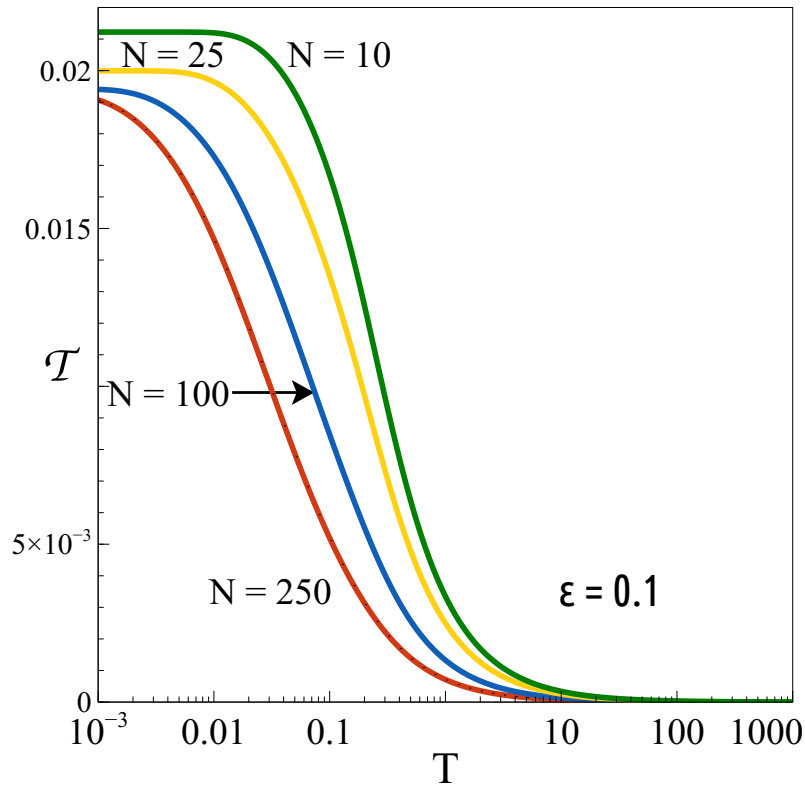


Figure 5.3: Variation of information trapping \mathcal{T} with temperature T , keeping the number of bath spins N as a parameter.

the amount of information trapped is greater for a smaller sized bath. This is consistent with the observation that a very large bath is required for \mathcal{T} to vanish. Fig. 5.4(a) and 5.4(b) lead to the observation that as the system-bath coupling gets stronger, the amount of information trapping, i.e. the dependence of the time averaged state on the initial state, also increases.

5.3 Canonical master equation and the process of equilibration

Finding the generator of a general dynamical evolution of a quantum system is one of the fundamental problems in the theory of open quantum systems, which leads to a better understanding of the actual nature of decoherence. It is our aim here to derive a canonical

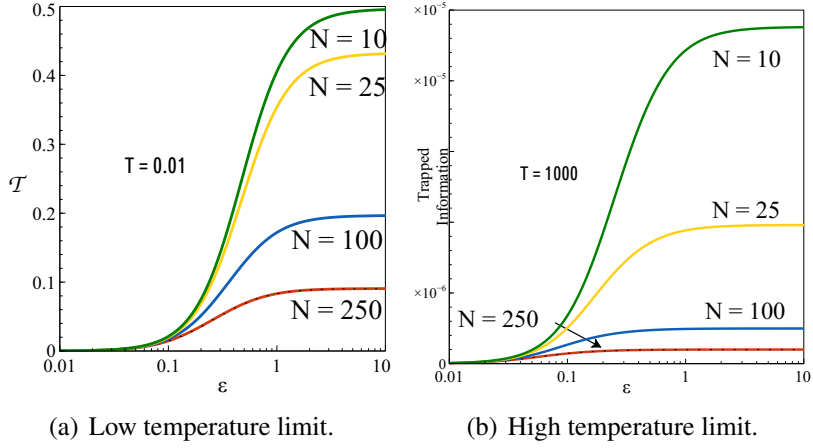


Figure 5.4: Variation of information trapping \mathcal{T} with interaction strength ϵ at (a) low temperature and (b) high temperature, keeping the number of bath spins N as a parameter.

master equation without resorting to the weak coupling and the Born-Markov approximation for the reduced dynamics presented in Eq. 5.12, by virtue of which we will later analyse various thermodynamic aspects of the qubit system. Using the formalism of [122], we obtain the following exact time local master equation for the central spin in the Lindblad form.

$$\begin{aligned}
\dot{\rho}(t) = & \frac{i}{\hbar} \delta(t) [\rho(t), \sigma_z] + \Gamma_{deph}(t) [\sigma_z \rho(t) \sigma_z - \rho(t)] \\
& + \Gamma_{dis}(t) \left[\sigma_- \rho(t) \sigma_+ - \frac{1}{2} \{ \sigma_+ \sigma_-, \rho(t) \} \right] \\
& + \Gamma_{abs}(t) \left[\sigma_+ \rho(t) \sigma_- - \frac{1}{2} \{ \sigma_- \sigma_+, \rho(t) \} \right],
\end{aligned} \tag{5.29}$$

where $\sigma_{\pm} = \frac{\sigma_x \pm i \sigma_y}{2}$, and $\Gamma_{dis}(t), \Gamma_{abs}(t), \Gamma_{deph}(t)$ are the rates of dissipation, absorption and dephasing processes respectively, and $\delta(t)$ corresponds to the unitary evolution, respec-

tively, given as

$$\begin{aligned}
\Gamma_{dis}(t) &= \left[\frac{d}{dt} \frac{(\alpha(t)-\beta(t))}{2} - \frac{(\alpha(t)-\beta(t)+1)}{2} \frac{d}{dt} \ln(1 - \alpha(t) - \beta(t)) \right], \\
\Gamma_{abs}(t) &= - \left[\frac{d}{dt} \frac{(\alpha(t)-\beta(t))}{2} - \frac{(\alpha(t)-\beta(t)-1)}{2} \frac{d}{dt} \ln(1 - \alpha(t) - \beta(t)) \right], \\
\Gamma_{deph}(t) &= \frac{1}{4} \frac{d}{dt} \left[\ln \left(\frac{1-\alpha(t)-\beta(t)}{|\Delta(t)|^2} \right) \right], \\
\delta(t) &= -\frac{1}{2} \frac{d}{dt} \left[\ln \left(1 + \left(\frac{\Delta_R(t)}{\Delta_I(t)} \right)^2 \right) \right].
\end{aligned} \tag{5.30}$$

For the detailed derivation of the master equation, one can look into the Refs. [183, 122]. Note that the system environment interaction generates a time dependent Hamiltonian evolution in the form of $\delta(t)$. This is analogous to the Lamb-shift correction in the unitary part of the evolution. Complete positivity [137, 66, 152, 153, 63, 65] is one of the important properties of a general quantum evolution, following the argument that for any valid quantum dynamical map, the positivity must be preserved if the map is acting on a system which is correlated to an ancilla of any possible dimension. For a Lindblad type evolution, this is guaranteed by the condition $\int_0^t \Gamma_i(s) ds \geq 0$ [157], which can be easily verified for the specific decay rates given in (5.30). However, since the dynamical map here is derived starting from an initial product state, complete positivity is always guaranteed [158, 89].

5.3.1 The principle of detailed balance

Here we investigate the process of approach towards steady state for the open system dynamics considered in this paper. There are various different approaches to explore the process of equilibration in an open system dynamics, each of which has their own merit [184]. In this work we carry out this investigation for the specific system considered here from a few different aspects, one of which is the method of quantum detailed balance. When two or more irreversible processes occur simultaneously, they naturally interfere

with each other. If due to the interplay between those different processes, over a sufficient period of evolution time, a certain balance condition between them is reached, then the system reaches a steady state. Consider the Pauli master equation for the atom undergoing such processes [91] given by

$$\dot{P}_n = \sum_m \gamma_{nm} P_m - \sum_m \gamma_{mn} P_n, \quad (5.31)$$

where P_n is the diagonal matrix element of the density operator and γ_{mn} is the transition probability for the process $|m\rangle \rightarrow |n\rangle$. The well known detailed balance condition [185, 186] for Pauli master equation is given as $\gamma_{nm} P_n^{(s)} = \gamma_{mn} P_m^{(s)}$, where $P_n^{(s)}$ is diagonal density matrix element at the steady state. We first derive a rate equation of the form of Eq.5.31 from the master equation 5.29 in order to study the detailed balance for our particular system [187, 188]. Let us consider the unitary matrix $U(t)$, which diagonalizes the system density matrix ($\rho(t)$) as $\rho_D(t) = U(t)\rho(t)U^\dagger(t)$. Then we can straightforwardly derive the equation of motion for the diagonalized density matrix as

$$\begin{aligned} \dot{\rho}_D(t) = & \frac{i}{\hbar} \delta(t) [\rho_D(t), \bar{\sigma}_z(t)] \\ & + \Gamma_{deph}(t) [\bar{\sigma}_z(t) \rho_D(t) \bar{\sigma}_z(t) - \rho_D(t)] \\ & + \Gamma_{dis}(t) \left[\bar{\sigma}_-(t) \rho_D(t) \bar{\sigma}_+(t) - \frac{1}{2} \{ \bar{\sigma}_+(t) \bar{\sigma}_-(t), \rho_D(t) \} \right] \\ & + \Gamma_{abs}(t) \left[\bar{\sigma}_+(t) \rho_D(t) \bar{\sigma}_-(t) - \frac{1}{2} \{ \bar{\sigma}_-(t) \bar{\sigma}_+(t), \rho_D(t) \} \right], \end{aligned} \quad (5.32)$$

where $\bar{A}_j(t) = U(t)A_j U^\dagger(t)$. Considering $P_a(t) = \langle a | \rho_D(t) | a \rangle$, we get the rate equation similar to the Pauli equation as

$$\dot{P}_a(t) = \sum_i \sum_b |\langle a | \bar{A}_i(t) | b \rangle|^2 P_b(t) - \sum_i \langle a | \bar{A}_i^\dagger(t) \bar{A}_i(t) | a \rangle P_a(t), \quad (5.33)$$

where $\bar{A}_i(t)$ s are all the Lindblad operators in the diagonal basis as given in Eq. 5.32. For the instantaneous steady state we must have $\dot{P}_a(t) = 0$, for all a . Thus, we have the

detailed balance condition

$$\frac{\sum_i \Gamma_i(t_s) \langle a | \bar{A}_i^\dagger(t_s) \bar{A}_i(t_s) | a \rangle P_a(t_s)}{\sum_i \sum_b \Gamma_i(t_s) |\langle a | \bar{A}_i(t_s) | b \rangle|^2 P_b(t_s)} = 1, \quad (5.34)$$

where t_s is the time at which the system comes to the steady state. From Eq. 5.32 and 5.34, we arrive at the following condition

$$D(t_s) = \frac{\Gamma_{dis}(t_s) P_a(t_s)}{\Gamma_{abs}(t_s) P_b(t_s)} = 1, \quad (5.35)$$

where $P_{a,b}(t) = \frac{1}{2}(1 \pm \sqrt{(\rho_{11}(t) - \rho_{22}(t))^2 + 4|\rho_{12}(t)|^2})$ are the eigenvalues of the system density matrix. Any deviation of $D(t)$ from its steady state value, implies that the system has not attained a steady state at that instant of time. The magnitude of such deviations may be regarded as a measure of how far away the system is from equilibrating. In the following we study the time dynamics of deviations from the detailed balance condition Eq. 5.35.

From Fig. 5.5, we observe that the deviations from detailed balance condition are quite persistent in the low temperature limit. In the opposite limit, as we go on increasing the bath temperature, Fig. 5.5 shows that the fluctuations in deviation from the detailed balance condition increasingly tend to damp down. In the limit of a completely unpolarized bath, the detailed balance condition is met if the system size is large enough. For an initially coherent central qubit, any study of approach towards steady state has to also take the coherence dynamics into account. In the very low temperature limit, the value of quantum coherence (Fig. 5.1(a)) is encapsulated within a narrow band whose width does not decay much over time. The persistence of coherence in this case implies the deviations are further away from $D(t) = 1$ than in Fig. 5.5. In the opposite limit of a high temperature bath, quantum coherence dies down very quickly, as seen in Fig. 5.1(a). This explains why, just like Fig. 5.5, $D(t)$ again approaches 1 in Fig. 5.6. In the intermediate regime, as we increase the temperature, the approach towards $D(t) = 1$ becomes faster.

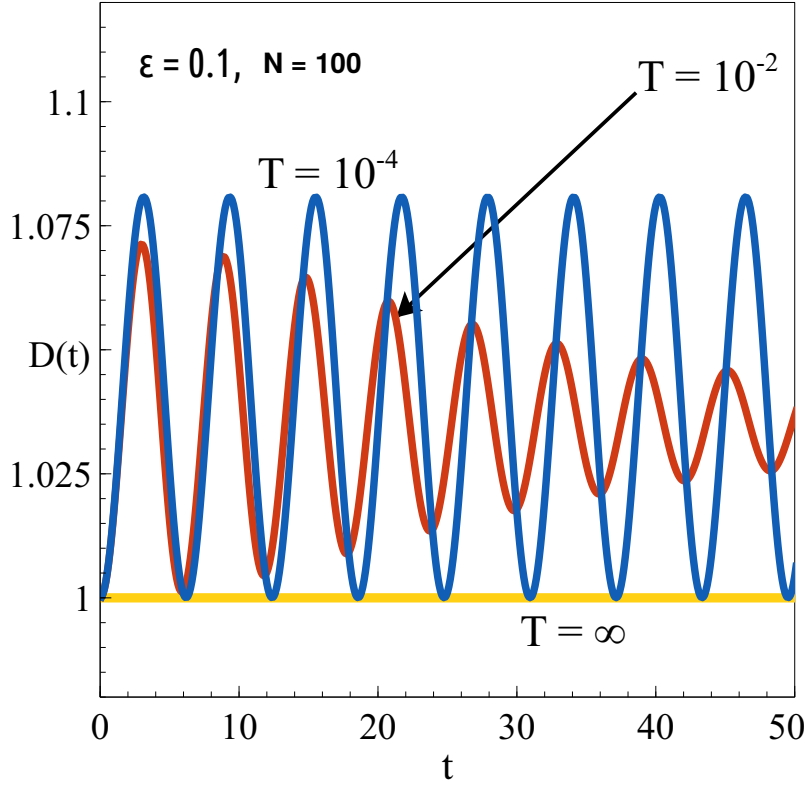


Figure 5.5: Variation of $D(t)$ with time, keeping temperature T as a parameter. $\rho_{11}(0) = 0.5, \rho_{12}(0) = 0$.

If the system-bath coupling strength is very weak, we see from Fig. 5.7 that the deviation of $D(t)$ from unity is very small. This is understandable because as the system-bath interaction gets weaker, the change in the state of the system due to the exposure of bath interaction becomes slower and the process becomes more and more quasi-static. Hence, the system remains close to its steady state. As we go on increasing the strength of the interaction, the fluctuations in population levels increase, implying that the deviation from detailed balance condition also increases which is confirmed in Fig. 5.7. With increasing the bath size, we see from Fig. 5.8 that deviations from detailed balance condition becomes smaller and smaller. This is fully consistent with the observation for many physical systems that energy exchange and consequent thermalization of a system is better facilitated by having a large bath rather than a small ancilla attached to it.

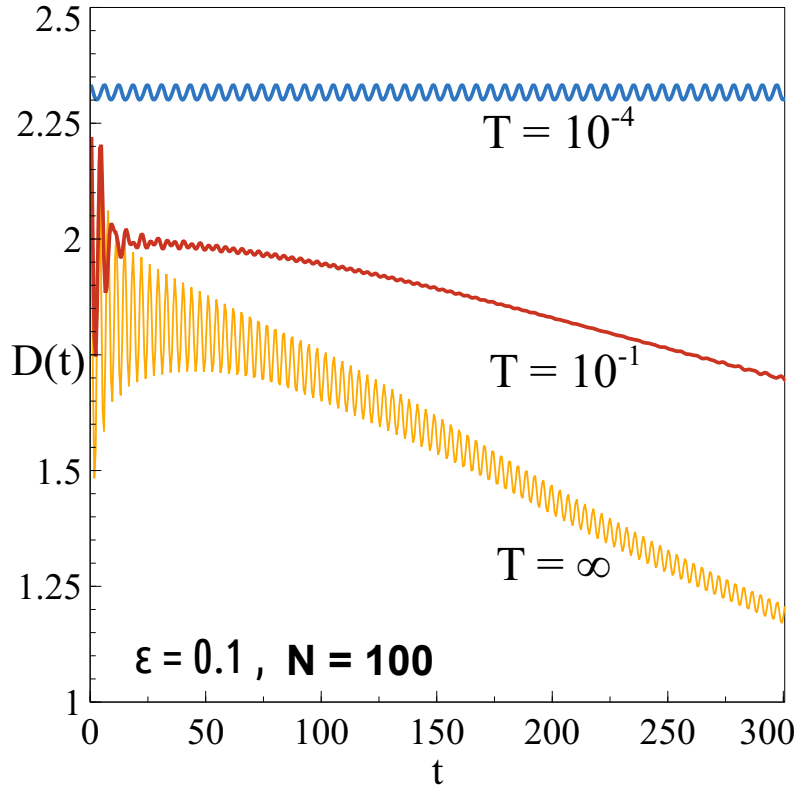


Figure 5.6: Variation of $D(t)$ with time, keeping temperature T as a parameter. $\rho_{11}(0) = 0.5$, $\rho_{12}(0) = 0.2$.

5.3.2 Irreversible Entropy production

Here we investigate how this system approaches towards a steady state from another thermodynamic perspective, i.e. the phenomenon of irreversible entropy production (IEP). The entropy production rate is formally defined as the negative rate of change of relative entropy between the instantaneous state and the steady state, i.e., $\Sigma(t) = -\frac{d}{dt}S(\rho(t)||\rho_{st})$. For an ideal Markovian evolution, $\Sigma(t)$ is always positive [150]. This happens for few ideal situations and in general is not satisfied.

The rate equation 5.33 can be compactly represented as $\dot{P}_a(t) = \sum_b \mathcal{L}_{ab}P_b(t)$, with

$$\mathcal{L} = \begin{pmatrix} -\Gamma_{dis}(t) & \Gamma_{abs}(t) \\ \Gamma_{dis}(t) & -\Gamma_{abs}(t) \end{pmatrix}.$$

The entropy of the system is defined as $S(t) = -\sum_b P_b(t) \ln P_b(t)$. By differentiating $S(t)$

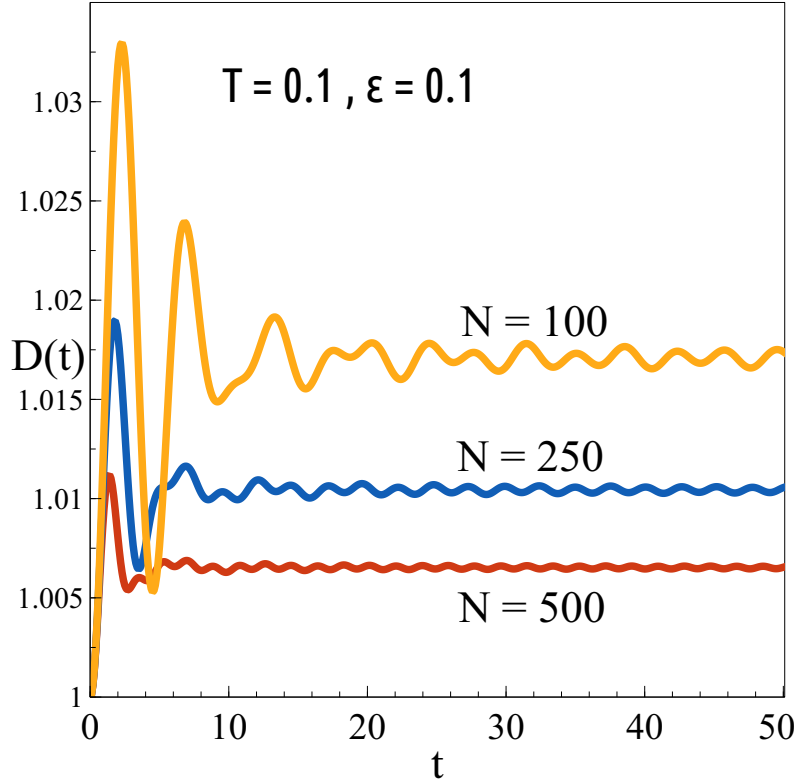


Figure 5.7: Variation of $D(t)$ with time, keeping interaction strength ϵ as a parameter. $\rho_{11}(0) = 0.5, \rho_{12}(0) = 0$.

with respect to time, it can be easily shown that

$$\begin{aligned} \dot{S}(t) &= \sum_{ab} \mathcal{L}_{ab} P_b(t) \ln \left(\frac{\mathcal{L}_{ab} P_b(t)}{\mathcal{L}_{ba} P_a(t)} \right) - \sum_{ab} \mathcal{L}_{ab} P_b(t) \ln \left(\frac{\mathcal{L}_{ab}}{\mathcal{L}_{ba}} \right), \\ &= \Sigma(t) + \Phi(t). \end{aligned} \quad (5.36)$$

The first term in the right hand side can be identified as the entropy production rate $\Sigma(t)$ and the second term $\Phi(t)$ defines the effective rate at which entropy is transferred from the environment to the system. For the particular central spin system considered in this paper, the IEP rate is given by

$$\Sigma(t) = (\Gamma_{dis}(t) P_a(t) - \Gamma_{abs}(t) P_b(t)) \ln \left(\frac{\Gamma_{dis}(t) P_a(t)}{\Gamma_{abs}(t) P_b(t)} \right). \quad (5.37)$$

We see from 5.37 that IEP rate is related to $D(t)$ and at the time (t_s) when system obeys the detailed balance condition, we have $\Sigma(t_s) = 0$. We also see from the expression of

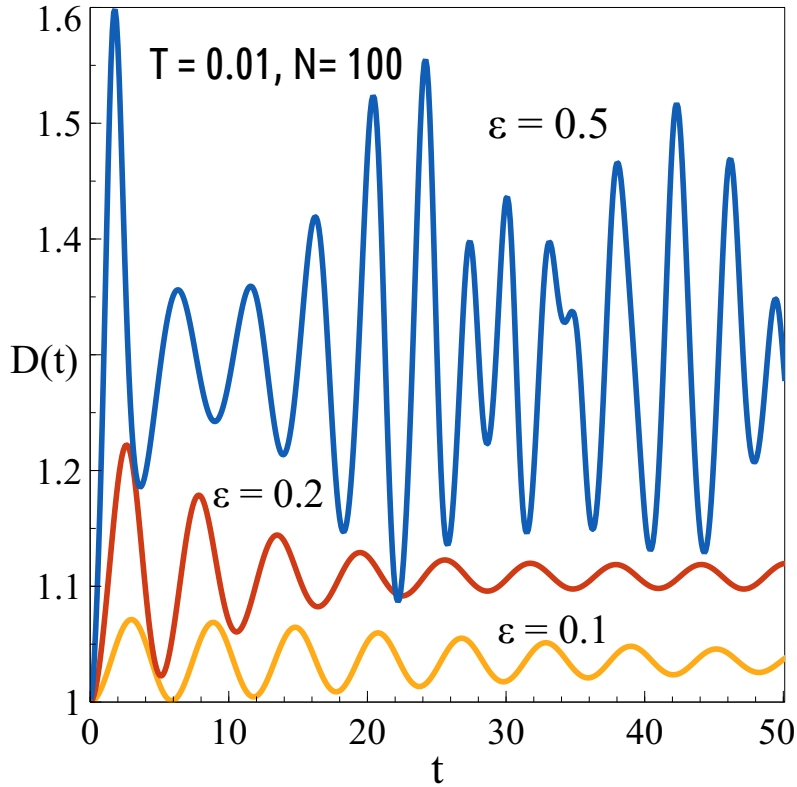


Figure 5.8: Variation of $D(t)$ with time, keeping N as a parameter. $\rho_{11}(0) = 0.5, \rho_{12}(0) = 0$.

IEP rate that for Markovian situation (i.e. $\Gamma_{dis}(t), \Gamma_{abs}(t) \geq 0$), it will always be non-negative. This behaviour is illustrated in Fig. 5.9. Whenever the irreversible entropy production rate $\Sigma(t)$ is negative, the absorption and dissipation rates are also negative and vice versa in the time span we probed. Since negativity of at least one Lindblad coefficient $\Gamma(t)$ is a necessary and sufficient condition [65] for non-Markovianity, this leads us to conclude that whenever this system is non-Markovian, a negative IEP rate $\Sigma(t)$ is obtained. While the negativity of IEP rate at any point in the dynamics necessarily implies that the dynamics is non-Markovian, the opposite is not true in general. However, in this illustration we note that the opposite is also true. If the bath temperature is very low, we have already seen from Fig. 5.1(a) that the quantum coherence of the central spin qubit persists for a long time, resulting in persistent deviations from the steady state detailed balance condition as depicted in Fig. 5.5. Therefore, it is expected that the IEP rate will also fluctuate and not show any sign of dying down to zero. This is indeed captured in

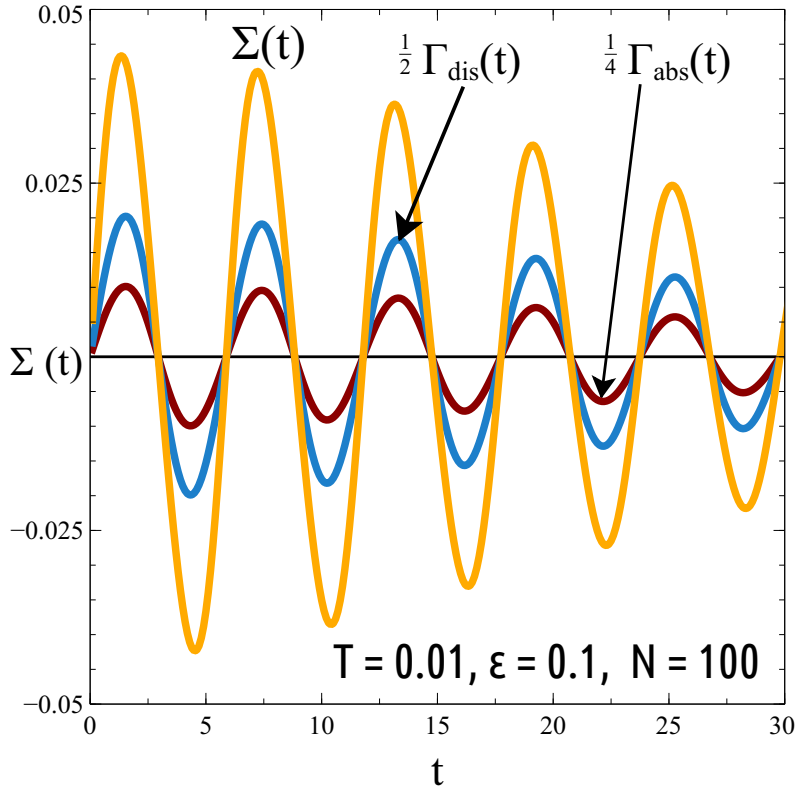


Figure 5.9: Variation of IEP rate $\Sigma(t)$ and Lindblad coefficients for absorption $\Gamma_{abs}(t)$ and dissipation $\Gamma_{dis}(t)$ with time t . Initial state $\rho(0)$ is chosen as $\frac{4}{5}|1\rangle\langle 1| + \frac{1}{5}|1\rangle\langle 0| + \frac{1}{5}|0\rangle\langle 1| + \frac{1}{5}|0\rangle\langle 0|$.

Fig. 5.10. In the opposite limit, as we go on increasing the bath temperature, as seen Fig. 5.5, the approach towards a steady state becomes quicker. This is again confirmed in Fig. 5.10, where the fluctuations in IEP rate die down more and more quickly for higher temperatures. As we have already observed in Fig. 5.8, the approach towards a steady state through exchange of energy between the system and the bath is quicker for a larger bath. This is again confirmed in Fig. 5.11 which shows the IEP rate becoming smaller and smaller as we increase the bath size. The period of fluctuations also diminish with increasing bath size.

5.4 Summary

- The exact finite temperature dynamics of the central spin model is studied.

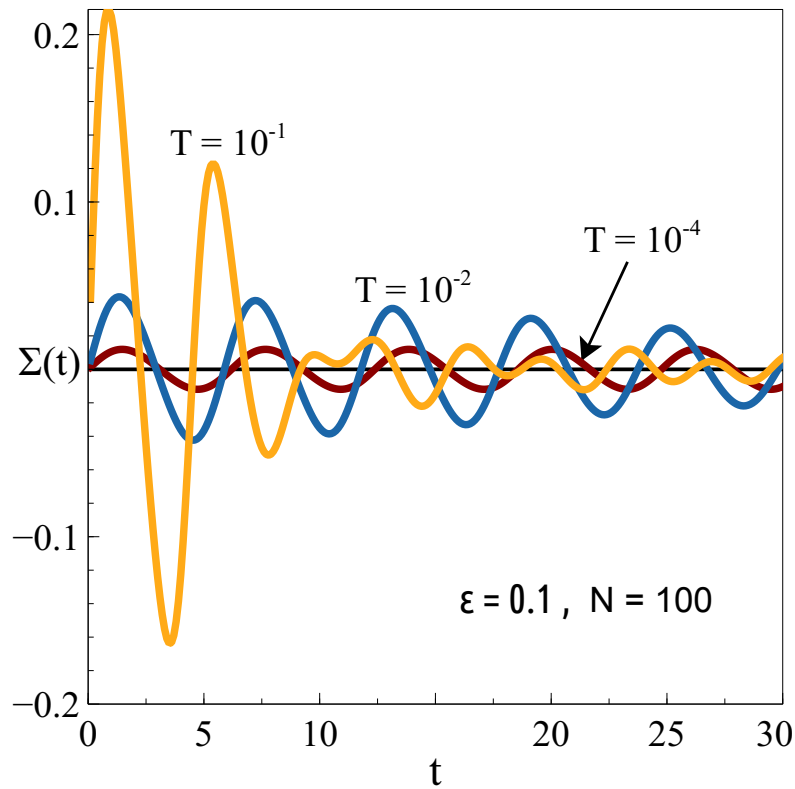


Figure 5.10: Variation of IEP rate $\Sigma(t)$ with time t for different bath temperatures. Initial state $\rho(0) = \frac{4}{5}|1\rangle\langle 1| + \frac{1}{5}|1\rangle\langle 0| + \frac{1}{5}|0\rangle\langle 1| + \frac{1}{5}|0\rangle\langle 0|$.

- Quantum master equation of the Lindblad type is derived.
- A resonance condition is obtained for the persistence of coherence in the long-time averaged state.
- Irreversible entropy production rate, and the deviation from ergodicity, as measured by trapped information, and departure from the detailed balance conditions have been thoroughly studied.

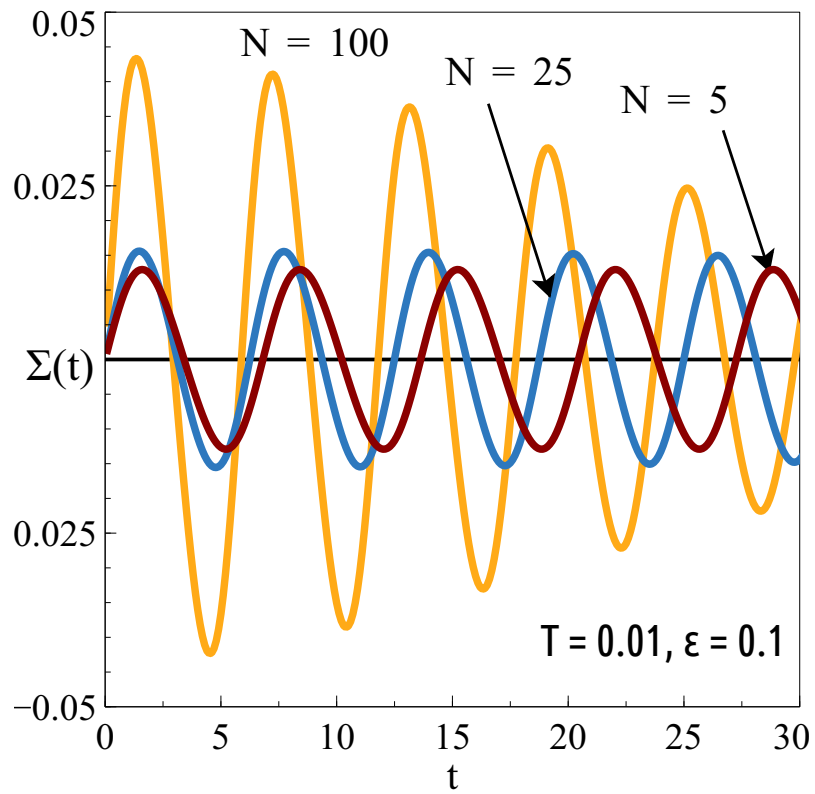


Figure 5.11: Variation of IEP rate $\Sigma(t)$ with time t for different number of bath spins. Initial state $\rho(0) = \frac{4}{5}|1\rangle\langle 1| + \frac{1}{5}|1\rangle\langle 0| + \frac{1}{5}|0\rangle\langle 1| + \frac{1}{5}|0\rangle\langle 0|$.

Quantum speed limit constraints on absorption refrigerators

1

In the last two chapters, we have analyzed the effect of a non-Markovian thermal bath on the preservation of quantum features of a system. In this chapter, we shall be concerned with the opposite question - viz, how does a genuinely quantum mechanical aspect of dynamics affect the performance of a thermal machine ?

In contradistinction with the implicit grounding of classical thermodynamics on a deterministic dynamical model, small scale thermal machines with constituents obeying laws of quantum theory have only recently come within our purview [189, 190]. However, these quantum machines still run up against the Carnot bound and barring non-thermal reservoirs like coherent [191] or squeezed baths [192, 193, 194, 195], generally fail to surpass it. Yet, the Carnot bound, attainable only through an infinitely slow process, is of limited practical utility compared to the performance of thermal devices at finite power. Classically, a bound on the efficiency at maximum power for cyclic thermal engines[196,

¹This chapter is based on the paper "*Quantum speed limit constraints on a nanoscale autonomous refrigerator*", published in Physical Review E, **97**, 062116 (2018).

197, 198] and refrigerators [199, 200, 201] was obtained in several works, as a figure of merit more relevant to practical scenarios. Investigations on finite time cyclic thermodynamic processes for quantum thermal machines [202, 203, 204] have already provided crucial physical insight on topics ranging from the origin of friction [205, 206, 207, 208] in thermal processes to the third law of thermodynamics [209, 210].

In this chapter, we shall work with self-contained thermal machines where the energy required to perform a task, e.g. cooling a cold bath, is provided by a third bath, thus requiring no external control. Motivated by algorithmic cooling, such a quantum absorption refrigerator (QAR) was proposed in [98], which provides the basis for our investigation. Numerous other proposals of QAR have already been put forward [211, 212, 213, 214], and experimental realization has been recently achieved in ion trap systems [215]. Depending upon the choice of initial parameters, such a setup at its steady state may be shown to act as a refrigerator.

The key motivation to the work presented in this chapter is the following - in addition to finding the steady state performance of such refrigerators, one should also consider how long it takes for the system to reach the steady state. If the system cools very reliably at steady state but only gets there very slowly, it is of limited utility. In this paper, we seek to understand the behaviour of QAR conditioned through the intrinsic restriction to evolution of a quantum system through its state space. The latter feature, known as the quantum speed limit is a fundamental feature of quantum dynamics and finds several applications in quantum computation, control theoretic settings and in the study of shortcut towards adiabaticity (See, for example, Ref. [216]. and references therein for an overview). To this end, we introduce and analyze a figure of merit, called the “*bounding second order cooling rate*” (*BSOCR*). This is defined as the product of the equilibrium cooling rate and the maximum possible speed of attaining equilibrium. We link the proposed figure of merit with the transient features of the refrigerator and go on to illustrate the dependence of BSOCR on various system parameters. We shall show that BSOCR increases linearly

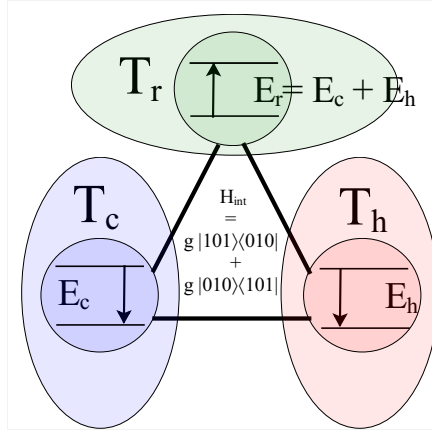


Figure 6.1: Schematic diagram of the absorption refrigerator model used in this work.

with the coupling strength. We shall also demonstrate that the presence of quantumness in the form of initial coherence in the system can boost the value of BSOCR. This is followed up by an investigation of the figure of merit vis-a-vis the refrigeration efficiency. We show that in the high temperature limit and subject to other specific conditions, we can recover an expression for efficiency at maximum value of BSOCR which scales similarly to the Curzon-Ahlborn bound.

6.1 Absorption refrigerator at steady state

We consider the model of three qubit absorption refrigerator introduced in Ref. [98]. A schematic diagram of the model is furnished in Fig. 6.1 above. The three qubits constituting the refrigerator are coupled to three different baths at different temperatures. The first qubit which is the object to be cooled, is coupled to the coldest bath at temperature T_c . The second qubit which takes energy from the first qubit and disposes into the environment, is coupled to a hotter bath at temperature T_r . The third and final qubit which provides the free energy for refrigeration is coupled to the hottest bath at temperature T_h . Here $T_c \leq T_r \leq T_h$. Without loss of generality, the ground state energy of all the qubits are considered

to be zero and the excited state energy of the i -th qubit is E_i , where $i \in \{c, r, h\}$. The free Hamiltonian of the combined system is $H_0 = \sum_{i \in \{c, r, h\}} E_i |1\rangle_i \langle 1|$. In thermal equilibrium the qubits are in the corresponding thermal states $\tau_i = r_i |0\rangle \langle 0| + \bar{r}_i |1\rangle \langle 1|$, where

$$r_i = (1 + e^{-\beta E_i})^{-1}, \quad (6.1)$$

is the probability of the i -th qubit to be in the ground state and $\bar{r}_i = 1 - r_i$. Here β is the inverse temperature $1/T$. The total system is initially in a product state of locally thermal qubits $\rho_0 = \tau_c \otimes \tau_r \otimes \tau_h$. The qubits interact via the interacting hamiltonian $H_{int} = g(|101\rangle \langle 010| + |010\rangle \langle 101|)$. Here the order of the qubits is c, r, h which is maintained throughout the chapter unless otherwise mentioned. The interaction strength g is taken weak enough compared to the energy spacings E_i , i.e., $g \ll E_i$, so that the energy levels and the energy eigenstates of the combined system are almost unaltered and the temperature of the each qubit can be defined neglecting the interaction energy [98]. The total Hamiltonian of the combined system is thus given by

$$H = \sum_{i \in \{c, r, h\}} E_i |1\rangle_i \langle 1| + g(|101\rangle \langle 010| + |010\rangle \langle 101|). \quad (6.2)$$

As the qubits are coupled with heat baths at each time step, we shall take the simplifying assumption that there is a finite probability that it will thermalize. Suppose p_i is the probability per unit time that the i -th qubit will revert back to its thermal state. Then the evolution of the combined system is given by the following master equation

$$\frac{\partial \rho}{\partial t} = -i[H, \rho] + \sum_{i \in \{c, r, h\}} p_i (\tau_i \otimes \text{tr}_i \rho - \rho). \quad (6.3)$$

It is necessary to mention that this master equation is valid only in the perturbative regime where the simultaneous thermalization of more than one qubit can be neglected. The steady state refrigeration with the aforementioned model has been demonstrated in great detail in Ref. [98, 217]. The steady state solution for this master equation, as obtained in

Ref. [217], is given as

$$\rho_f = \tau_c \otimes \tau_r \otimes \tau_h + \gamma \sigma_{crh}, \quad (6.4)$$

where

$$\begin{aligned} \sigma_{crh} = & \left(Q_{rh} Z_c \tau_r \tau_h + Q_{ch} \tau_c Z_r \tau_h + Q_{cr} \tau_c \tau_r Z_h \right. \\ & \left. + q_c \tau_c Z_{rh} + q_r \tau_r Z_{ch} + q_h Z_{cr} \tau_h + Z_{crh} + \frac{q}{2g} Y_{crh} \right). \end{aligned} \quad (6.5)$$

Here, $Y_{crh} = i|101\rangle\langle 010| - i|010\rangle\langle 101|$ and $Z_{crh} = |010\rangle\langle 010| - |101\rangle\langle 101|$, $Z_{ij} = \text{tr}_k Z_{ijk}$, where $\{i, j, k\} \in \{c, r, h\}$ and q_i and Q_{jk} , are given as follows $q_i = \frac{p_i}{q-p_i}$, $Q_{jk} = \frac{p_j q_k + p_k q_j}{q-p_j-p_k}$, where $q = p_c + p_r + p_h$. The parameter γ in Eq. 6.4 is given by

$$\gamma = \frac{-\Delta}{2 + \frac{q^2}{2g^2} + \sum_i q_i + \sum_{jk} Q_{jk} \Omega_{jk}} \quad (6.6)$$

where $\Delta = r_1(1-r_2)r_3 - (1-r_1)r_2(1-r_3)$, $\Omega_{jk} = r'_j(1-r'_k) + (1-r'_j)r_k$. Here $r'_i = (1-r_i)$ for $i = r$, otherwise $r'_i = r_i$. The cooling rate for the cold bath is given as

$$Q_c = q\gamma E_c, \quad (6.7)$$

which clearly shows that the machine acts as a refrigerator only when $\gamma > 0$. It has been shown that the efficiency η of this refrigerator is equal to E_c/E_h [217].

6.2 Quantum speed limit

Quantum evolution for a closed system is a unitary map. It has been shown that the fluctuation [218, 219] or the average value [220, 221] of the generator of such maps determines the maximum rate of unitary evolution of a quantum system through the corresponding state space, giving rise to the concept of a limiting speed for dynamical evolution. For

pure quantum states, this speed of evolution was introduced by Anandan and Aharonov [219] utilizing the Fubini-Study metric, with subsequent works [222, 223] building on the concept. Generalizations for mixed states in the case of unitary evolutions were proposed [23] and tightness of bounds found earlier were proved in some cases [224]. For a generalized quantum evolution characterized by CPTP maps, it is possible to find similar speed limits [225, 226, 227, 228, 229]. In particular, for a Markovian channel on an open quantum system expressed via a dynamical subgroup \mathcal{L} , the following lower bound on the time $t_{\text{evolution}}$ required for evolution of a quantum system from initial state ρ_0 to a state ρ_f was given in Ref. [230] as

$$t_{\text{evolution}} \geq \frac{|\cos \theta - 1| \text{tr} \rho_0^2}{\sqrt{\text{tr} (\mathcal{L}^\dagger \rho_0)^2}} = \tau, \quad (6.8)$$

where $\theta = \cos^{-1} \frac{\text{tr}(\rho_0 \rho_f)}{\text{tr}(\rho_0^2)}$ is expressed in terms of relative purity between the initial and the final state. Thus, $1/\tau$ can be interpreted as the maximum speed of the evolution. In this paper, using this maximum speed of evolution, we show how the existence of a quantum speed limit constrains the performance of the QAR.

6.3 Effects on the performance of quantum refrigerator from quantum speed limit

In this section, we establish a link between the cooling rate of the QAR at its steady state and the minimum time that it takes to reach the steady state. We define the novel figure of merit, i.e., the product of the steady cooling power of the QAR and the maximum speed of evolution to the steady state as

$$\chi = \frac{Q_c}{\tau}. \quad (6.9)$$

Note that, for better performance, we need higher χ , i.e., higher cooling rate as well as faster evolution to the steady state. Interestingly, we observe that there lies a trade-off between these two desired criteria. It will be interesting to explore in detail how the performance of steady QAR depends on χ , as well as how χ itself depends on the system parameters. Before doing so, we would like to digress a bit towards transient refrigeration by QAR.

The efficiency and cooling rate in the transient regime by QAR have been extensively studied in Ref. [104]. The figure of merit χ is the upper bound on the temporal average of time derivatives of the instantaneous cooling rate. The latter quantity, say $P(t)$, is defined as $P(t) = \frac{dQ_c(t)}{dt}$, where $Q_c(t)$ is the instantaneous cooling rate. Now, the time average

$$\overline{P(t)} = \frac{1}{t_{\text{evolution}}} \int_0^{t_{\text{evolution}}} \frac{dQ_c(t')}{dt'} dt' = \frac{Q_c}{t_{\text{evolution}}} \leq \frac{Q_c}{\tau} = \chi, \quad (6.10)$$

justifying our assertion. Thus the time-derivative of the transient cooling rate, averaged over the entire duration of dynamics, is upper bounded by our figure of merit. The transient cooling rate is, of course, the amount of heat drawn from the bath per unit time during the transient regime. Thus, the time derivative of cooling rate may be argued as a second order time-derivative of the amount of heat drawn from the bath during transient dynamics. Since our figure of merit represents an upper bound on the average time-derivative of the transient cooling rate, we coin the term *bounding second order cooling rate (BSOCR)* for the figure of merit χ . To avoid any potential confusion for the reader, we emphasize that the exact expression for χ is homogeneous to Q_c , i.e., the steady cooling rate, and not to the time derivative of the transient cooling rate. The BSOCR can be expressed in terms of the initial state ρ_0 via (6.4), (6.6), and (6.8) as

$$\frac{Q_c}{\tau} = \frac{qE_c}{[\text{tr}(\rho_0 \sigma_{crh})] / \left[\sqrt{\text{tr}([H_{int}, \rho_0]^2)} \right]} \quad (6.11)$$

Using the equation above, we demonstrate the trade-off between the steady cooling power

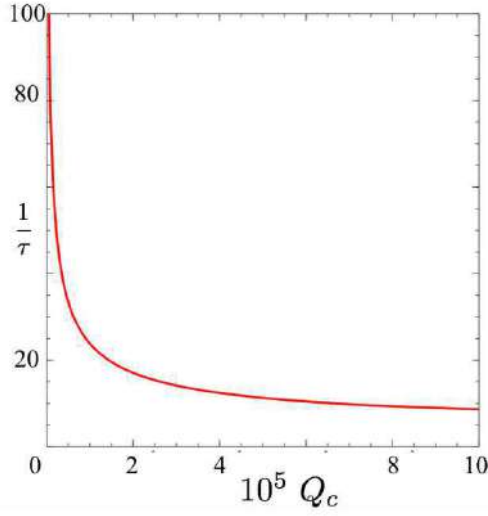


Figure 6.2: Demonstration that high equilibrium cooling power Q_c can come at the cost of slow evolution to equilibrium state. When all parameters other than g are fixed, steady cooling rate Q_c and the inverse of evolution time $1/\tau$, both functions of g , are parametrically plotted by varying the interaction strength g from 10^{-4} to 10^{-1} . The parameters are chosen as $E_c = 1$, $p_c = p_r = p_h = 0.1$, $\eta = 1$, $T_c = 1$, $T_r = 5$, $T_h = 10$.

and the maximum speed of evolution. As Q_c and $1/\tau$ both are function of the interaction strength g , we plot these quantities by varying the interaction strength g . Fig. 6.2 clearly demonstrates the trade-off between steady cooling power Q_c and maximum speed of evolution $1/\tau$, implying one can only get better cooling rate by compromising on the speed of evolution. This sets up the main crux of our investigation. It is also surprising that the performance of an autonomous quantum thermal machine at the steady state depends on the minimum time taken to reach the steady state. In the rest of the section, we shall study how the BSOCR χ depends on the parameters of the QAR. We shall also investigate whether initial quantumness can enhance the performance of the steady QAR.

Let us now note that the cooling rate Q_c is expressible explicitly in terms of the parameters of the model in the form

$$Q_c = \frac{\xi_1}{\Upsilon_1 + \frac{\Upsilon_2}{g^2}} \quad (6.12)$$

and the inverse speed limit, i.e. minimum time required for evolution to the steady state

is similarly expressible in the form

$$\tau = \frac{\xi_2/g}{\Upsilon_1 + \frac{\Upsilon_2}{g^2}}, \quad (6.13)$$

where the parameters $\Upsilon_1, \Upsilon_2, \xi_1, \xi_2$ all depend on the system parameters other than g . All these parameters are explicitly expressed as $\xi_1 = qE_c\Delta, \xi_2 = \frac{\Delta \text{tr}(\tau_c \tau_r \tau_h \sigma_{crh})}{\sqrt{2}(r_1 r_3 + r_2(r_1 + r_3 - 2r_1 r_3 - 1))}, \Upsilon_1 = 2 + \sum_i q_i + \sum_{jk} Q_{jk} \Omega_{jk}, \Upsilon_2 = q^2/2$. Thus, if other system parameters are kept fixed and only the interaction strength g is tuned, then the above parametric relation yields the following link between Q_c and τ , which is valid for any interaction strength.

$$\tau^2 = \left(\frac{\xi_2^2}{\xi_1} \right) Q_c - \Upsilon_1 \frac{\xi_2^2}{\xi_1^2} Q_c^2 \quad (6.14)$$

In case the first term of the RHS dominates over the second term, this immediately reveals that there exists a trade-off between the speed of evolution and the steady state cooling rate, which provides the rationale for investigating this tradeoff through our figure of merit. In general, if the cooling rate Q_c is small, the quadratic term is subleading, and the tradeoff is always observed. More specifically, in the scenarios we illustrated in the paper, the first term indeed dominates and this trade-off is observed. The expression for BSOCR may now be calculated explicitly. For the sake of simplicity, we assume equal reset probabilities, i.e., on putting $p_c = p_r = p_h = p$, the expression for BSOCR written in terms of the excited state probabilities $\{\bar{r}_i\}$ reduces to

$$\chi = \frac{3\sqrt{2}gpE_c f_1(\bar{r}_c, \bar{r}_r, \bar{r}_h)}{f_2(\bar{r}_c, \bar{r}_r, \bar{r}_h)}. \quad (6.15)$$

Where the numerator f_1 is given by $f_1 = \bar{r}_c r_h - \bar{r}_r (1 - \bar{r}_c - \bar{r}_h + 2\bar{r}_c \bar{r}_h)$, and the denominator f_2 is given by $f_2 = \frac{3}{2} - 3\bar{r}_h + \bar{r}_r(-1 + 3\bar{r}_h + \bar{r}_h^2) + \bar{r}_r^2(5 - 9\bar{r}_h + 4\bar{r}_h^2) + \bar{r}_c^2(\bar{r}_r + \bar{r}_r^2(4 - 8\bar{r}_h) + 8\bar{r}_r \bar{r}_h^2 - \bar{r}_h(1 + 4\bar{r}_h)) - \bar{r}_c(3 - 5\bar{r}_h + \bar{r}_h^2 + 6\bar{r}_r \bar{r}_h - 3\bar{r}_r + \bar{r}_r^2(9 - 16\bar{r}_h + 8\bar{r}_h^2))$.

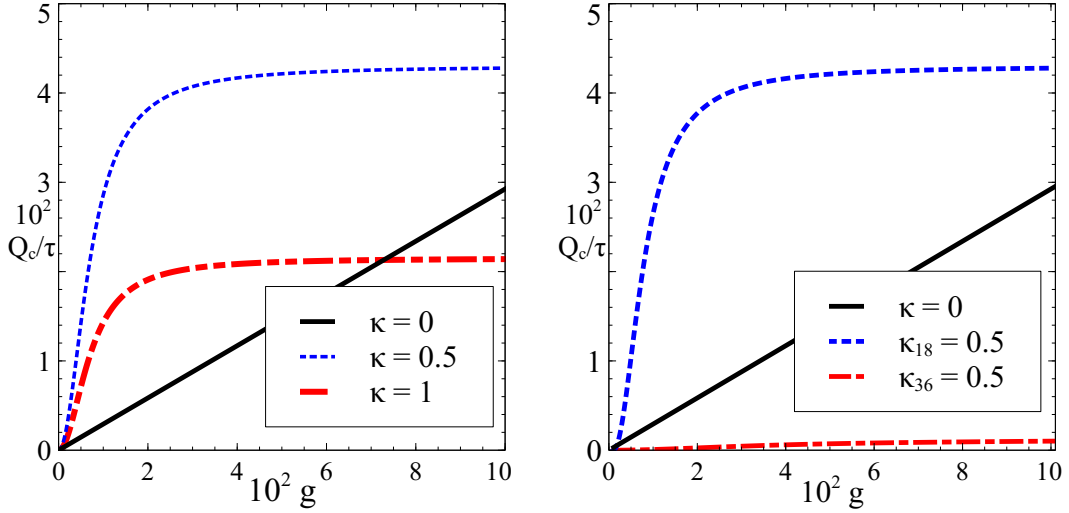


Figure 6.3: Variation of BSOCR with interaction strength g . *Left*: for different strengths of initial coherence κ applied to the $|000\rangle\langle 111|$ subspace as well as *Right* : for same amount of coherence in different subspaces viz., the $|101\rangle\langle 010|$, and the $|000\rangle\langle 111|$ subspaces. The reset probabilities have been taken as $p_c = p_r = p_h = p$ throughout. The other parameters are taken as $T_c = 1, T_r = 2, T_h = 10, \eta = 0.5, p = 0.05, E_c = 1$.

6.3.1 Dependence of the figure of merit on model parameters : role of initial coherence

In this subsection, we investigate the role the choice of model parameters, namely, the strength of thermalization, as well as the three qubit interaction, plays in determining the magnitude of the BSOCR. We know that the three-body interaction cools the cold qubit and draws heat from the cold bath. Hence, the more the interaction strength, the stronger the biasing facilitating the refrigeration. However, the cooling power depends in a complicated way on the strength g of the three-body interaction. On the contrary, from Eq. 6.11, when the resetting probabilities $\{p_i\}$ are equal), we observe that *the BSOCR grows linearly with the strength g of the three-body interaction H_{int} when the qubits are initialized in their respective local thermal states.*

In Fig. 6.3, we demonstrate the linear dependence of the BSOCR on the interaction strength. It will be interesting to inquire whether some initial coherence in the three qubit QAR can boost the BSOCR beyond the linear increase with the interaction strength g seen

above. We add an additional real off-diagonal part to the $|000\rangle\langle 111|$ and the corresponding adjoint element of the diagonal initial density matrix ρ_0 with the following magnitude

$$= \kappa \sqrt{\prod_{i=c,r,h} r_i \bar{r}_i} \quad ; \quad 0 \leq \kappa \leq 1. \quad (6.16)$$

. Now, the corresponding BSOCR is given by

$$\frac{Q_c}{\tau} = \frac{qE_c \sqrt{\text{tr}(-i[H, \rho_0 + \mu] - q\mu)^2}}{\left| \text{tr}(\rho_0 \sigma + \mu \sigma) - \frac{1}{\gamma} \text{tr}(\rho_0 \mu + \mu^2) \right|}, \quad (6.17)$$

where $\mu = \kappa \sqrt{\prod_{i=c,r,h} r_i \bar{r}_i} (|0_c 0_r 0_h\rangle\langle 1_c 1_r 1_h| + h.c.)$. Explicitly computing this expression yields the following expression for BSOCR

$$= 3pE_c \sqrt{\frac{N_1 p^2 + N_2 p + N_3}{D_1 p^4 + D_2 p^2 + D_3}}, \quad (6.18)$$

where $N_1 = 9 \text{tr} \mu^2$, $N_2 = -6 \text{tr} M \mu$, $N_3 = \text{tr} M^2$, $D_1 = 81 \frac{\Pi_2^2}{4g^4 \Delta^2}$, $D_2 = 18 \left(\Pi_1 + \frac{\lambda \Pi_2}{\Delta} \right) \frac{\Pi_2}{2g^2 \Delta}$, $D_3 = \left(\Pi_1 + \frac{\lambda \Pi_2}{\Delta} \right)^2$, $\lambda = 2 + \sum_i q_i + \sum_{jk} Q_{jk} \Omega_{jk}$, and the corresponding meta-parameters are given as $M = -i[H, \rho_0 + \mu]$, $\gamma = \frac{-\Delta}{\lambda + \frac{9p^2}{2g^2}}$, $\Pi_1 = \text{tr}(\rho_0 \sigma + \mu \sigma)$, $\Pi_2 = \text{tr}(\rho_0 \mu + \mu^2)$.

Clearly only N_3 and D_3 coefficients survive in the absence of initial coherence, i.e., $\kappa = 0$, thus giving rise to the linearity with p in that case. One may easily check now for $\mu = 0$ that $\frac{N_3}{D_3}$ is proportional to g^2 , thus confirming the linearity of BSOCR with interaction strength. In fact it may be shown that the BSOCR can be expressed in the following alternate way

$$= gE_c \sqrt{\frac{N'_1 g^2 + N'_2 g + N'_3}{D'_1 g^4 + D'_2 g^2 + D'_3}}, \quad (6.19)$$

with only the coefficients N'_3, D'_3 surviving in the special case of $\kappa = 0$, i.e., one with no initial coherence.

Fig. 6.3 confirms that the injection of initial coherence can indeed significantly increase the BSOCR. Thus, quantum coherence, already identified as a useful resource in quantum

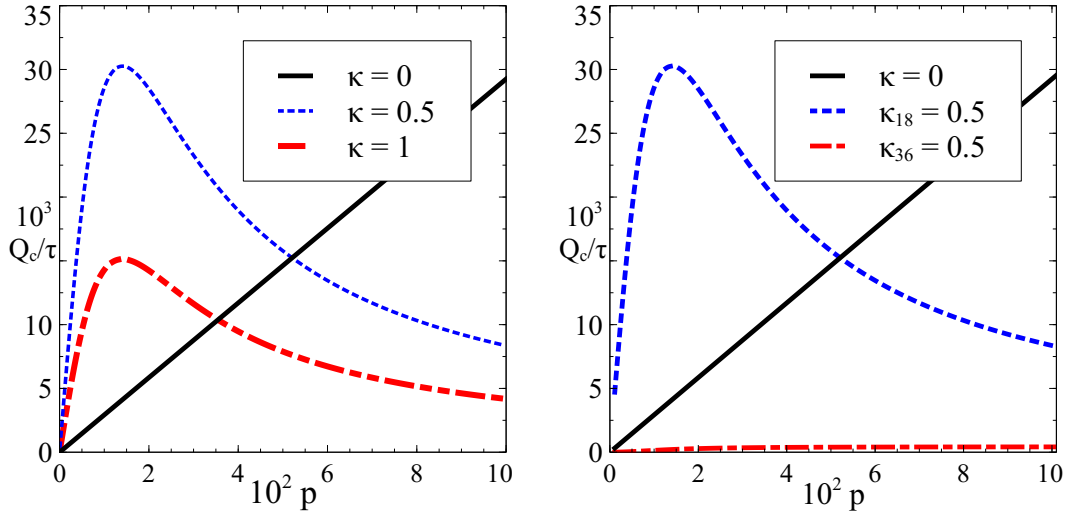


Figure 6.4: Variation of BSOCR with reset probability $p_c = p_r = p_h = p$. *Left* : for different strengths of initial coherence κ in the $|000\rangle\langle 111|$ subspace as well as *Right* : for same amount of coherence in different subspaces viz. the $|101\rangle\langle 010|$, and the $|000\rangle\langle 111|$ subspaces. The other parameters are taken as $T_c = 1, T_r = 2, T_h = 10, \eta = 0.5, g = 0.05, E_c = 1$.

information theory and quantum thermodynamics [231, 40, 232, 41], can enhance the performance of the QAR for a fixed interaction strength by reducing the minimum time taken to reach the steady state. It is worth mentioning that in Ref. [233], it has been pointed out that coherence can enhance the cooling of the cold qubit in the transient regime. In this work, we show that coherence can also enhance the performance of the steady heat machine. This is consistent with the assertion made in Ref. [227] that quantum coherence can serve to augment the speed limit for general dynamics. At this juncture, we want to emphasize that the present treatment of adding initial coherence to the system is different from having a bath which is coherent. The choice of adding coherence only to the $|000\rangle\langle 111|$ subspace may seem restrictive, but it can be shown that the nature of functional dependence of the BSOCR on the interaction strength or reset probabilities does not change whether we add the coherence in any other density matrix element, say, $|010\rangle\langle 101|$. However, the numerical value of the BSCOR depends on the subspace to which coherence is added. In Fig. 6.3, we show that as far as the efficacy of applying coherence to facilitate cooling is concerned, applying coherence to $|000\rangle\langle 111|$ subspace is far better than applying the same amount of coherence to $|010\rangle\langle 101|$ subspace.

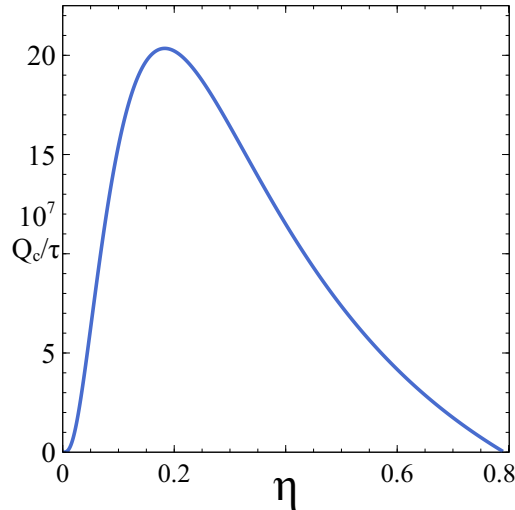


Figure 6.5: Variation of BSOCR with steady state efficiency η for fixed parameter values $p_c = 0.01$, $p_r = 0.02$, $p_h = 0.05$, $T_c = 1$, $T_r = 2$, $T_h = 10$, $E_c = 1$, $g = 0.01$.

Again, one can verify that this simple linear relation does not hold for the heat extracted from the cold bath. Now, let us start with a slightly more general case where the density matrix corresponding to the initial state ρ_0 possesses some non-local coherence, the latter typified by non-zero elements as in Eq. (6.16) in the earlier section. It is readily verified that the reduced states are still Gibbsian in their respective energy eigenbases. Fig. 6.4 shows that although the BSOCR increases rapidly with increasing reset probability if the p is very low, it decays considerably as we go on increasing p . However, we add the following note of caution - one can not indefinitely go on increasing the reset probability due to the weak coupling assumption used in the derivation of this master equation.

6.3.2 Efficiency at maximal figure of merit

For finite time thermodynamic cycles, finding the efficiency at maximum power is a well-motivated pursuit. For QAR models, in addition to finding the efficiency at maximum power [213], it makes sense to find the efficiency of the QAR when the BSOCR, the figure of merit encompassing both steady power characteristics and speed of evolution, is maximal. Let us now focus on how the BSOCR depends on the efficiency of the machine. For this model, the efficiency η is expressed as E_c/E_h . This allows us to explicitly com-

pute the BSOCR for any efficiency. We demonstrate in Fig. 6.5 that in a generic case, the BSOCR vanishes when there is no cooling as well as at the Carnot point, and attains its maximal value at some intermediate point. Exactly calculating the efficiency at maximal BSOCR in the most general case is quite cumbersome, therefore we restrict ourselves to the case of equal reset probabilities and use the expression for BSOCR derived earlier. In the high temperature limit and with the following assumptions, this allows us to derive the following crucial result.

If the reset probabilities p_c, p_r, p_h are equal and $T_h \gg T_r \gg T_c \gg E_c$ along with the condition that $\frac{T_c}{T_r} \approx \frac{T_r}{T_h}$, the efficiency at maximal BSOCR equals

$$\frac{T_c}{T_r} \left(1 - \sqrt{\frac{T_c}{T_h}} \right). \quad (6.20)$$

Proof : In the high temperature limit, the occupancies of the excited states of qubits are approximated by

$$\bar{r}_i \cong \frac{1}{2} - \frac{x_i}{4} - \frac{x_i^2}{8} + \frac{x_i^3}{4} \quad ; \quad x_i = \frac{E_i}{T_i}. \quad (6.21)$$

Putting them in the expression for BSOCR and weeding out higher order terms using the fact that $T_h \gg T_r \gg T_c \gg E_c$ leads to the following reasonably simple expression for the BSOCR

$$\frac{Q_c}{\tau} \cong \frac{3\sqrt{2}gpE_c}{3 - \frac{x_c x_r (x_c - x_r)}{3(x_c - x_r + x_h)}} = \frac{3\sqrt{2}gpE_c}{3 - \frac{1}{3}F}. \quad (6.22)$$

Now optimizing the BSOCR reduces to maximizing F . Putting $x_c = \frac{E_c}{T_c}$, $x_r = \frac{E_c}{T_r} \left(1 + \frac{1}{\eta} \right)$, $x_h = \frac{E_c}{\eta T_h}$, we differentiate F with respect to η to obtain the efficiency at maximal BSOCR. The solution to the equation $\frac{\partial F}{\partial \eta} = 0$ yields the following nontrivial solutions for efficiency at extremal BSOCR -

$$\eta_{opt} = \frac{-T_c^2 T_r + T_c^2 T_h - T_c T_r T_h \pm \sqrt{T_c^4 T_r^2 + T_c^3 T_r^2 T_h}}{2T_c^2 T_r - T_c T_r^2 - T_c^2 T_h + 2T_c T_r T_h - T_r^2 T_h}. \quad (6.23)$$

Applying the condition $T_h \gg T_r \gg T_c$, we now have the expression for efficiency at extremal BSOCR as

$$\eta_{opt} \cong \frac{T_c T_r T_h - T_c^2 T_h \mp \sqrt{T_c^3 T_r^2 T_h}}{(T_r - T_c)^2 T_h} = \frac{T_c}{T_r - T_c} \mp \frac{T_c T_r}{(T_r - T_c)^2} \sqrt{\frac{T_c}{T_h}}, \quad (6.24)$$

Noting that $T_r - T_c \approx T_r$, we arrive at the following expression for efficiency at optimal BSOCR

$$\eta_{opt} = \frac{T_c}{T_r} \left(1 \mp \sqrt{\frac{T_c}{T_h}} \right). \quad (6.25)$$

Now one can show that only the minus sign corresponds to the *maximal* BSOCR, taking into account the fact $\frac{T_c}{T_r} \sim \frac{T_r}{T_h}$. the other solution lies beyond the Carnot efficiency and consequently the efficiency at maximal BSOCR is given by $\frac{T_c}{T_r} \left(1 - \sqrt{\frac{T_c}{T_h}} \right)$ - thus completing the proof.

Now, let us mention that in the limit considered above, the Carnot efficiency for this refrigerator is given by

$$\eta_{Carnot} = \frac{T_c}{T_r} \left(1 - \frac{T_c}{T_h} \right). \quad (6.26)$$

We immediately see that the relation between Eq. 6.20 and Eq. 6.26 is remarkably similar to the relation between the expressions for Carnot bound and Curzon-Ahlborn (CA) bound for efficiency heretofore derived for various cyclic heat pumps [202, 199].

6.4 Summary

- A tradeoff in the steady state cooling power of an absorption refrigerator with the time required to reach the steady state is obtained.
- A new figure of merit is introduced, which takes into account both the steady state cooling power, as well as the minimal time required to reach the steady state configuration.
- The magnitude of the new figure of merit, called the BSOCR, may be significantly bolstered by the initial injection of quantum coherence.
- The expression for efficiency at maximal BSOCR is derived in the high temperature scenario, subject to suitable conditions. The expression bears a strong resemblance to the Curzon-Ahlborn expression for efficiency at maximal power.

Autonomous creation of quantum resources

1

In the previous chapter, we have seen how quantum features like the presence of a speed limit or the injection of quantum coherence impacts the performance of an autonomous thermal machine. In this chapter, we shall investigate how similarly conceived autonomous machines may allow us to create quantum resources. These are particularly useful since autonomous machines do not require precise time control. Completely sealing off quantum systems from the environment is very difficult anyway, therefore we may alternately ask - can we somehow use the environment as an ally instead of an impediment [234, 235] ? This broad area of research has received renewed attention in recent years with the advent of bath-engineering techniques as well as works on non-Markovian environments [236, 237, 238, 95, 239, 240, 241]. One particular realization in the recent past is of the fact that apart from heat baths, baths such as spin baths can be used to overcome the Landauer erasure energy cost[11, 242, 243], although a corresponding cost has to be paid in

¹This chapter is based on the paper "*Generating steady state quantum coherence and magic through an autonomous thermodynamic machine by utilizing a spin bath*", published in Physical Review A, **98**, 012102 (2018).

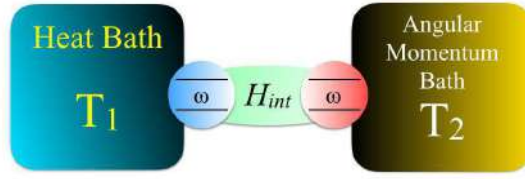


Figure 7.1: Schematic diagram of model used in the work.

terms of angular momentum. .

In this work, we show, in a self-contained model, how to impart quantum properties to the steady state of a qubit system interacting with a thermal bath utilizing an angular momentum bath interacting with another qubit. We propose the setup and using a simple reset model, explicitly find the steady state configuration. This enables us to observe how non-classicality in the form of quantum coherence and magic builds up in the steady state. Simply equilibrating a qubit in the angular momentum bath instead of the heat bath may yield coherence in the energy eigenbasis, but may not yield magic. However, in the proposed setup, we shall show that the reduced qubit in its steady state may indeed have non-zero magic, i.e., be useful as ancilla for injection in the paradigm of stabilizer quantum computation.

7.1 Autonomous thermal machine

In statistical mechanics, a basic concept is that of the canonical ensemble, where a physical system exchanges energy with the environment to equilibrate. It can be shown using the MaxEnt principle that the population of equilibrium density matrix of the state which maximizes the information theoretic entropy for a given amount of average energy follows the Gibbs distribution with a potential-like parameter T , which we term as *temperature*. However, instead of energy, we can envision a situation where the system exchanges spin angular momentum along a specified direction, say \vec{k} . In this situation, again maximizing

the information theoretic entropy for a given amount of average spin angular momentum along \vec{k} -direction yields an equilibrium state which follows the Gibbs distribution with a potential-like parameter which plays a role similar to the role of temperature for heat baths. In this chapter, we shall loosely call this parameter as temperature of the angular momentum bath. However we warn the reader, that this *temperature* in this context, is to be understood as something different from the way temperature is used in the *usual* sense for thermal baths. It is natural to wonder about the theoretical as well as experimental basis for assuming such baths. Theoretically, the motivation comes chiefly from Vaccaro and Barnett's [242] pioneering work, showing such baths can give rise to Landauer erasure without energy cost. More recent resource theoretic works [243, 244, 245] consider even more general kinds of baths with any number of conserved charges, of which the bath proposed above is a very special case. Works on cyclic thermal machines between a thermal and a spin reservoir have also been performed [246]. However, practical realization of these baths seem to be rather difficult, as has been pointed out, for example, in [247]. Hence, we reserve comment on the actual practical realization of our model. In this context, we also note for clarity that the spin bath is *not* a thermal resource in the usual sense, and hence the quantumness generation procedure outlined in this work, although autonomous, is not altogether thermal. One compare and contrast this approach with another recent work [248].

7.1.1 Scheme and master equation

Let us now introduce the setup in Fig. 7.1. The first qubit is immersed in a heat bath of temperature T_1 , where the energy eigenbasis is along the z direction. The second qubit is immersed in a spin bath of temperature T_2 , where the spin angular momenta along x

direction are exchanged. The Hamiltonian corresponding to the first qubit is

$$H_1 = \frac{1}{2}\omega_1|1\rangle\langle 1|$$

and the Hamiltonian corresponding to the second qubit is

$$H_2 = \frac{1}{2}\omega_2|1\rangle\langle 1|$$

We also assume an energy swapping interaction $H_{int} = g(|01\rangle\langle 10| + |10\rangle\langle 01|)$

between the two qubits. We assume the resonance condition $\omega_1 = \omega_2 = \omega$. In subsequent calculations, we shall assume $\omega = 1$ without loss of generality. Thus the collective Hamiltonian reads as

$$H = H_1 \otimes \mathbb{I} + \mathbb{I} \otimes H_2 + H_{int} \tag{7.3}$$

The thermal state of a particle, immersed in the heat bath of inverse temperature $\beta_1 = 1/T_1$, now reads as

$$\tau_1 = \frac{1}{1 + e^{-\beta_1}}|0\rangle\langle 0| + \frac{e^{-\beta_1}}{1 + e^{-\beta_1}}|1\rangle\langle 1|$$

The corresponding equilibrium state of a particle, immersed in the spin bath of inverse temperature $\beta_2 = 1/T_2$, is given by

$$\tau_2 = \frac{1}{1 + e^{-\beta_2}}(|+\rangle\langle +| + |-\rangle\langle -|)$$

$$+| + \frac{e^{-\beta_2}}{1+e^{-\beta_2}}| - |$$

-(7.5)

During each small time interval δt of the dynamics, one of the qubits of the two qubit state $\rho_{12}(t)$ can thermalize back to its respective equilibrium configuration (that is, τ_1 for the first qubit and τ_2 for the second qubit) with probabilities p_1 and p_2 respectively. We assume that the probability of both the qubits equilibrating in δt interval is negligible. Thus, the master equation for the two qubits read as the following

$$\frac{d\rho_{12}(t)}{dt} = -i[H, \rho_{12}] + \sum_i p_i (\tau_i \otimes \text{tr}_i \rho_{12}(t) - \rho_{12}(t)) \quad (7.6)$$

In general, the steady state of a qubit immersed in a bath and oblivious to any other system, and the the state that the same qubit wants to revert to, *while* interacting with another system, may be different. This may be especially prominent if the qubit in question is coupled very strongly with the other qubit, when compared with the coupling with the bath. Thus, we shall restrict ourselves to the weak interaction strength, i.e., g being small, when using the above master equation. We have also assumed that the probability of both the qubits resetting back to their respective equilibrium configurations is too small, which means $p_1 p_2$ is quite small. The steady state ρ_{12}^{steady} is obtained by solving for vanishing right hand side of the evolution master equation 7.6. Since a general two-qubit density matrix has fifteen real parameters, this implies solving a system of linear equations with fifteen variables. However, the general expression for the steady state is algebraically quite cumbersome - therefore we shall state and use simplifying assumptions in the rest of the paper.

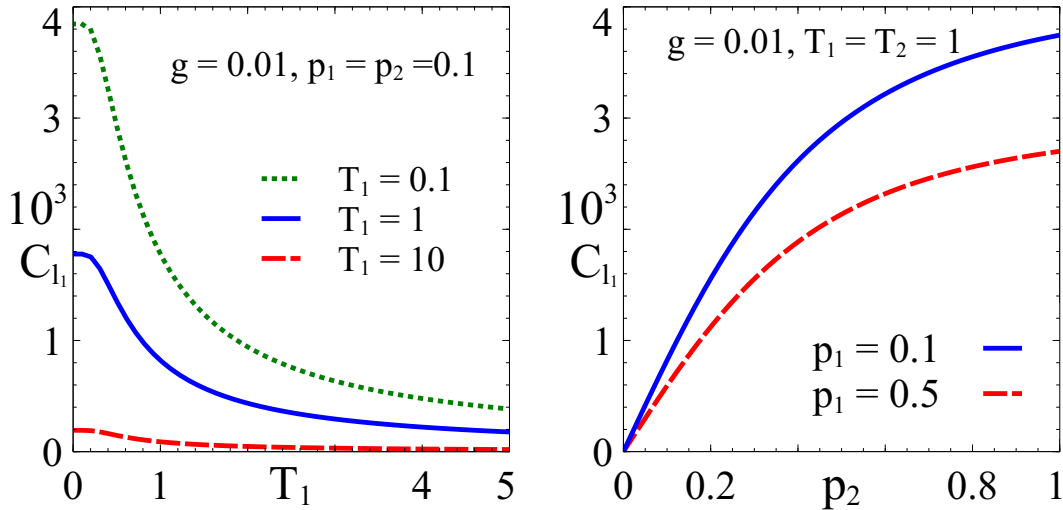


Figure 7.2: Dependence of the steady state coherence of the first qubit on the heat bath temperature T_1 (left) and the reset probability for the spin bath p_2 (right).

7.2 Quantum coherence generation in the reduced qubit

As we discussed in the first chapter of the thesis, quantum coherence is regarded as a genuinely quantum mechanical resource. From the perspective of autonomous quantum thermal machines, initial coherence is a resource for augmenting the performance of an absorption refrigerator, as we also saw in the previous chapter. The inverse problem of creating coherence in finite dimensional systems using thermal resources has also attracted recent attention [249, 248]. As we shall show below, the reduced steady state of the qubit attached to the heat bath is coherent in the energy eigenbasis. Thus, when the steady state is reached in our setup, if we simply strip the other components of the present model (except the heat bath and the attached qubit) away and replace them with the hot and cold heat baths of the quantum absorption refrigerator setup, we can benefit from the initial coherence in the absorption refrigerator setup.

From the general steady state solution, if one performs a perturbative expansion for small interaction strength g , the l_1 -norm of coherence in the reduced qubit attached to the heat

bath reads as

$$C_{l_1} = \frac{4gp_2}{\sqrt{(1+4p_1^2)(1+4p_2^2)}} \left| \tanh\left(\frac{1}{2T_1}\right) \tanh\left(\frac{1}{2T_2}\right) \right| + \mathcal{O}(g^2) \quad (7.7)$$

The first observation is that increased thermalization probability p_1 leads to a decrease of the steady coherence. The second observation is that for small thermalization probability p_2 , increasing it also increases the magnitude of steady coherence. However, as we go on increasing the reset probability p_2 , the magnitude of steady coherence asymptotically reaches a maximum. Regarding the bath temperatures, we observe that the magnitude of steady coherence is increased if the bath temperatures are low.

7.3 Generation of magic in the reduced qubit

Many fault-tolerant quantum algorithms use the so called *stabilizer operations*, i.e., unitary gates and measurements chosen from a specific set. It can be shown via the Gottesmann-Knill theorem, that these set of operations are efficiently simulable via classical means. Thus, for universal quantum computation, if one only allows for *stabilizer* operations, one must introduce additional ancilla states along with the original system. Stabilizer operations may then be performed over the larger Hilbert space consisting of the original system plus the ancilla to effectively implement non-stabilizer operations on the actual system. In order to facilitate non-stabilizer operations on the original system, the ancilla states must lie outside the convex hull of pure states, which are known as *stabilizer states*. States which satisfy this property are defined to be endowed with *magic*. Thus, just as quantum entanglement is the operational resource underlying the superiority of quantum communication protocols, *magic* is the resource for classically non-simulable gate implementation [54, 58]. Thus, creation of magic in a quantum system is vital for quantum technology. Indeed, if we simply immerse a qubit to the heat bath, it thermalizes

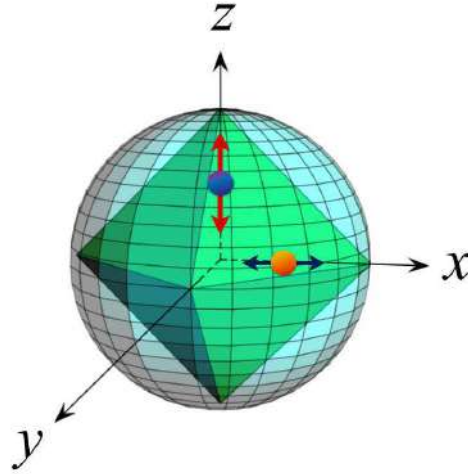


Figure 7.3: If a qubit state equilibrates on the z -axis of the Bloch sphere (blue blob) or on the x -axis of the Bloch sphere (golden blob) - the state lies within the stabilizer polytope. The first scenario is associated with the thermal state of the heat bath, the second with the equilibrium state of the angular momentum bath depicted in our model.

at an equilibrium state which lies on the z -axis of the Bloch sphere, i.e., always within the stabilizer polytope. More interestingly, if a qubit is immersed in the spin bath described above, then the steady state lies on the x -axis of the Bloch sphere, i.e., again within the stabilizer polytope, although it may be coherent in the energy eigenbasis. See Fig. 7.3 for an illustration. Nonetheless, we shall now show that the magic can be indeed imparted in the steady state of the qubit attached to the heat bath through our setup.

In the qubit case, the states which can *not* be used as ancilla to implement classically non-simulable gates, lie inside the convex polytope formed by the eigenvectors of the mutually unbiased operators σ_x , σ_y , and σ_z . Any state outside this so called *stabilizer* polytope is said to possess magic. In terms of the Bloch vector $\vec{r} = (r_x, r_y, r_z)$ of a quantum state, the condition for the state lying within the stabilizer polytope is when all the following inequalities are simultaneously met [56].

$$-1 \leq r_x \pm r_y \pm r_z \leq 1. \quad (7.8)$$

For qutrit and other higher prime power dimensional states, the negativity of the discrete

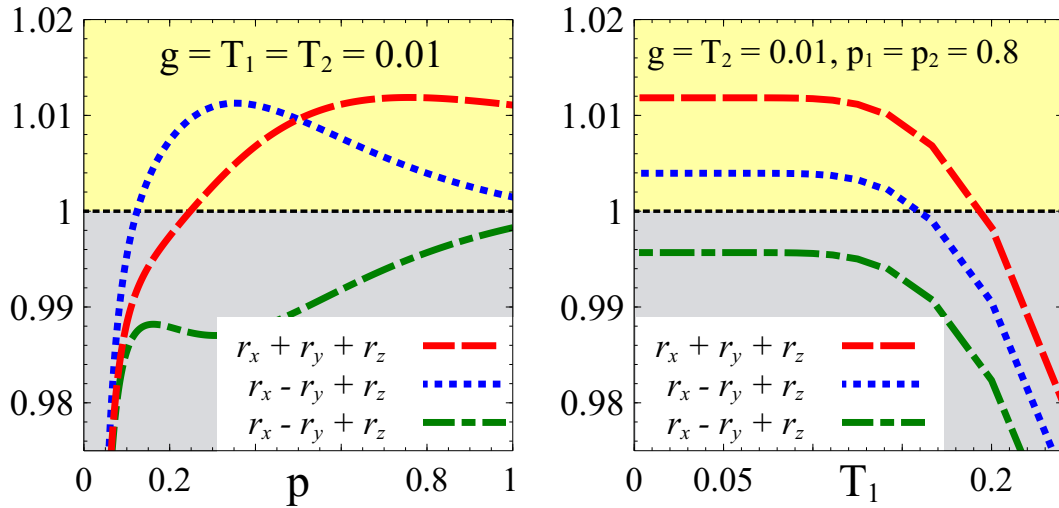


Figure 7.4: Values of linear functions of Bloch vector (cf. 7.8 of the reduced qubit attached to the heat bath vs. the reset probability $p_1 = p_2 = p$ (left) and the heat bath temperature T_1 (right). Any one of the curves falling in the pale yellow region indicates the presence of magic. If all three lines lie in the light grey region, that indicates the state is within the stabilizer polytope.

Wigner function is an analytically computable magic monotone. However, for qubits, the situation is less fortunate. While magic monotones like relative entropy of magic [54], robustness of magic [58] or semi-definite programming based measures [56] indeed exist in the qubit case - they are not amenable to simple analytical calculations. Thus, we would only investigate the condition for the existence of magic. Fig 7.4 depicts the results for the exact steady-state solution, which indicate that the above quantities in 7.8 can indeed exceed unity and thus create magic in the reduced qubit attached to the heat bath. Fig 7.4 also allows us to observe that as we go on increasing the heat bath temperature, the value of the quantities in 7.8 eventually stop exceeding unity. Thus there seems to be a critical temperature associated with the heat bath above which magic creation may not be possible in the reduced qubit attached to the heat bath.

Proving the above results from the full steady state solution, which is algebraically messy, is quite challenging. Instead, as a way of simplification, we will follow a perturbative approach, inspired by the fact that the quantum master equation 7.6 holds true if the interaction strength g is weak. From the general expression for the Bloch vectors of the qubit attached to the heat bath of temperature T_1 , we may write down the leading order

terms for the perturbation expansion for small g -

$$\begin{aligned}
r_x + r_y + r_z &= \tanh\left(\frac{1}{2T_1}\right) \left[1 + 4g \frac{p_2(-1 + 2p_2 + 2p_1 + 4p_1p_2) \tanh\left(\frac{1}{2T_2}\right)}{(1 + 4p_1^2)(1 + 4p_2^2)} + 2g^2 \frac{[-1 - 2p_2^2 - 4p_1(p_1 + 4p_1p_2)]}{p_1(p_1 + p_2)(1 + 4p_1^2)} \right] \\
r_x - r_y + r_z &= \tanh\left(\frac{1}{2T_1}\right) \left[1 + 4g \frac{p_2(1 + 2p_2 + 2p_1 - 4p_1p_2) \tanh\left(\frac{1}{2T_2}\right)}{(1 + 4p_1^2)(1 + 4p_2^2)} + 2g^2 \frac{[-1 - 2p_2^2 - 4p_1(p_1 + 4p_1p_2)]}{p_1(p_1 + p_2)(1 + 4p_1^2)} \right] \\
-r_x + r_y + r_z &= \tanh\left(\frac{1}{2T_1}\right) \left[1 + 4g \frac{p_2(-1 - 2p_2 - 2p_1 + 4p_1p_2) \tanh\left(\frac{1}{2T_2}\right)}{(1 + 4p_1^2)(1 + 4p_2^2)} + 2g^2 \frac{[-1 - 2p_2^2 - 4p_1(p_1 + 4p_1p_2)]}{p_1(p_1 + p_2)(1 + 4p_1^2)} \right]
\end{aligned}$$

Let us now concentrate on specific parameter domains to explicitly find out the condition for existence of magic. We begin with the assumption that the temperature T_2 is very low and assume further that the reset probabilities p_1 and p_2 are equal in magnitude and have the value, say, p . Under these conditions

$$r_x + r_y + r_z \approx \tanh\left(\frac{1}{2T_1}\right) \left[1 + 4gp \frac{4p^2 + 4p - 1}{(1 + 4p^2)^2} - g^2 \frac{1 + 6p^2 + 24p^4}{p^2(1 + 4p^2)^2} \right] \quad (7.10)$$

Noting that the condition $r_x + r_y + r_z > 1$ is sufficient for the existence of magic in the reduced qubit, we express this condition under the above assumptions as

$$1 + 4g \frac{p(4p^2 + 4p - 1)}{(1 + 4p^2)^2} - g^2 \frac{1 + 6p^2 + 24p^4}{p^2(1 + 4p^2)^2} > \coth\left(\frac{1}{2T_1}\right) \quad (7.11)$$

Let us now designate $f_1 = \frac{p(4p^2 + 4p - 1)}{(1 + 4p^2)^2}$, $f_2 = \frac{1 + 6p^2 + 24p^4}{p^2(1 + 4p^2)^2}$, and $\lambda = \coth\left(\frac{1}{2T_1}\right) - 1$, thus the

expression above is written as

$$g^2 - 4g\frac{f_1}{f_2} + \frac{\lambda}{f_2} < 0, \quad (7.12)$$

which yields the condition

$$\left(g - 2\frac{f_1}{f_2}\right)^2 < 4\frac{f_1^2}{f_2^2} - \frac{\lambda}{f_2} \quad (7.13)$$

Note that, it becomes possible to satisfy the above criteria, only if the right hand side of the above expression is positive. If the reset probabilities are fixed, this implies the existence of a threshold temperature of the hot bath, say T_{crit}^1 above which $r_x + r_y + r_z$ can never exceed unity. Similarly analyzing the conditions for $r_x - r_y + r_z$ and $r_y - r_x + r_z$ to exceed unity, give rise to threshold temperatures T_{crit}^2 , and T_{crit}^3 respectively. The actual threshold temperature of the heat bath beyond which magic can not be generated is thus the maximum of these three threshold temperatures, i.e.,

$$T_{\text{crit}} = \max \left[T_{\text{crit}}^1, T_{\text{crit}}^2, T_{\text{crit}}^3 \right], \quad (7.14)$$

where we have assumed $g_1 = \frac{p(1+4p-4p^2)}{(1+4p^2)^2}$, $h_1 = \frac{p(4p^2-4p-1)}{(1+4p^2)^2}$, and the critical temperatures are explicitly expressed as

$$T_{\text{crit}}^1 = \frac{1}{\ln\left(1 + \frac{f_2}{2f_1^2}\right)}, T_{\text{crit}}^2 = \frac{1}{\ln\left(1 + \frac{f_2}{2g_1^2}\right)}, T_{\text{crit}}^3 = \frac{1}{\ln\left(1 + \frac{f_2}{2h_1^2}\right)}. \quad (7.15)$$

Fig. 7.5 illustrates that the critical temperature increases with the reset probability p . However, even if the temperature of the heat bath is less than T_{crit} , the interaction strength g must satisfy 7.13 or similar conditions for $r_x - r_y + r_z$ or $r_y - r_x + r_z$ for creation of magic. This effect is demonstrated in Fig. 7.5, which shows that the allowed range of interaction strength g steady decreases until it vanishes at the critical temperature T_{crit} .

Let us now explore the opposite limit, that is, the spin bath temperature T_2 being very high, and again make the simplifying assumption that $p_1 = p_2 = p$. We recall that, for

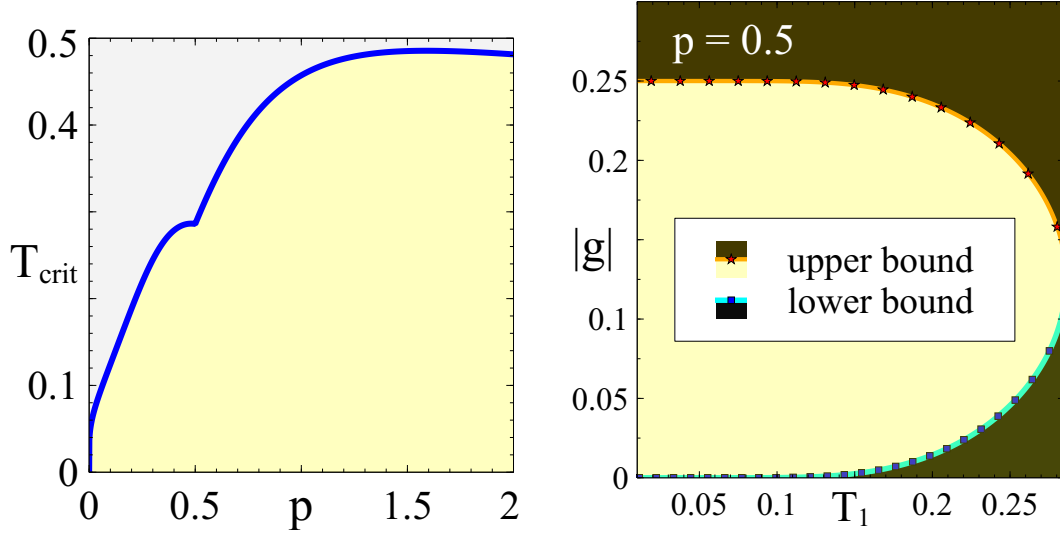


Figure 7.5: Magic creation in the limit of low spin bath temperature T_2 . Left : dependence of critical temperature T_{crit} on the reset probability $p_1 = p_2 = p$. Creation of magic is possible in the pale yellow region and impossible in the light gray region. Right : allowed interval for interaction strength g with respect to heat bath temperature T_1 for creation of magic. Creation of magic is possible in the pale yellow region and impossible in the dark brown region.

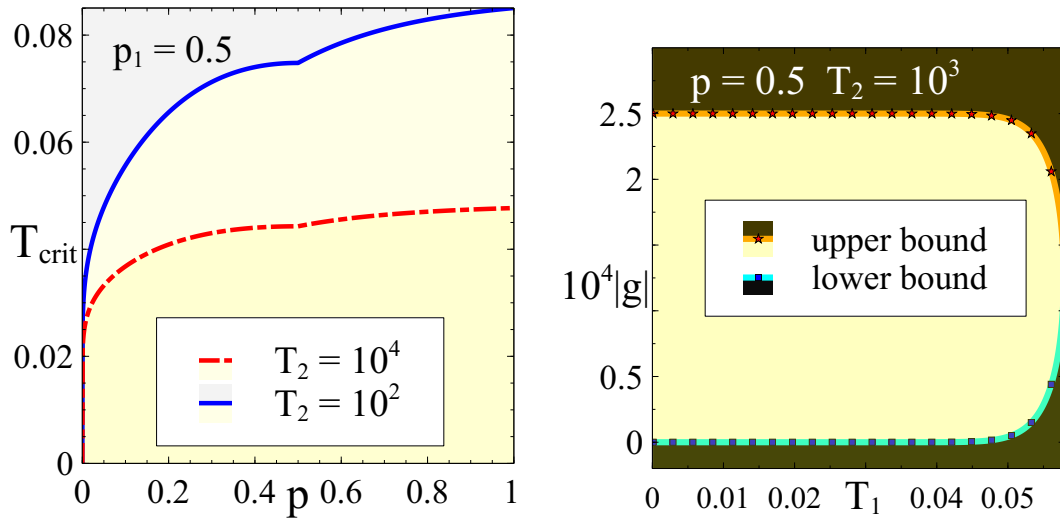


Figure 7.6: Condition for creation of magic for high spin bath temperature T_2 . Left : dependence of critical temperature T_{crit} on the reset probability $p_1 = p_2 = p$. Creation of magic is possible in the pale yellow region and impossible in the light gray region. Right : Allowed interval for interaction strength g with respect to heat bath temperature T_1 for creation of magic. Creation of magic is possible in the pale yellow region and impossible in the dark brown region.

$x \rightarrow \infty$, $\tanh(1/x) \approx 1/x$, and $\cosh(1/x) \approx 1$. Making these approximations yield the following result

$$r_x + r_y + r_z \approx \tanh\left(\frac{1}{2T_1}\right) \left[1 + 2g \frac{p(4p^2 + 4p - 1)}{T_2(1 + 4p^2)^2} - \frac{g^2}{p^2} \right] \quad (7.16)$$

From the above formula, following the approach earlier, the condition that $r_x + r_y + r_z > 1$ can be shown to be equivalent to

$$\left(g - \frac{F_1}{F_2}\right)^2 < \frac{F_1^2}{F_2^2} - \frac{\lambda}{F_2}, \quad (7.17)$$

where $F_1 = \frac{p(4p^2+4p-1)}{T_2(1+4p^2)^2}$, and $F_2 = 1/p^2$. Similar to before, the critical threshold temperature T_{crit} of the heat bath is the maximum of the critical threshold temperatures corresponding to the conditions for $r_x \pm r_y + r_z$, or $r_y - r_x + r_z$ surpassing unity respectively.

That is,

$$T_{\text{crit}} = \max \left[\frac{1}{\ln\left(1 + \frac{F_2}{F_1}\right)}, \frac{1}{\ln\left(1 + \frac{F_2}{G_1}\right)}, \frac{1}{\ln\left(1 + \frac{F_2}{H_1}\right)} \right], \quad (7.18)$$

where $G_1 = \frac{p(1+4p-4p^2)}{T_2(1+4p^2)^2}$, and $H_1 = \frac{p(4p^2-4p-1)}{T_2(1+4p^2)^2}$. In case the temperature of the heat bath is less than the critical temperature, the interaction strength g must again satisfy either 7.17 or its analogues. The above situations are pictorially depicted in Fig 7.6 from which we observe that the critical heat bath temperature for creation of magic is enhanced if the spin bath temperature is lowered. From Fig 7.6, we also affirm that similar to the low temperature case, the window of interaction strength g for which magic creation is possible becomes narrower and narrower with increasing heat bath temperature T_1 until vanishing when the heat bath temperature exceeds the critical temperature T_{crit} . In line with our naive expectation that it becomes harder and harder to extract quantumness from a system in presence of large classical noise, Fig 7.6 illustrates that for increased spin bath temperature T_2 , the critical temperature of the thermal bath for creation of magic is significantly depressed.

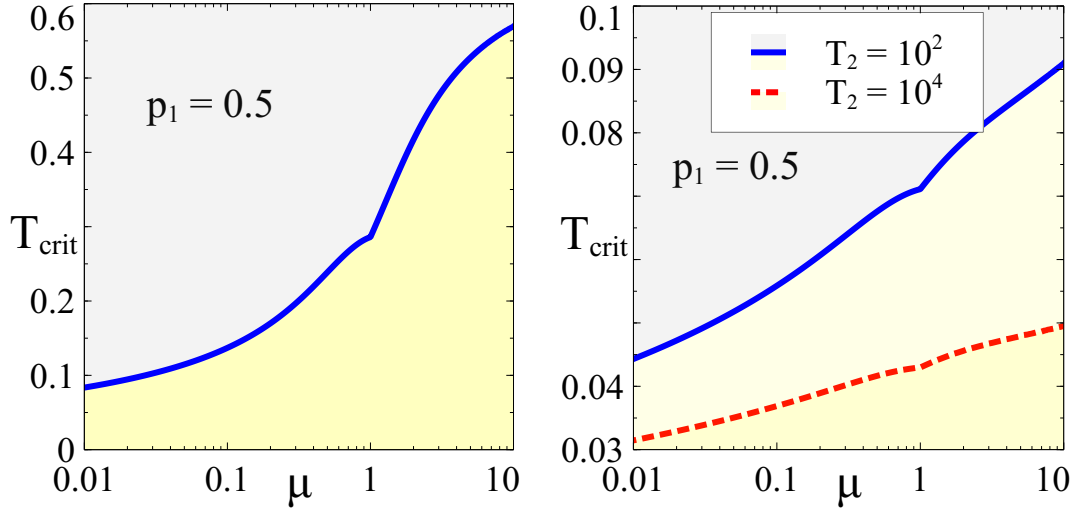


Figure 7.7: Effect of asymmetry μ between the reset probabilities p_1 and $p_2 = \mu p_1$ on the critical temperature T_{crit} for creation of magic in the low spin bath temperature T_2 limit (left) and high spin bath temperature T_2 limit (right). Creation of magic is possible in the pale yellow region and impossible in the light gray region.

Until now, we have made the simplifying assumption that the reset probabilities are equal. Let us now study, in the low T_2 limit, the effect of asymmetry between the reset probabilities. Suppose $p_1 = p$ and $p_2 = \mu p$. Thus, in the low T_2 limit, the corresponding expressions are

$$r_x + r_y + r_z \approx \tanh\left(\frac{1}{2T_1}\right) \left[1 + 4g\mu p \frac{4\mu p^2 + 2\mu p + 2p - 1}{(1 + 4p^2)(1 + 4\mu^2 p^2)} - 2g^2 \frac{1 + 2\mu^2 p^2 + 4p^2 + 16\mu^2 p^4 + 8\mu^3 p^4}{p^2(1 + \mu)(1 + 4p^2)(1 + 4\mu^2 p^2)} \right] \quad (7.19)$$

$$r_x - r_y + r_z \approx \tanh\left(\frac{1}{2T_1}\right) \left[1 + 4g\mu p \frac{1 + 2\mu p + 2p - 4\mu p^2}{(1 + 4p^2)(1 + 4\mu^2 p^2)} - 2g^2 \frac{1 + 2\mu^2 p^2 + 4p^2 + 16\mu^2 p^4 + 8\mu^3 p^4}{p^2(1 + \mu)(1 + 4p^2)(1 + 4\mu^2 p^2)} \right] \quad (7.20)$$

$$-r_x + r_y + r_z \approx \tanh\left(\frac{1}{2T_1}\right) \left[1 + 4g\mu p \frac{4\mu p^2 - 2\mu p - 2p - 1}{(1 + 4p^2)(1 + 4\mu^2 p^2)} - 2g^2 \frac{1 + 2\mu^2 p^2 + 4p^2 + 16\mu^2 p^4 + 8\mu^3 p^4}{p^2(1 + \mu)(1 + 4p^2)(1 + 4\mu^2 p^2)} \right] \quad (7.21)$$

In the opposite, i.e., high T_2 limit, using previously stated approximations, viz., $\tanh(1/x) \approx 1/x$ and $\cosh(1/x) \approx 1$ for $x \rightarrow \infty$, the expressions for linear functions of Bloch vectors

are given by

$$r_x + r_y + r_z \approx \tanh\left(\frac{1}{2T_1}\right) \left[1 + 2g\mu p \frac{4\mu p^2 + 2\mu p + 2p - 1}{T_2(1 + 4p^2)(1 + 4\mu^2 p^2)} - 2g^2 \frac{1}{p^2(1 + \mu)} \right], \quad (7.22)$$

$$r_x - r_y + r_z \approx \tanh\left(\frac{1}{2T_1}\right) \left[1 + 2g\mu p \frac{1 + 2\mu p + 2p - 4\mu p^2}{T_2(1 + 4p^2)(1 + 4\mu^2 p^2)} - 2g^2 \frac{1}{p^2(1 + \mu)} \right]. \quad (7.23)$$

$$-r_x + r_y + r_z \approx \tanh\left(\frac{1}{2T_1}\right) \left[1 + 2g\mu p \frac{4\mu p^2 - 2\mu p - 2p - 1}{T_2(1 + 4p^2)(1 + 4\mu^2 p^2)} - 2g^2 \frac{1}{p^2(1 + \mu)} \right]. \quad (7.24)$$

Fig 7.7 illustrates that, in both the low T_2 and high T_2 limit, the larger the reset probability of the spin bath is compared with the reset probability of the heat bath, the more the magnitude of critical temperature for creation of magic.

However, when considering these results, one must also keep in mind that they have been obtained through a perturbation expansion in g . Thus, the cases where magic creation seems possible from the relations like 7.13 or 7.17, yet the interaction strength is quite high, have to be more carefully treated. Moreover, if the interaction strength is quite high, the reset model master equation itself may not work.

7.4 Summary

- An autonomous model of creating steady quantum coherence and magic is proposed.
- The amount of coherence generated in this model increases for increased couplings to the respective baths, and with lowering of temperature.
- There exists a critical temperature below which it is possible to autonomously generate magic in the steady state.
- The interaction parameter between the qubits should neither be too small, nor be too large for the creation of magic. The allowed window of the magnitude of the interaction parameter shrinks, *ceteris paribus*, if the spin bath temperature increases.

Indefinite causal order as a resource for thermometry

1

Until this point, we have mostly treated the thermal environment as one endowed with a known temperature. However, temperature is not a dynamical variable, and hence can not be directly measured. Thus, the problem of thermometry becomes interesting in its own right. The importance of discovering better quantum thermometric schemes stems from two distinct motivations. Firstly, low temperature sensing is of utmost importance in numerous instances ranging from many body physics [250, 251] to biophysics [252]. For various engineered baths, which may themselves be small in size, one has to necessarily take quantum effects into consideration. Secondly, quantum features may enhance the ultimate precision reachable through thermometry. One of the challenges in thermometry lies in the fact that macroscopic probes may disturb the bath by distorting its thermal profile [253]. Quantum thermometry [254, 255, 256, 257, 258, 259, 260, 261] is thus important, as it aims at improving the precision of nanoscale probes. In the case of metrology and parameter estimation, it is well known that spatial entanglement [51, 262] between

¹This chapter is based on the preprint "*Superposition of causal order as a metrological resource for quantum thermometry*" appearing in arXiv, with arXiv number 1812.07508

two distinct parties sometimes allows for a better scaling than the so called *standard quantum limit* [263]. However, it has now been realized that quantum mechanics also allows for operations with superposition of causal order [69, 70, 79, 73, 81]. This idea has been recently exploited, among others, towards enhancing the classical capacity of channels [72, 76], reducing communication complexity of tasks [70], and improving teleportation protocols in noisy scenarios [264]. Experimental implementations of quantum switches have also been achieved [71, 265] using optical setups. Thus, an inevitable question arises, can we get a metrological advantage in the presence of superposition of causal order? In this chapter, we discuss a simple way to use superposition of processes to enhance the precision of thermometry. We show that, by using a quantum switch it is possible to estimate the temperature of a bath significantly more precisely than previously considered *optimal qubit probes* [266, 254]. While an optimal conventional qubit probe is outperformed by a Harmonic oscillator probe with infinite levels, we show that the same qubit probe, augmented with a quantum switch, can outperform the conventional Harmonic oscillator probe in the operating temperature window. We also derive thermodynamic uncertainty relations in the presence of the quantum switch.

8.1 A brief prologue on quantum thermometry

We first briefly review the existing theory of optimal qubit thermometry following [266, 254]. The imprecision in estimating the inverse temperature β from a probe which has attained equilibration in a thermal bath of inverse temperature β is bounded from below by the quantum Cramer Rao bound which assumes the form

$$\delta\beta \geq \frac{1}{\sqrt{v \mathcal{F}_\beta}}, \quad (8.1)$$

with ν being the number of runs which is assumed to be one throughout, and \mathcal{F}_β being the *quantum* Fisher information (QFI) of the thermalized probe state ρ , is given by [267]

$$\mathcal{F}_\beta(\rho) = \sum_k \frac{(\partial_\beta p_k)^2}{p_k} + 2 \sum_{n \neq m} \frac{(p_m - p_n)^2}{p_m + p_n} |\langle \psi_n | \partial_\beta \psi_m \rangle|^2, \quad (8.2)$$

where $\{p_k\}$, and $\{|\psi_k\rangle\}$ are the eigenvalues and eigenvectors of the state ρ . For a single copy of the probe with a Hamiltonian H , the QFI equals the variance ΔH^2 of the Hamiltonian. Thus, the above expression amounts to the following thermodynamic uncertainty relation

$$\delta\beta\Delta H \geq 1 \quad (8.3)$$

For *optimal* quantum thermometry in case of a qubit probe, one optimizes the QFI for the temperature over the parameter $x = \epsilon/T$, where ϵ is the energy gap of the probe Hamiltonian, and T being the bath temperature, and thus obtains the following transcendental equation for $x = x^*$ [266]

$$e^{x^*} = \frac{x^* + 2}{x^* - 2}. \quad (8.4)$$

The above equation can be numerically shown to have the solution $x^* \approx 2.399$. The resulting QFI for temperature has a peak, which determines the operating window of the thermometer.

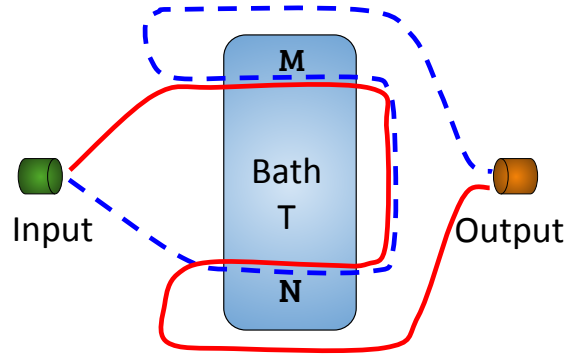


Figure 8.1: Schematic of the protocol. The input probe is being sent in two possible pathways (red solid line, which implements $N \circ M$ and blue dashed line, which implements $M \circ N$) based upon the configuration of the control. N and M are identical thermalizing channels.

8.2 Quantum switch enhanced thermometry

8.2.1 Protocol

Let us now introduce the protocol for enhancing the precision of quantum thermometry. Thermometry, in its simplest form, consists of the following. The bath, whose temperature is to be estimated precisely, is at temperature T . A probe is sent to the bath, and then recovered. During this time interval, the probe interacts with the bath, resulting in the final state of the probe imbibing some information about the bath temperature T . An estimate of the bath temperature is then obtained by analyzing the probe. Our protocol is based on the above model with the following crucial difference. The probe interacts with the bath twice in succession, and the ordering between these two interactions is superposed with the help of a control qubit. If the control state is $|0\rangle$, one such ordering is followed, i.e., in Fig.8.1, the channel M is encountered first, followed by the identical channel N . If the control is at the orthogonal state $|1\rangle$, then the alternative ordering is followed, i.e., the channel N is encountered first, followed by the identical channel M . Now, if the control is in a superposition of these two orthogonal states, no specific and definite ordering remains, and the resulting configuration is called a *quantum switch*. For

simplicity, we assume that the probe is a qubit, and when in contact with the bath, undergoes thermalization, which can be modelled by a generalized amplitude damping channel \mathcal{N} with the following Kraus operators [51]

$$K_0 = \sqrt{p} \begin{pmatrix} 1 & 0 \\ 0 & \sqrt{1-\lambda} \end{pmatrix}, K_1 = \sqrt{p} \begin{pmatrix} 0 & \sqrt{\lambda} \\ 0 & 0 \end{pmatrix}, \quad (8.5)$$

$$K_2 = \sqrt{1-p} \begin{pmatrix} \sqrt{1-\lambda} & 0 \\ 0 & 1 \end{pmatrix}, K_3 = \sqrt{1-p} \begin{pmatrix} 0 & 0 \\ \sqrt{\lambda} & 0 \end{pmatrix}, p = \frac{1}{1 + e^{-\beta\epsilon}}, \lambda = 1 - e^{-t/\tau}, \quad (8.6)$$

where t is the time of interaction with the bath, ϵ is the energy spacing in the probe qubit, τ is the relaxation time of the bath, and $\beta = 1/T$ is the inverse temperature of the bath. The Kraus operators are normalized, i.e., $\sum_i K_i^\dagger K_i = \mathbb{I}$. If the control state is initially $\rho_c = |\psi_c\rangle\langle\psi_c|$, where $|\psi_c\rangle = \sqrt{\alpha}|0\rangle + \sqrt{1-\alpha}|1\rangle$, then the output state of the correlated system-control is given by [72]

$$\mathcal{E}[\rho \otimes \rho_c] = \sum_i \sum_j W_{ij}(\rho \otimes \rho_c) W_{ij}^\dagger, \quad (8.7)$$

where $W_{ij} = K_i K_j \otimes |0\rangle\langle 0| + K_j K_i \otimes |1\rangle\langle 1|$ are the Kraus operators for the combined probe-control joint system. We note, that the representability of any dynamics in the operator-sum form does not depend on further assumptions about dynamics, e.g., the Markov approximation, beyond the fact that every such dynamics can be dilated to a global unitary. Consequently, there is no guarantee that one can easily write down the corresponding master equation in the canonical Lindblad Gorini Kossakowski Sudarshan (LGKS) form, although progress in this direction has been made [268, 122, 269, 171]. We further note that, setting $t \gg \tau$, and $\beta = 1/T = 0$ for the generalized amplitude damping channel is equivalent to considering a depolarizing channel. Such channels have been considered in the context of quantum switches, both theoretically [72, 76, 270], and experimentally [270, 265]. However, beyond the formalism, our end goal is different from

enhancing the classical capacity of channels [72, 76, 270].

It is clear that tracing out the control from the output state leaves us back with the same state which we would have obtained in the absence of the control. However, the correlation between the control and the probe established through the thermalizing channel may also store some information about the bath temperature, thus enhancing the precision of estimation of temperature. In the present work, we quantitatively investigate this phenomenon. At this point, we note in passing that there is an ongoing debate on whether the superposition of causal order offers the same operational advantage as a coherent control, especially in the case of enhancement of channel capacity, dubbed *causal activation* [76, 71, 73], which is beyond the scope of the present work. We also clarify that the present scheme is different from just using two different qubits as probes, as the control qubit does not interact with the bath and has no energy spectrum. We also reiterate that the control qubit is never sent through the bath. The bath always experiences only a single probe qubit passing through it. This should not be confused with sending two qubits to the bath. In the latter case, since QFI is additive, it is self-evident that the precision should increase vis-a-vis a single qubit probe.

Thermometric precision

For simplicity, we assume that the time spent by the probe inside the bath is much longer than the relaxation time τ of the bath, or $\lambda = 1 - e^{-t/\tau}$ tends to unity vide 8.6. Hence, following 8.7, the joint output state of the probe and the control reads as

$$\rho_{\text{out}} = \begin{pmatrix} \alpha p & p^2 \sqrt{\alpha(1-\alpha)} & 0 & 0 \\ p^2 \sqrt{\alpha(1-\alpha)} & p(1-\alpha) & 0 & 0 \\ 0 & 0 & \alpha(1-p) & 0 \\ 0 & 0 & 0 & (1-p)(1-\alpha) \end{pmatrix}.$$

Note that the above density matrix without coherence in the control qubit is a diagonal one, hence the off-diagonal, or genuinely quantum contributions to QFI in 8.2 does not exist. However, in the case of an initially coherent control qubit, there is a non-zero magnitude of genuinely quantum contribution to the QFI. This affirms that qubit thermometry at equilibrium does benefit from quantum features other than the mere discreteness of levels. The QFI for the output state above with respect to the parameter β is expressed in the following form

$$\mathcal{F}_\beta(\rho_{\text{out}}) = \epsilon^2 \frac{[2 + 4\alpha(1 - \alpha)]e^{3\beta\epsilon} + 3e^{2\beta\epsilon} + e^{\beta\epsilon}}{(1 + e^{\beta\epsilon})^3(1 + 2e^{\beta\epsilon})}. \quad (8.8)$$

If we parametrize $\beta\epsilon = \epsilon/T = x$ and optimize over x to maximize the QFI, the corresponding condition is given by $\partial_x \mathcal{F}_\beta(x) = 0$, which, upon simplification, yields the following transcendental equation for optimal $x = x^*$

$$\xi = \frac{(1 + e^{x^*})(1 + 2e^{x^*})^2 [(x^* - 2)e^{x^*} - (x^* + 2)]}{e^{2x^*} [(2 + 3x^*) + (6 + 4x^*)e^{x^*} + (4 - 2x^*)e^{2x^*}]}, \quad (8.9)$$

where $\xi = 4\alpha(1 - \alpha)$ indicates the amount of superposition initially in the control qubit. In term of resource theory of coherence [33], ξ is the square of the l_1 -norm of coherence C_{l_1} , i.e., $\xi = C_{l_1}^2(|\psi_c\rangle)$. If $\xi = 0$, this indicates the presence of a definite causal order, and $\xi = 1$ corresponds to the maximal superposition in the control qubit. For $\xi = 0$, the condition above reduces to the optimization condition 8.4 derived in Ref. [266]. In case of maximal superposition, i.e., $\xi = 1$, the condition above leads to the solution $x^* \approx 2.4741$, which is quite close to the solution of the optimality condition in the presence of a definite causal order. Thus, other things equal, the operating window of the thermometer does not shift much in presence of the switch. See Fig. 8.2 for an illustration of how the QFI depends on the energy gap.

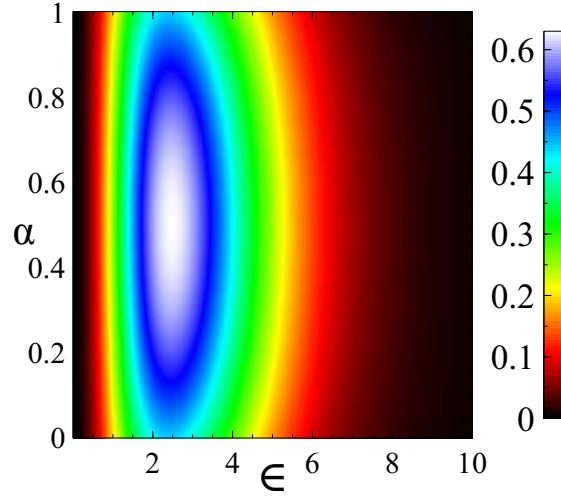


Figure 8.2: Density plot of QFI for the inverse temperature β on the gap ϵ as well as the superposition parameter α . Temperature is fixed at $T = 1$.

8.2.2 Thermodynamic uncertainty relations

Thermodynamic uncertainty relations have a long history, which we shall not dwell upon here [271, 272]. We note that the thermodynamic uncertainty relation in 8.1 is analogous to the familiar uncertainty relation for incompatible observables. It is well known [273, 274] that the presence of quantum entanglement and quantum superposition can reduce uncertainty. Thus, it is natural to wonder whether the quantum switch induces a similar effect for the thermodynamic uncertainty relation. Indeed, starting from 8.8, and the quantum Cramer Rao bound, yields the following version of the thermodynamic uncertainty relation

$$\delta\beta\Delta H \geq \frac{1}{\sqrt{1 + \frac{\xi\epsilon^2}{(1+e^{-\beta\epsilon})(2+e^{-\beta\epsilon})}}}. \quad (8.10)$$

Since the quantum Cramer Rao bound for estimating a single parameter is tight, it is possible to saturate the above uncertainty relation as well. We now concentrate on limiting cases. If the bath temperature is very low, i.e., $\beta = 1/T \rightarrow \infty$, this reads as

$$\delta\beta\Delta H \geq \frac{1}{\sqrt{1 + \frac{\xi\epsilon^2}{2}}}. \quad (8.11)$$

On the other hand, if the bath temperature is very high, i.e., $\beta = 1/T \rightarrow 0$, the corresponding thermodynamic uncertainty relation is given by

$$\delta\beta\Delta H \geq \frac{1}{\sqrt{1 + \frac{\xi\xi^2}{6}}}. \quad (8.12)$$

The lower bound depends on the quantum coherence of the control qubit and the energy gap of the probe qubit. Therefore, one can see that similar to earlier results [273, 274], quantum coherence reduces thermodynamic uncertainty. Also, it is evident from the above that a large gap in the probe Hamiltonian reduces the thermodynamic uncertainty. However, it is easy to see that the average energy of the probe in such a case becomes very big. Thus, the assumption that the probe is much smaller in comparison to the bath may no longer hold.

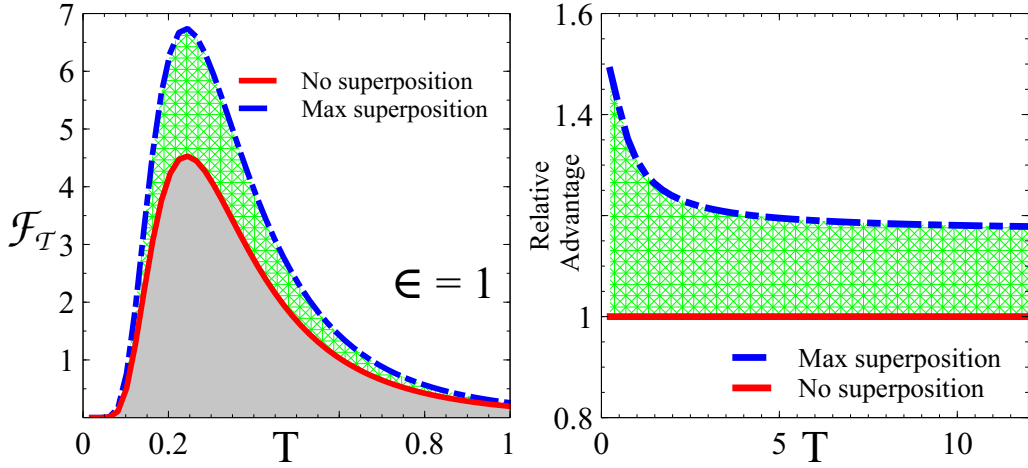


Figure 8.3: *Left*: QFI for temperature T vs. temperature T . *Right*: Relative advantage in terms of QFI gained through the use of quantum switch. The red solid line indicates the qubit probe used without any switch, the blue dash-dotted line indicates the qubit probe used with a maximally coherent switch. Green shaded regions are only accessible when using a quantum switch in the qubit protocol.

8.2.3 Performance advantage

Let us now quantify the relative advantage gained through the use of the qubit probe with a quantum switch vis-a-vis a conventional qubit probe. The relative gain in QFI through the use of a quantum switch utilizing a maximally coherent control qubit, with respect to a conventional qubit probe, reads as

$$\chi = \frac{\mathcal{F}_\beta^{\text{switch}}}{\mathcal{F}_\beta^{\text{no switch}}} = \frac{(2 + \xi)e^{3\beta\epsilon} + 3e^{2\beta\epsilon} + e^{\beta\epsilon}}{2e^{3\beta\epsilon} + 3e^{2\beta\epsilon} + e^{\beta\epsilon}}. \quad (8.13)$$

In the limit of very high temperature, i.e., $\beta \rightarrow 0$, and maximal superposition between paths, the ratio $\chi \approx 7/6$, whereas in the limit of very low temperature, i.e., $\beta \rightarrow \infty$ and maximal superposition between paths, the ratio $\chi \approx 1.5$. Expressed in terms of precision of estimation of temperature, this translates to $\approx 8\%$ more precision for estimating a very high temperature, and $\approx 22\%$ more precision for estimating a very low temperature. Thus, our protocol performs much better than the other qubit thermometry protocols in the low-temperature regime, while retaining the advantage vis-a-vis other protocols in the high-temperature regime as well. See Fig. 8.3 for an illustration of the advantage gained through the use of the quantum switch.

Comparison with a Harmonic Oscillator probe - A qubit has only two energy levels, therefore the problem of optimizing the Hamiltonian spectrum does not arise in general except optimizing over the value of the energy gap. Extending the optimal thermometry scheme [266] for N -level systems leads us to an optimal Hamiltonian spectrum with a gapped ground state and a $N - 1$ fold energetically degenerate energy eigenstates. Clearly, designing such probes is practically quite challenging. In contrast, Harmonic oscillators with equispaced energy levels are far more accessible. It was shown [266] that they are superior to qubit probes with the same energy gap ϵ in terms of precision as well as the breadth of the operating window. The corresponding QFI for the conventional Harmonic

oscillator probe is given by [254]

$$\mathcal{F}_\beta^{\text{HO}} = \epsilon^2 \frac{e^{-\beta\epsilon}}{(1 - e^{-\beta\epsilon})^2} \quad (8.14)$$

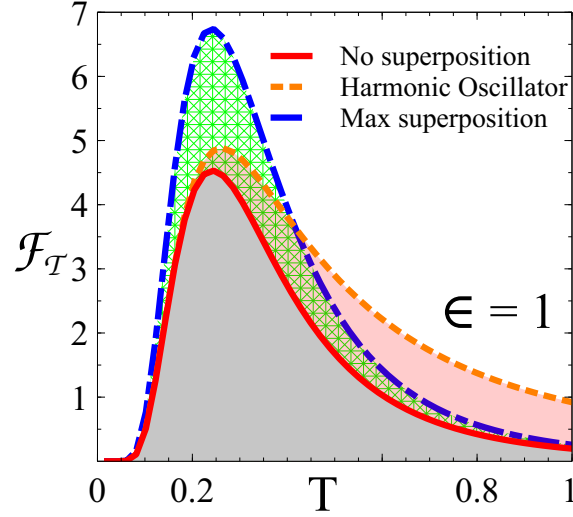


Figure 8.4: Comparison of the QFI for temperature with temperature T for the qubit probe without quantum switch (red solid line), qubit probe with a maximally coherent quantum switch (blue dash dotted line), and a harmonic oscillator probe (orange dotted line). The energy level spacing in every case is $\epsilon = 1$.

Comparing (8.14) with the expression (8.8) of QFI for a qubit probe with a quantum switch reveals an interesting phenomenon. Below a certain threshold temperature, our qubit probe with a maximally coherent control outperforms the conventional Harmonic oscillator probe. Even better, this region includes the operating ranges of our probe as well the conventional harmonic oscillator probe. See Fig 8.4 for illustration. Thus, it is actually better to use a qubit probe in conjunction with a quantum switch rather than a conventional Harmonic oscillator probe, even though the latter has an infinite number of energy levels. The threshold temperature is obtained from equating the QFI expressions for the qubit probe with a quantum switch 8.8, and the conventional harmonic oscillator probe 8.14, which yields the following equation for $\beta\epsilon = x$

$$\frac{3e^{3x} + 3e^{2x} + e^x}{(1 + e^x)^3(1 + 2e^x)} = \frac{e^{-x}}{(1 - e^{-x})^2}. \quad (8.15)$$

This is an algebraic quartic equation in e^x and can be shown to have a non-zero real solution of $x \approx 2.40$. For example, assuming $\epsilon = 1$ yields the threshold temperature to be $T_{\text{threshold}} \approx 0.4157$, which is not in the optimal temperature window for our scheme.

8.3 Summary

- Quantum switch enhances the precision of equilibrium thermometry with a single qubit probe.
- Thermal channels under the influence of a coherent control lead to a new uncertainty relation with smaller-than-usual uncertainty.
- Although a single qubit probe steady state thermometry always performs poorly when compared against a harmonic oscillator probe, it is possible to surpass the optimal precision obtained by harmonic oscillator probes through the use of a quantum switch.

Thermometry using weak quantum measurements

1

In the previous chapter, we had described a possible way to improve the performance of quantum thermometers. The principle aim of quantum thermometry is always to avoid strong interactions, which may either be detrimental to the original thermal profile of the bath, or be damaging to the probing device itself. In this context, schemes which are, in some sense gentle, are called for. This way of gathering information about a quantum system through *weak measurement* scheme [275, 276, 277, 278], has recently come to the fore. Weak measurement is a technique of extracting information about physical quantities by allowing a *weak* interaction between the system and the measurement apparatus generated by the observable, followed up by a strong *post selection* measurement on the system. The weak measurement protocol helps one obtain *weak values* of an observable, which are, in general, complex numbers, and whose range may vastly exceed the range of the corresponding observable. This property, known as *weak value amplification* (WVA), is quite popular in the context of measuring quantities which may or may not

¹This chapter is based on the preprint "*Quantum precision thermometry with weak measurement*" appearing in arXiv, with arXiv number 1901.07415.

have quantum mechanical observables associated with them, for example, the geometric phase [279], non-Hermitian observables [280], tomographic estimation of quantum states [281, 282, 283, 284, 285], or amount of entanglement within a quantum state [286, 287]. The WVA technique has found applications in observations of the spin Hall effect [288], photon trajectories [289], or the time lag between rapidly occurring processes [290] as well. Thus, it is perhaps a natural logical step to coonsider weak measurement based thermometric protocols. In this chapter, such a scheme is investigated in detail.

In this chapter, we confine our analysis to finite dimensional probes, with an emphasis on qubit probes. As we shall show, the protocol offers better precision for a certain temperature window, which is a generic feature of many thermometric schemes [256, 266, 291, 292]. At the same time, the scheme discussed in this chapter is more flexible in the sense of enabling the experimenter to shift the optimal precision window, even when the probe spectrum is fixed, by simply tweaking the choice of the post-selected state. As a further potential advantage of this scheme, the measuring apparatus interacts with the thermal qubit belonging to the bath only weakly, thus it is usable in situations where a strongly interacting apparatus may destroy itself.

2

9.1 Weak measurement

Let us briefly introduce the protocol of weak measurement with respect to an observable \hat{A} . A state of a quantum mechanical system S is *pre-selected* as $|\psi_i\rangle_S$ – which is the initial state of S . The measuring apparatus M is prepared initially in a (fixed) state $|\phi\rangle_M$ with the position of the pointer being governed by the wave function $\phi(x)$. The interaction Hamiltonian $H_{int} \equiv g\hat{A} \otimes \hat{P}_x$ acts on the system and the measuring apparatus jointly during

²According to the formulation of the weak measurement protocol, described in section 9.2, it is enough to consider $g\tau \ll 1$, even if we allow hot probes. Note that, for performing the post-selection strong measurement, the assumption $g\tau \ll 1$ may be dropped. Nevertheless, the issue of the measuring apparatus getting destroyed due to the hot probe can be circumvented by considering a different measuring apparatus.

a very small time interval τ , where g is the weak interaction strength and \hat{P}_x is the linear momentum of M , canonically conjugate to the position observable \hat{X} (say) of M . After the action of the measurement interaction, the system S is then *post-selected* in some state $|\psi_f\rangle$ – via an appropriate selective (strong) measurement on M . Thus, the time-evolved state of $S + M$ before post-selection is given by

$$\begin{aligned} |\Psi\rangle &= e^{-ig\hat{A}\otimes\hat{P}_x} [|\psi_i\rangle \otimes |\phi\rangle_M] \\ &\approx (I_S \otimes I_M - ig\hat{A} \otimes \hat{P}_x) [|\psi_i\rangle \otimes |\phi\rangle_M], \end{aligned} \quad (9.1)$$

where we have ignored quadratic and higher order terms for g , since the interaction is assumed to be weak. The unnormalized reduced state $|\tilde{\Psi}\rangle_{SM}$ of the measuring apparatus M is given by

$$|\tilde{\phi}_f\rangle_M \approx \left(\langle\psi_f|\psi_i\rangle |\psi_f\rangle_M - ig \langle\psi_f|\hat{A}|\psi_i\rangle \hat{P}_x |\phi\rangle_M \right), \quad (9.2)$$

Upon normalization, this reads as

$$|\phi_f\rangle_M \approx (1 - igA_w \hat{P}_x) |\phi\rangle_M \approx e^{-igA_w \hat{P}_x} |\phi\rangle_M, \quad (9.3)$$

where $A_w \equiv \langle\psi_f|\hat{A}|\psi_i\rangle / \langle\psi_f|\psi_i\rangle$ is said to be the *weak value* corresponding to the operator \hat{A} . Let us note two important features of the weak value, firstly, A_w need not be a real quantity and secondly, it may take values which are not constrained by the range of the spectrum corresponding to the observable \hat{A} .

The imaginary and real components of the weak value A_w may be experimentally ascertained through investigating certain features of the final state $|\phi_f\rangle_M$ of the pointer. These features include deviation in momentum and position with respect to the initial state $|\phi\rangle_M$, dispersion of the wave function in momentum space, and rate of change of the wave function in position space [293]. Laguerre-Gaussian modes of an optical beam have also been used to measure the real and imaginary parts of a weak value [294, 295]. Other proposals to completely determine the weak value, based upon interference visibility and phase

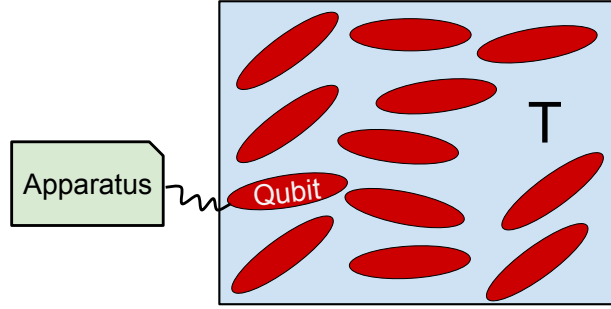


Figure 9.1: Schematic of the weak measurement based thermometric scheme. The bath is a collection of thermalized qubits. We couple the measuring apparatus to one of these qubits for a very small time-interval.

shifts [296], have also been put forward.

9.2 Assessing temperature through weak values

Consider a d dimensional quantum system S under the action of a time-independent Hamiltonian \hat{H} having non-degenerate energy eigenvalues E_1, E_2, \dots, E_d and the corresponding energy eigenstates $|\psi_1\rangle, |\psi_2\rangle, \dots, |\psi_d\rangle$. Assume that S is in contact with a heat bath of temperature T and S has reached the thermal equilibrium state $\rho_T \equiv e^{-\beta\hat{H}} / (\text{Tr}[e^{-\beta\hat{H}}]) = (\sum_{n=1}^d e^{-\beta E_n} |\psi_n\rangle \langle \psi_n|) / (\sum_{n=1}^d e^{-\beta E_n})$. Here $\beta = 1/(k_B T)$, with k_B being taken as unity. Prepare the measuring apparatus M in a state $|\phi\rangle$, having position wave function $\phi(x)$. Note that here M is considered to be a continuous-variable system, in general. We would like to perform measurement of an observable \hat{A} on the system S .

Consider now evolution of $S + M$ under the action of an interaction Hamiltonian $\hat{H}_{int} = g\hat{A} \otimes \hat{P}_x$ for a brief period of time τ . The interaction strength g is also considered to be small – in the regime of weak interaction between S and M . Here \hat{P}_x is the momentum observable of M canonically conjugate to the position observable \hat{X} . We assume here that

during the time interval $[0, \tau]$, S and M are under the action of *only* the Hamiltonian \hat{H}_{int} . This may be fulfilled in different ways: (i) We may decouple the system S at time $t = 0$ from the heat bath (after S achieves the thermal equilibrium state ρ_T) and thereby switch on the interaction Hamiltonian \hat{H}_{int} for the time duration $[0, \tau]$. (ii) On the other hand, we may think of assuming here that the strength g of interaction is much higher than that of the system Hamiltonian \hat{H} , so that due to action of \hat{H}_{int} for a small time span τ , it is enough to consider the change in states of S under the action of \hat{H}_{int} only. The time span τ should be small enough so that in spite of taking the strength g of the interaction Hamiltonian H_{int} being greater than the free Hamiltonian, $g\tau \ll 1$. At the end of the action of the interaction Hamiltonian, the joint state of $S + M$ becomes:

$$\begin{aligned}
\rho_{SM}(\tau) &= e^{-ig\tau\hat{A}\otimes\hat{P}_x}(\rho_T \otimes |\phi\rangle\langle\phi|)e^{ig\tau\hat{A}\otimes\hat{P}_x} \\
&\approx (I_S \otimes I_M - ig\tau\hat{A} \otimes \hat{P}_x)(\rho_T \otimes |\phi\rangle\langle\phi|) \\
&\times (I_S \otimes I_M + ig\tau\hat{A} \otimes \hat{P}_x) \\
&\approx \rho_T \otimes |\phi\rangle\langle\phi| - ig\tau[\hat{A} \otimes \hat{P}_x, \rho_T \otimes |\phi\rangle\langle\phi|].
\end{aligned} \tag{9.4}$$

Now we post-select the state of S to be $|\psi_f\rangle$. Then M will get collapsed into the following (unnormalized) state as given by

$$\begin{aligned}
\tilde{\eta}(\tau) &= \langle\psi_f|\rho_T|\psi_f\rangle|\psi_f\rangle\langle\psi_f| |\phi\rangle\langle\phi| \\
&- ig\tau(\langle\psi_f|\hat{A}\rho_T|\psi_f\rangle\hat{P}_x|\phi\rangle\langle\phi| - \langle\psi_f|\rho_T\hat{A}|\psi_f\rangle\langle\phi|\langle\phi|\hat{P}_x) \\
&= \langle\psi_f|\rho_T|\psi_f\rangle [|\phi\rangle\langle\phi| \\
&- ig\tau(A_w\hat{P}_x|\phi\rangle\langle\phi| - A_w^*|\phi\rangle\langle\phi|\hat{P}_x)] \\
&\approx \langle\psi_f|\rho_T|\psi_f\rangle \times \eta(\tau),
\end{aligned} \tag{9.5}$$

with the corresponding normalized collapsed state of M being given by:

$$\eta(\tau) = e^{-ig\tau A_w \hat{P}_x} |\phi\rangle\langle\phi| e^{ig\tau A_w \hat{P}_x} \tag{9.6}$$

and the corresponding weak value is given by:

$$A_w = \frac{\langle \psi_f | \hat{A} \rho_T | \psi_f \rangle}{\langle \psi_f | \rho_T | \psi_f \rangle}. \quad (9.7)$$

Using the value of A_w together with *a priori* knowledge of $|\psi_f\rangle$, \hat{A} , and the energy eigen spectrum of the system Hamiltonian \hat{H} , one can, in principle, find out the value of the temperature T – with the help of eqn. (9.7). Let us note in passing that the operator A must not commute with the relevant energy eigenbasis, else the weak value ceases to depend on the inverse temperature β , and thus, measuring the weak value furnishes no thermometric advantage.

High temperature regime- Let us now consider the case where the bath temperature is high, that is, $\beta \rightarrow 0$. Thus, we can replace $e^{-\beta} \approx 1 - \beta$. Now, assuming the spectral decomposition of \hat{A} with eigenvalues a_j and corresponding eigenstates $|a_j\rangle$ for $j = 1, 2, \dots, d$, in conjunction with eqn. (9.7), helps us to obtain the following expression for the weak value.

$$\begin{aligned} A_w &= \frac{\sum_{j,k=1}^d a_j e^{-\beta E_k} \langle \psi_f | a_j \rangle \langle \psi_f | a_j \rangle \langle a_j | \psi_k \rangle \langle a_j | \psi_k \rangle \langle \psi_k | \psi_f \rangle \langle \psi_k | \psi_f \rangle}{\sum_{l=1}^d e^{-\beta E_l} |\langle \psi_f | \psi_l \rangle \langle \psi_f | \psi_l \rangle|^2} \\ &\approx \frac{\langle \psi_f | \hat{A} | \psi_f \rangle - \beta \langle \psi_f | \hat{A} \hat{H} | \psi_f \rangle}{1 - \beta \langle \psi_f | \hat{H} | \psi_f \rangle} \\ &\approx (\langle \psi_f | \hat{A} | \psi_f \rangle - \beta \langle \psi_f | \hat{A} \hat{H} | \psi_f \rangle) (1 + \beta \langle \psi_f | \hat{H} | \psi_f \rangle) \end{aligned} \quad (9.8)$$

$$\begin{aligned} &\approx \langle \psi_f | \hat{A} | \psi_f \rangle \\ &+ \beta (\langle \psi_f | \hat{A} | \psi_f \rangle \times \langle \psi_f | \hat{H} | \psi_f \rangle - \langle \psi_f | \hat{A} \hat{H} | \psi_f \rangle) \end{aligned} \quad (9.9)$$

Inverting this expression, in the high temperature limit, the inverse temperature is expressible in terms of the weak value of the observable A as

$$\beta \approx \frac{A_w - \langle \psi_f | \hat{A} | \psi_f \rangle}{\langle \psi_f | \hat{A} | \psi_f \rangle \times \langle \psi_f | \hat{H} | \psi_f \rangle - \langle \psi_f | \hat{A} \hat{H} | \psi_f \rangle}. \quad (9.10)$$

Let us now analyze the right hand side of the above result in further detail. We denote the standard deviation of an observable O as ΔO . According to Vaidman's formula [223], $A|\psi_f\rangle = \langle A\rangle|\psi_f\rangle + \Delta A|\bar{\psi}_f\rangle$, which implies the following expression for the weak value

$$A_w = \langle A\rangle + \Delta A \frac{\langle \bar{\psi}_f | \rho_T | \psi_f \rangle}{\langle \psi_f | \rho_T | \psi_f \rangle}. \quad (9.11)$$

Here $|\bar{\psi}\rangle$ indicates that it is a state orthogonal to $|\psi\rangle$. This formula has been proved [223] in the following way - we can always decompose the state $|\psi\rangle$ as $|\psi\rangle = \alpha|\psi\rangle + \beta|\bar{\psi}\rangle$. Now, $\langle A\rangle = \langle \psi | A | \psi \rangle = \alpha$, and $\Delta A = \sqrt{\langle A^2 \rangle - \alpha^2} = \sqrt{\langle \psi | A^\dagger A | \psi \rangle - \alpha^2} = \sqrt{\alpha^2 + \beta^2 - \alpha^2} = \beta$. Similarly applying Vaidman's formula for the density operator ρ_T yields $\rho_T|\psi_f\rangle = \langle \rho_T \rangle + \Delta \rho_T |\bar{\psi}_f\rangle$, where $|\bar{\psi}_f\rangle$ is another state perpendicular to $|\psi_f\rangle$. Plugging in this expression to the earlier equation for weak value of A yields the following expression for the inverse temperature

$$\beta = -\frac{\Delta A \Delta \rho_T \langle \bar{\psi}_f | \bar{\psi}_f \rangle}{\text{Cov}(A, H) \langle \psi_f | \rho_T | \psi_f \rangle} \quad (9.12)$$

For a qubit state, the corresponding orthogonal state is unique. Hence, $|\bar{\psi}_f\rangle = |\bar{\psi}_f\rangle$, which, when plugged in, yields the following expression

$$\beta = -\frac{\Delta A \Delta \rho_T}{\text{Cov}(A, H) \langle \psi_f | \rho_T | \psi_f \rangle}. \quad (9.13)$$

The above equation may be of independent interest. Let us now note that the anomalous weak value $\delta A = |\text{Re}(A_w) - \langle A \rangle|$, is expressible as $\delta A = |\text{Cov}(A, \rho_T)| / |\langle \rho_T \rangle|$. Now, $\langle \rho_T \rangle = \langle \exp(-\beta H) \rangle / Z \leq 1 / (Z(1 - \beta \langle H \rangle))$, where Z is the corresponding canonical partition function. Combining these results together, we obtain the following lower bound for the temperature

$$T \geq \frac{\langle H \rangle}{1 - \frac{|\text{Cov}(A, \rho_T)|}{Z \delta A}} \quad (9.14)$$

In the above equation, the anomalous weak value δA is a truly quantum mechanical quantity. It is easy to note that the achievable lower bound on the temperature is stronger, if δA is large in magnitude.

Qubit case - Let us now consider the generic situation in the case of the simplest non-trivial quantum system, which is a qubit, for arbitrary temperature. Consider $H = \sum_{i=1}^d E_i |\psi_i\rangle\langle\psi_i|$. If we take now $\hat{A} = -i|\psi_1\rangle\langle\psi_2| + i|\psi_2\rangle\langle\psi_1|$ and $|\psi_f\rangle = (1/\sqrt{2})(|\psi_1\rangle + |\psi_2\rangle)$, then the weak value A_w is given by:

$$A_w \equiv \langle\psi_f|\hat{A}\rho_T|\psi_f\rangle/\langle\psi_f|\rho_T|\psi_f\rangle = i\frac{e^{-\beta E_1} - e^{-\beta E_2}}{e^{-\beta E_1} + e^{-\beta E_2}}. \quad (9.15)$$

Note that here $\langle\psi_f|\hat{A}|\psi_f\rangle = 0$, $\langle\psi_f|\hat{H}|\psi_f\rangle = (E_1 + E_2)/2$, $\langle\psi_f|\hat{A}\hat{H}|\psi_f\rangle = i(E_1 - E_2)/2$. For the high temperature limit, we have the following (approximate) expression for the inverse temperature of the bath in the qubit case, which may be shown to be consistent with (9.10).

$$\beta \approx \frac{-2iA_w}{E_2 - E_1}. \quad (9.16)$$

Now, based upon the existing methods of identifying/measuring the weak value A_w [293, 294], one can, in principle, get an estimate of the (inverse) temperature β in eqn. (9.16). One of the advantages of the present scheme is that the measuring apparatus is brought into contact with the heat bath for a very short time, hence reducing the chance of damage to the apparatus. We add here that the rationale behind choosing the operator A in this form is the following, if A is chosen as being along the z-axis of the Bloch sphere, there is no information to be obtained about the temperature from the weak value. In case of thermalization, the azimuthal symmetry of the state in the Bloch sphere picture means it is equally feasible choosing any operator A along the $x - y$ plane of the Bloch sphere, thus we may assume the above form of A without loss of generality. Once A is fixed, the azimuthal symmetry of the problem is lost, and one has to choose the post selected state carefully. Above, we assumed an example of the post selected state, however a more

general analysis of the precision of our scheme depending upon different post-selections have been performed in the following sections.

9.3 Precision in measurement of temperature

It is natural to wonder about the optimal temperature window where the present scheme works best, that is, most precisely. The usual procedure for determining the precision of quantum thermometers is through finding the corresponding quantum Cramer Rao bound. In this section, we adopt a different approach. We restrict to qubit systems for simplicity. However, the present analysis can be extended to higher dimensions in a similar fashion.

9.3.1 Precision analysis for imperfect thermalization

Let us assume that the initial pre-measurement state is not exactly a thermal state, but very close to it, and written in the following manner

$$\rho_T^{(\delta)} = (1 - \delta)\rho_T + \delta|\chi(\theta, \phi)\rangle\langle\chi(\theta, \phi)|, \quad (9.17)$$

where $0 \leq \delta \ll 1$, and $|\chi\rangle$ is a random pure qubit state with corresponding Bloch sphere parameters θ , and ϕ . Physically this indicates imperfect thermalization, which is experimentally relevant, especially in situations where the thermalization timescale is not extremely fast compared to the time available for sensing. The corresponding weak value is denoted by A_w^δ . Now, an experimentalist may use the formula (9.15) to find the apparent inverse temperature $\tilde{\beta}$ of the bath as

$$\tilde{\beta} = \frac{2}{E_2 - E_1}(-iA_w^{(\delta)}) \quad (9.18)$$

It is of obvious practical interest to us that the inferred value of temperature does not

change wildly if the thermalization is imperfect. In order to quantify this, we invoke the idea of quantifying a relative error, which is the difference between the temperature furnished from imperfect thermalization, and the genuine temperature of the bath, divided by the bath temperature, and scaled by the imperfection δ . The squared relative error introduced through imperfect thermalization may thus be taken to be $|\tilde{\beta} - \beta|^2 / (\delta^2 \beta^2)$. It is this quantity we shall concentrate upon. To remove the effect of $|\chi\rangle$, which may conceivably capture some information about the state in which the probe was initialized, we shall finally average over the pure states $|\chi\rangle$. We will write $E_2 - E_1$ as the gap Δ from here on. Performing a perturbation expansion for $A_w^{(\delta)}$ around $\delta = 0$, and retaining terms upto first order in δ , the expression for $\tilde{\beta}$ is given by

$$\tilde{\beta} = \frac{2}{\Delta} \left(c_1 \tanh \frac{\beta \Delta}{2} - i c_2 \right), \quad (9.19)$$

where $c_1 = 1 - \delta \frac{\langle \psi_f | \chi \rangle^2}{\langle \psi_f | \rho_T | \psi_f \rangle}$, and $c_2 = \delta \frac{\langle \psi_f | A | \chi \rangle \langle \chi | \psi_f \rangle}{\langle \psi_f | \rho_T | \psi_f \rangle}$. Note that, c_1 and c_2 are functions of the Bloch sphere angles $\{\theta, \phi\}$ of the state χ . Thus, averaging over them, the resulting root mean squared relative error \mathcal{N}_β for the particular weak measurement strategy adopted in the previous section, is written as a function of inverse temperature as

$$\mathcal{N}_\beta^2 = \frac{1}{4\pi} \iint \frac{|\tilde{\beta} - \beta|^2}{\beta^2 \delta^2} \sin \theta d\theta d\phi = \frac{1}{4\pi \delta^2} \int_{\theta=0}^{\pi} \int_{\phi=0}^{2\pi} \left| \frac{2}{\beta \Delta} \left[c_1(\theta, \phi) \tanh \frac{\beta \Delta}{2} - i c_2(\theta, \phi) \right] - 1 \right|^2 \sin \theta d\theta d\phi. \quad (9.20)$$

Now, neglecting the second and the higher order coefficients of δ , we note that the expression for relative RMS error is written as

$$\mathcal{N}_\beta^2 = \frac{1}{4\pi} \iint \frac{4|v_1 \tanh \frac{\beta \Delta}{2} + i v_2|^2}{\Delta^2 \beta^2 (1 - \tanh^2 \frac{\beta \Delta}{2})^2} \sin \theta d\theta d\phi \quad (9.21)$$

where $v_1 = (1 - c_1)/\delta$, and $v_2 = c_2/\delta$. At this point, let us fix the observable $A = -i|\psi_1\rangle\langle\psi_2| + i|\psi_2\rangle\langle\psi_1|$, as in the previous section, and assume the arbitrary post selected

state $|\psi_f\rangle = \cos(\xi/2)|\psi_1\rangle + e^{i\nu} \sin(\xi/2)|\psi_2\rangle$. We also assume, without loss of generality, that the energy gap $\Delta = 1$. The expression for root mean squared relative error \mathcal{N}_β is given by

$$\frac{\sqrt{(13 - \cos 2\nu) \cosh \beta - 4 \cos 2\xi \sin^2 \nu \cosh^2(\frac{\beta}{2}) - (3 + \cos 2\nu)}}{3\beta [\cosh(\beta/2) + \cos \xi \sinh(\beta/2)] [1 - \tanh^2(\beta/2)]}. \quad (9.22)$$

For specific choices of the post selected state, the above equation yields the expression for error, and consequently, the inverse quantity signifies the precision of measurement. For example, assuming $|\psi_f\rangle = \frac{1}{\sqrt{2}} (|\psi_1\rangle + |\psi_2\rangle)$, as in the previous section, the relative error reads as

$$\mathcal{N}_\beta^+ = \sqrt{\frac{1 + 4 \cosh \beta + 3 \cosh 2\beta}{3\beta^2}}. \quad (9.23)$$

Fig. 9.2 shows that the precision, which is defined as the inverse of the relative error, attains a relatively narrow peak at a finite temperature, which determines the best operating window of the scheme. While the qubit thermometric schemes [256, 266, 254, 297] based on the strong measurement are different in conception than the present scheme, it is nonetheless noteworthy that the phenomenon of a narrow peak in the precision corresponding to an optimal temperature window is present in both the cases. We also note that for the QFI based analysis of optimal qubit thermometric probes with unit energy gap, the peak is situated at $T \approx 0.41$ [256, 266], which is obtained through solving the transcendental equation [256, 266] $e^{1/T} = (1+2T)/(1-2T)$. In comparison, in the present scheme, for a specific post-selected state $|\psi_f\rangle$, the location of the peak for optimal precision is obtained by the vanishing of the first derivative with respect to the inverse temperature β of the expression in (9.22). In particular, for the specific example $|\psi\rangle = \frac{1}{\sqrt{2}} (|\psi_1\rangle + |\psi_2\rangle)$ discussed in the previous section, the equation takes the form

$$\beta = \frac{3 \cosh \beta - 1}{3 \sinh \beta - 2 \tanh \frac{\beta}{2}}, \quad (9.24)$$

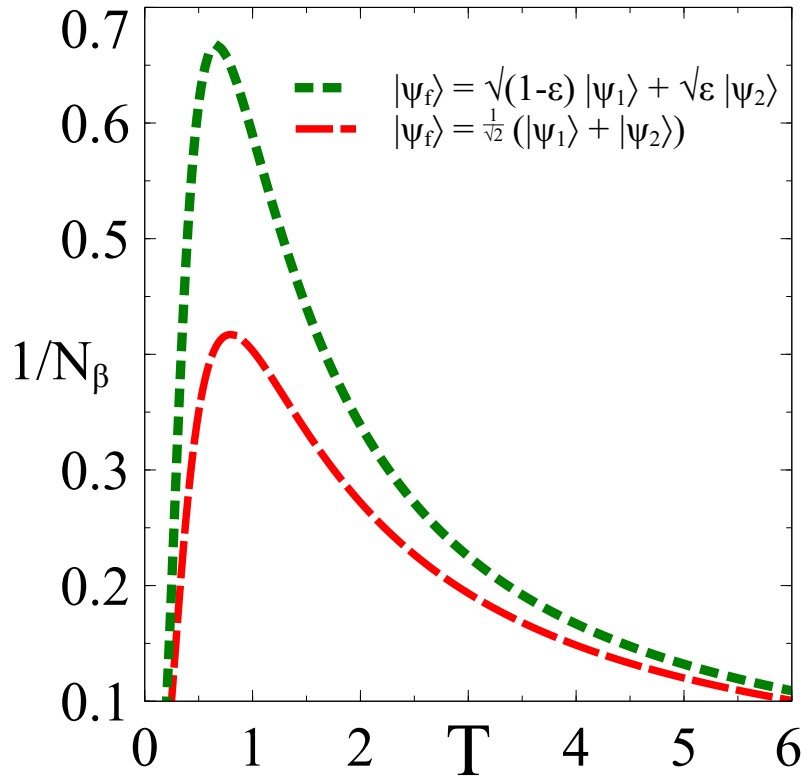


Figure 9.2: Precision of the scheme plotted against the temperature for the specific choice of post-selected states $|\psi_f\rangle = \sqrt{1-\epsilon}|\psi_1\rangle + \sqrt{\epsilon}|\psi_2\rangle$ (green dotted curve), $|\psi_f\rangle = \frac{1}{\sqrt{2}}(|\psi_1\rangle + |\psi_2\rangle)$ (red dashed curve). Energy gap between ground and excited states is unity in each case. $\epsilon = 0.01$ is assumed.

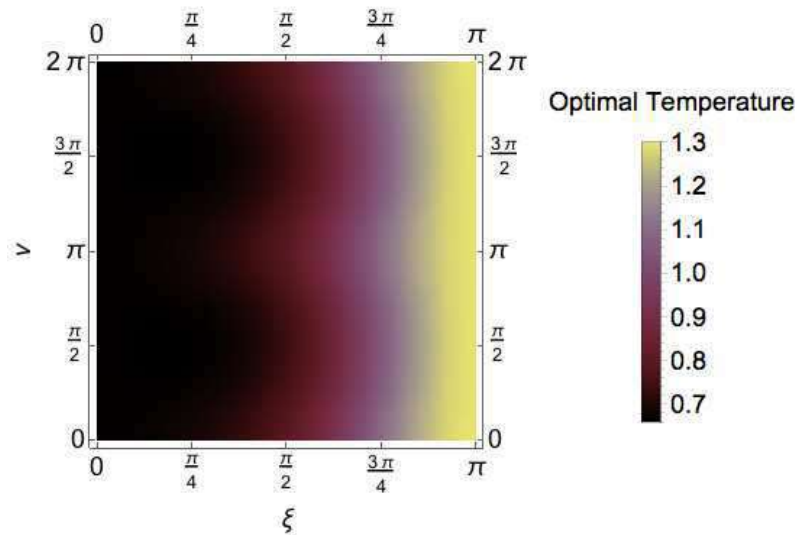


Figure 9.3: The temperature at which the optimal precision is achieved is plotted against the parameters ξ and ν of the post selected state $|\psi_f\rangle$.

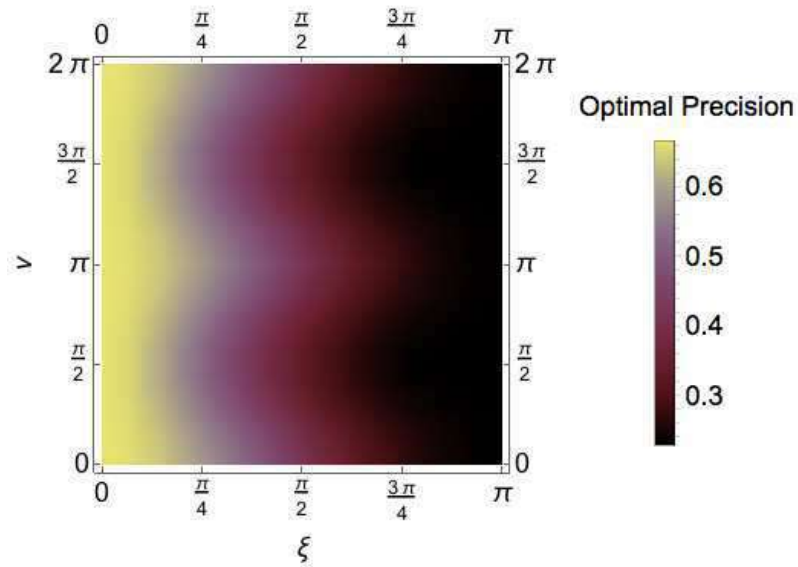


Figure 9.4: The magnitude of precision at optimal temperature is plotted against the parameters ξ and ν of the post selected state $|\psi_f\rangle$.

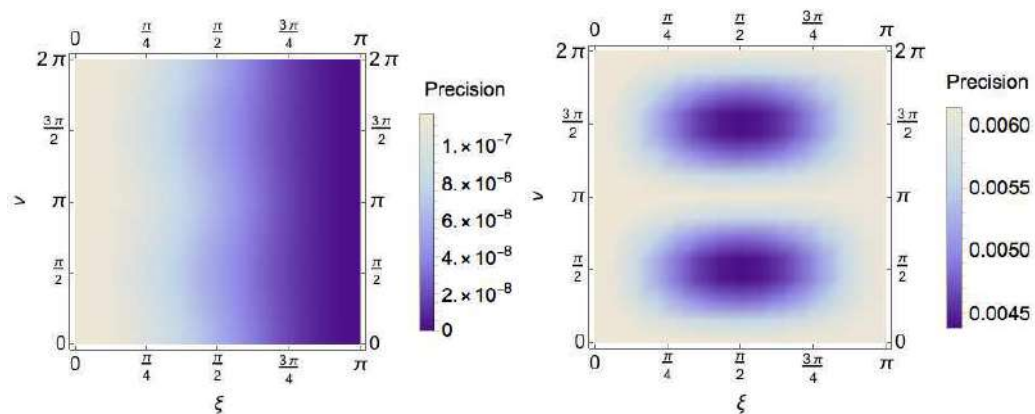


Figure 9.5: The magnitude of precision is plotted against the parameters ξ and ν of the post selected state $|\psi_f\rangle$ for (left) low temperature $T = 0.05$, and (right) high temperature $T = 100$.

which has the solution $T \approx 0.79$. The temperatures corresponding to optimal precision for other choices of post-selected states are depicted in Fig 9.3. Interestingly, for every $|\psi_f\rangle$, the corresponding optimal temperature is significantly higher than 0.41. This indicates the possibility that the present scheme may be better than the strong measurement based one based one for the relevant temperature range. It is natural to wonder about the post-selected state $|\psi_f\rangle$ which corresponds to maximum precision. From Fig 9.4 as well as Fig 9.5, it may be concluded that for any arbitrary temperature, $|\psi_f\rangle$ close to $|\psi_1\rangle$ maximizes the precision. Here, let us add a note of caution, from the definition, the weak value is independent of the temperature when $|\psi_f\rangle$ is exactly $|\psi_1\rangle$, hence measuring the weak value furnishes no information about the temperature. Thus, we must take $|\psi_f\rangle$ to be extremely close to $|\psi_1\rangle$, but not identically equal.

9.3.2 Precision analysis for unsharp post-selection

Let us now consider another potential source of error in the present scheme, that is, the post selection may be unsharp. Let us assume the unsharp post-measurement qubit state in the form

$$\rho_f^{(\epsilon)} = (1 - \epsilon)|\psi_f\rangle\langle\psi_f| + \frac{\epsilon}{2} \quad (9.25)$$

Thus, the corresponding perturbed weak value of the observable A is given by

$$A_w^\epsilon = \frac{\text{Tr}(\rho_f^{(\epsilon)} A \rho_T)}{\text{Tr}(\rho_f^{(\epsilon)} \rho_T)} \approx A_w \left[1 + \frac{\epsilon}{A_w} \left(\frac{\text{Tr}(A \rho_T) - 1}{\langle \psi_f | \rho_T | \psi_f \rangle} \right) \right] + O(\epsilon^2) \quad (9.26)$$

Now, using (9.15), the corresponding expression for shifted inverse temperature is $\tilde{\beta} = \frac{2}{\Delta}(-iA_w^\epsilon)$. From which, the formula for the squared relative error incurred is given by

$$\mathcal{N}_\beta^2 = \frac{|\tilde{\beta} - \beta|^2}{\epsilon^2 \beta^2} = \frac{4}{\Delta^2 \beta^2 [1 - \tanh^2(\beta \Delta / 2)]^2} \left| \frac{\text{Tr}(A \rho_T) - 1}{\langle \psi_f | \rho_T | \psi_f \rangle} \right|^2. \quad (9.27)$$

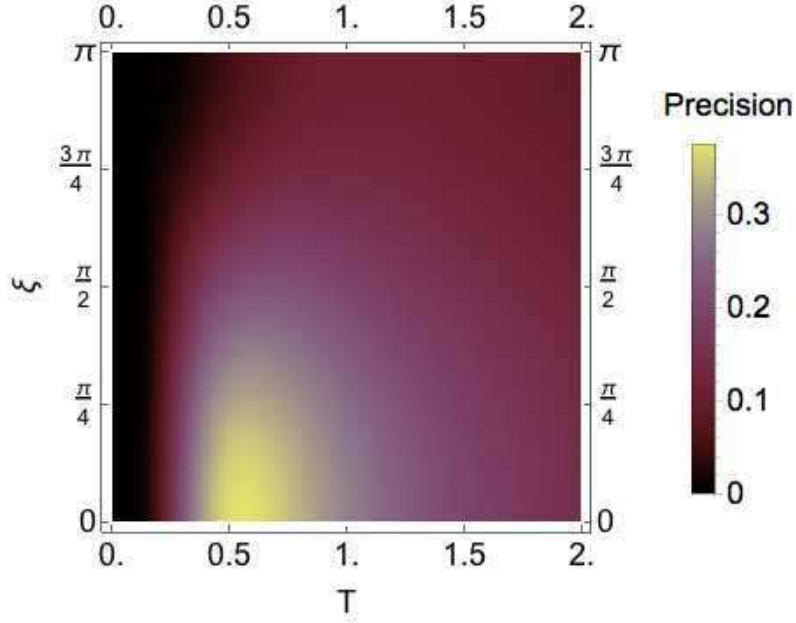


Figure 9.6: The magnitude of precision at optimal temperature is plotted against the temperature T and the polar angle ξ of the post selected state $|\psi_f\rangle$.

As in the previous section, if one chooses $A = -i|\psi_1\rangle\langle\psi_2| + i|\psi_2\rangle\langle\psi_1|$, then, assuming $\Delta = 1$ without loss of generality, the corresponding expression for relative error reads as

$$\mathcal{N}_\beta = \frac{4}{\beta \left[1 - \tanh^2 \frac{\beta}{2} \right] (1 + \cos \xi \tanh \frac{\beta}{2})}, \quad (9.28)$$

where ξ is the polar angle of the pure post selection state $|\psi_f\rangle$. For the specific choice $|\psi_f\rangle = \frac{1}{\sqrt{2}} (|\psi_1\rangle + |\psi_2\rangle)$ in the last section, this amounts to the following expression for precision, which is defined as the inverse of the error

$$1/\mathcal{N}_\beta(|+\rangle) = \frac{4}{\beta \left[1 - \tanh^2 \frac{\beta}{2} \right]}, \quad (9.29)$$

It can be seen from Fig. 9.6 that the precision, defined as the inverse of the relative error, attains a peak at some temperature, which determines the corresponding optimal temperature window for thermometry. Fig. 9.7 reveals that the optimal temperature for the scheme varies from $T_{\text{opt}} \approx 0.54$ to $T_{\text{opt}} \approx 1.12$. Solution of the following transcendental

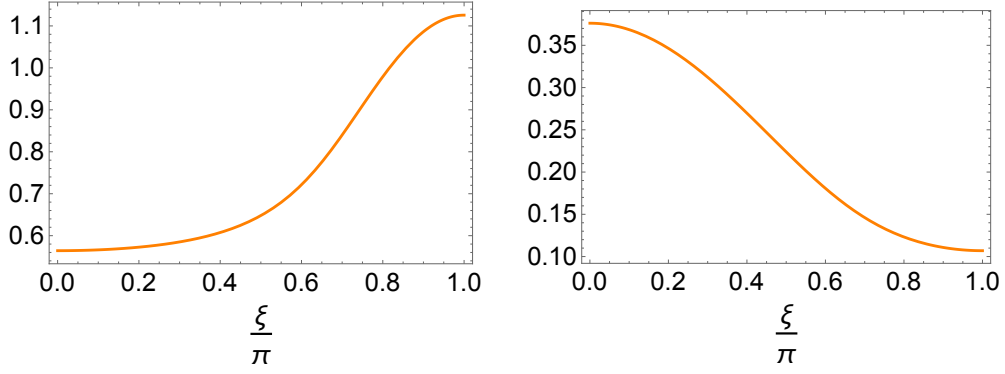


Figure 9.7: *Left-* optimal temperature, and *Right-* precision at optimal temperature, as a function of the polar angle ξ of the post measurement state $|\psi_f\rangle$.

equation determines the location of the optimal temperature T^* for any given post-selected state $|\psi_f\rangle$ with the polar angle ξ

$$\cos \xi = \frac{\sinh \frac{1}{T^*} - T^*(1 + \cosh \frac{1}{T^*})}{T^* \sinh \frac{1}{T^*} - \cosh \frac{1}{T^*} + 2} \quad (9.30)$$

An interesting feature we observe in Fig 9.7 is that there is a shift in the optimal temperature window towards the right, and higher temperatures is associated with the reduction in the optimal precision attainable through the present scheme. This is in line with the intuition that, as a distinctly quantum mechanical scheme, the weak measurement protocol should work best in the low temperature regime.

9.4 Quantum Fisher Information based analysis of precision of weak thermometry protocol

Until now, we have looked at the robustness of precision of the weak measurement based thermometric protocol. In this section, we present the complementary analysis of thermometric precision in this protocol through the usual quantum estimation theoretic methods. Let us first recall the relevant bound on fluctuation Δu of estimation of a single parameter u , which is known as the *quantum Cramer-Rao bound (QCRB)*.

$$\Delta u \geq \frac{1}{\sqrt{n\mathcal{F}_u(\rho_u)}}, \quad (9.31)$$

where \mathcal{F} is the quantum Fisher Information for the state ρ_u , and n is the number of runs. For the single parameter estimation case, it is always possible to saturate the lower bound. We now remember that the final state of the pointer after the post-selection in state $|\psi_f\rangle$ is given in (9.6), which is a pure state. For a pure state $|\psi_u\rangle$ with the corresponding parameter u , we recall that the QFI is given by [298]

$$\mathcal{F}_u = 4\langle \dot{\psi}_u | \dot{\psi}_u \rangle - 4|\langle \psi_u | \dot{\psi}_u \rangle|^2, \quad (9.32)$$

where $|\dot{\psi}_u\rangle$ denotes the first derivative of the state $|\psi_u\rangle$ with respect to the parameter u . Putting this in (9.6), we obtain the following expression for QFI for temperature T after a little algebra

$$\mathcal{F}_T = g^2 \tau^2 \left(\frac{dA_w}{dT} \right)^2 (\xi - \xi^2) \quad (9.33)$$

Here $\xi = \langle \phi | e^{igA_w^* \hat{P}_x} \hat{P}_x e^{-igA_w \hat{P}_x} | \phi \rangle = |\langle \phi | x \rangle|^2 e^{2g\tau \text{Im}(A_w)}$. Thus, upto leading order, the square-root of QFI is proportional to

$$\sqrt{\mathcal{F}_T} \propto \tilde{\mathcal{F}} = \left| \frac{dA_w}{dT} \right| = \left| \frac{\langle \psi_f | A \frac{d\rho_T}{dT} | \psi_f \rangle}{\langle \psi_f | \rho_T | \psi_f \rangle} - \frac{\langle \psi_f | \frac{d\rho_T}{dT} | \psi_f \rangle \langle \psi_f | A \rho_T | \psi_f \rangle}{(\langle \psi_f | \rho_T | \psi_f \rangle)^2} \right| \quad (9.34)$$

Once more, we assume $\hat{A} = \hat{\sigma}_y$ unless otherwise mentioned. Expressing an arbitrary post-selected state as $|\psi_f\rangle = \cos \frac{\theta}{2} |0\rangle + \sin \frac{\theta}{2} e^{i\phi} |1\rangle$, we obtain the expression for scaled precision $\tilde{\mathcal{F}}$ as being

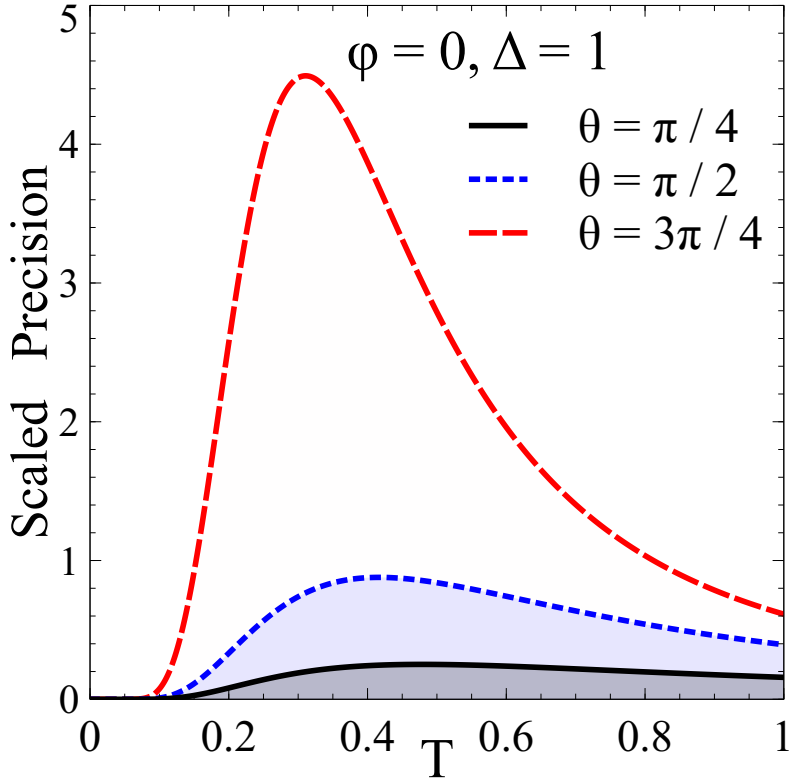


Figure 9.8: Scaled precision \tilde{F} plotted against temperature for various choices of post-selected state parameter θ . The energy gap Δ is taken to be unity, and the azimuthal angle ϕ of the post-selected state is assumed to be zero.

$$\tilde{F} = \frac{2e^{\Delta/T} \Delta \sin \theta \sqrt{\cos^2 \phi + \cos^2 \theta \sin^2 \phi}}{T^2 [1 - \cos \theta + e^{\Delta/T} (1 + \cos \theta)]^2} \quad (9.35)$$

Some specific illustrations for different values of θ are demonstrated in Fig. 9.8. The existence of an optimal temperature window is once more observed, as is the feature of a shift in the optimal temperature window by shifting the choice of the post selection. As earlier, attempt to shift this optimal temperature window towards the right, i.e., to higher temperatures by judiciously choosing the post-selection state, inevitably results in a loss of optimal precision. Thus, the QFI based analysis yields the same qualitative picture as the analysis performed earlier.

9.5 Summary

- A thermometric protocol in terms of the weak measurement scheme is proposed. The weakness of interactions is suggested to be beneficial in case the probe is highly susceptible to damage from the thermal environment.
- The optimal temperature window for this scheme can be tweaked by changing the choice of post-selected states, and not solely determined by the energy spectrum of the probe.
- There is a trade off involved in shifting the optimal temperature window towards higher temperatures, and the precision as well as the robustness of precision.

Future directions of work

We have finally come to the conclusion of the present thesis. We have seen how quantum resources like coherence and magic are interlinked, analysed the role non-Markovian dynamic plays in affecting the quantum features of a central spin system, studied a quantum autonomous refrigerator model from the perspective of limitations set forth by the existence of a quantum speed limit, proposed an autonomous thermal machine for steady state creation of quantum resources, and proposed two different novel methods of quantum thermometry. The natural question is - what's next ? While we strive to provide some possible answers to this question - it should be borne in mind that some of these directions may eventually turn out to be blind alleys, while unforeseen directions may spring up.

Firstly, unlike other quantum resources, for example, entanglement, the potential of condensed matter spin chain systems for the purpose of magic state quantum computation is underexplored. We have very recently started investigation on how to quantify the magic in simple spin chain systems, and this avenue of research looks promising indeed.

Secondly, The present thesis dwells almost entirely on the finite dimensional quantum systems. However, the basic question that the thesis seeks to address, namely, the interplay between thermal and quantum features of systems, is equally relevant for infinite dimensional systems. For example, the discrete Wigner function based approach to magic has a

very strong resonance to the resource theory of non-Gaussianity and Wigner negativity in the Bosonic case.

Thirdly, the quantum switch based protocol for thermometry as laid down in the penultimate main chapter of the thesis, can easily be generalized to more general metrological protocols, and indeed, beyond metrology as well. We hope to provide more concrete and operationally important results in this direction soon.

Fourthly, quantum networks with nodes rich in quantum resources are going to be operationally crucial in the age of quantum computers. The analysis of growth models of quantum networks in different environments has to take quantum thermodynamic limitations into consideration, just as thermodynamic considerations are relevant for classical network science. Moreover, the growth and dynamics of such networks must be affected by the monogamy of quantum correlations, unlike classical networks, where preferential attachment based growth models are very successful. Thus, the study of quantum dynamics in these systems is going to be a necessary component of building a genuinely quantum network.

Finally, with the recent emphasis on environmental concerns and a potentially looming crisis of resources, doing less with more is more important than ever. Hence suitable analysis of energetic cost of implementing various protocols and creating useable resources is an extremely practical question, and for that purpose, it is vital to envisage how quantum resources may be created using environments as potential allies, instead of enemies.

Bibliography

- [1] A. Einstein, B. Podolsky, and N. Rosen. Can quantum-mechanical description of physical reality be considered complete? *Phys. Rev.*, 47:777–780, May 1935.
- [2] R.P Feynman and F.L Vernon. The theory of a general quantum system interacting with a linear dissipative system. *Annals of Physics*, 24:118 – 173, 1963.
- [3] Paul Benioff. The computer as a physical system: A microscopic quantum mechanical hamiltonian model of computers as represented by turing machines. *Journal of Statistical Physics*, 22(5):563–591, May 1980.
- [4] J. S. Bell. On the einstein podolsky rosen paradox. *Physics Physique Fizika*, 1:195–200, Nov 1964.
- [5] SIMON KOCHEN and E. P. SPECKER. The problem of hidden variables in quantum mechanics. *Journal of Mathematics and Mechanics*, 17(1):59–87, 1967.
- [6] C.E. Shannon and W. Weaver. *The Mathematical Theory of Communication*. University of Illinois Press, 1998.
- [7] T.M. Cover and J.A. Thomas. *Elements of Information Theory*. Wiley, 2012.
- [8] Rajesh P. N. Rao, Nisha Yadav, Mayank N. Vahia, Hrishikesh Joglekar, R. Adhikari, and Iravatham Mahadevan. A markov model of the indus script. *Proceedings of the National Academy of Sciences*, 106(33):13685–13690, 2009.

- [9] Hector Zenil and Jean-Paul Delahaye. An algorithmic information-theoretic approach to the behaviour of financial markets, 2010.
- [10] Leo Szilard. Über die ausdehnung der phänomenologischen thermodynamik auf die schwankungserscheinungen. *Zeitschrift für Physik*, 32(1):753–788, Dec 1925.
- [11] Rolf Landauer. Irreversibility and heat generation in the computing process. *IBM Journal of Research and Development*, 5(3):183–191, 1961.
- [12] Charles H. Bennett and Stephen J. Wiesner. Communication via one- and two-particle operators on einstein-podolsky-rosen states. *Phys. Rev. Lett.*, 69:2881–2884, Nov 1992.
- [13] Charles H. Bennett, Gilles Brassard, Claude Crépeau, Richard Jozsa, Asher Peres, and William K. Wootters. Teleporting an unknown quantum state via dual classical and einstein-podolsky-rosen channels. *Phys. Rev. Lett.*, 70:1895–1899, Mar 1993.
- [14] Asher Peres. All the bell inequalities, 1998.
- [15] Tamás Vértesi and Nicolas Brunner. Disproving the Peres conjecture by showing Bell nonlocality from bound entanglement. *Nature Communications*, 5:5297, Nov 2014.
- [16] William K. Wootters. Entanglement of formation of an arbitrary state of two qubits. *Phys. Rev. Lett.*, 80:2245–2248, Mar 1998.
- [17] G. Vidal, W. Dür, and J. I. Cirac. Entanglement cost of bipartite mixed states. *Phys. Rev. Lett.*, 89:027901, Jun 2002.
- [18] Charles H. Bennett, Herbert J. Bernstein, Sandu Popescu, and Benjamin Schumacher. Concentrating partial entanglement by local operations. *Phys. Rev. A*, 53:2046–2052, Apr 1996.
- [19] G. Vidal and R. F. Werner. Computable measure of entanglement. *Phys. Rev. A*, 65:032314, Feb 2002.

- [20] Matthias Christandl and Andreas Winter. “squashed entanglement”: An additive entanglement measure. *Journal of Mathematical Physics*, 45(3):829–840, Mar 2004.
- [21] Arun K. Pati. Minimum classical bit for remote preparation and measurement of a qubit. *Phys. Rev. A*, 63:014302, Dec 2000.
- [22] Özen c Güngör and Sadi Turgut. Entanglement-assisted state discrimination and entanglement preservation. *Phys. Rev. A*, 94:032330, Sep 2016.
- [23] V. Giovannetti, S. Lloyd, and L. Maccone. The speed limit of quantum unitary evolution. *Journal of Optics B: Quantum and Semiclassical Optics*, 6:S807–S810, August 2004.
- [24] W. Dür, G. Vidal, and J. I. Cirac. Three qubits can be entangled in two inequivalent ways. *Physical Review A*, 62(6), Nov 2000.
- [25] Tobias J. Osborne and Frank Verstraete. General monogamy inequality for bipartite qubit entanglement. *Physical Review Letters*, 96(22), Jun 2006.
- [26] L Henderson and V Vedral. Classical, quantum and total correlations. *Journal of Physics A: Mathematical and General*, 34(35):6899–6905, Aug 2001.
- [27] Harold Ollivier and Wojciech H. Zurek. Quantum discord: A measure of the quantumness of correlations. *Phys. Rev. Lett.*, 88:017901, Dec 2001.
- [28] Borivoje Dakić, Vlatko Vedral, and Āaslav Brukner. Necessary and sufficient condition for nonzero quantum discord. *Phys. Rev. Lett.*, 105:190502, Nov 2010.
- [29] Jonathan Oppenheim, Michał Horodecki, Paweł Horodecki, and Ryszard Horodecki. Thermodynamical approach to quantifying quantum correlations. *Physical Review Letters*, 89(18), Oct 2002.

- [30] Davide Girolami, Tommaso Tufarelli, and Gerardo Adesso. Characterizing non-classical correlations via local quantum uncertainty. *Physical Review Letters*, 110(24), Jun 2013.
- [31] Animesh Datta, Anil Shaji, and Carlton M. Caves. Quantum discord and the power of one qubit. *Phys. Rev. Lett.*, 100:050502, Feb 2008.
- [32] Lectures on general quantum correlations and their applications. *Quantum Science and Technology*, 2017.
- [33] T. Baumgratz, M. Cramer, and M. B. Plenio. Quantifying coherence. *Phys. Rev. Lett.*, 113:140401, Sep 2014.
- [34] Carmine Napoli, Thomas R. Bromley, Marco Cianciaruso, Marco Piani, Nathaniel Johnston, and Gerardo Adesso. Robustness of coherence: An operational and observable measure of quantum coherence. *Phys. Rev. Lett.*, 116:150502, Apr 2016.
- [35] Marco Piani, Marco Cianciaruso, Thomas R. Bromley, Carmine Napoli, Nathaniel Johnston, and Gerardo Adesso. Robustness of asymmetry and coherence of quantum states. *Phys. Rev. A*, 93:042107, Apr 2016.
- [36] Sumana Karmakar, Ajoy Sen, Indrani Chattopadhyay, Amit Bhar, and Debasis Sarkar. Coherence fraction. *Quantum Information Processing*, 18(9):275, Jul 2019.
- [37] Alexander Streltsov, Uttam Singh, Himadri Shekhar Dhar, Manabendra Nath Bera, and Gerardo Adesso. Measuring quantum coherence with entanglement. *Phys. Rev. Lett.*, 115:020403, Jul 2015.
- [38] N. Killoran, F. E. S. Steinhoff, and M. B. Plenio. Converting nonclassicality into entanglement. *Phys. Rev. Lett.*, 116:080402, Feb 2016.
- [39] Chiranjib Mukhopadhyay, Sk Sazim, and Arun Kumar Pati. Coherence makes quantum systems ‘magical’. *Journal of Physics A: Mathematical and Theoretical*, 51(41):414006, sep 2018.

- [40] Iman Marvian, Robert W. Spekkens, and Paolo Zanardi. Quantum speed limits, coherence, and asymmetry. *Phys. Rev. A*, 93:052331, May 2016.
- [41] M. Lostaglio, D. Jennings, and T. Rudolph. Description of quantum coherence in thermodynamic processes requires constraints beyond free energy. *Nature Communications*, 6:6383, March 2015.
- [42] Peter W. Shor. Polynomial-time algorithms for prime factorization and discrete logarithms on a quantum computer. *SIAM J. Comput.*, 26(5):1484–1509, October 1997.
- [43] Lov K. Grover. A fast quantum mechanical algorithm for database search. *arXiv e-prints*, pages quant-ph/9605043, May 1996.
- [44] Richard Jozsa and Noah Linden. On the role of entanglement in quantum-computational speed-up. *Proceedings of the Royal Society of London A: Mathematical, Physical and Engineering Sciences*, 459(2036):2011–2032, 2003.
- [45] S. L. Braunstein and A. K. Pati. Speed-up and entanglement in quantum searching. *Quantum Information and Computation*, 2:399, 2002.
- [46] A. K. Pati and S. L. Braunstein. *Special Issue Indian Institute of Science*, 89:295, 2009.
- [47] D Deutsch and R Jozsa. Rapid solution of problems by quantum computation. *Proceedings of the Royal Society of London A: Mathematical, Physical and Engineering Sciences*, 439(1907):553–558, 1992.
- [48] Mark Hillery. Coherence as a resource in decision problems: The deutsch-jozsa algorithm and a variation. *Phys. Rev. A*, 93:012111, Jan 2016.
- [49] Hai-Long Shi, Si-Yuan Liu, Xiao-Hui Wang, Wen-Li Yang, Zhan-Ying Yang, and Heng Fan. Coherence depletion in the grover quantum search algorithm. *Phys. Rev. A*, 95:032307, Mar 2017.

- [50] N. Anand and A. K. Pati. Coherence and Entanglement Monogamy in the Discrete Analogue of Analog Grover Search. *ArXiv e-prints*, November 2016.
- [51] M.A. Nielsen and I.L. Chuang. *Quantum Computation and Quantum Information*. Cambridge Series on Information and the Natural Sciences. Cambridge University Press, 2000.
- [52] Daniel Gottesman. The Heisenberg Representation of Quantum Computers. *arXiv e-prints*, pages quant-ph/9807006, Jul 1998.
- [53] Sergey Bravyi and Alexei Kitaev. Universal quantum computation with ideal clifford gates and noisy ancillas. *Phys. Rev. A*, 71:022316, Feb 2005.
- [54] V. Veitch, S. A. Hamed Mousavian, D. Gottesman, and J. Emerson. The resource theory of stabilizer quantum computation. *New J. Phys.*, 16(1):013009, January 2014.
- [55] Mark Howard and Earl Campbell. Application of a resource theory for magic states to fault-tolerant quantum computing. *Phys. Rev. Lett.*, 118:090501, Mar 2017.
- [56] M. Ahmadi, H. Bui Dang, G. Gour, and B. C. Sanders. Quantification and manipulation of magic states. *ArXiv e-prints*, June 2017.
- [57] B. Regula. Convex geometry of quantum resource quantification. *ArXiv e-prints*, July 2017.
- [58] M. Howard, J. Wallman, V. Veitch, and J. Emerson. Contextuality supplies the ‘magic’ for quantum computation. *Nature*, 510:351–355, June 2014.
- [59] B. Bylicka, M. Tukiainen, D. Chruściński, J. Piilo, and S. Maniscalco. Thermodynamic power of non-Markovianity. *Scientific Reports*, 6:27989, June 2016.
- [60] Alex W. Chin, Susana F. Huelga, and Martin B. Plenio. Quantum metrology in non-markovian environments. *Phys. Rev. Lett.*, 109:233601, Dec 2012.

- [61] B. Bellomo, R. Lo Franco, and G. Compagno. Non-markovian effects on the dynamics of entanglement. *Phys. Rev. Lett.*, 99:160502, Oct 2007.
- [62] Heinz-Peter Breuer, Elsi-Mari Laine, and Jyrki Piilo. Measure for the degree of non-markovian behavior of quantum processes in open systems. *Phys. Rev. Lett.*, 103:210401, Nov 2009.
- [63] Elsi-Mari Laine, Jyrki Piilo, and Heinz-Peter Breuer. Measure for the non-markovianity of quantum processes. *Phys. Rev. A*, 81:062115, Jun 2010.
- [64] Titas Chanda and Samyadeb Bhattacharya. Delineating incoherent non-markovian dynamics using quantum coherence. *Annals of Physics*, 366:1 – 12, 2016.
- [65] Ángel Rivas, Susana F. Huelga, and Martin B. Plenio. Entanglement and non-markovianity of quantum evolutions. *Phys. Rev. Lett.*, 105:050403, Jul 2010.
- [66] A Rivas, Susana F Huelga, and Martin B Plenio. Quantum non-markovianity: characterization, quantification and detection. *Reports on Progress in Physics*, 77(9):094001, 2014.
- [67] Simon Milz, Felix A. Pollock, and Kavan Modi. An introduction to operational quantum dynamics. *Open Systems Information Dynamics*, 24(04):1740016, Dec 2017.
- [68] Felix A. Pollock, César Rodríguez-Rosario, Thomas Frauenheim, Mauro Paternostro, and Kavan Modi. Non-markovian quantum processes: Complete framework and efficient characterization. *Phys. Rev. A*, 97:012127, Jan 2018.
- [69] Yakir Aharonov, Jeeva Anandan, Sandu Popescu, and Lev Vaidman. Superpositions of time evolutions of a quantum system and a quantum time-translation machine. *Phys. Rev. Lett.*, 64:2965–2968, Jun 1990.

- [70] Giulio Chiribella, Giacomo Mauro D’Ariano, Paolo Perinotti, and Benoit Valiron. Quantum computations without definite causal structure. *Phys. Rev. A*, 88:022318, Aug 2013.
- [71] K. Goswami, C. Giarmatzi, M. Kewming, F. Costa, C. Branciard, J. Romero, and A. G. White. Indefinite causal order in a quantum switch. *Phys. Rev. Lett.*, 121:090503, Aug 2018.
- [72] Daniel Ebler, Sina Salek, and Giulio Chiribella. Enhanced communication with the assistance of indefinite causal order. *Phys. Rev. Lett.*, 120:120502, Mar 2018.
- [73] Lorenzo M. Procopio, Amir Moqanaki, Mateus Araújo, Fabio Costa, Irati Alonso Calafell, Emma G. Dowd, Deny R. Hamel, Lee A. Rozema, Časlav Brukner, and Philip Walther. Experimental superposition of orders of quantum gates. *Nature Communications*, 6:7913 EP –, 08 2015.
- [74] Giulia Rubino, Lee A. Rozema, Adrien Feix, Mateus Araújo, Jonas M. Zeuner, Lorenzo M. Procopio, Časlav Brukner, and Philip Walther. Experimental verification of an indefinite causal order. *Science Advances*, 3(3):e1602589, Mar 2017.
- [75] Adrien Feix, Mateus Araújo, and Časlav Brukner. Quantum superposition of the order of parties as a communication resource. *Phys. Rev. A*, 92:052326, Nov 2015.
- [76] G. Chiribella, M. Banik, S. Sankar Bhattacharya, T. Guha, M. Alimuddin, A. Roy, S. Saha, S. Agrawal, and G. Kar. Indefinite causal order enables perfect quantum communication with zero capacity channel. *ArXiv e-prints*, October 2018.
- [77] Mateus Araújo, Fabio Costa, and Časlav Brukner. Computational advantage from quantum-controlled ordering of gates. *Phys. Rev. Lett.*, 113:250402, Dec 2014.
- [78] Chiranjib Mukhopadhyay and Arun Kumar Pati. Superposition of causal order enables perfect quantum teleportation with very noisy singlets, 2019.

- [79] Ognyan Oreshkov, Fabio Costa, and Časlav Brukner. Quantum correlations with no causal order. *Nature Communications*, 3:1092, October 2012.
- [80] Alastair A. Abbott, Julian Wechs, Dominic Horsman, Mehdi Mhalla, and Cyril Branciard. Communication through coherent control of quantum channels. *arXiv e-prints*, page arXiv:1810.09826, Oct 2018.
- [81] Giulio Chiribella and Hlér Kristjánsson. A second-quantised Shannon theory. *arXiv e-prints*, page arXiv:1812.05292, December 2018.
- [82] Bob Coecke, Tobias Fritz, and Robert W. Spekkens. A mathematical theory of resources. *Information and Computation*, 250:59 – 86, 2016. Quantum Physics and Logic.
- [83] Fernando G. S. L. Brandão and Gilad Gour. Reversible framework for quantum resource theories. *Phys. Rev. Lett.*, 115:070503, Aug 2015.
- [84] Wojciech Hubert Zurek. Decoherence, einselection, and the quantum origins of the classical. *Rev. Mod. Phys.*, 75:715–775, May 2003.
- [85] Daniel A. Lidar. *Review of Decoherence-Free Subspaces, Noiseless Subsystems, and Dynamical Decoupling*, pages 295–354. John Wiley Sons, Ltd, 2014.
- [86] Lorenza Viola, Emanuel Knill, and Seth Lloyd. Dynamical decoupling of open quantum systems. *Phys. Rev. Lett.*, 82:2417–2421, Mar 1999.
- [87] Lorenza Viola and Seth Lloyd. Dynamical suppression of decoherence in two-state quantum systems. *Phys. Rev. A*, 58:2733–2744, Oct 1998.
- [88] E. C. G. Sudarshan, P. M. Mathews, and Jayaseetha Rau. Stochastic dynamics of quantum-mechanical systems. *Phys. Rev.*, 121:920–924, Feb 1961.
- [89] Philip Pechukas. Reduced dynamics need not be completely positive. *Phys. Rev. Lett.*, 73:1060–1062, Aug 1994.

- [90] Anil Shaji and E.C.G. Sudarshan. Who's afraid of not completely positive maps? *Physics Letters A*, 341(1):48 – 54, 2005.
- [91] H. P. Breuer and F. Petruccione. *The theory of open quantum systems*. Oxford University Press, Great Clarendon Street, 2002.
- [92] G. Lindblad. On the generators of quantum dynamical semigroups. *Communications in Mathematical Physics*, 48:119–130, June 1976.
- [93] V. Gorini, A. Kossakowski, and E. C. G. Sudarshan. Completely positive dynamical semigroups of N-level systems. *Journal of Mathematical Physics*, 17:821–825, May 1976.
- [94] Felix A. Pollock, César Rodríguez-Rosario, Thomas Frauenheim, Mauro Paternostro, and Kavan Modi. Non-markovian quantum processes: Complete framework and efficient characterization. *Phys. Rev. A*, 97:012127, Jan 2018.
- [95] Á. Rivas, S. F. Huelga, and M. B. Plenio. Quantum non-Markovianity: characterization, quantification and detection. *Reports on Progress in Physics*, 77(9):094001, September 2014.
- [96] Francesco Buscemi. Complete positivity, markovianity, and the quantum data-processing inequality, in the presence of initial system-environment correlations. *Phys. Rev. Lett.*, 113:140502, Oct 2014.
- [97] Dariusz Chruściński, Andrzej Kossakowski, and Ángel Rivas. Measures of non-markovianity: Divisibility versus backflow of information. *Phys. Rev. A*, 83:052128, May 2011.
- [98] Noah Linden, Sandu Popescu, and Paul Skrzypczyk. How small can thermal machines be? the smallest possible refrigerator. *Phys. Rev. Lett.*, 105:130401, Sep 2010.

- [99] Amikam Levy and Ronnie Kosloff. Quantum absorption refrigerator. *Phys. Rev. Lett.*, 108:070604, Feb 2012.
- [100] Mark T Mitchison, Marcus Huber, Javier Prior, Mischa P Woods, and Martin B Plenio. Realising a quantum absorption refrigerator with an atom-cavity system. *Quantum Science and Technology*, 1(1):015001, 2016.
- [101] P. P. Hofer, M. Perarnau-Llobet, J. Bohr Brask, R. Silva, M. Huber, and N. Brunner. Autonomous Quantum Refrigerator in a Circuit-QED Architecture Based on a Josephson Junction. *ArXiv e-prints*, July 2016.
- [102] Luis A. Correa, José P. Palao, Gerardo Adesso, and Daniel Alonso. Performance bound for quantum absorption refrigerators. *Phys. Rev. E*, 87:042131, Apr 2013.
- [103] Mark T Mitchison, Mischa P Woods, Javier Prior, and Marcus Huber. Coherence-assisted single-shot cooling by quantum absorption refrigerators. *New Journal of Physics*, 17(11):115013, 2015.
- [104] S. Das, A. Misra, A. K. Pal, A. S. De, and U. Sen. Necessarily transient quantum refrigerator. *ArXiv e-prints*, June 2016.
- [105] Karl Joulain, Jérémie Drevillon, Younès Ezzahri, and Jose Ordonez-Miranda. Quantum thermal transistor. *Phys. Rev. Lett.*, 116:200601, May 2016.
- [106] W. K. Wootters. The discrete wigner functiona. *Annals of the New York Academy of Sciences*, 480(1):275–282, 1986.
- [107] S. Chaturvedi. Aspects of mutually unbiased bases in odd-prime-power dimensions. *Phys. Rev. A*, 65:044301, Mar 2002.
- [108] D. Gross. Hudson’s theorem for finite-dimensional quantum systems. *Journal of Mathematical Physics*, 47(12):122107–122107, December 2006.
- [109] M.O. Scully and M.S. Zubairy. *Quantum Optics*. Cambridge University Press, 1997.

- [110] WOOTTERS WILLIAM K. The discrete wigner functiona. *Annals of the New York Academy of Sciences*, 480(1):275–282.
- [111] A Luis and J Perina. Discrete wigner function for finite-dimensional systems. *Journal of Physics A: Mathematical and General*, 31(5):1423, 1998.
- [112] S. Chaturvedi, E. Ercolessi, G. Marmo, G. Morandi, N. Mukunda, and R. Simon. Wigner distributions for finite dimensional quantum systems: An algebraic approach. *Pramana*, 65(6):981–993, Dec 2005.
- [113] Xiao-Dong Yu, Da-Jian Zhang, G. F. Xu, and D. M. Tong. Alternative framework for quantifying coherence. *Phys. Rev. A*, 94:060302, Dec 2016.
- [114] Eric Chitambar and Gilad Gour. Critical examination of incoherent operations and a physically consistent resource theory of quantum coherence. *Phys. Rev. Lett.*, 117:030401, Jul 2016.
- [115] Eric Chitambar and Gilad Gour. Comparison of incoherent operations and measures of coherence. *Phys. Rev. A*, 94:052336, Nov 2016.
- [116] J. I. de Vicente and A. Streltsov. Genuine quantum coherence. *J. Phys. A*, 50(4):045301, 2016.
- [117] C. Mukhopadhyay, U. Kamal Sharma, and I. Chakrabarty. A note on robustness of coherence for multipartite quantum states.
- [118] Alexander A. Klyachko, M. Ali Can, Sinem Binicioğlu, and Alexander S. Shumovsky. Simple test for hidden variables in spin-1 systems. *Phys. Rev. Lett.*, 101:020403, Jul 2008.
- [119] A. Grudka, K. Horodecki, M. Horodecki, P. Horodecki, R. Horodecki, P. Joshi, W. Kłobus, and A. Wójcik. Quantifying contextuality. *Phys. Rev. Lett.*, 112:120401, Mar 2014.

- [120] B. Amaral, A. Cabello, M. Terra Cunha, and L. Aolita. Noncontextual wirings. *ArXiv e-prints*.
- [121] Uttam Singh, Manabendra Nath Bera, Himadri Shekhar Dhar, and Arun Kumar Pati. Maximally coherent mixed states: Complementarity between maximal coherence and mixedness. *Phys. Rev. A*, 91:052115, May 2015.
- [122] Shuming Cheng and Michael J. W. Hall. Complementarity relations for quantum coherence. *Phys. Rev. A*, 92:042101, Oct 2015.
- [123] Xiang Zhan, Xin Zhang, Jian Li, Yongsheng Zhang, Barry C. Sanders, and Peng Xue. Realization of the contextuality-nonlocality tradeoff with a qubit-qutrit photon pair. *Phys. Rev. Lett.*, 116:090401, Feb 2016.
- [124] H. P. Breuer and F. Petruccione. *The theory of open quantum systems*. Oxford University Press, Great Clarendon Street, 2002.
- [125] N V Prokof'ev and P C E Stamp. Theory of the spin bath. *Reports on Progress in Physics*, 63(4):669, 2000.
- [126] A. J. Leggett, S. Chakravarty, A. T. Dorsey, Matthew P. A. Fisher, Anupam Garg, and W. Zwerger. Dynamics of the dissipative two-state system. *Rev. Mod. Phys.*, 59:1–85, Jan 1987.
- [127] U Weiss. *Quantum Dissipative Systems*, volume 10 of *Series in Modern Condensed Matter Physics*. World Scientific, 2 edition, 1999.
- [128] A. O. Caldeira and A. J. Leggett. Quantum tunnelling in a dissipative system. *Annals of Physics*, 149:374–456, September 1983.
- [129] J. B. Parkinson and D. J. J. Farnell. *An Introduction to Quantum Spin Systems*, volume 816 of *Lect. Notes Phys*. Springer, Berlin, 2010.
- [130] Thomas F Rosenbaum. Quantum magnets and glasses. *Journal of Physics: Condensed Matter*, 8(48):9759, 1996.

- [131] A. J. Leggett, S. Chakravarty, A. T. Dorsey, Matthew P. A. Fisher, Anupam Garg, and W. Zwerger. Dynamics of the dissipative two-state system. *Rev. Mod. Phys.*, 59:1–85, Jan 1987.
- [132] Sadao Nakajima. On quantum theory of transport phenomena: Steady diffusion. *Progress of Theoretical Physics*, 20(6):948–959, 1958.
- [133] Robert Zwanzig. Ensemble method in the theory of irreversibility. *The Journal of Chemical Physics*, 33(5):1338–1341, 1960.
- [134] Heinz-Peter Breuer, Daniel Burgarth, and Francesco Petruccione. Non-markovian dynamics in a spin star system: Exact solution and approximation techniques. *Phys. Rev. B*, 70:045323, Jul 2004.
- [135] Jan Fischer and Heinz-Peter Breuer. Correlated projection operator approach to non-markovian dynamics in spin baths. *Phys. Rev. A*, 76:052119, Nov 2007.
- [136] V. Semin, I. Sinayskiy, and F. Petruccione. Initial correlation in a system of a spin coupled to a spin bath through an intermediate spin. *Phys. Rev. A*, 86:062114, Dec 2012.
- [137] Heinz-Peter Breuer, Elsi-Mari Laine, Jyrki Piilo, and Bassano Vacchini. *Colloquium* : Non-markovian dynamics in open quantum systems. *Rev. Mod. Phys.*, 88:021002, Apr 2016.
- [138] B. Bylicka, D. Chruściński, and S. Maniscalco. Non-markovianity and reservoir memory of quantum channels: a quantum information theory perspective. *Scientific Reports*, 4:5720, Jul 2014.
- [139] Arend G. Dijkstra and Yoshitaka Tanimura. Non-markovian entanglement dynamics in the presence of system-bath coherence. *Phys. Rev. Lett.*, 104:250401, Jun 2010.

- [140] M. Pezzutto, M. Paternostro, and Y. Omar. Implications of non-Markovian dynamics for the Landauer bound. *ArXiv e-prints*, August 2016.
- [141] David Gelbwaser-Klimovsky, Wolfgang Niedenzu, and Gershon Kurizki. Chapter twelve - thermodynamics of quantum systems under dynamical control. volume 64 of *Advances In Atomic, Molecular, and Optical Physics*, pages 329 – 407. Academic Press, 2015.
- [142] Yuichiro Matsuzaki, Simon C. Benjamin, and Joseph Fitzsimons. Magnetic field sensing beyond the standard quantum limit under the effect of decoherence. *Phys. Rev. A*, 84:012103, Jul 2011.
- [143] Himadri Shekhar Dhar, Manabendra Nath Bera, and Gerardo Adesso. Characterizing non-markovianity via quantum interferometric power. *Phys. Rev. A*, 91:032115, Mar 2015.
- [144] C. Tietz, S. Schuler, T. Speck, U. Seifert, and J. Wrachtrup. Measurement of stochastic entropy production. *Phys. Rev. Lett.*, 97:050602, Aug 2006.
- [145] K. Turitsyn, M. Chertkov, V. Y. Chernyak, and A. Puliafito. Statistics of entropy production in linearized stochastic systems. *Phys. Rev. Lett.*, 98:180603, May 2007.
- [146] Benjamin Andrae, Jonas Cremer, Tobias Reichenbach, and Erwin Frey. Entropy production of cyclic population dynamics. *Phys. Rev. Lett.*, 104:218102, May 2010.
- [147] Pankaj Mehta and Natan Andrei. Nonequilibrium quantum impurities: From entropy production to information theory. *Phys. Rev. Lett.*, 100:086804, Feb 2008.
- [148] Anatoli Polkovnikov, Krishnendu Sengupta, Alessandro Silva, and Mukund Vengalattore. *Colloquium* : Nonequilibrium dynamics of closed interacting quantum systems. *Rev. Mod. Phys.*, 83:863–883, Aug 2011.
- [149] Sebastian Deffner and Eric Lutz. Nonequilibrium entropy production for open quantum systems. *Phys. Rev. Lett.*, 107:140404, Sep 2011.

- [150] Herbert Spohn. Entropy production for quantum dynamical semigroups. *Journal of Mathematical Physics*, 19(5):1227–1230, 1978.
- [151] Erika Andersson, James D. Cresser, and Michael J. W. Hall. Finding the kraus decomposition from a master equation and vice versa. *Journal of Modern Optics*, 54(12):1695–1716, 2007.
- [152] A. R. Usha Devi, A. K. Rajagopal, and Sudha. Open-system quantum dynamics with correlated initial states, not completely positive maps, and non-markovianity. *Phys. Rev. A*, 83:022109, Feb 2011.
- [153] A. R. Usha Devi, A. K. Rajagopal, S. Shenoy, and R.W. Rendell. Interplay of quantum stochastic and dynamical maps to discern markovian and non-markovian transitions. *JQIS*, 2:47, June 2012.
- [154] M. M. Wolf, J. Eisert, T. S. Cubitt, and J. I. Cirac. Assessing non-markovian quantum dynamics. *Phys. Rev. Lett.*, 101:150402, Oct 2008.
- [155] A. K. Rajagopal, A. R. Usha Devi, and R. W. Rendell. Kraus representation of quantum evolution and fidelity as manifestations of markovian and non-markovian forms. *Phys. Rev. A*, 82:042107, Oct 2010.
- [156] Heinz-Peter Breuer. Foundations and measures of quantum non-markovianity. *Journal of Physics B: Atomic, Molecular and Optical Physics*, 45(15):154001, 2012.
- [157] Dariusz Chruściński and Andrzej Kossakowski. Non-markovian quantum dynamics: Local versus nonlocal. *Phys. Rev. Lett.*, 104:070406, Feb 2010.
- [158] R Alicki. The quantum open system as a model of the heat engine. *Journal of Physics A: Mathematical and General*, 12(5):L103, 1979.
- [159] Debbie W. Leung. Choi’s proof as a recipe for quantum process tomography. *Journal of Mathematical Physics*, 44(2):528–533, 2003.

- [160] Man-Duen Choi. Completely positive linear maps on complex matrices. *Linear Algebra and its Applications*, 10(3):285 – 290, 1975.
- [161] Ruggero Vasile, Sabrina Maniscalco, Matteo G. A. Paris, Heinz-Peter Breuer, and Jyrki Piilo. Quantifying non-markovianity of continuous-variable gaussian dynamical maps. *Phys. Rev. A*, 84:052118, Nov 2011.
- [162] Xiao-Ming Lu, Xiaoguang Wang, and C. P. Sun. Quantum fisher information flow and non-markovian processes of open systems. *Phys. Rev. A*, 82:042103, Oct 2010.
- [163] Shunlong Luo. Wigner-yanase skew information and uncertainty relations. *Phys. Rev. Lett.*, 91:180403, Oct 2003.
- [164] x. Non-markovianity through accessible information. *Phys. Rev. Lett.*, 112:210402, May 2014.
- [165] S. Haseli, G. Karpat, S. Salimi, A. S. Khorashad, F. F. Fanchini, B. akmak, G. H. Aguilar, S. P. Walborn, and P. H. S. Ribeiro. Non-markovianity through flow of information between a system and an environment. *Phys. Rev. A*, 90:052118, Nov 2014.
- [166] M. B. Ruskai. Beyond strong subadditivity ? improved bounds on the contraction of generalized relative entropy. *Reviews in Mathematical Physics*, 06(05a):1147–1161, 1994.
- [167] P. Haikka, J. D. Cresser, and S. Maniscalco. Comparing different non-markovianity measures in a driven qubit system. *Phys. Rev. A*, 83:012112, Jan 2011.
- [168] N. Erez, G. Gordon, M. Nest, and G. Kurizki. Thermodynamic control by frequent quantum measurements. , 452:724–727, April 2008.
- [169] Goren Gordon, Guy Bensky, David Gelbwaser-Klimovsky, D D Bhaktavatsala Rao, Noam Erez, and Gershon Kurizki. Cooling down quantum bits on ultrashort time scales. *New Journal of Physics*, 11(12):123025, 2009.

- [170] P. Facchi, S. Pascazio, V. Vedral, and K. Yuasa. Quantumness and entanglement witnesses. *Journal of Physics A Mathematical General*, 45(10):105302, March 2012.
- [171] S. Bhattacharya, S. Banerjee, and A. K. Pati. Effect of non-Markovianity on the dynamics of coherence, concurrence and Fisher information. *ArXiv e-prints*, January 2016.
- [172] A. J. Daley, H. Pichler, J. Schachenmayer, and P. Zoller. Measuring entanglement growth in quench dynamics of bosons in an optical lattice. *Phys. Rev. Lett.*, 109:020505, Jul 2012.
- [173] Artur K. Ekert, Carolina Moura Alves, Daniel K. L. Oi, Michał Horodecki, Paweł Horodecki, and L. C. Kwek. Direct estimations of linear and nonlinear functionals of a quantum state. *Phys. Rev. Lett.*, 88:217901, May 2002.
- [174] Fabio Antonio Bovino, Giuseppe Castagnoli, Artur Ekert, Paweł Horodecki, Carolina Moura Alves, and Alexander Vladimir Sergienko. Direct measurement of nonlinear properties of bipartite quantum states. *Phys. Rev. Lett.*, 95:240407, Dec 2005.
- [175] M. V. Gurudev Dutt, L. Childress, L. Jiang, E. Togan, J. Maze, F. Jelezko, A. S. Zibrov, P. R. Hemmer, and M. D. Lukin. Quantum register based on individual electronic and nuclear spin qubits in diamond. *Science*, 316(5829):1312–1316, 2007.
- [176] A Smirne, E-M Laine, H-P Breuer, J Piilo, and B Vacchini. Role of correlations in the thermalization of quantum systems. *New Journal of Physics*, 14(11):113034, 2012.
- [177] Ting Yu and J. H. Eberly. Finite-time disentanglement via spontaneous emission. *Phys. Rev. Lett.*, 93:140404, Sep 2004.

- [178] T. Yu and J. H. Eberly. Sudden Death of Entanglement. *Science*, 323:598, January 2009.
- [179] Thomas Konrad, Fernando de Melo, Markus Tiersch, Christian Kasztelan, Adriano Aragao, and Andreas Buchleitner. Evolution equation for quantum entanglement. *Nat Phys*, 4:99–102, 2008.
- [180] Pei Pei, Chong Li, Jia-Sen Jin, and He-Shan Song. Quantum coherence versus quantum discord in two coupled semiconductor double-dot molecules via a transmission line resonator. *Journal of Physics B: Atomic, Molecular and Optical Physics*, 44(3):035501, 2011.
- [181] M. Cianciaruso, T. R. Bromley, W. Roga, R. Lo Franco, and G. Adesso. Universal freezing of quantum correlations within the geometric approach. *Scientific Reports*, 5:10177, June 2015.
- [182] Thomas R. Bromley, Marco Cianciaruso, and Gerardo Adesso. Frozen quantum coherence. *Phys. Rev. Lett.*, 114:210401, May 2015.
- [183] Samyadeb Bhattacharya, Avijit Misra, Chiranjib Mukhopadhyay, and Arun Kumar Pati. Exact master equation for a spin interacting with a spin bath: Non-markovianity and negative entropy production rate. *Phys. Rev. A*, 95:012122, Jan 2017.
- [184] Christian Gogolin and Jens Eisert. Equilibration, thermalisation, and the emergence of statistical mechanics in closed quantum systems. *Reports on Progress in Physics*, 79(5):056001, 2016.
- [185] Ryogo Kubo. Statistical-mechanical theory of irreversible processes. i. general theory and simple applications to magnetic and conduction problems. *Journal of the Physical Society of Japan*, 12(6):570–586, 1957.

- [186] Paul C. Martin and Julian Schwinger. Theory of many-particle systems. i. *Phys. Rev.*, 115:1342–1373, Sep 1959.
- [187] Takahiro Hatano and Shin-ichi Sasa. Steady-state thermodynamics of langevin systems. *Phys. Rev. Lett.*, 86:3463–3466, Apr 2001.
- [188] Massimiliano Esposito and Shaul Mukamel. Fluctuation theorems for quantum master equations. *Physical Review E*, 73(4), Apr 2006.
- [189] J. Goold, M. Huber, A. Riera, L. del Rio, and P. Skrzypczyk. The role of quantum information in thermodynamicsa topical review. *Journal of Physics A Mathematical General*, 49(14):143001, April 2016.
- [190] R. Kosloff. Quantum Thermodynamics: A Dynamical Viewpoint. *Entropy*, 15:2100–2128, May 2013.
- [191] Marlan O. Scully. Extracting work from a single heat bath via vanishing quantum coherence ii: Microscopic model. *AIP Conference Proceedings*, 643(1):83–91, 2002.
- [192] J. Roßnagel, O. Abah, F. Schmidt-Kaler, K. Singer, and E. Lutz. Nanoscale heat engine beyond the carnot limit. *Phys. Rev. Lett.*, 112:030602, Jan 2014.
- [193] Wolfgang Niedenzu, David Gelbwaser-Klimovsky, Abraham G Kofman, and Gershon Kurizki. On the operation of machines powered by quantum non-thermal baths. *New Journal of Physics*, 18(8):083012, 2016.
- [194] W. Niedenzu, V. Mukherjee, A. Ghosh, A. G. Kofman, and G. Kurizki. Universal thermodynamic limit of quantum engine efficiency. *ArXiv e-prints*, March 2017.
- [195] J. Klaers, S. Faelt, A. Imamoglu, and E. Togan. Squeezed thermal reservoirs as a resource for a nano-mechanical engine beyond the Carnot limit. *ArXiv e-prints*, March 2017.

- [196] H.B. Reitlinger and A. Duchesne. *Sur l'Utilisation de la chaleur dans les machines à feu*. Imprimerie H. Vaillant-Carmanne, 1929.
- [197] I. Novikov. Effektivnyj koefitsient poleznovo deystvia atomnoy energeticeskoj ustanojki. *Atomnaya Energiya*, 3:409, 1957.
- [198] F. L. Curzon and B. Ahlborn. Efficiency of a Carnot engine at maximum power output. *American Journal of Physics*, 43:22–24, January 1975.
- [199] Z. Yan. *Cryogenics*, 3:17, 1984.
- [200] Zijun Yan and Jincan Chen. A class of irreversible carnot refrigeration cycles with a general heat transfer law. *Journal of Physics D: Applied Physics*, 23(2):136, 1990.
- [201] S. Velasco, J. M. M. Roco, A. Medina, and A. Calvo Hernández. New performance bounds for a finite-time carnot refrigerator. *Phys. Rev. Lett.*, 78:3241–3244, Apr 1997.
- [202] Obinna Abah and Eric Lutz. Optimal performance of a quantum otto refrigerator. *EPL (Europhysics Letters)*, 113(6):60002, 2016.
- [203] D. Gelbwaser-Klimovsky, W. Niedenzu, and G. Kurizki. Thermodynamics of Quantum Systems Under Dynamical Control. *Advances in Atomic Molecular and Optical Physics*, 64:329, 2015.
- [204] Raam Uzdin, Amikam Levy, and Ronnie Kosloff. Equivalence of quantum heat machines, and quantum-thermodynamic signatures. *Phys. Rev. X*, 5:031044, Sep 2015.
- [205] Tova Feldmann and Ronnie Kosloff. Performance of discrete heat engines and heat pumps in finite time. *Phys. Rev. E*, 61:4774–4790, May 2000.
- [206] Ronnie Kosloff and Tova Feldmann. Discrete four-stroke quantum heat engine exploring the origin of friction. *Phys. Rev. E*, 65:055102, May 2002.

- [207] A. Alecce, F. Galve, N. Lo Gullo, L. Dell'Anna, F. Plastina, and R. Zambrini. Quantum Otto cycle with inner friction: finite-time and disorder effects. *New Journal of Physics*, 17(7):075007, July 2015.
- [208] Selcuk Cakmak, Ferdi Altintas, Azmi Gencten, and Özgür E. Müstecaplıoğlu. Irreversible work and internal friction in a quantum otto cycle of a single arbitrary spin. *The European Physical Journal D*, 71(3):75, 2017.
- [209] Y. Rezek, P. Salamon, K. H. Hoffmann, and R. Kosloff. The quantum refrigerator: The quest for absolute zero. *EPL (Europhysics Letters)*, 85(3):30008, 2009.
- [210] Amikam Levy, Robert Alicki, and Ronnie Kosloff. Quantum refrigerators and the third law of thermodynamics. *Phys. Rev. E*, 85:061126, Jun 2012.
- [211] Amikam Levy and Ronnie Kosloff. Quantum absorption refrigerator. *Phys. Rev. Lett.*, 108:070604, Feb 2012.
- [212] Ralph Silva, Gonzalo Manzano, Paul Skrzypczyk, and Nicolas Brunner. Performance of autonomous quantum thermal machines: Hilbert space dimension as a thermodynamical resource. *Phys. Rev. E*, 94:032120, Sep 2016.
- [213] Luis A. Correa, José P. Palao, Gerardo Adesso, and Daniel Alonso. Performance bound for quantum absorption refrigerators. *Phys. Rev. E*, 87:042131, Apr 2013.
- [214] Ralph Silva, Paul Skrzypczyk, and Nicolas Brunner. Small quantum absorption refrigerator with reversed couplings. *Phys. Rev. E*, 92:012136, Jul 2015.
- [215] G. Maslennikov, S. Ding, R. Hablutzel, J. Gan, A. Roulet, S. Nimmrichter, J. Dai, V. Scarani, and D. Matsukevich. Quantum absorption refrigerator with trapped ions. *ArXiv e-prints*, February 2017.
- [216] S. Deffner and S. Campbell. Quantum speed limits: from Heisenbergs uncertainty principle to optimal quantum control. *Journal of Physics A Mathematical General*, 50:453001, November 2017.

- [217] Paul Skrzypczyk, Nicolas Brunner, Noah Linden, and Sandu Popescu. The smallest refrigerators can reach maximal efficiency. *Journal of Physics A: Mathematical and Theoretical*, 44(49):492002, 2011.
- [218] L. I. Mandelshtam and I. E Tamm. The uncertainty relation between energy and time in nonrelativistic quantum mechanics. *J. Phys. (USSR)*, 9:249, 1945.
- [219] J. Anandan and Y. Aharonov. Geometry of quantum evolution. *Phys. Rev. Lett.*, 65:1697–1700, Oct 1990.
- [220] N. Margolus and L. B. Levitin. The maximum speed of dynamical evolution. *Physica D Nonlinear Phenomena*, 120:188–195, September 1998.
- [221] G. De Palma, A. Mari, S. Lloyd, and V. Giovannetti. Multimode quantum entropy power inequality. *Phys. Rev. A*, 91:032320, Mar 2015.
- [222] A. K. Pati. Uncertainty relation of Anandan-Aharonov and intelligent states. *Physics Letters A*, 262:296–301, November 1999.
- [223] Lev Vaidman. Minimum time for the evolution to an orthogonal quantum state. *American Journal of Physics*, 60(2):182–183, 1992.
- [224] Lev B. Levitin and Tommaso Toffoli. Fundamental limit on the rate of quantum dynamics: The unified bound is tight. *Phys. Rev. Lett.*, 103:160502, Oct 2009.
- [225] D. Mondal and A. K. Pati. Quantum speed limit for mixed states using an experimentally realizable metric. *Physics Letters A*, 380:1395–1400, April 2016.
- [226] Sebastian Deffner and Eric Lutz. Quantum speed limit for non-markovian dynamics. *Phys. Rev. Lett.*, 111:010402, Jul 2013.
- [227] Debasis Mondal, Shrobona Bagchi, and Arun Kumar Pati. Tighter uncertainty and reverse uncertainty relations. *Phys. Rev. A*, 95:052117, May 2017.

- [228] M. M. Taddei, B. M. Escher, L. Davidovich, and R. L. de Matos Filho. Quantum speed limit for physical processes. *Phys. Rev. Lett.*, 110:050402, Jan 2013.
- [229] Diego Paiva Pires, Marco Cianciaruso, Lucas C. Céleri, Gerardo Adesso, and Diogo O. Soares-Pinto. Generalized geometric quantum speed limits. *Phys. Rev. X*, 6:021031, Jun 2016.
- [230] A. del Campo, I. L. Egusquiza, M. B. Plenio, and S. F. Huelga. Quantum speed limits in open system dynamics. *Phys. Rev. Lett.*, 110:050403, Jan 2013.
- [231] Alexander Streltsov, Gerardo Adesso, and Martin B. Plenio. Colloquium. *Rev. Mod. Phys.*, 89:041003, Oct 2017.
- [232] U. Singh, M. Nath Bera, A. Misra, and A. K. Pati. Erasing Quantum Coherence: An Operational Approach.
- [233] Mark T Mitchison, Mischa P Woods, Javier Prior, and Marcus Huber. Coherence-assisted single-shot cooling by quantum absorption refrigerators. *New Journal of Physics*, 17(11):115013, 2015.
- [234] Alexander Pechen and Herschel Rabitz. Teaching the environment to control quantum systems. *Phys. Rev. A*, 73:062102, Jun 2006.
- [235] H. P. Breuer and F. Petruccione. *The theory of open quantum systems*. Oxford University Press, Great Clarendon Street, 2002.
- [236] K. W. Murch, U. Vool, D. Zhou, S. J. Weber, S. M. Girvin, and I. Siddiqi. Cavity-assisted quantum bath engineering. *Phys. Rev. Lett.*, 109:183602, Oct 2012.
- [237] Alireza Shabani and Hartmut Neven. Artificial quantum thermal bath: Engineering temperature for a many-body quantum system. *Phys. Rev. A*, 94:052301, Nov 2016.
- [238] Vitalii Semin, Ilya Sinayskiy, and Francesco Petruccione. Arbitrary spin in a spin bath: Exact dynamics and approximation techniques. *Phys. Rev. A*, 89:012107, Jan 2014.

- [239] Inés de Vega and Daniel Alonso. Dynamics of non-markovian open quantum systems. *Rev. Mod. Phys.*, 89:015001, Jan 2017.
- [240] Samyadeb Bhattacharya, Avijit Misra, Chiranjib Mukhopadhyay, and Arun Kumar Pati. Exact master equation for a spin interacting with a spin bath: Non-markovianity and negative entropy production rate. *Phys. Rev. A*, 95:012122, Jan 2017.
- [241] Chiranjib Mukhopadhyay, Samyadeb Bhattacharya, Avijit Misra, and Arun Kumar Pati. Dynamics and thermodynamics of a central spin immersed in a spin bath. *Phys. Rev. A*, 96:052125, Nov 2017.
- [242] Stephen M. Barnett and Joan A. Vaccaro. Beyond landauer erasure. *Entropy*, 15(11):4956–4968, 2013.
- [243] M. Lostaglio, D. Jennings, and T. Rudolph. Thermodynamic resource theories, non-commutativity and maximum entropy principles. *New Journal of Physics*, 19(4):043008, April 2017.
- [244] Y. Guryanova, S. Popescu, A. J. Short, R. Silva, and P. Skrzypczyk. Thermodynamics of quantum systems with multiple conserved quantities. *Nature Communications*, 7:12049, July 2016.
- [245] N. Yunger Halpern, P. Faist, J. Oppenheim, and A. Winter. Microcanonical and resource-theoretic derivations of the thermal state of a quantum system with non-commuting charges. *Nature Communications*, 7:12051, July 2016.
- [246] Jackson S. S. T. Wright, Tim Gould, André R. R. Carvalho, Salil Bedkihal, and Joan A. Vaccaro. Quantum heat engine operating between thermal and spin reservoirs. *Phys. Rev. A*, 97:052104, May 2018.
- [247] Scientists show how to erase information without using energy. <https://phys.org/news/2011-01-scientists-erase-energy.html>.

- [248] G. Manzano, R. Silva, and J. M. R. Parrondo. Autonomous thermal machine for amplification and control of energetic coherence. *ArXiv e-prints*, September 2017.
- [249] Avijit Misra, Uttam Singh, Samyadeb Bhattacharya, and Arun Kumar Pati. Energy cost of creating quantum coherence. *Phys. Rev. A*, 93:052335, May 2016.
- [250] A. E. Leanhardt, T. A. Pasquini, M. Saba, A. Schirotzek, Y. Shin, D. Kielpinski, D. E. Pritchard, and W. Ketterle. Cooling bose-einstein condensates below 500 picokelvin. *Science*, 301(5639):1513–1515, 2003.
- [251] Immanuel Bloch, Jean Dalibard, and Wilhelm Zwerger. Many-body physics with ultracold gases. *Rev. Mod. Phys.*, 80:885–964, Jul 2008.
- [252] Piali Sengupta and Paul Garrity. Sensing temperature. *Current Biology*, 23(8):R304 – R307, 2013.
- [253] Luigi Seveso and Matteo G. A. Paris. Trade-off between information and disturbance in qubit thermometry. *Phys. Rev. A*, 97:032129, Mar 2018.
- [254] Mohammad Mehboudi, Anna Sanpera, and Luis A. Correa. Thermometry in the quantum regime: Recent theoretical progress. *arXiv e-prints*, page arXiv:1811.03988, November 2018.
- [255] Antonella De Pasquale and Thomas M. Stace. Quantum Thermometry. *arXiv e-prints*, page arXiv:1807.05762, July 2018.
- [256] Thomas M. Stace. Quantum limits of thermometry. *Phys. Rev. A*, 82:011611, Jul 2010.
- [257] Matteo Brunelli, Stefano Olivares, and Matteo G. A. Paris. Qubit thermometry for micromechanical resonators. *Phys. Rev. A*, 84:032105, Sep 2011.
- [258] Matteo Brunelli, Stefano Olivares, Mauro Paternostro, and Matteo G. A. Paris. Qubit-assisted thermometry of a quantum harmonic oscillator. *Phys. Rev. A*, 86:012125, Jul 2012.

- [259] Dong Xie, Chunling Xu, and An Min Wang. Optimal quantum thermometry by dephasing. *Quantum Information Processing*, 16:155, June 2017.
- [260] Patrick P. Hofer, Jonatan Bohr Brask, Martí Perarnau-Llobet, and Nicolas Brunner. Quantum thermal machine as a thermometer. *Phys. Rev. Lett.*, 119:090603, Sep 2017.
- [261] Peter A. Ivanov. Quantum Thermometry with Trapped Ions. *arXiv e-prints*, page arXiv:1809.01451, September 2018.
- [262] Ryszard Horodecki, Paweł Horodecki, Michał Horodecki, and Karol Horodecki. Quantum entanglement. *Rev. Mod. Phys.*, 81:865–942, Jun 2009.
- [263] Vittorio Giovannetti, Seth Lloyd, and Lorenzo Maccone. Advances in quantum metrology. *Nature Photonics*, 5:222–229, April 2011.
- [264] Chiranjib Mukhopadhyay and Arun Kumar Pati. Superposition of causal order enables perfect quantum teleportation with very noisy singlets. *arXiv e-prints*, page arXiv:1901.07626, January 2019.
- [265] Yu Guo, Xiao-Min Hu, Zhi-Bo Hou, Huan Cao, Jin-Ming Cui, Bi-Heng Liu, Yun-Feng Huang, Chuan-Feng Li, and Guang-Can Guo. Experimental investigating communication in a superposition of causal orders. *arXiv e-prints*, page arXiv:1811.07526, November 2018.
- [266] Luis A. Correa, Mohammad Mehboudi, Gerardo Adesso, and Anna Sanpera. Individual quantum probes for optimal thermometry. *Phys. Rev. Lett.*, 114:220405, Jun 2015.
- [267] MATTEO G. A. PARIS. Quantum estimation for quantum technology. *International Journal of Quantum Information*, 07(supp01):125–137, 2009.

- [268] Timothy F. Havel. Robust procedures for converting among lindblad, kraus and matrix representations of quantum dynamical semigroups. *Journal of Mathematical Physics*, 44(2):534–557, 2003.
- [269] Asoka Biswas and Paul Brumer. Generic construction of kraus operators: d-level systems in a thermal bosonic bath. *Israel Journal of Chemistry*, 52(5):461–466.
- [270] K. Goswami, J. Romero, and A. G. White. Communicating via ignorance. *arXiv e-prints*, page arXiv:1807.07383, July 2018.
- [271] J. Uffink and J. H. van Lith-van Dis. Thermodynamic uncertainty relations. *arXiv e-prints*, pages cond-mat/9806102, June 1998.
- [272] H. J. D. Miller and J. Anders. Energy-temperature uncertainty relation in quantum thermodynamics. *Nature Communications*, 9:2203, June 2018.
- [273] Mario Berta, Matthias Christandl, Roger Colbeck, Joseph M. Renes, and Renato Renner. The uncertainty principle in the presence of quantum memory. *Nature Physics*, 6:659–662, September 2010.
- [274] Arun Kumar Pati, Mark M. Wilde, A. R. Usha Devi, A. K. Rajagopal, and Sudha. Quantum discord and classical correlation can tighten the uncertainty principle in the presence of quantum memory. *Phys. Rev. A*, 86:042105, Oct 2012.
- [275] Yakir Aharonov, David Z. Albert, and Lev Vaidman. How the result of a measurement of a component of the spin of a spin-1/2 particle can turn out to be 100. *Phys. Rev. Lett.*, 60:1351–1354, Apr 1988.
- [276] Amir Feizpour, Xingxing Xing, and Aephraim M. Steinberg. Amplifying single-photon nonlinearity using weak measurements. *Phys. Rev. Lett.*, 107:133603, Sep 2011.

- [277] Jérémie Harris, Robert W. Boyd, and Jeff S. Lundeen. Weak value amplification can outperform conventional measurement in the presence of detector saturation. *Phys. Rev. Lett.*, 118:070802, Feb 2017.
- [278] Andrew N. Jordan, Julián Martínez-Rincón, and John C. Howell. Technical advantages for weak-value amplification: When less is more. *Phys. Rev. X*, 4:011031, Mar 2014.
- [279] Erik Sjöqvist. Geometric phase in weak measurements. *Physics Letters A*, 359(3):187 – 189, 2006.
- [280] Arun Kumar Pati, Uttam Singh, and Urbasi Sinha. Measuring non-hermitian operators via weak values. *Phys. Rev. A*, 92:052120, Nov 2015.
- [281] Jeff S. Lundeen and Charles Bamber. Procedure for direct measurement of general quantum states using weak measurement. *Phys. Rev. Lett.*, 108:070402, Feb 2012.
- [282] Erkkka Haapasalo, Pekka Lahti, and Jussi Schultz. Weak versus approximate values in quantum state determination. *Phys. Rev. A*, 84:052107, Nov 2011.
- [283] Mehul Malik, Mohammad Mirhosseini, Martin PJ Lavery, Jonathan Leach, Miles J Padgett, and Robert W Boyd. Direct measurement of a 27-dimensional orbital-angular-momentum state vector. *Nature communications*, 5:3115, 2014.
- [284] Gerardo I. Viza, Julián Martínez-Rincón, Gabriel B. Alves, Andrew N. Jordan, and John C. Howell. Experimentally quantifying the advantages of weak-value-based metrology. *Phys. Rev. A*, 92:032127, Sep 2015.
- [285] Josiah Sinclair, Matin Hallaji, Aephraim M. Steinberg, Jeff Tollaksen, and Andrew N. Jordan. Weak-value amplification and optimal parameter estimation in the presence of correlated noise. *Phys. Rev. A*, 96:052128, Nov 2017.
- [286] Mikko Tukiainen, Hirokazu Kobayashi, and Yutaka Shikano. Quantification of concurrence via weak measurement. *Phys. Rev. A*, 95:052301, May 2017.

- [287] Suchetana Goswami, Sagnik Chakraborty, Sibasish Ghosh, and A. S. Majumdar. Universal detection of entanglement in two-qubit states using only two copies. *Phys. Rev. A*, 99:012327, Jan 2019.
- [288] Onur Hosten and Paul Kwiat. Observation of the spin hall effect of light via weak measurements. *Science*, 319(5864):787–790, 2008.
- [289] Sacha Kocsis, Boris Braverman, Sylvain Ravets, Martin J Stevens, Richard P Mirin, L Krister Shalm, and Aepraim M Steinberg. Observing the average trajectories of single photons in a two-slit interferometer. *Science*, 332(6034):1170–1173, 2011.
- [290] Grégory Strübi and C. Bruder. Measuring ultrasmall time delays of light by joint weak measurements. *Phys. Rev. Lett.*, 110:083605, Feb 2013.
- [291] Dong Xie, Chunling Xu, and An Min Wang. Optimal quantum thermometry by dephasing. *Quantum Information Processing*, 16(6):155, May 2017.
- [292] Matteo G A Paris. Achieving the landau bound to precision of quantum thermometry in systems with vanishing gap. *Journal of Physics A: Mathematical and Theoretical*, 49(3):03LT02, 2016.
- [293] Graeme Mitchison, Richard Jozsa, and Sandu Popescu. Sequential weak measurement. *Phys. Rev. A*, 76:062105, Dec 2007.
- [294] Hirokazu Kobayashi, Koji Nonaka, and Yutaka Shikano. Stereographical visualization of a polarization state using weak measurements with an optical-vortex beam. *Phys. Rev. A*, 89:053816, May 2014.
- [295] Justin Dressel and Andrew N. Jordan. Weak values are universal in von neumann measurements. *Phys. Rev. Lett.*, 109:230402, Dec 2012.

- [296] Gaurav Nirala, Surya Narayan Sahoo, Arun K Pati, and Urbasi Sinha. Measuring average of non-Hermitian operator with weak value in a Mach-Zehnder interferometer. *arXiv e-prints*, page arXiv:1807.09014, July 2018.
- [297] Chiranjib Mukhopadhyay, Manish K. Gupta, and Arun Kumar Pati. Superposition of causal order as a metrological resource for quantum thermometry. *arXiv e-prints*, page arXiv:1812.07508, December 2018.
- [298] D. Petz and C. Ghinea. Introduction to Quantum Fisher Information. In Rolando Rebolledo and Miguel Orszag, editors, *Quantum Probability and Related Topics*, pages 261–281, Jan 2011.